

**DEVELOPMENT OF TARGET-SPECIFIC ^{99m}Tc -RADIOTRACERS
AS POTENTIAL
RADIOPHARMACEUTICALS FOR DIAGNOSTIC APPLICATION**

By

V. KUSUM VATS
CHEM01201204011

Bhabha Atomic Research Centre, Mumbai

*A thesis submitted to the
Board of Studies in Chemical Sciences
In partial fulfillment of requirements
for the Degree of*

DOCTOR OF PHILOSOPHY

of

HOMI BHABHA NATIONAL INSTITUTE



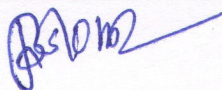
August, 2017

Homi Bhabha National Institute

Recommendations of the Viva Voce Committee

As members of the Viva Voce Committee, we certify that we have read the dissertation prepared by V. KUSUM VATS entitled "Development of target-specific ^{99m}Tc -radiotracers as potential radiopharmaceuticals for diagnostic application" and recommend that it may be accepted as fulfilling the thesis requirement for the award of Degree of Doctor of Philosophy.

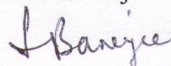
Chairman - Dr. B. S. Tomar



Date:

10.1.2018

Guide / Convener - Dr. (Smt.) Sharmila Banerjee



Date:

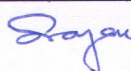
10/1/2018

Examiner - Dr. M. A. Neelakanta



Date:

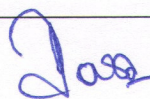
Member 1- Dr. S. K. Nayak



Date:

10/01/2018

Member 2- Dr. A. Dash



Date:

10/01/2018

Member 3- Dr. S. Kannan



Date:

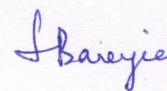
10.1.18

Final approval and acceptance of this thesis is contingent upon the candidate's submission of the final copies of the thesis to HBNI.

I/We hereby certify that I/we have read this thesis prepared under my/our direction and recommend that it may be accepted as fulfilling the thesis requirement.

Date: 10/1/2018

Place: BARC



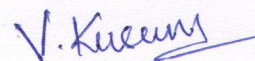
Guide

(Dr. (Smt.) Sharmila Banerjee)

STATEMENT BY AUTHOR

This dissertation has been submitted in partial fulfillment of requirements for an advanced degree at Homi Bhabha National Institute (HBNI) and is deposited in the Library to be made available to borrowers under rules of the HBNI.

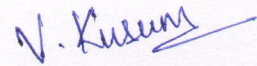
Brief quotations from this dissertation are allowable without special permission, provided that accurate acknowledgement of source is made. Requests for permission for extended quotation from or reproduction of this manuscript in whole or in part may be granted by the Competent Authority of HBNI when in his or her judgment the proposed use of the material is in the interests of scholarship. In all other instances, however, permission must be obtained from the author.



(V. KUSUM VATS)

DECLARATION

I, hereby declare that the investigation presented in the thesis has been carried out by me. The work is original and has not been submitted earlier as a whole or in part for a degree / diploma at this or any other Institution / University.



(V. KUSUM VATS)

List of Publications arising from the thesis

Journal

1. Radio synthesis and Evaluation of a ^{99m}Tc -Folic Acid Radiotracer prepared using $[\text{}^{99m}\text{TcN}(\text{PNP})]^{2+}$ Metal Fragment.
Kusum Vats, Suresh Subramanian, Anupam Mathur, Haladhar Dev Sarma, Sharmila Banerjee. *Bioorganic and Medicinal Chemistry Letters*, 27, 1329-1332 (2017).
2. Synthesis and Comparative In Vivo Evaluation of $^{99m}\text{Tc}(\text{CO})_3$ -labeled PEGylated and non-PEGylated cRGDFK Peptide Monomers.
Kusum Vats, Drishty Satpati, Haladhar Dev Sarma, Sharmila Banerjee. *Chemical Biology and Drug Design*, 89, 371-378 (2017).
3. '4+1' Mixed Ligand Strategy for the Preparation of ^{99m}Tc -Radiopharmaceuticals for Hypoxia Detecting Applications.
Kusum Vats, Madhava B Mallia, Anupam Mathur, Haladhar Dev Sarma, Sharmila Banerjee. *Chemistry Select*, 2, 2910-2916 (2017).
4. Preparation and Comparative evaluation of ^{99m}Tc -HYNIC-cNGR and ^{99m}Tc -HYNIC-PEG₂-cNGR as Tumor Targeting Molecular Imaging Probes.
Kusum Vats, Drishty Satpati, Rohit Sharma, Chandan Kumar, Haladhar Dev Sarma, Sharmila Banerjee. *Journal of Labelled Compounds and Radiopharmaceuticals*. doi/10.1002/jlcr.3585

Conferences

1. $^{99m}\text{Tc}(\text{CO})_3$ -labeling and Comparative In-Vivo Evaluation of Two Clicked cRGDFK Peptide Derivatives.
Kusum Vats, Drishty Satpati, Haladhar D Sarma, Sharmila Banerjee. *EJNMMI Radiopharmacy and Chemistry*; Vol 1, Supplement 1, PP 31 (2016).
2. ^{99m}Tc -HYNIC- labeled peptide c(KCNGRC) and peptide-drug conjugate c(KCNGRC)-CLB as radiomarkers for tumor angiogenesis.
Kusum Vats, Drishty Satpati, Haladhar Deb Sarma, Sharmila Banerjee. *Journal of Radiation and Cancer Research*, Vol 7, Special issue 1, PP 35 (2016).

3. Synthesis and in vivo evaluation of ^{99m}Tc -Hynic labeled tumor homing cyclic NGR peptide.

Kusum Vats, Drishty Satpati, Haladhar D Sarma, Sharmila Banerjee. *Asia Oceania Journal of Nuclear Medicine and Biology*, Vol 3, Supplement 1, S73 (2015).

4. Preparation of ^{99m}Tc -‘4+1’ Mixed Ligand Complex of 2-Nitroimidazole as a Marker for Tumor Hypoxia.

Kusum Vats, Madhava B Mallia, Anupam Mathur, Haladhar D Sarma, Sharmila Banerjee. *Indian Journal of Nuclear Medicine*, Vol 30, S56 (2015).

Others

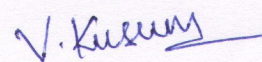
1. Radiolabeling, stability studies and pharmacokinetic evaluation of Thulium-170 labeled acyclic and cyclic polyaminopolyphosphonic acids.

Kusum Vats, Tapas Das, Haladhar Dev Sarma, Sharmila Banerjee, M R A Pillai. *Cancer Biotherapy and Radiopharmaceuticals*, 28, 737-745 (2013).

2. Synthesis and evaluation of a novel $^{99m}\text{TcN}(\text{PNP})$ -complex with metronidazole isocyanide ligand: as a marker for tumor hypoxia.

Kusum Vats, Madhava B Mallia, Anupam Mathur, Haladhar Dev Sarma, Sharmila Banerjee. *Journal of Radioanalytical Nuclear Chemistry*, 308, 363-369 (2016).

3. ^{99m}Tc -labeled NGR-chlorambucil conjugate, ^{99m}Tc -HYNIC-CLB-c(NGR) for targeted chemotherapy and molecular imaging. Kusum Vats, Drishty Satpati, Rohit Sharma, Chandan Kumar, Haladhar Dev Sarma, Ashutosh Dash. *Journal of Labelled Compounds and Radiopharmaceuticals*. doi/10.1002/jlcr.3522



V. Kusum Vats

Dedicated to my Parents....

ACKNOWLEDGEMENTS

First and Foremost, I would like to express my sincere gratitude to my guide Dr. (Smt) Sharmila Banerjee, Head, Radiation Medicine Centre and erstwhile Head of Radiopharmaceutical Chemistry Section, RC & IG, for her unwavering support, motivation and encouragement. Her observations and comments helped me to establish the overall direction of the research and to move forward with investigation in depth. I am thankful to her for sharing her knowledge and scientific understanding during the fruitful discussions with me throughout the work. I consider it as a great opportunity to do my doctoral programme under her guidance and to learn from her research expertise.

It gives me a great pleasure to acknowledge Dr. Ashutosh Dash, Head Radiopharmaceuticals Division, for his help and support in facilitating my work in Radiopharmaceuticals Division as well as for his inspiring words, encouragement and good wishes throughout my research tenure.

I owe a great deal of appreciation and gratitude to Dr. Drishti Satpati, my immediate superior, who inculcated in me the interest for peptide chemistry and taught me the solid phase peptide synthesis method. Her guidance helped me in all the time of research and also during the preparation of some of the manuscripts included in my thesis. I thank her deep from my heart for her unstinted inspiration, guidance and encouragement as well as for sharing her scientific and experimental knowledge with me.

I am grateful to Dr. Madhava B. Mallia for providing me hands-on-training in a number of laboratory techniques and some of the organic synthesis methodologies. His invaluable constructive criticisms and suggestions on academic level have always been extremely helpful to me. I also thank Dr. Anupam Mathur for providing the PNP compound and also for sharing his work experience and scientific knowledge with me.

I wish to pay my sincere thanks to Dr. Tapas Das, Head Radiopharmaceutical Chemistry Section, for his helpful suggestions and encouragement as well as for teaching me the practical aspects of radiochemistry initially, when I joined Radiopharmaceuticals Division.

My sincere thanks to Dr. Haladhar D. Sarma, Head, Experimental Animal Facility and Radioisotope Laboratory, Radiation Biology and Health Sciences Division for his kind help in carrying out biological evaluations of the compounds reported in this thesis.

I am also grateful to the chairman, Prof. B. S. Tomar (Director, Radiochemistry and Isotope Group, BARC), former chairman, Prof. K. L. Ramakumar (Former Director, Radiochemistry and Isotope Group, BARC), and the members Dr. S. K. Nayak (Head, Bio-organic Division), Dr. Ashutosh Dash (Head, Radiopharmaceuticals Division) and Dr. S. Kannan (Head, Fuel Chemistry Division) of the doctoral committee, for their critical reviews and suggestions during the annual progress reviews and pre-synopsis viva-voce.

My sincere thanks are due to all of my colleagues from Radiopharmaceuticals Chemistry Section for their help and support. Special thanks to Dr. (Smt.) Mohini Guleria for her moral support, encouraging words and helpful suggestions throughout the course of work.

Now, I would like to thank my colleagues of Radiochemistry Section for regularly supplying ^{99}Mo activity for carrying out the radiolabeling studies reported in this thesis. I am also thankful to colleagues from Radiopharmaceuticals Evaluation Section for carrying out in-vitro cell binding studies. I sincerely acknowledge all my colleagues from Radiopharmaceuticals Division for their help and support. I would also like to thank Shri Laxminaryan of Radiation Medicine Centre for his help and support.

I thankfully acknowledge the help and technical assistance received from Mr. Umesh Kumar and Mr. G. Gandhale throughout the course of work.

Finally I would like to thank my friends and family for continued support and encouragement. Most importantly, I would like to pay high regards to my parents who encouraged and helped me at every stage of my personal and academic life, and longed to see this achievement come true. I salute them for their selfless love, care, pain and sacrifice to shape my life. I would not have made it this far without their help and support. Last but not least, I want to thank my husband Bal Govind Vats for his encouragement and support which provided me the strength and patience to complete this challenging task.

CONTENTS

	Page No.
SYNOPSIS	(i)
LIST OF FIGURES	(xv)
LIST OF TABLES	(xix)
Chapter 1: General Introduction	
1.1. Radiopharmaceuticals	4
1.1.1. Target specific radiopharmaceuticals	4
1.1.2. Diagnostic radiopharmaceuticals	6
1.1.3. Therapeutic radiopharmaceuticals	8
1.2. Technetium-99m in nuclear medicine	10
1.3. ⁹⁹Mo-^{99m}Tc generator	11
1.4. Technetium Chemistry: different approaches of radiolabeling	12
1.4.1. Radiolabeling with ^{99m}Tc-oxo/dioxo core ($[\text{}^{99\text{m}}\text{TcO}]^{3+}$ or $[\text{}^{99\text{m}}\text{TcO}_2]^+$)	14
1.4.2. Radiolabeling with $[\text{}^{99\text{m}}\text{Tc}(\text{CO})_3]^+$ core	16
1.4.3. Radiolabeling with ^{99m}Tc-HYNIC core	18
1.4.4. ‘4+1’ mixed ligand approach of radiolabeling	19
1.4.5. Radiolabeling with $[\text{}^{99\text{m}}\text{TcN}]^{2+}$ and $[\text{}^{99\text{m}}\text{TcN}(\text{PNP})]^{2+}$ core	20
1.5. Biomolecules used in the present study	22
1.6. Quality control of radiotracers	23
1.6.1. Physicochemical tests	23
1.6.1.1. Chemical purity	24
1.6.1.2. Radionuclidic purity	24
1.6.1.3. Radiochemical purity	25
1.6.2. Biological tests	26
1.7. Thesis-outline	26
Chapter 2: Preparation of $[\text{}^{99\text{m}}\text{Tc}(\text{CO})_3]^+$ labeled cyclic RGD peptide derivatives for targeting tumor angiogenesis	
2.1. Introduction	31

2.1.1. Click-chemistry: Cu(I) catalyzed azide-alkyne cycloaddition (CuAAC) reaction	32
2.1.2. RGD peptide: Valuable tool for targeting tumor angiogenesis	33
2.2. Experimental	35
2.2.1. Materials and methods	35
2.2.2. Synthesis	36
2.2.2.1. Synthesis of cRGDfK-CH ₂ -Tz-Pra (2a)	36
2.2.2.2. Synthesis of cRGDfK-PEG ₇ -Tz-Pra (2b)	36
2.2.2.3. Preparation of Re(CO) ₃ complexes, Re(CO) ₃ -Pra-Tz-CH ₂ -cRGDfK (2c) & Re(CO) ₃ -Pra-Tz-PEG ₇ -cRGDfK (2d)	37
2.2.3. Radiolabeling	37
2.2.3.1. Preparation of [^{99m} Tc(CO) ₃ (H ₂ O) ₃] ⁺ precursor	37
2.2.3.2. Preparation of ^{99m} Tc(CO) ₃ -Pra-Tz-CH ₂ -cRGDfK (2e) & ^{99m} Tc(CO) ₃ -Pra-Tz-PEG ₇ -cRGDfK (2f)	38
2.2.3.3. Quality control	38
2.2.3.4. Determination of octanol-water partition coefficient (Log P _{o/w})	38
2.2.3.5. Stability studies	39
2.2.4. <i>In vitro</i> cell studies	39
2.2.5. Biodistribution studies	40
2.2.6. Data analysis	40
2.3. Results and Discussion	40
2.3.1. Synthesis	40
2.3.2. Radiolabeling	42
2.3.3. <i>In vitro</i> cell studies	45
2.3.4. Biodistribution studies	45
2.4. Conclusion	49
Chapter 3: Preparation of ^{99m}Tc-HYNIC labeled cyclic NGR peptide derivatives for targeting CD13 specific tumors	
3.1. Introduction	53
3.1.1. Radiolabeled peptides for imaging of tumors	54
3.1.2. NGR motif for targeting APN/CD13 expressing tumor	55

3.1.3. Solid phase peptide synthesis	57
3.2. Experimental	58
3.2.1. Materials and method	58
3.2.2. Synthesis	59
3.2.2.1. Synthesis of HYNIC-Boc (3a)	59
3.2.2.2. Synthesis HYNIC conjugated cyclic NGR peptides (3b and 3c)	60
3.2.3. Radiolabeling and quality control	65
3.2.3.1. Preparation of ^{99m} Tc-HYNIC-c(NGR) and ^{99m} Tc-HYNIC-PEG ₂ -c(NGR)	65
3.2.3.2. Determination of octanol-water partition coefficient (Log P _{o/w})	65
3.2.3.3. Stability studies	65
3.2.4. <i>In vitro</i> cell uptake studies	66
3.2.5. Biodistribution studies	66
3.2.6. Data analysis	67
3.3. Results and discussion	67
3.3.1. Synthesis	67
3.3.2. Radiolabeling	68
3.3.3. <i>In vitro</i> cell uptake studies	70
3.3.4. Biodistribution studies	71
3.4. Conclusion	75
Chapter 4: Preparation of ^{99m}Tc-‘4+1’ mixed ligand complexes of nitroimidazole ligands for targeting tumor hypoxia	
4.1. Introduction	79
4.1.1. Hypoxia	79
4.1.2. Nitroimidazoles as hypoxia markers	80
4.1.3. Nitroimidazole radiopharmaceuticals	81
4.2. Experimental	83
4.2.1. Materials and methods	83
4.2.2. Synthesis	84
4.2.2.1. Synthesis of tris(2-chloroethyl)amine (4a)	85

4.2.2.2. Synthesis of tris(S-ethylethanethioate)amine (4b)	85
4.2.2.3. Synthesis of 2,2',2''-nitrilotrisethanethiol (NS ₃) (4c)	85
4.2.2.4. Synthesis of tert-Butyl-3-(2-nitro-1H-imidazol-1-yl)propylcarbamate (4d)	88
4.2.2.5. Synthesis of 3-(2-nitro-1H-imidazol-1-yl)propan-1-amine hydrochloride (4e)	90
4.2.2.6. Synthesis of N-(3-(2-nitro-1H-imidazol-1-yl)propyl)formamide (4f)	90
4.2.2.7. Synthesis of 1-(3-isocyanopropyl)-2-nitro-1H-imidazole (2NimNC) (4g)	91
4.2.2.8. Synthesis of N-(2-(2-methyl-5-nitro-1H-imidazol-1-yl)ethyl)formamide (4h)	93
4.2.2.9. Synthesis of 1-(2-isocyanoethyl)-2-methyl-5-nitro-1H-imidazole (MetNC) (4i)	94
4.2.2.10. Preparation of inactive Rhenium (^{185/187} Re) analogs of ^{99m} Tc-complexes (4j & 4k)	96
4.2.3. Radiolabeling	99
4.2.3.1. Preparation of ^{99m} Tc-EDTA complex	99
4.2.3.2. General procedure for preparation of ^{99m} Tc(NS ₃)-complex	99
4.2.4. Quality Control	99
4.2.4.1. TLC of ^{99m} Tc-EDTA complex	99
4.2.4.2. HPLC	99
4.2.4.3. Octanol-water partition co-efficient (LogP _{o/w})	100
4.2.4.4. <i>In-vitro</i> serum stability	100
4.2.5. Cyclic voltametry studies	100
4.2.6. <i>In vivo</i> studies	101
4.3. Results and discussion	102
4.3.1. Synthesis	102
4.3.2. Radiolabeling	103
4.3.3. Preparation of inactive Rhenium (^{185/187} Re) analogs of ^{99m} Tc-complexes	107
4.3.4. Cyclic voltametry studies	110

4.3.5. <i>In vivo</i> studies	113
4.4. Conclusions	116
Chapter 5: Preparation of a ^{99m}Tc-Folic Acid radiotracer using [^{99m}TcN(PNP)]²⁺ metal fragment	
5.1. Introduction	119
5.2. Experimental	121
5.2.1. Materials and methods	121
5.2.2. Synthesis	122
5.2.2.1. Synthesis of S-trityl cysteine ester (5a)	122
5.2.2.2. Synthesis of (Ethyl, S-trityl cysteinyl amido) Folic acid (5b)	123
5.2.2.3. Synthesis of (S-trityl cysteinyl amido) Folic acid (5c)	123
5.2.2.4. Synthesis of (cysteinyl amido) folic acid (5d)	125
5.2.3. Radiolabeling	126
5.2.4. Quality control studies	127
5.2.4.1. HPLC	127
5.2.4.2. Octanol-Water partition coefficient (Log P _{o/w})	127
5.2.4.3. Stability studies	128
5.2.5. <i>In vitro</i> cell binding studies	128
5.2.5.1. Estimation of IC ₅₀	128
5.2.5.2. Cell uptake studies of [^{99m} TcN(PNP)]-folic acid complex	129
5.2.6. <i>In vivo</i> evaluation studies	130
5.3. Results and discussion	130
5.3.1. Synthesis	131
5.3.2. Radiolabeling and quality control	132
5.3.3. <i>In vitro</i> cell binding studies	133
5.3.4. <i>In vivo</i> biodistribution studies	135
5.4. Conclusion	137
Summary	139
References	143

SYNOPSIS

The survival and quality of life of cancer patients can be improved by early detection, staging and management of the disease. This has now become possible with specific and targeted imaging of cancer related molecular events using highly sensitive molecular imaging techniques. While conventional imaging techniques like X-ray, CT, MRI etc. provide anatomical imaging, molecular imaging effectively allows the non-invasive visualization, characterization and measurement of biological processes at the molecular and cellular level in the human body [1]. Of the various molecular imaging techniques, use of nuclear medicine that employs radiopharmaceuticals is most promising with respect to imaging specific biological targets present at low concentrations [2,3]. As a result, there is a great interest in the development of novel target-specific radiolabeled agents for diagnostic application.

Radiopharmaceuticals are radiolabeled drugs or molecules with a definite composition and are used routinely in nuclear medicine for the diagnosis or therapy of various diseases. Radiopharmaceuticals are classified on the basis of their biological distribution, as metal essential radiopharmaceuticals where there is no targeting molecule and the biodistribution depends on the chemical and physical properties of the radio-complex; and target-specific radiopharmaceuticals where the *in vivo* localization is determined by the specific biological interactions such as receptor binding, enzymatic reduction, antigen-antibody interaction etc. Depending on their use in nuclear medicine and the nuclear characteristics of the radionuclide used, radiopharmaceuticals can be classified as diagnostic and therapeutic radiopharmaceuticals.

Diagnostic radiopharmaceuticals are molecules labeled with preferably pure gamma emitting isotopes or positron emitting isotopes, used to provide information related to morphological structure of organ or tissue as well as their physiological functions when they

localize in the particular organ. Therapeutic radiopharmaceuticals are molecules designed to deliver therapeutic doses of ionizing radiation to the diseased site. Diagnostic application in nuclear medicine relies on two main imaging modalities: SPECT (Single photon emission computed tomography) and PET (positron emission tomography) [4]. PET offers higher resolution and sensitivity, however, the use of more readily available, longer lived radionuclides and the relatively lower costs of gamma cameras make SPECT imaging much more attractive and affordable for larger population. Among different SPECT radioisotopes used in diagnostic nuclear medicine, ^{99m}Tc with its ideal nuclear characteristics ($t_{1/2} = 6$ h, 140 keV), cost effectiveness, easy availability from $^{99}\text{Mo}/^{99m}\text{Tc}$ generator and ready formulation of radiopharmaceuticals through cold kits, becomes the obvious choice. ^{99m}Tc being routinely and most widely used medical isotope accounting for approximately 20-25 million diagnostic procedures annually, comprising ~80% of all diagnostic Nuclear Medicine procedures worldwide, continues to be the ‘work-horse’ of diagnostic Nuclear Medicine [5].

Technetium belongs to the group VII B of the periodic table with a neutral electronic configuration of $[\text{Kr}]4d^65s^1$. Being a transition metal the coordination chemistry of ^{99m}Tc is very complex: a large number of oxidation states (+7 to -1) and a wide variety of coordination geometries (square pyramidal, trigonal bipyramidal and octahedral) are possible [6]. The oxidation state and stability of Tc-complex depends on the type of ligand used and the chemical environment. The most stable oxidation states of technetium in water are +7 as $^{99m}\text{TcO}_4^-$ and +4 as the insoluble hydrolyzed reduction product, $\text{TcO}_2 \cdot \text{H}_2\text{O}$. The other oxidation states (+5, +3, +2, +1) are stabilized on complexation with the suitable ligand [5,7]. The diverse redox chemistry of technetium led to different strategies for labeling biomolecules with ^{99m}Tc , in terms of metal cores, oxidation states and selection of BFCAs [5-9]. The ^{99m}Tc -oxo core ($[\text{O}^{99m}\text{TcO}]^{3+}$ or

$[\text{}^{99\text{m}}\text{TcO}_2]^+$) is the earliest and most commonly used $^{99\text{m}}\text{Tc}$ -core. However, the conventional method of radiolabeling with $^{99\text{m}}\text{Tc}$ where in situ formation of $^{99\text{m}}\text{Tc}$ -oxo core ($[\text{}^{99\text{m}}\text{TcO}]^{3+}$ or $[\text{}^{99\text{m}}\text{TcO}_2]^+$) occurs has the inherent disadvantage of requiring large excess of ligand [9]. Use of large excess of ligand is a drawback in preparation of target-specific radiopharmaceuticals as there will be a competition between the radiolabeled ligand and the unlabeled ligand for the limited number of receptors on the cancerous cells. Thus novel and improved methods of radiolabeling were introduced, which make use of cores such as $[\text{}^{99\text{m}}\text{TcN}]^{2+}$, $[\text{}^{99\text{m}}\text{Tc}(\text{CO})_3]^+$, bifunctional chelating agents (BFCA) like HYNIC (6-hydrazine nicotinic acid) and $^{99\text{m}}\text{Tc}$ -‘4+1’ mixed ligand approach etc. Since the labeling using these preformed cores requires less ligand concentration, it opened up the possibility of preparing high-specific activity $^{99\text{m}}\text{Tc}$ -complexes using low ligand concentration [8,9].

In the present thesis an attempt has been made to prepare $^{99\text{m}}\text{Tc}$ -labeled target-specific molecular imaging probes for specific targeting of different tumors using novel technetium cores such as $[\text{}^{99\text{m}}\text{TcN}]^{2+}$, $[\text{}^{99\text{m}}\text{Tc}(\text{CO})_3]^+$, $^{99\text{m}}\text{Tc}$ -HYNIC and $^{99\text{m}}\text{Tc}$ -‘4 + 1’ mixed ligand approach. Different tumors have different characteristic features such as specific receptor over-expression; hypoxic condition etc., which are the guiding parameters for selecting the carrier molecule in the radiopharmaceutical. Towards this, the biological vectors like peptide ligands having high affinity towards receptors over-expressed in numerous cancers, folic acid having high affinity for folate receptors over-expressed in many human tumor cells and nitroimidazole ligands for selective accumulation in hypoxic tumors were synthesized or derivatized and radiolabeled with $^{99\text{m}}\text{Tc}$. The thesis consists of four chapters and the contents of each chapter are briefly outlined below.

Chapter 1: Introduction

This chapter deals with the basic concepts of radiopharmaceuticals and their use in nuclear medicine. Radiopharmaceuticals have been classified according to their medical applications as ‘diagnostic’ and ‘therapeutic’ and ‘target-specific’ on the basis of their biodistribution. This chapter also brings to light the importance of ^{99m}Tc in diagnostic nuclear medicine. Different labeling approaches with ^{99m}Tc are discussed with emphasis on novel technetium chemistry like $[\text{}^{99m}\text{TcN}]^{2+}$ core, $[\text{}^{99m}\text{Tc}(\text{CO})_3]^+$ core, HYNIC and ‘4 + 1’ mixed ligand approach. Advantages of using novel technetium chemistry over the conventional ^{99m}Tc -oxo core ($[\text{}^{99m}\text{TcO}]^{3+}$ or $[\text{}^{99m}\text{TcO}_2]^+$) for preparing target-specific radiotracers are discussed. An introduction to bi-functional chelating agents (BFCA), their importance in preparation of stable complexes as well as their role in improving the pharmacokinetic behavior of resultant radiopharmaceutical has also been discussed. A brief description of different targeting molecules used viz. peptides, folic acid and nitroimidazoles is also provided in this chapter. Various quality control methods, biological study protocols etc. for evaluating different labeled molecules are described briefly.

Chapter 2: Preparation of $[\text{}^{99m}\text{Tc}(\text{CO})_3]^+$ -labeled cyclic RGD peptide derivatives for targeting tumor angiogenesis

For targeted molecular imaging applications with ^{99m}Tc , the $[\text{}^{99m}\text{Tc}(\text{CO})_3(\text{H}_2\text{O})_3]^+$ precursor complex introduced by Alberto et al. is an attractive option of preparing ^{99m}Tc -labeled targeted radiotracers. By using this strategy of using the $[\text{}^{99m}\text{Tc}(\text{CO})_3(\text{H}_2\text{O})_3]^+$ core, high specific activity complexes can be prepared, as ^{99m}Tc is already stabilized in +1 oxidation state and hence use of excess ligand is not required during radiolabeling [10]. The $[\text{}^{99m}\text{Tc}(\text{CO})_3(\text{H}_2\text{O})_3]^+$ core can be easily prepared by purging carbon monoxide (CO) gas into $^{99m}\text{TcO}_4^-$ in the presence of NaBH_4 .¹⁰ The three coordinated water molecules can be easily replaced by variety of functional

groups (e.g., amines, thiols, carboxylates etc) to give stable complexes [11]. For radiolabeling with $^{99m}\text{Tc}(\text{CO})_3$ core, the biomolecule is synthetically modified to incorporate appropriate ligands and subsequently reacted with $[\text{}^{99m}\text{Tc}(\text{CO})_3(\text{H}_2\text{O})_3]^+$ precursor complex. This chapter demonstrates the application of click chemistry in the preparation of $^{99m}\text{Tc}(\text{CO})_3$ complexes of cRGDfK peptide derivatives. Ease of incorporation of azide and alkyne in variety of substrates (peptides, antibodies, small molecules) has popularized, 'click reaction', as an effective strategy for introduction of a metal chelator in a biological vector [12]. Copper catalyzed azide and alkyne click reaction product 1,4-substituted 1,2,3-triazole (Tz) forms an integral part of a tridentate chelating system needed for coordination and preparation of kinetically inert $[\text{}^{99m}\text{Tc}(\text{CO})_3]$ -radiotracers [13].

RGD (arginine-glycine-aspartic acid) peptides radiolabeled with different ^{99m}Tc cores have been widely investigated for targeting integrin $\alpha_v\beta_3$ receptors overexpressed in certain specific cancers [14]. Integrin $\alpha_v\beta_3$, a well-established target for tumor angiogenesis and metastasis is also upregulated in various types of cancer particularly in melanoma, glioblastoma, ovarian and breast carcinoma [15]. Therefore, RGD peptides have been widely explored for development of imaging agents as markers of tumor angiogenesis. There is a constant effort by the scientists worldwide to modify and prepare potential RGD-based radiotracers with improved pharmacokinetics for targeted angiogenesis imaging.

In this work, click reaction has been employed for synthesis of two modified cRGDfK peptides with different spacer units, PEG was incorporated as the hydrophilic linker in one of the azide-modified cRGDfK peptide analogue and the comparative studies with its counterpart, azide-modified cRGDfK without the PEG unit were carried out. Towards this, two different azide moieties, $\text{N}_3\text{CH}_2\text{COOH}$ and $\text{N}_3\text{-PEG}_7\text{-COOH}$ were introduced by amide bond formation

with cRGDfK peptide which were then clicked with propargyl glycine (Pra) to introduce a tridentate chelator for radiolabeling with $[^{99m}\text{Tc}(\text{CO})_3(\text{H}_2\text{O})_3]^+$ precursor. The ligands synthesized were characterized and subsequently radiolabeled using $[^{99m}\text{Tc}(\text{CO})_3(\text{H}_2\text{O})_3]^+$ core to form neutral complexes of cRGDfK [Fig. 1]. The radiotracers, $^{99m}\text{Tc}(\text{CO})_3\text{-Pra-Tz-CH}_2\text{-cRGDfK}$ and $^{99m}\text{Tc}(\text{CO})_3\text{-Pra-Tz-PEG}_7\text{-cRGDfK}$ were obtained in >90% RCP. For the purpose of characterization of the ^{99m}Tc complexes, corresponding rhenium complexes, $\text{Re}(\text{CO})_3\text{-Pra-Tz-CH}_2\text{-cRGDfK}$ and $\text{Re}(\text{CO})_3\text{-Pra-Tz-PEG}_7\text{-cRGDfK}$ were synthesized using the $[\text{NEt}_4]_2[\text{ReBr}_3(\text{CO})_3]$ precursor. The biological efficacy of the radiotracers was evaluated by carrying out *in vitro* and *in vivo* studies in $\alpha_v\beta_3$ -positive murine melanoma (B16F10) tumor model. The two radiotracers showed specificity towards the $\alpha_v\beta_3$ receptors. The PEGylated cRGDfK peptide analogue ($^{99m}\text{Tc}(\text{CO})_3\text{-Pra-Tz-PEG}_7\text{-cRGDfK}$) had higher tumor uptake than the non-PEGylated analogue ($^{99m}\text{Tc}(\text{CO})_3\text{-Pra-Tz-CH}_2\text{-cRGDfK}$) but its high uptake in other non-target organs resulted in lower target/non-target ratios.

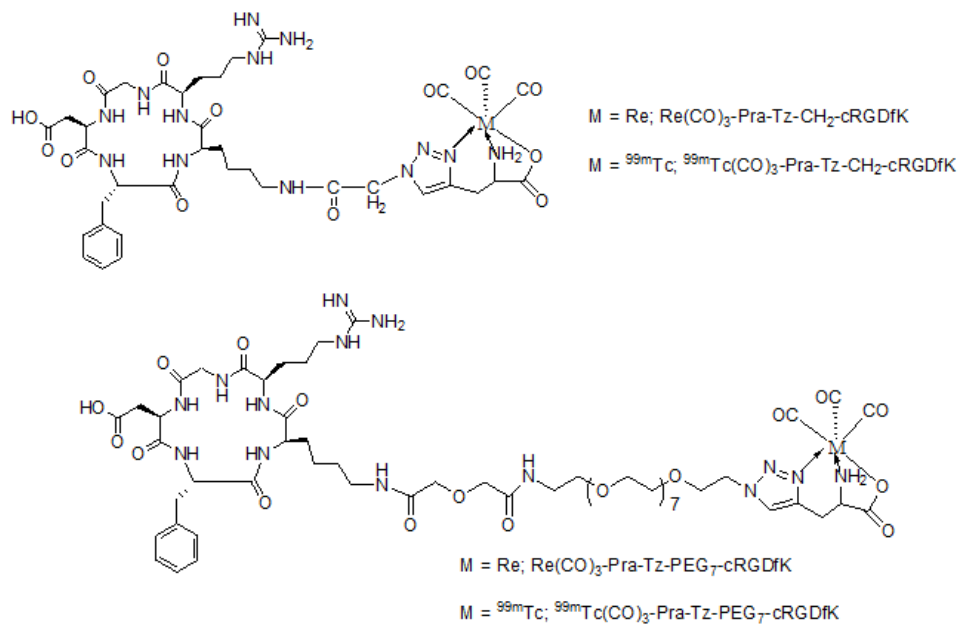


Fig. 1: Technetium and rhenium carbonyl complexes of triazole functionalized cRGDfK peptide analogues

Chapter 3: Preparation of ^{99m}Tc -HYNIC labeled cyclic NGR peptide derivatives for targeting CD13 specific tumors

Radiolabeled peptides offer multiple advantages of simple and rapid preparation, high target efficacy, and fast clearance from non-target organs and low immunogenicity. Therefore, they serve as key tools for molecular imaging of different cancers [16]. The diverse and rich chemistry of ^{99m}Tc allows the use of different strategies for labeling peptides with ^{99m}Tc , with respect to the choice of metal cores as well as bifunctional chelating agents (BFCAs) [6-9]. Amongst them, HYNIC is one of the most promising bifunctional chelating agent (BFCA) generally used for radiolabeling peptides with ^{99m}Tc . The advantage of using HYNIC as BFCA is its high radiolabeling efficiency which allows for preparation of radio-complexes with high specific activity [9,17]. The appropriate choice of co-ligands allows easy modification of pharmacokinetic profile of the ^{99m}Tc -labeled biomolecules, since the hydrophilicity/lipophilicity of the resultant complex can be tailored [9,17]. HYNIC also has an advantage of simple and easier conjugation with peptides either on-resin during solid phase peptide synthesis or in the solution phase.

Peptide ligands containing asparagine-glycine-arginine (NGR) sequence specifically target aminopeptidase receptors (APN or CD13) over-expressed on tumor cells or tumor vasculature [18]. CD13 receptors reportedly have high expression on various human solid tumors including melanoma, prostate, lung and ovarian cancer [19]. Thus radiolabeled NGR peptides can be potential radiotracers for imaging and detection of CD13 receptor-positive tumors as well as for monitoring the response of cancer sites towards therapy. In the present work cyclic NGR peptide, cKCNGRC was synthesized and conjugated with HYNIC chelator for radiolabeling with ^{99m}Tc . With the aim of increasing the circulating half-life of the peptide and modulating the

pharmacokinetics, polyethylene glycol moiety (PEG₂) was introduced as a spacer at the N-terminus of the peptide prior to conjugation with HYNIC. The two HYNIC conjugated peptides, HYNIC-cKCNGRC (HYNIC-cNGR) and HYNIC-PEG₂-cKCNGRC (HYNIC-PEG₂-cNGR) [Fig. 2] were subsequently radiolabeled with ^{99m}Tc and their efficacy for targeting CD13 receptors was investigated. The radiotracers, ^{99m}Tc-HYNIC-c(NGR) and ^{99m}Tc-HYNIC-PEG₂-c(NGR) could be prepared in >95% radiochemical purity (RCP) and exhibited excellent in vitro as well as in vivo stability. Both the radiotracers exhibited high selectivity towards CD13 receptors.

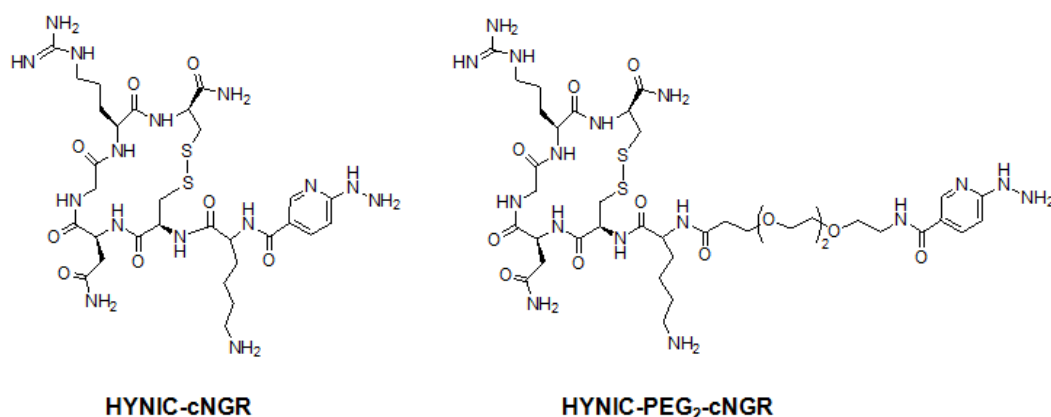


Fig. 2: HYNIC conjugated cyclic NGR peptide derivatives

In vivo evaluation studies revealed similar uptake of ^{99m}Tc-HYNIC-c(NGR) and ^{99m}Tc-HYNIC-PEG₂-c(NGR) in HT-1080 tumor xenografts at all the time points studied. The insertion of PEG₂ linker did not significantly affect the tumor uptake and retention. However target/non-target ratios (tumor/blood, tumor/muscle, tumor/liver) were observed to be higher for ^{99m}Tc-HYNIC-PEG₂-c(NGR) at 3 h p.i. in comparison to that of ^{99m}Tc-HYNIC-c(NGR). The two radiotracers were excreted through renal pathway and cleared rapidly from blood, liver and intestine.

Chapter 4: Preparation of ^{99m}Tc -‘4+1’ mixed ligand complexes of nitroimidazole ligands for targeting tumor hypoxia.

The ‘4+1’ mixed ligand approach is a relatively less explored strategy for radiolabeling molecules with ^{99m}Tc . The ‘4+1’ mixed-ligand complexes consist of central Tc(III) metal atom coordinated to a tetradentate tripodal chelator 2,2',2''-nitrilotriethanethiol (NS_3) and a monodentate isocyanide group tethered to a biomolecule [20]. The ‘4+1’ mixed ligand complexes are neutral and can be prepared in excellent yield under mild reaction conditions. Additionally, they exhibit high kinetic stability against ligand exchange *in vivo* [20,21]. The present work describes the use of ‘4+1’ mixed ligand strategy to design ^{99m}Tc -radiotracers for the detection of *in vivo* tissue hypoxia. The ^{99m}Tc -labeling is affected using the tripodal tetradentate NS_3 chelator and nitroimidazole-isocyanide as the monodentate ligand.

Hypoxia is a pathophysiological condition in a locally advanced solid tumor arising from an imbalance between the oxygen supply it receives and its consumption therein. Presence of hypoxic regions in tumors is one of the major reasons for the resistance to conventional radiotherapy and chemotherapy. Nitroimidazoles, which show selective accumulation in hypoxic cells, are the most widely explored molecules for delineating hypoxic tumor cells from normoxic cells [22]. In the present work, isocyanide derivatives of 2-nitroimidazole (2-NimNC) and metronidazole (MetNC) were synthesized and characterized by IR, ^1H -NMR and ^{13}C -NMR. Subsequently, the ^{99m}Tc mixed ligand complexes [$^{99m}\text{Tc}(\text{NS}_3)(2\text{-NimNC})$] and [$^{99m}\text{Tc}(\text{NS}_3)(\text{MetNC})$] were prepared by substitution using ^{99m}Tc -EDTA complex as precursor [Fig. 3]. The complexes [$^{99m}\text{Tc}(\text{NS}_3)(2\text{-NimNC})$] and [$^{99m}\text{Tc}(\text{NS}_3)(\text{MetNC})$] were prepared in >90% RCP and exhibited excellent *in vitro* and *in vivo* stability. The structure of ^{99m}Tc complexes was corroborated using stable rhenium ($^{185/187}\text{Re}$) as surrogate for technetium. The

rhenium complexes were prepared by substitution of ligands 2-NimNC and MetNC on the rhenium precursor complex $[\text{Re}(\text{NS}_3)(\text{PMe}_2\text{Ph})]$. UV-HPLC chromatograms of the two rhenium complexes matched with that of the HPLC profile of the corresponding $^{99\text{m}}\text{Tc}$ -‘4+1’ complexes, indicating the formation of structurally similar types of complexes in both cases. Cyclic voltammetry studies of the ligand and rhenium complexes clearly indicated that there is no significant change in SERP value of nitroimidazole ligand upon forming the complex. Preliminary biological evaluation of $[\text{}^{99\text{m}}\text{Tc}(\text{NS}_3)(2\text{NimNC})]$ and $[\text{}^{99\text{m}}\text{Tc}(\text{NS}_3)(\text{MetNC})]$ in Swiss mice bearing fibrosarcoma tumor showed uptake and retention of the complex in tumor.

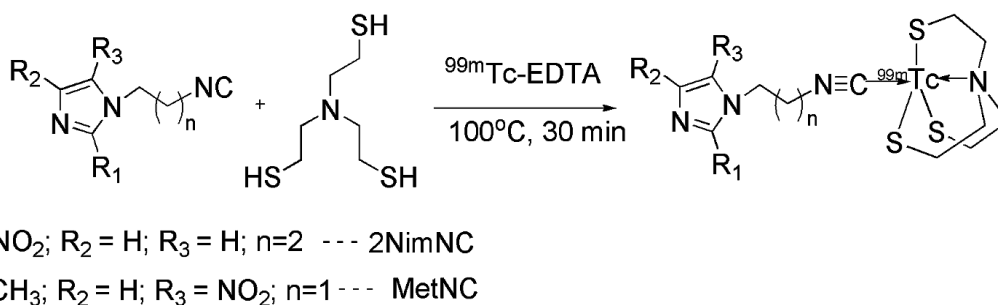


Fig. 3: Preparation of $^{99\text{m}}\text{Tc}$ -‘4+1’ complexes of isocyanide derivatives of nitroimidazole

Chapter 5: Preparation of a $^{99\text{m}}\text{Tc}$ -Folic Acid radiotracer using $[\text{}^{99\text{m}}\text{TcN}(\text{PNP})]^{2+}$ metal fragment

This chapter gives a brief overview of the usefulness of $[\text{}^{99\text{m}}\text{TcN}]^{2+}$ core for preparing target specific radiotracers. There are two general approaches for radiolabeling molecules with $[\text{}^{99\text{m}}\text{TcN}]^{2+}$ core. While the first approach involves two bidentate σ -donor ligands such as dithiocarbamates, xanthates, cysteine, etc., which form a symmetrical $[2 + 2]$ complex [23], the second approach makes use of a combination of ‘pseudotridentate’ σ -donors π -acceptors diphosphinoamines (PNP) and bidentate σ -donor ligand forming an asymmetrical complex via the formation of $[\text{}^{99\text{m}}\text{TcN}(\text{PNP})]^{2+}$ core [24]. This approach is particularly useful for $^{99\text{m}}\text{Tc}$

labeling of bulky biomolecules where a symmetric [2+2] complex formation would probably result in loss of biological activity due to the steric hindrance of the resultant ^{99m}TcN -complex. In this chapter use of $[\text{}^{99m}\text{TcN(PNP)}]^{2+}$ precursor for radiolabeling folic acid with ^{99m}Tc is demonstrated.

Radiolabeled folate conjugates are radiotracers for targeting folate receptors (FRs) overexpressed on various tumors and thus act as important molecular imaging entities for staging and monitoring of FR-positive cancers [25]. A number of ^{99m}Tc -folate radioconjugates have been developed in the past. However high renal uptake where FRs is densely populated acts as a drawback towards their utility as radiotracer for FR positive cancers [25]. This behavior is attributable to the highly hydrophilic nature of the ^{99m}Tc -folate complexes, which facilitates clearance mainly via the renal pathway. In this direction, use of the $[\text{}^{99m}\text{TcN(PNP)}]^{2+}$ precursor which is known to form lipophilic complexes and facilitate *in vivo* clearance of the complex via the hepatic route, was chosen for labeling the parent folic acid molecule.

In the present work, conjugation of γ - carboxylic acid of folic acid with the amino group of cysteine BFCA was carried out, resulting in the formation of the folic acid-cysteine conjugate, which was subsequently radiolabeled with $[\text{}^{99m}\text{TcN(PNP)}]^{2+}$ metal fragment to yield the final $[\text{}^{99m}\text{TcN(PNP)}]$ -folic acid complex [Fig. 4]. The $[\text{}^{99m}\text{TcN(PNP)}]$ -folic acid complex was prepared with ~90% RCP. The radiolabeled complex after purification by HPLC was used for further studies. The $\text{LogP}_{\text{o/w}}$ value, a measure of lipophilicity, was found to be 0.87 which is higher than the $\text{LogP}_{\text{o/w}}$ value for previously reported radiofolates [25,26], thus showing that $[\text{}^{99m}\text{TcN(PNP)}]$ -folic acid complex is more lipophilic compared to previously reported radiofolates. The *in vitro* cell uptake studies in KB-31 cells known to express FR, revealed reduction in the affinity of the radiotracer on complexation with the $[\text{}^{99m}\text{TcN(PNP)}]$ moiety.

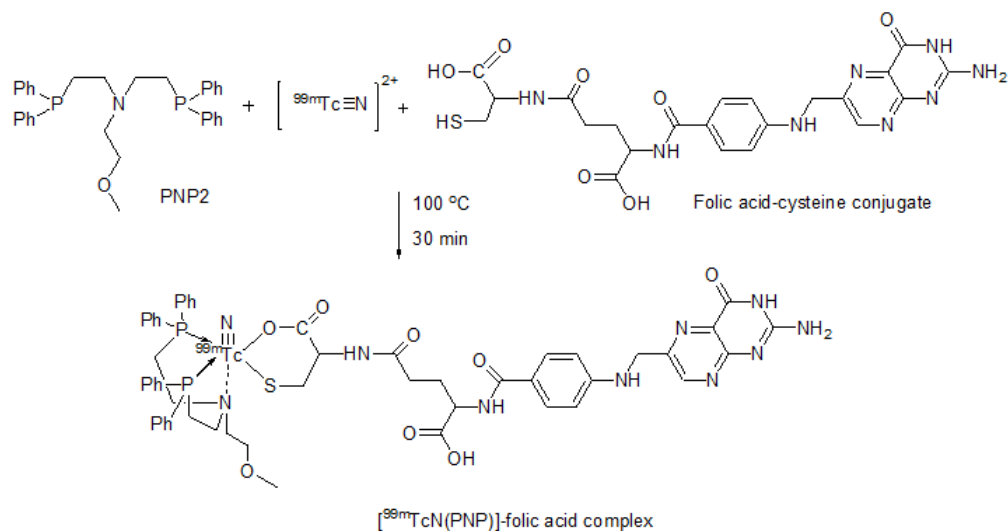


Fig. 4: Preparation of $[\text{}^{99\text{m}}\text{TcN(PNP)}]\text{-folic acid complex}$

The *in vivo* experiment in normal swiss mice revealed clearance of the radiotracer via the hepatic route as envisaged in the study design. The study provided pertinent insights towards improving the receptor uptake by designing a similar $[\text{}^{99\text{m}}\text{TcN(PNP)}]\text{-folic acid radiotracer}$ by suitable structural modification.

References:

1. Pimlott S. L., Sutherland A. *Chem Soc Rev* **2011**, *40*, 149–162.
2. Bartholomä M. D., Louie A. S., Valliant J. F., Zubieta Jon. *Chem Rev* **2010**, *110*, 2903–2920.
3. Correia J. D. G., Paulo A., Raposinho P. D., Santos I. *Dalton Trans* **2011**, *40*, 6144–6167.
4. Coleman R. E. *Cancer* **1991**, *67*, 1261-1270.
5. Banerjee S., Pillai M. R. A., Ramamoorthy N. *Semin Nucl Med* **2001**, *31*, 260–277.
6. Liu S. *Chem Soc Rev* **2004**, *33*, 445–461.
7. Liu S., Edwards D. S., Barrett J. A. *Bioconjugate Chem* **1997**, *8*, 621–636.
8. Jurisson S. S., Lydon J. D. *Chem Rev* **1999**, *99*, 2205–2218.

9. Alberto R. in *Technetium-99m Radiopharmaceuticals: Status and Trends*, IAEA, 2009, ch. 2, pp. 19–34.
10. Alberto R., Schibli R., Egli A., Schubiger, A. P. *J. Am. Chem. Soc.*, **1998**, *120*, 7987.
11. Alberto R., Schibli R., Waibel R., Abram U., Schubiger A. P. *Coord Chem Rev* **1999**, *190–192*, 901–919.
12. Zeng D., Zeglis B. M., Lewis J. S., Anderson C. J. *J Nucl Med* **2013**, *54*, 829–832.
13. Mindt T. L., Muller C., Melis M., de Jong M., Schibli R. *Bioconjug Chem* **2008**, *19*, 1689–1695.
14. Decristoforo C., Santos I., Pietzsch H. J., Kuenstler J. U., Duatti A., Smith C. J., Rey A., Alberto R., Von Guggenber E., Hauber R. *Q J Nucl Med Mol Imaging* **2007**, *51*, 33–41.
15. Gasparini G, Brooks P. C, Biganzoli E et al *Clin Cancer Res* **1998**, *4*, 2625–2634.
16. Fani M, Maecke H. R., Okarvi S. M. *Theranostics* **2012**, *2*, 481–501.
17. Liu S, Edwards D. S. *Chem Rev* **1999**, *99*, 2235–2268.
18. Arap W., Pasqualini R., Ruoslahti E. *Science* **1998**, *279*, 377–378.
19. Chen K, Ma W, Li G, Wang J, Yang W, Yap L.P., Hughes L. D., Park R., Conti P. S. *Mol Pharm* **2013**, *10*, 417–427.
20. Spies H., Glaser M., Pietzsch H. J., Hahn F. E., Lugger T., *Inorg Chim Acta* **1995**, *240*, 465–478.
21. Kunstler J. U., Seidel G., Bergmann R., Gniazdowska E., Walther M., Schiller E., Decristoforo C., Stephan H., Haubner R., Steinbach J., Pietzsch H. J. *Eur J Med Chem* **2010**, *45*, 3645–3655.
22. Krohn K. A., Link J. M., Mason R. P. *J Nucl Med* **2008**, *Suppl 2*, 129S.

23. Pasqualini R, Duatti A, Bellande E, Comazzi V, Brucato V, Hoffschir D, Fagret D, Comet M
J Nucl Med **1994**, 35, 334-341.
24. Bolzati C, Boschi A, Uccelli L, Tisato F, Refesco F, Cagnolini A, Duatti A, Prakash S,
Bandoli G, Vittadini A. *J Am Chem Soc* **2002**, 124, 11468-11479.
25. Müller C., Schibli R. *J Nucl Med* **2011**, 52, 1-4.
26. Lu J., Pang Y., Xie F., Guo H., Li Y., Yang Z., Wang X. *Nucl Med Biol* **2011**, 38, 557-565.

LIST OF FIGURES

	Page No.
Fig.1.1. Typical design of a radiopharmaceutical using BFCA approach	5
Fig.1.2. Simplified ^{99}Mo decay scheme	10
Fig.1.3. Some $^{99\text{m}}\text{Tc}$ -radiopharmaceuticals having $^{99\text{m}}\text{Tc}$ -oxo or dioxo core	15
Fig.1.4. Typical structure of $[\text{}^{99\text{m}}\text{Tc}(\text{CO})_3(\text{H}_2\text{O})_3]^+$ precursor complex	16
Fig.1.5. Examples of few tridentate chelators for labeling with $[\text{}^{99\text{m}}\text{Tc}(\text{CO})_3]^+$ core.	17
Fig.1.6. Typical structure $^{99\text{m}}\text{Tc}$ -HYNIC-biomolecule complex using (a) tricine as co-ligand (b) EDDA/tricine as co-ligand and (c) TPPTS/tricine co-ligand	18
Fig.1.7. Typical structure $^{99\text{m}}\text{Tc}$ -‘4+1’ mixed ligand complex with tetradentate NS_3 ligand and monodentate isocyanide ligand conjugated to the biomolecule	20
Fig.1.8. (a) Typical structure of symmetric [2+2] complex with $[\text{}^{99\text{m}}\text{TcN}]^{2+}$ core and (b) structure of asymmetric [2+2] $[\text{}^{99\text{m}}\text{TcN}(\text{PNP})]$ -biomolecule complex	21
Fig.2.1. Schematic representation of the synthesis of 1,2,3-triazolyl ligand systems for complexation with $[\text{}^{99\text{m}}\text{Tc}(\text{CO})_3(\text{H}_2\text{O})_3]^+$ precursor.	33
Fig.2.2. Synthesis scheme of triazole functionalized PEGylated and non-PEGylated cRGDfK peptide analogues	41
Fig.2.3. Metal carbonyl complexes of triazole functionalized cRGDfK peptide analogues	43
Fig.2.4. HPLC profile of (a) $\text{Re}(\text{CO})_3\text{-Pra-Tz-CH}_2\text{-cRGDfK}$ (b) $^{99\text{m}}\text{Tc}(\text{CO})_3\text{-Pra-Tz-CH}_2\text{-cRGDfK}$ (c) $\text{Re}(\text{CO})_3\text{-Pra-Tz-PEG}_7\text{-cRGDfK}$ and (d) $^{99\text{m}}\text{Tc}(\text{CO})_3\text{-Pra-Tz-PEG}_7\text{-cRGDfK}$	44
Fig.2.5. Comparison in the uptake of (a) $^{99\text{m}}\text{Tc}(\text{CO})_3\text{-Pra-Tz-CH}_2\text{-cRGDfK}$ and (b) $^{99\text{m}}\text{Tc}(\text{CO})_3\text{-Pra-Tz-PEG}_7\text{-cRGDfK}$ in different organs/tissue of C57BL/6 mice bearing melanoma tumor with/without receptor blockade at 180 min p.i.	48
Fig.3.1. ESI-MS of HYNIC-Boc (3a)	60

Fig.3.2. Synthesis scheme of HYNIC-c(NGR) and HYNIC-PEG ₂ -c(NGR)	62
Fig.3.3. ESI-MS of HYNIC-c(NGR) (3b)	63
Fig.3.4. ESI-MS of HYNIC-PEG ₂ -c(NGR) (3c)	64
Fig.3.5. Radiosynthesis of ^{99m} Tc-HYNIC-c(NGR) and ^{99m} Tc-HYNIC-PEG ₂ -c(NGR)	69
Fig.3.6. HPLC profile of (a) ^{99m} Tc-HYNIC-c(NGR) and (b) ^{99m} Tc-HYNIC-PEG ₂ -c(NGR)	70
Fig.3.7. Cell binding of ^{99m} Tc-HYNIC-c(NGR) and ^{99m} Tc-HYNIC-PEG ₂ -c(NGR) in HT-1080 cells and MCF7 cells	71
Fig.3.8. Radio-HPLC chromatogram of (a) ^{99m} Tc-HYNIC-c(NGR) and (b) ^{99m} Tc-HYNIC-PEG ₂ -c(NGR) in the urine sample of nude mice bearing HT-1080 tumor at 3 h p.i.	74
Fig.3.9. Tumor uptake of ^{99m} Tc-HYNIC-c(NGR) and ^{99m} Tc-HYNIC-PEG ₂ -c(NGR) in human fibrosarcoma (HT-1080) tumor with and without receptor blockade at 1 h p.i.	74
Fig.4.1. Schematic representation of reduction of nitroimidazole	81
Fig.4.2. Synthesis scheme of tetradentate ligand (NS ₃)	84
Fig.4.3. ¹ H-NMR spectra of tris(<i>S</i> -ethylethanethioate)amine (4b)	86
Fig.4.4. ESI-MS of tris(<i>S</i> -ethylethanethioate)amine (4b)	87
Fig.4.5. ESI-MS of 2,2',2''-nitriлотrisethanethiol (NS ₃) (4c)	88
Fig.4.6. ¹ H-NMR spectra of tert-Butyl-3-(2-nitro-1H-imidazol-1-yl)propylcarbamate (4d)	89
Fig.4.7. ¹ H-NMR spectra of N-(3-(2-nitro-1H-imidazol-1-yl)propyl)formamide (4f)	91
Fig.4.8. ¹ H-NMR spectra of 1-(3-isocyanopropyl)-2-nitro-1H-imidazole (2NimNC) (4g)	92
Fig.4.9. ¹³ C-NMR spectra of 1-(3-isocyanopropyl)-2-nitro-1H-imidazole (2NimNC) (4g)	93

Fig.4.10. ¹ H-NMR spectra of N-(2-(2-methyl-5-nitro-1H-imidazol-1-yl)ethyl)formamide (4h)	94
Fig.4.11. ¹ H-NMR spectra of 1-(2-isocyanoethyl)-2-methyl-5-nitro-1H-imidazole (MetNC) (4i)	95
Fig.4.12. ¹ H-NMR spectra of [Re(NS ₃)(2NimNC)] (4j)	97
Fig.4.13. ESI-HRMS of [Re(NS ₃)(2NimNC)] complex (4j)	97
Fig.4.14. ¹ H-NMR spectra of [Re(NS ₃)(MetNC)] (4k)	98
Fig.4.15. ESI-HRMS of [Re(NS ₃)(MetNC)] complex (4k)	98
Fig. 4.16. Synthesis of isocyanide derivative of 2-nitroimidazole (2NimNC, 4g) and metronidazole (MetNC, 4i)	103
Fig. 4.17. TLC of ^{99m} Tc-EDTA complex in (a) acetone and (b) water	105
Fig. 4.18. HPLC elution profile of (a) [^{99m} Tc(NS ₃)(2NimNC)] and (b) [Re(NS ₃)(2NimNC)], (c) [^{99m} Tc(NS ₃)(MetNC)] and (d) [Re(NS ₃)(MetNC)]	106
Fig. 4.19. HPLC elution profile of (a) [^{99m} Tc(NS ₃)(2-NimNC)] and (b) supernatant obtained after the precipitation of serum proteins	107
Fig. 4.20. Preparation of Re-‘4+1’ complexes of isocyanide derivatives of nitroimidazole	108
Fig. 4.21. IR absorption of N≡C bond in ligands (a) 2NimNC and (b) MetNC, their respective Re-‘4+1’ complexes (c) [Re(NS ₃)(2NimNC)] and (d) [Re(NS ₃)(MetNC)]	109
Fig. 4.22. Voltammogram of (a) 2NimNC and [Re(NS ₃)(2NimNC)] and (b) MetNC and [Re(NS ₃)(MetNC)]	112
Fig.5.1. Chemical structure of folic acid	121
Fig.5.2. ¹ H-NMR spectra of compound 5b	124
Fig.5.3. ESI-MS of compound 5c	125
Fig.5.4. ESI-MS of compound 5d	126
Fig. 5.5. Synthesis scheme of folic acid-cysteine conjugate (5d)	131
Fig. 5.6. Radiolabeling of folic acid-cysteine conjugate (5d)	132

Fig. 5.7. HPLC profile of (a) $[\text{}^{99\text{m}}\text{Tc}(\text{N})\text{PNP2}]^{2+}$ intermediate and (b) $[\text{}^{99\text{m}}\text{Tc}(\text{N})\text{PNP}]$ -folic acid complex 5e	133
Fig. 5.8. Comparison of inhibition of $[\text{}^3\text{H}]$ -folic acid uptake in KB-31 cells by a) Folic acid-cysteine conjugate 5d and b) Native folic acid	135

LIST OF TABLES

	Page No.
Table 1.1. List of gamma emitting radionuclides useful for SPECT imaging	07
Table 1.2. List of positron emitting radionuclides useful for PET imaging	07
Table 1.3. List of β -emitting radionuclides	09
Table 1.4. List of α -emitting radionuclides	09
Table 1.5. Some of the ^{99m}Tc -based diagnostic radiopharmaceuticals	11
Table 1.6. Oxidation states and Coordination geometries of Technetium	13
Table 2.1. Percentage binding and inhibition of $^{99m}\text{Tc}(\text{CO})_3\text{-Pra-Tz-CH}_2\text{-cRGDfK}$ (2e) and $^{99m}\text{Tc}(\text{CO})_3\text{-Pra-Tz-PEG}_7\text{-cRGDfK}$ (2f) in B16F10 murine melanoma cells	45
Table 2.2. Biodistribution pattern of $^{99m}\text{Tc}(\text{CO})_3\text{-Pra-Tz-CH}_2\text{-cRGDfK}$ (2e) and $^{99m}\text{Tc}(\text{CO})_3\text{-Pra-Tz-PEG}_7\text{-cRGDfK}$ (2f) in C57BL/6 mice bearing melanoma tumor	46
Table 3.1. List of few radiolabeled peptides and the corresponding target receptors	54
Table 3.2. Biodistribution pattern of $^{99m}\text{Tc-HYNIC-c(NGR)}$ and $^{99m}\text{Tc-HYNIC-PEG}_2\text{-c(NGR)}$ in athymic nude mice bearing human fibrosarcoma, HT-1080 tumor	72
Table 4.1. Distribution pattern of nitroimidazole- $^{99m}\text{Tc}(\text{NS}_3)$ complexes ($[\text{}^{99m}\text{Tc}(\text{NS}_3)(2\text{NimNC})]$ and $[\text{}^{99m}\text{Tc}(\text{NS}_3)(\text{MetNC})]$) in various organs at different time points	114
Table 4.2. Activity of nitroimidazole- $^{99m}\text{Tc}(\text{NS}_3)$ complexes ($[\text{}^{99m}\text{Tc}(\text{NS}_3)(2\text{NimNC})]$ and $[\text{}^{99m}\text{Tc}(\text{NS}_3)(\text{MetNC})]$) and $[\text{}^{18}\text{F}]\text{FMISO}$ observed in tumor and blood at different time points	115
Table 5.1. Biodistribution studies of $[\text{}^{99m}\text{TcN}(\text{PNP})]\text{-folic acid complex}$ (5e) in normal Swiss mice	136

CHAPTER 1

GENERAL INTRODUCTION

Introduction

Cancer is one of the leading causes of death worldwide [1]. The early diagnosis of malignant alterations is of utmost importance in the treatment of cancer. Since, the disease begins with microscopic changes in the cellular level, it is important to visualize these early changes in cellular metabolism. '*Molecular imaging*' enables the detection of disease at the level when cellular or molecular changes occur inside the human body with high sensitivity and specificity [2-4]. Molecular imaging differs from traditional imaging in that probes known as biomarkers or molecular vectors are used to image particular targets or pathways based on their localization and biological behavior within the body. While conventional imaging procedures such as X-rays, computed tomography (CT), MRI and ultrasound offer information of anatomical structure, molecular imaging enables to view the *in vivo* functioning of the chemical and biological processes [5,6] occurring at the cellular level. Unlike the conventional anatomical imaging techniques which have the limitation of not being able to detect diseases until structural changes are large enough to be detected, molecular imaging agents have the potential to identify disease at an early stage. Early detection in turn helps in disease management in a more effective manner. Among the various molecular imaging techniques, '*Nuclear medicine*' that employs '*Radiopharmaceuticals*' is the most popular and promising modality, owing to the simplicity, ease as well as economical aspects involved in its application [7,8].

Molecular imaging in nuclear medicine uses radiolabeled molecules in very low concentrations (tracers) for *in vivo* imaging and in larger amounts for therapeutic purpose [8]. In nuclear medicine imaging the gamma radiation emitted by the radionuclide is detected by special type of cameras that work with computers to provide very precise pictures of the area of the body being imaged. *Single photon emission tomography* (SPECT) and *positron emission tomography*

(PET) are the two imaging modalities used in nuclear medicine depending on the type of emission by the radionuclide [9-11].

1.1. Radiopharmaceuticals

Radiopharmaceuticals are preparations with high purity and definite composition containing a radionuclide that are used routinely in nuclear medicine for the diagnosis or therapy of various diseases [12]. Radiopharmaceuticals monitor the functional changes *in-vivo* and thus form an important part of nuclear medicine. The radiopharmaceutical has two components: a ‘radionuclide’ and an organic, inorganic, medicinal or a natural compound, ‘pharmaceutical’ in a definite composition. The organic molecule acts as a targeting vector for localization of radiopharmaceutical in a particular organ while the nature of the radionuclide decides whether the intended use is for diagnosis or for therapy [13,14]. Radiopharmaceuticals can be of two types viz. ‘metal essential radiopharmaceuticals’ where the chemical and physical property of the complex decides its biological distribution and ‘target specific radiopharmaceuticals’ where the ultimate distribution is driven by specific biochemical interactions like receptor binding, enzymatic reduction, antigen-antibody interaction etc [15].

1.1.1. Target specific radiopharmaceuticals

Target specific radiopharmaceuticals are being increasingly utilized in imaging and treatment of cancer because they provide a unique tool for target specific delivery of radionuclides to the diseased tissues. In target specific radiopharmaceutical, a carrier molecule which serves as vehicle is tethered to the radionuclide in order to direct the latter to the diseased tissue [13-15]. Accumulation of the radiotracer at the diseased site relies on the target-specificity and localization of the carrier molecule that binds to the receptor with high affinity and specificity. The high specificity of the carrier molecule results in selective uptake and

distribution of the radiotracer at the diseased site and thus has the ability to accurately target the tumor lesions/cancer while sparing the non-target major vital organs.

The target specific radiopharmaceutical can be prepared in two ways: (i) integrated approach, which involves replacement of a part of high affinity receptor ligand by metal chelate in such a way that there are minimal changes in size, conformation, and receptor binding affinity. This approach often results in a more synthetically challenging target molecule or the loss of receptor binding affinity. (ii) The bi-functional chelating agent (BFCA) approach, where the targeting molecule is radiolabeled using a pendant moiety known as bifunctional chelating agent (**Fig. 1.1**). A bi-functional chelating agent is a molecule which possesses a derivatizable residue on one end that can be linked to the carrier molecule and an array of coordinating donors on the other end for complexing with the radionuclide [13,16].

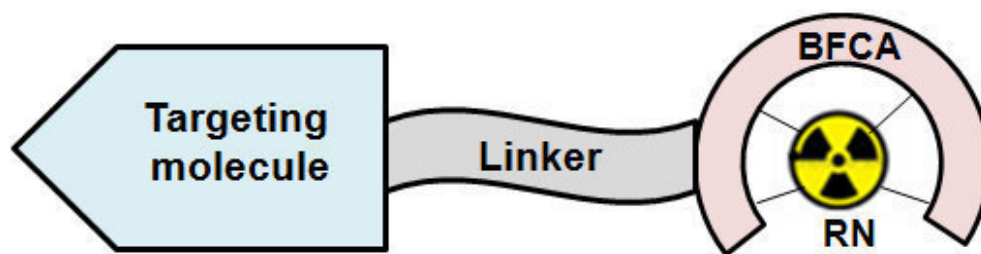


Fig. 1.1. Typical design of a radiopharmaceutical using BFCA approach

The choice of BFCA is determined by the nature and oxidation state of the radionuclide as each radionuclide has different coordination chemistry. The BFCA should form a stable complex with the radionuclide in relatively high yield. This is the most commonly used approach for designing a target specific radiopharmaceutical as the targeting affinity of the carrier

molecule can be retained by careful choice of BFCA for radiolabeling. This approach combines the ease of direct labeling with well-defined chemistry of the preformed chelate approach.

Depending upon the type of radionuclide used, the radiopharmaceuticals are divided into two primary classes: '*diagnostic radiopharmaceuticals*' and '*therapeutic radiopharmaceuticals*'.

1.1.2. Diagnostic Radiopharmaceuticals:

A diagnostic radiopharmaceutical is the molecule labeled with a gamma-emitting isotope for single photon emission computed tomography (SPECT) or a positron-emitting isotope for positron emission tomography (PET) [13,17]. The diagnostic radiopharmaceuticals are used at very low concentrations in the range 10^{-6} to 10^{-8} M and are intended to provide detailed description of morphologic structure of organs or tissues and physiological functions *in vivo*, through accumulation of the radiopharmaceutical. Diagnostic radiopharmaceuticals provide a non-invasive method of assessing the disease or diseased states by SPECT or PET and monitoring the efficacy of a specific therapeutic treatment.

Single photon emission computed tomography (SPECT) is a nuclear medicine tomographic imaging technique where radiopharmaceuticals containing gamma emitting radionuclides are used for the diagnostic purpose. These gamma cameras are fitted with NaI (TI) detectors which are sensitive to the photons in the range of 80-200 keV. The image obtained is a 2-D view of 3-D distribution of a radionuclide. To the 2-D image is then applied a tomographic reconstruction algorithm using a computer to yield a 3-D data set.

Positron emission tomography (PET) is another nuclear medicine imaging technique where the imaging agents are radiolabeled with radionuclides that decay by the emission of a positively charged particle called the positron (β^+). This is based on the coincident detection of two 511 keV gamma rays emitted simultaneously at 180° to each other following positron and

electron annihilation. The bismuth germanium oxide (BGO) scintillation detectors which are capable of efficiently detecting high energy gamma rays are arranged in a circular array with coincidence circuits designed to specifically detect the 511 keV photons emitted in opposite directions [18,19]. A few SPECT radioisotopes and PET radioisotopes are listed in **Table 1.1** and **Table 1.2** respectively.

Table 1.1. List of gamma emitting radionuclides useful for SPECT imaging [20,21]

Radionuclide	Half-life	E_{γ} in keV (% Abundance)
^{99m}Tc	6.02 h	140.5 (89.0)
^{123}I	13.27 h	159.0 (82.8)
^{67}Ga	3.26 d	93.3 (38.3)
^{111}In	2.80 d	245.4 (94.2)
^{201}Tl	72.91 h	167.4 (10.0)

Table 1.2. List of positron emitting radionuclides useful for PET imaging [20,21]

Radionuclide	Half-life	E_{max} in MeV (% Abundance)
^{18}F	110 min	0.63 (96.9)
^{11}C	20.4 min	0.96 (99.8)
^{13}N	10.0 min	1.20 (99.8)
^{15}O	2 min	1.73 (99.9)
^{68}Ga	68 min	1.90 (89.1)
^{64}Cu	12.7 h	0.65 (17.5)

PET offers higher resolution and sensitivity over that obtained by SPECT, however, the use of more readily available, longer lived radionuclides and the relatively lower costs of gamma cameras make SPECT imaging much more attractive and affordable for larger population. Additionally, improvement in SPECT technology has tremendously reduced the gap in the spatial resolution achievable with a SPECT and PET machine [19].

Among different radioisotopes used in diagnostic nuclear medicine, ^{99m}Tc with its ideal nuclear characteristics ($t_{1/2} = 6$ h, 140 keV), cost effectiveness, easy availability from $^{99}\text{Mo}/^{99m}\text{Tc}$ generator and ready formulation of radiopharmaceuticals through cold kits, occupies a premier position in nuclear medicine. ^{99m}Tc continues to be the ‘work-horse’ of diagnostic Nuclear Medicine and is routinely and most widely used medical isotope accounting for approximately 30 million diagnostic procedures annually comprising ~80% of all diagnostic Nuclear Medicine procedures worldwide [22-24].

1.1.3. Therapeutic radiopharmaceuticals

Therapeutic radiopharmaceuticals are radiolabeled molecules designed to deliver therapeutic doses of ionizing radiation to specific disease sites (most often cancerous tumors) with high specificity in the body [25]. Radionuclides that decay by particle emission viz. beta emission, alpha emission and Auger electron emission are used in therapeutic radiopharmaceuticals. Therapeutic radiopharmaceuticals should localize at the diseased site in sufficient concentration with high specificity in order to deliver a cytotoxic radiation dose to the cancerous cells while sparing the normal cells or producing tolerable radiation damage to normal cells. A list of few beta and alpha emitting radionuclides is presented in **Table 1.3** and **Table 1.4** respectively.

Table 1.3. List of β -emitting radionuclides [20,25]

Radionuclide	Half-life (days)	Max E_{β} (MeV)	Principal E_{γ} in keV (% Abundance)
^{177}Lu	6.7	0.50	112.95 (6.4) 208.36 (11.0)
^{153}Sm	1.9	0.8	103.18 (28.3)
^{131}I	8.0	0.81	364.48 (81.2)
^{186}Re	3.8	1.07	137.16 (8.6)
^{188}Re	0.7	2.11	155.04 (14.9)
^{89}Sr	50.5	1.46	Nil
^{32}P	14.3	1.71	Nil
^{90}Y	2.7	2.27	Nil

Table 1.4. List of α -emitting radionuclides [20,25]

Radionuclide	Half-life	Particulate Energy (MeV)	Principal E_{γ} in keV (% Abundance)
^{225}Ac	10.00 d	5.93	99.70 (3.5)
^{223}Ra	11.44 d	5.98	269.41 (13.6)
^{213}Bi	45.59 min	5.98	439.70 (27.3)
^{212}Bi	60.55 min	6.21	727.17 (11.8)

1.2. Technetium-99m in nuclear medicine:

Technetium was first isolated by Segre and Perrier in 1938 from a molybdenum target plate that had been bombarded with deuterons in the Berkeley cyclotron [26]. Two years later, Segre and Seaborg discovered the metastable isotope ^{99m}Tc . In 1959, Brookhaven National Laboratory developed $^{99}\text{Mo}/^{99m}\text{Tc}$ generator, which paved the way for ready availability of ^{99m}Tc and thus opened up the possibility of wide applications of ^{99m}Tc in diagnostic nuclear medicine [26]. Technetium-99m is used in about 30 million medical diagnostic procedures annually throughout the world, comprising 80% of all diagnostic studies in nuclear medicine [27].

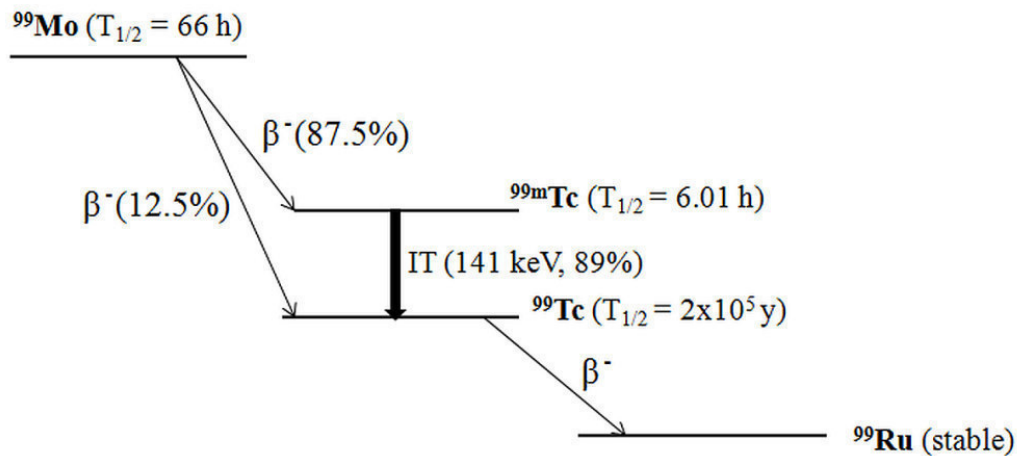


Fig. 1.2. Simplified ^{99}Mo decay scheme

^{99m}Tc is the most preferred isotope in designing radiopharmaceuticals due to its optimal nuclear characteristics and ease of availability through a commercial ^{99}Mo - ^{99m}Tc generator. The 6 h half-life is long enough for preparing the radiopharmaceutical, performing quality control procedures and injecting into the patient for collecting useful images. At the same time, it is short enough to permit administration of millicurie amounts of ^{99m}Tc without incurring significant radiation dose to patient. ^{99m}Tc decays by ‘isomeric transition’ emitting gamma photons of energy 141 KeV

with 89% abundance (**Fig. 1.2**), which is readily collimated to give images of high resolution. Furthermore, due to its versatile chemistry, ^{99m}Tc can be incorporated into a wide variety of suitably modified biologically active molecules [27-30]. Because of the above ideal characteristics ^{99m}Tc is the ‘work-horse’ of nuclear medicine. Some of the ^{99m}Tc -based radiopharmaceuticals used in nuclear medicine are given in **Table 1.5**.

Table 1.5. Some of the ^{99m}Tc -based diagnostic radiopharmaceuticals [28,31]

Radiopharmaceutical	Function
^{99m}Tc -ECD, ^{99m}Tc -TRODAT, ^{99m}Tc -HMPAO	Brain imaging
^{99m}Tc -MIBI, ^{99m}Tc -Tetrofosmin, ^{99m}Tc -Pyrophosphates	Cardiac imaging
^{99m}Tc -Phytate, ^{99m}Tc -Sulphur colloid	Liver imaging
^{99m}Tc -Mebrofenin	Hepatobiliary function
^{99m}Tc -HSA microspheres/macroaggregates,	Lung imaging
^{99m}Tc -MDP	Bone imaging
^{99m}Tc -GHA, ^{99m}Tc (III)-DMSA, ^{99m}Tc -DTPA, ^{99m}Tc -EC	Kidney imaging
^{99m}Tc -Leucocytes, ^{99m}Tc -HIgG, ^{99m}Tc -ciprofloxacin, ^{99m}Tc -UBI	Infection/Inflammation
^{99m}Tc (V)-DMSA, ^{99m}Tc -HYNIC-TOC, ^{99m}Tc -HYNIC-TATE	Tumor imaging

1.3. ^{99}Mo - ^{99m}Tc generator

The practical use of ^{99m}Tc for regular imaging is possible due to the ready availability of ^{99m}Tc from ^{99}Mo - ^{99m}Tc generator [32]. A radionuclide generator is a device in which a long-lived parent and short-lived daughter exist in radioactive equilibrium, from which the daughter activity could be separated conveniently at regular intervals. A major advantage of the generators is that they are easily transportable and serve as source of short-lived radionuclide in

hospitals/institutions far from the site of cyclotron or reactor facility [33]. Thus by having a supply of parent on hand at a facility, the daughter is continually generated on site.

The radionuclide, ^{99}Mo is produced either by fission of ^{235}U (n,f) or by neutron activation of ^{98}Mo (n, γ) in the nuclear reactor. Since the parent nuclide ^{99}Mo ($T_{1/2} = 66$ h) is longer lived than the daughter $^{99\text{m}}\text{Tc}$, there exists an equilibrium between these isotopes after a certain time, when the rate of growth of $^{99\text{m}}\text{Tc}$ becomes equal to the rate of its decay. The transient equilibrium between parent ^{99}Mo and daughter $^{99\text{m}}\text{Tc}$ helps accumulation of $^{99\text{m}}\text{Tc}$ to maximum concentration after every 23 hours. There are different types of ^{99}Mo - $^{99\text{m}}\text{Tc}$ generator systems available depending upon the method used for separating $^{99\text{m}}\text{Tc}$ from ^{99}Mo . Some of the methods are, (i) column chromatography over acidic alumina, (ii) solvent extraction of $^{99\text{m}}\text{Tc}$ with methylethyl ketone (MEK), (iii) sublimation of Tc oxides from Mo oxides and (iv) elution of $^{99\text{m}}\text{Tc}$ from gel-column generator with ^{99}Mo in the form of ZrMoO_4 . Among these, the generator based on alumina column is the most commonly used method. In this, ^{99}Mo in $\text{Mo}_6\text{O}_{24}^{4-}$ chemical form is adsorbed to an acidic alumina column and when the column is flushed with saline, $^{99\text{m}}\text{Tc}$ formed by the decay of ^{99}Mo is preferentially eluted. The final eluate contains $^{99\text{m}}\text{Tc}$ as $\text{Na}^{99\text{m}}\text{TcO}_4$ in saline [32,34].

1.4. Technetium Chemistry: different approaches of radiolabeling

Technetium belongs to the group VII B of the periodic table with a neutral electronic configuration of $[\text{Kr}]4\text{d}^65\text{s}^1$. Being a transition metal the coordination chemistry of $^{99\text{m}}\text{Tc}$ is very complex. A large number of oxidation states (+7 to -1) and a wide variety of coordination geometries (square pyramidal, trigonal bipyramidal and octahedral) are possible for Tc-complexes with various ligands [10,16,30,35-37]. **Table 1.6** summarizes various oxidation states

and coordination geometries of technetium. The oxidation state and stability of Tc-complex depends on the type of ligand used and the chemical environment.

Table 1.6. Oxidation states and Coordination geometries of Technetium

Oxidation state	Example	Coordination Geometry	Coordination Number
+7 (d ⁰)	TcO ₄ ⁻	Tetrahedron	4
	[TcH ₉] ²⁻	Trigonal prism	9
+6 (d ¹)	TcO ₄ ²⁻	Tetrahedron	4
+5 (d ²)	Tc-oxo complexes	Square pyramidal	5
	Tc-dioxo complexes	Octahedron	6
+4 (d ³)	TcO ₂ .H ₂ O	Octahedron	6
	[TcCl ₆] ²⁻	Octahedron	6
+3 (d ⁴)	Tc- '4+1' mixed ligand complexes	Trigonal bipyramidal	5
	[Tc(Diars) ₂ Cl ₂] ⁺	Octahedron	6
+2 (d ⁵)	[TcCl ₂ (PhP(OEt) ₂) ₄]	Octahedron	6
+1 (d ⁶)	Tc(CO) ₃ complexes	Octahedron	6
	Tc-sestamibi	Octahedron	6
0 (d ⁷)	[Tc ₂ (CO) ₁₀]	Octahedron	6
-1 (d ⁸)	[Tc(CO) ₅] ⁻	Trigonal bipyramidal	5

The most stable oxidation states of technetium in water are +7 as ^{99m}TcO₄⁻ and +4 as the insoluble hydrolyzed reduction product, TcO₂.H₂O. The other oxidation states (+5, +3, +2, +1)

are stabilized on complexation with the suitable ligand [27]. The diverse redox chemistry of technetium led to different strategies for labeling biomolecules with ^{99m}Tc , in terms of metal cores, oxidation states and selection of BFCAs [38-45]. Some of them are ^{99m}Tc -oxo core ($[\text{}^{99m}\text{TcO}]^{3+}$ or $[\text{}^{99m}\text{TcO}_2]^+$), ^{99m}Tc -nitrido core $[\text{}^{99m}\text{TcN}]^{2+}$, ^{99m}Tc -tricarbonyl core $[\text{}^{99m}\text{Tc}(\text{CO})_3]^+$, ^{99m}Tc -HYNIC core (HYNIC: 6-hydrazino nicotinic acid) and ^{99m}Tc -‘4+1’ mixed ligand approach.

1.4.1. Radiolabeling with ^{99m}Tc -oxo/dioxo core ($[\text{}^{99m}\text{TcO}]^{3+}$ or $[\text{}^{99m}\text{TcO}_2]^+$):

The $[\text{}^{99m}\text{TcO}]^{3+}$ and $[\text{}^{99m}\text{TcO}_2]^+$ cores are the first ones to be used and are by far the most commonly used ^{99m}Tc -core for the preparation of radiopharmaceuticals in clinical nuclear medicine. A plethora of ^{99m}Tc -radiopharmaceuticals for cerebral imaging, renal and myocardial perfusion imaging have been prepared using ^{99m}Tc -oxo core where technetium exists in +5 oxidation state [27,46-49]. Some of the ^{99m}Tc -radiopharmaceuticals containing ^{99m}Tc -oxo or dioxo core is shown in **Fig. 1.3**. The $[\text{}^{99m}\text{TcO}]^{3+}$ core forms square pyramidal complexes with tetradentate N, mixed NS or NO type ligands [50-55] whereas, $[\text{}^{99m}\text{TcO}_2]^+$ core forms octahedral complexes with polydentate ligands with either amine N/thioether S donors phosphine P donor atoms [56,57]. ^{99m}Tc -oxo/dioxo core can be readily formed by in-situ reduction of $^{99m}\text{TcO}_4^-$ with suitable reducing agent like stannous chloride, however requirement of a large excess of ligand for stabilizing the resultant complex leads to formation of low specific activity complexes, using this approach. In the absence of sufficient amount of stabilizing ligand, reduction of $^{99m}\text{TcO}_4^-$ leads to the formation of colloidal $^{99m}\text{Tc}(\text{IV})\text{O}_2$ [58]. Thus, this approach of labeling is not suitable for target specific biomolecules such as peptides, antibody, steroids etc. as the antigen or receptors present on the target site have low concentrations. Use of large excess of ligand is a drawback in preparation of target specific radiopharmaceuticals as there will be a competition

between the radiolabeled ligand and the unlabeled ligand for the limited number of receptors on the cancerous cells. Thus, novel and improved methods of radiolabeling were introduced which make use of cores such as $[^{99m}\text{TcN}]^{2+}$, $[^{99m}\text{Tc}(\text{CO})_3]^+$, bifunctional chelating agents (BFCA) like HYNIC and ^{99m}Tc -‘4+1’ mixed ligand approach. Since the labeling using these preformed cores requires less ligand concentration, it opened up the possibility of preparing high-specific activity ^{99m}Tc -complexes using low ligand concentration.

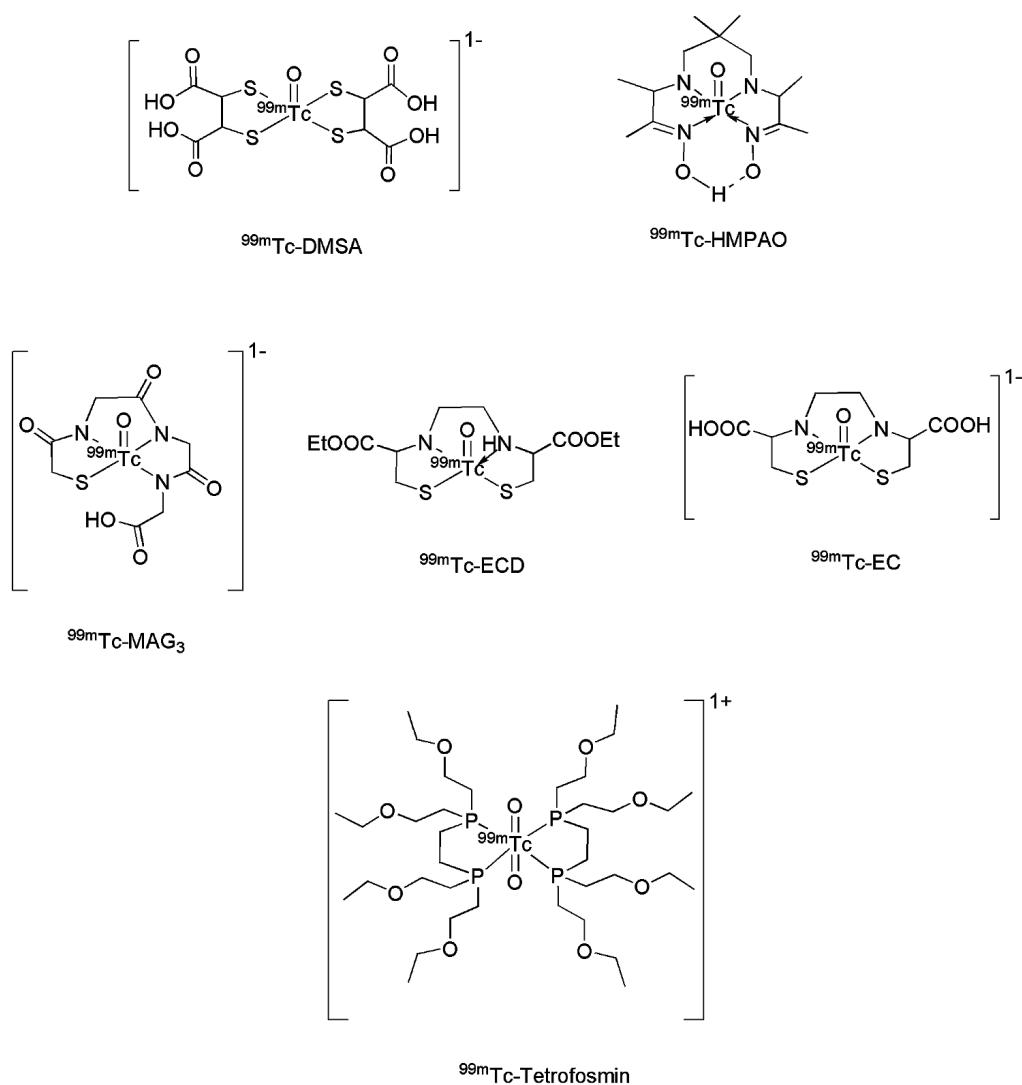


Fig. 1.3. Some ^{99m}Tc -radiopharmaceuticals having ^{99m}Tc -oxo or dioxo core

1.4.2. Radiolabeling with $^{99m}\text{Tc}(\text{CO})_3]^+$ core

The organometallic core “*fac*- $^{99m}\text{Tc}(\text{CO})_3(\text{H}_2\text{O})]^+$ ” developed by Alberto and coworkers [59], with its stability, significantly smaller size and easy synthesis offers varying possibilities for labeling of several target-specific molecules. This core can be prepared by two methods, either by using commercially available potassium boranocarbonate (Isolink[®]) kits [60] or by conventional method of purging carbon monoxide (CO) gas at 1 atmosphere pressure into $^{99m}\text{TcO}_4^-$ in the presence of sodium borohydride (NaBH_4) as reducing agent [59]. In $^{99m}\text{Tc}(\text{CO})_3(\text{H}_2\text{O})]^+$ precursor complex, ^{99m}Tc exists in +1 oxidation state. The low oxidation state is stabilized by π -back bonding from filled d-orbital of the metal to empty anti-bonding orbital of CO ligand which is a strong sigma doner and π -acceptor moiety. The Tc(I) state possesses d^6 electronic configuration in the precursor complex $^{99m}\text{Tc}(\text{CO})_3(\text{H}_2\text{O})]^+$ which imparts the property to be chemically inert. The $^{99m}\text{Tc}(\text{CO})_3(\text{H}_2\text{O})]^+$ precursor complex has an octahedral geometry with the three CO ligands occupying the facial position (**Fig. 1.4**). The other three positions are occupied by substitution labile water molecules which can be replaced by variety of ligands having appropriate donor atoms such as N, O, P, S etc. to form the $^{99m}\text{Tc}(\text{CO})_3$ -complexes [61-73].

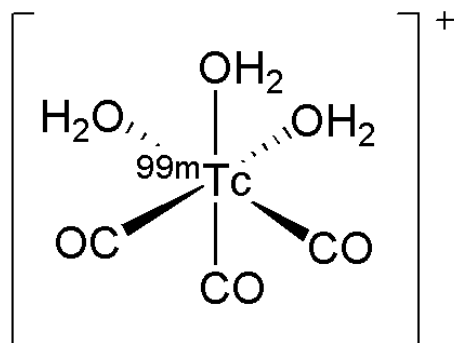


Fig. 1.4. Typical structure of $^{99m}\text{Tc}(\text{CO})_3(\text{H}_2\text{O})]^+$ precursor complex

The ligands can be three monodentate ligands, a set of one monodentate and one bidentate ligand or a tridentate ligand, thus opening up different possibilities leading to the formation of a variety of complexes [61-73]. However, monodentate and bidentate ligands often form $^{99m}\text{Tc}(\text{CO})_3$ -complexes with low solution stability, which results in high protein binding and high background activity in the blood stream. In contrast, a tridentate ligand forms more stable $^{99m}\text{Tc}(\text{CO})_3$ -complex due to chelate effect [74]. **Fig 1.5** shows a few tridentate chelators used for labeling biomolecules with $[\text{}^{99m}\text{Tc}(\text{CO})_3]^+$ core. Thus, for radiolabeling using ^{99m}Tc -tricarbonyl core approach, the biomolecule is synthetically modified to incorporate the tridentate chelator, which is subsequently reacted with $[\text{}^{99m}\text{Tc}(\text{CO})_3(\text{H}_2\text{O})_3]^+$ precursor complex. Radiolabeling using this core can be achieved at low ligand concentration and the complexes obtained exhibit high thermodynamic stability and are kinetically inert, thus making it suitable for radiolabeling of target-specific biomolecules [70,75-77].

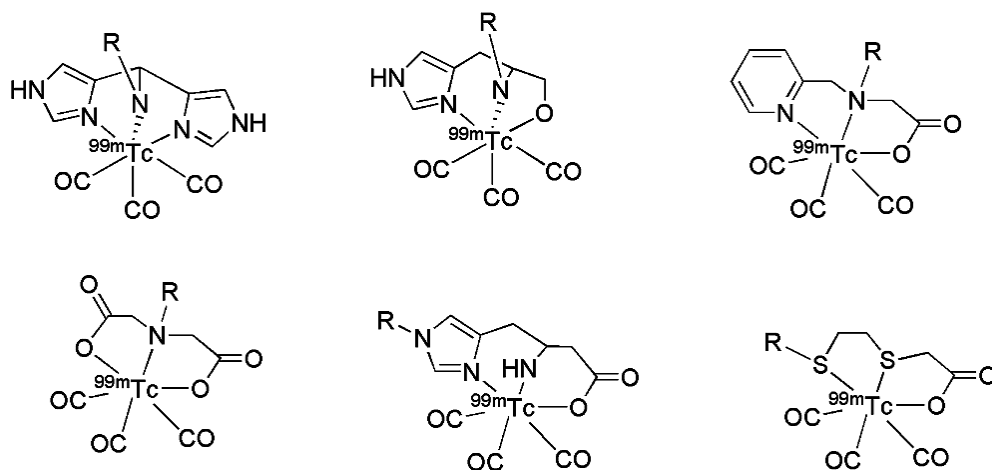


Fig.1.5. Examples of few tridentate chelators for labeling with $[\text{}^{99m}\text{Tc}(\text{CO})_3]^+$ core. The R group may be a biomolecule or linker attached to biomolecule

1.4.3. Radiolabeling with ^{99m}Tc -HYNIC core:

Hydrazinonicotinic acid [HYNIC] is a BFCA, preferentially used for radiolabeling of peptides, antibodies and antibody fragments with ^{99m}Tc [78-86]. The HYNIC moiety is conjugated to the biomolecule at one end and it coordinates to ^{99m}Tc through hydrazine nitrogen at the other end. In ^{99m}Tc -HYNIC core, ^{99m}Tc exist in +5 oxidation state. Since HYNIC acts as a monodentate ligand, coligands are required to complete the octahedral coordination sphere of technetium (Fig. 1.6) [78,87].

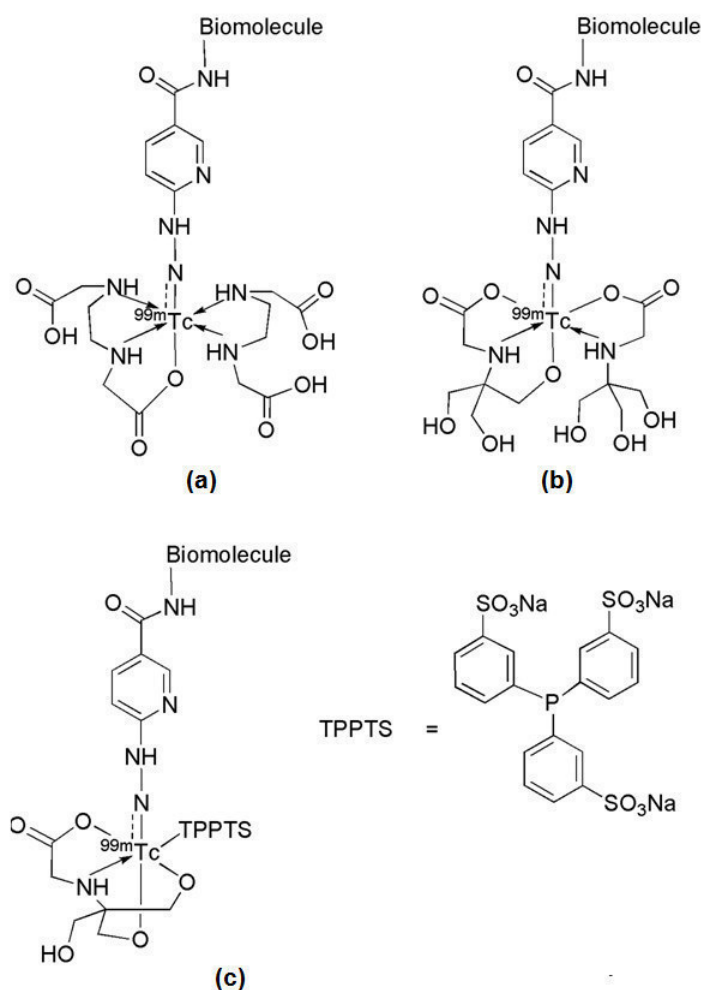


Fig. 1.6. Typical structure ^{99m}Tc -HYNIC-biomolecule complex using (a) tricine as co-ligand (b) EDDA/tricine as co-ligand and (c) TPPTS/tricine co-ligand

Most commonly used coligands are tricine and ethylenediaminediacetic acid (EDDA) [86]. The advantage of using HYNIC as BFCA is its high radiolabeling efficiency which allows for preparation of radio-complexes with high specific activity. The appropriate choice of co-ligands allows easy modification of *in vivo* pharmacokinetic profile of the ^{99m}Tc -labeled biomolecules, since the hydrophilicity/lipophilicity of the resultant complex can be tailored [13-16,88,89]. The use of tricine as the only coligand often results in complexes with significant solution instability and leads to formation of multiple species. To overcome this problem, Liu and coworkers have reported the use of water soluble phosphine ligands like trisodium triphenylphosphine-3,3',3''-trisulfonate (TPPTS) along with tricine to prepare ^{99m}Tc -HYNIC complexes [90,91]. These ternary ligand technetium complexes, [$^{99m}\text{Tc}(\text{HYNIC-bimolecule})(\text{tricine})(\text{phosphine})$] are formed with high specific activity and have very high solution stability.

1.4.4. '4+1' mixed ligand approach

The '4+1' mixed ligand complexes are formed by a combination of tetradentate tripodal chelator 2,2',2''-nitrilotriethanethiol (NS_3) and a monodentate ligand which is usually a soft donor such as an isocyanide or a phosphine [92,93]. In '4+1' mixed ligand complexes, ^{99m}Tc exists in +3 oxidation state. The tripodal tetradentate ligand NS_3 stabilizes $\text{Tc}(\text{III})$ in less common trigonal bipyramidal geometry with one of the position being occupied by monodentate (isocyanide/phosphine) ligand (**Fig. 1.7**). The NS_3 coordination of $\text{Tc}(\text{III})$ generates an electron-rich metal fragment which in turn is engaged in strong back-bonding to the coordinated isocyanides/phosphines. The biomolecule can either be linked to a functionalized tetra-dentate ligand (e.g., $\text{NS}_3\text{-COOH}$) or can be an intergral part of the mono-dentate ligand for getting attached to the $^{99m}\text{Tc}(\text{III})$ centre [94-99]. However, the later approach is mostly used as it

contributes little to the overall molecular framework of the complex with minimum distortion to the biomolecule attached to the monodentate isocyanide ligand [98].

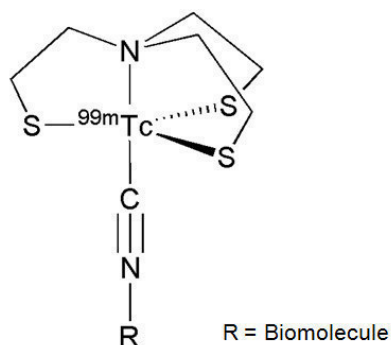


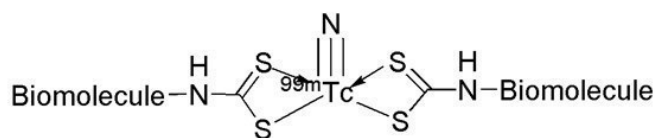
Fig. 1.7. Typical structure ^{99m}Tc -‘4+1’ mixed ligand complex with tetradentate NS_3 ligand and monodentate isocyanide ligand conjugated to the biomolecule

A significant advantage of the $^{99m}\text{Tc(III)}$ approach is that the ^{99m}Tc building block is small. The ‘4+1’ mixed ligand complexes are neutral and can be prepared in excellent yield under mild reaction conditions. Additionally, they exhibit high kinetic stability towards ligand exchange in vivo. The ‘4+1’ mixed ligand chemistry can be adapted with minor changes for preparation of analogous ^{188}Re complexes which can be used for therapeutic purpose [99].

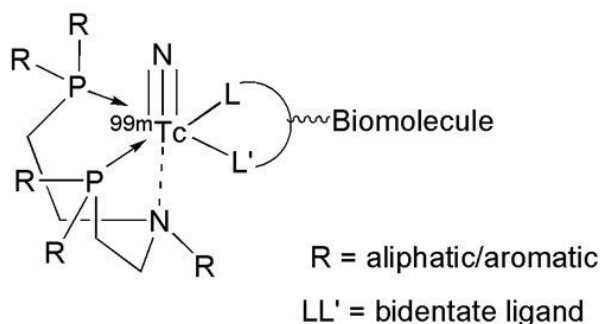
1.4.5. Radiolabeling with $[^{99m}\text{TcN}]^{2+}$ and $[^{99m}\text{TcN(PNP)}]^{2+}$ core:

The $[^{99m}\text{TcN}]^{2+}$ core was introduced by Baldas and Bonnyman in 1981 [100,101]. This core is isoelectronic with the conventional $[^{99m}\text{TcO}]^{3+}$ core, with ^{99m}Tc existing in the +5 oxidation state. The nitride N^{3-} ion is a strong π -electron donor and shows a high capacity to stabilize transition metals in higher oxidation states [13,101,102]. The $[^{99m}\text{TcN}]^{2+}$ core is stable under redox conditions and varying conditions of pH compared to the conventional $[^{99m}\text{TcO}]^{3+}$ core [103]. This feature imparts structural robustness to the nitrido core and thus facilitates

complexation with small amounts of ligand, leading to high specific activity complexes, which is a prerequisite for the target-specific radiotracers. Unlike ^{99m}Tc -oxo core which forms stable complexes with tetradentate ligands, the ^{99m}Tc -nitrido core favours complexation with two bidentate donor ligands due to steric constraint by the nitrido group. The ^{99m}Tc -nitrido core forms stable complexes with ligands containing soft donor atoms like sulphur [101]. Dithiocarbamates and xanthates containing two S donor atoms act as bidentate ligands and form stable symmetric [2+2] complexes with $[\text{}^{99m}\text{TcN}]^{2+}$ core [104-106]. The symmetric [2+2] complex has distorted square pyramidal geometry with nitride group at the apical position and the four S-donor atoms of dithiocarbamate/xanthate occupying the basal plane (**Fig. 1.8(a)**).



(a)



(b)

Fig. 1.8. (a) Typical structure of symmetric [2+2] complex with $[\text{}^{99m}\text{TcN}]^{2+}$ core and (b) structure of asymmetric [2+2] $[\text{}^{99m}\text{TcN}(\text{PNP})]$ -biomolecule complex

The symmetric [2+2] ^{99m}Tc -nitrido approach of radiolabeling bioactive molecules leads to formation of a complex carrying two molecules of biologically active species, each acting as a bidentate donor ligand. In order to design a complex with a single unit of biological substrate, another approach i.e asymmetric [2+2] was developed [107-112] using long chain bidentate phosphorous co-ligand (PNP) (**Fig. 1.8(b)**). Here the two bidentate ligands are different; with the two cis positions of the basal plane of the square pyramidal geometry occupied by PNP ligand and the other two cis positions left for coordinating to bidentate π -donor ligands having NS/ OS/ SS donor atoms [111,112]. Thus, the biomolecule is generally derivatized to incorporate bidentate π -donor ligands containing NS/ OS/ SS donor atoms group for linking it to $[\text{}^{99m}\text{TcN}(\text{PNP})]^{2+}$ core. Dithiocarbamate, dithiols and cysteine are the most commonly used bifunctional chelator for this metal fragment. This approach is particularly useful for ^{99m}Tc labeling of bulky biomolecules where a symmetric [2+2] complex formation would probably result in loss of biological activity due to the steric hindrance of the resultant ^{99m}TcN -complex. The pharmacokinetics of the final complex can be tuned by altering the lipophilicity of the complex through appropriate selection of pendant groups in PNP ligand [113].

1.5. Biomolecules used in the present study

To design a new target-specific radiopharmaceutical, the choice of biomolecule is made so as ensure the delivery of the radionuclide to the specific diseased tissue. Many biomolecules like monoclonal antibodies, peptides, peptidomimetics, small receptor-specific organic molecules etc are used as targeting vectors in designing radiopharmaceuticals. While preparing a radiopharmaceutical, it is important to consider the structure-activity relationship of the biomolecule. The structure-activity relationship gives an insight of the portion of the biomolecule which can be synthetically derivetized in order to attach the radionuclide without

significantly affecting the target-specificity of the biomolecule. The biomolecules used in the present work are RGD (Arginine-Glycine-Aspartic acid) peptide having high affinity towards integrin $\alpha_v\beta_3$ receptors over-expressed in numerous cancers, NGR (Asparagine-Glycine-Arginine) peptide having high affinity towards CD13 receptors over-expressed in different types of cancers, folic acid having high affinity for folate receptors over-expressed in many human tumor cells and nitroimidazole ligands for selective accumulation in hypoxic tumors. These biomolecules were synthetically derivetized to incorporate ^{99m}Tc using novel technetium chemistry, which make use of preformed cores such as $[\text{}^{99m}\text{TcN}]^{2+}$, $[\text{}^{99m}\text{Tc}(\text{CO})_3]^+$, ^{99m}Tc -HYNIC and ^{99m}Tc -‘4+1’ mixed ligand approach. Each of the cores has been used in labeling of different biomolecule to examine the efficacy of radiolabeling methodology. The work involves synthetic derivetization of the biomolecule, preparation of different cores, radiolabeling and bioevaluation in suitable animal model. A detailed description of the biomolecules used, RGD peptide, NGR peptide, folic acid and nitroimidazoles is given in the respective chapters.

1.6. Quality control of radiotracers

Quality control of the radiopharmaceuticals is mandatory before it can be administered as an *in vivo* injectable preparation. Quality control procedures involve several specific tests and measurements that ensure the purity, potency, product identity, biologic safety and efficacy of the radiopharmaceuticals [114]. These procedures include tests for radiochemical purity, radionuclidic purity, and chemical purity as well as general tests relevant for pharmaceutical safety. The quality control tests are categorized into physicochemical tests and biological tests.

1.6.1. Physicochemical tests

Various physicochemical tests are performed to check different physical parameters such as pH, physical appearance etc. and chemical parameters such as radiochemical purity,

radionuclidic purity, chemical purity, specific activity and radioactive concentration during the quality control of a radiopharmaceutical. The pH of the radiopharmaceutical is determined by the pH paper. Generally, the pH of the radiopharmaceutical preparation should be between 7 and 8 from point of view of suitability for *in vivo* administration. The radiopharmaceutical preparation is visually inspected to check for turbidity or suspended particles and certified w.r.t visual clarity.

1.6.1.1. Chemical purity

Chemical purity of a radiopharmaceutical refers to the proportion of the preparation that is in the specified chemical form regardless of the presence of radioactivity. Chemical impurities may come in a radiopharmaceutical preparation as some undesired species present in the ligand or radioactivity used for labeling or due to decomposition of materials before and after labeling. The presence of chemical impurity may affect radiolabeling thus resulting in undesired labeled molecules or directly produce adverse biological effects. In the present thesis purification of ligands was carried out using column chromatography, semi-preparative and preparative TLC.

1.6.1.2. Radionuclidic purity

Radionuclidic purity of the radiopharmaceutical refers to the percentage of total radioactivity due to the specific radionuclide. Radionuclidic impurities can originate from extraneous nuclear reactions as a result of isotopic impurities present in the target material or due to the fission process occurring in a reactor. The radionuclidic purity is an important factor as the presence of these extraneous radionuclides as impurities increases the radiation dose to the patient as well as impacts the image quality. Thus, accurate determination of the level of radionuclidic impurity is very important and it is mostly assessed by γ -ray spectrometry using an HPGe detector.

1.6.1.3. Radiochemical purity

Radiochemical purity (RCP) of a radiopharmaceutical is defined as the percent of the total radioactivity present in the desired chemical form. Radiochemical impurities in a radiopharmaceutical preparation can come from the chemical impurities present in the target ligand or from its decomposition on storage due to the action of solvent, change of temperature and pH, presence of oxidizing or reducing agents and radiolysis. In ^{99m}Tc -Radiopharmaceuticals, the radiochemical impurities are mostly, free pertechnetate ($^{99m}\text{TcO}_4^-$), hydrolyzed-reduced technetium ($^{99m}\text{TcO}_2 \cdot \text{H}_2\text{O}$) and ^{99m}Tc -labeled to transfer ligands (e.g., ^{99m}Tc gluconate in tetrofosmin). Radiochemical purity is an important factor to be considered in radiopharmaceutical preparation since it is the radiochemical form which determines the *in vivo* biodistribution of the agent. Radiochemical impurities will have different patterns of biodistribution which may obscure the diagnostic image and increase undue radiation exposure to the patient. Radiochemical purity is assessed by a variety of analytical techniques such as liquid chromatography, paper chromatography, thin-layer chromatography and electrophoresis. In the present thesis, some of these techniques viz. paper and thin layer chromatography, HPLC coupled with a well type NaI(Tl) detector were used to detect and determine the extent of radiochemical impurities present in various radiochemical preparations.

Determination of radiochemical purity of the radio-complexes by HPLC

High performance liquid chromatography (HPLC) measurements were performed on a JASCO PU 2080 Plus dual pump HPLC system, Japan, with a JASCO 2075 Plus tunable absorption detector and a Gina Star radiometric detector system, using a C18 reversed phase HiQ Sil column (5 μm , 4 x 250 mm). The eluting solvents used in HPLC were water with 0.1% trifluoroacetic acid (solvent A) and acetonitrile with 0.1% trifluoroacetic acid (solvent B). The

flow rate was kept at 1mL/min. Radiochemical purity (RCP) of ^{99m}Tc -complexes was determined by peak area measurement from the elution profile.

1.6.2. Biological tests

Biological quality control tests of radiopharmaceuticals are essentially identical with that of non-radioactive pharmaceutical preparation and these include determination of sterility, toxicity and apyrogenicity of the radiolabeled preparations [114].

To check the stability and efficacy of the radiolabeled agent, preliminary bioevaluation studies are carried out. These involve *in vitro* evaluation of the radiolabeled agents in serum and in cancer cell lines and *in vivo* evaluation of the agents in normal animals and/or animals bearing specific tumors.

1.7. Thesis-outline

The work in this thesis describes preparation of ^{99m}Tc -labeled target-specific radiotracers for specific targeting of different tumors using novel technetium cores such as $[\text{}^{99m}\text{TcN}]^{2+}$, $[\text{}^{99m}\text{Tc}(\text{CO})_3]^+$, ^{99m}Tc -HYNIC and ^{99m}Tc -‘4 + 1’ mixed ligand approach. In this respect, the biomolecules like peptide ligands (RGD and NGR), folic acid and nitroimidazole ligands were derivatized to radiolabel with ^{99m}Tc . Each of these cores has been utilized to radiolabel different biomolecule. The work carried out is divided into four chapters (Chapter 2, 3, 4 and 5).

In Chapter 2, two neutral $^{99m}\text{Tc}(\text{CO})_3$ complexes of cRGDfK peptide derivatives with different spacers were prepared via Click chemistry route. In one of the derivative methylene unit ($-\text{CH}_2-$) was used as the spacer whereas in the other derivative PEG₇ was incorporated as linker with an aim of increasing the biological half-life of the peptide. Click chemistry was used to introduce a tridentate chelator for radiolabeling with $[\text{}^{99m}\text{Tc}(\text{CO})_3]^+$ core. Both the radiotracers showed specificity towards the $\alpha_v\beta_3$ receptors. The PEGylated cRGDfK peptide analogue

exhibited higher tumor uptake than the non-PEGylated analogue but its high uptake in other non-target organs resulted in lower target/non-target ratios.

In Chapter 3, ^{99m}Tc -HYNIC approach is utilized for labeling NGR peptides targeting CD13 receptors over-expressed in various tumor cells. In this regard, two NGR peptide ligands, HYNIC-c(NGR) and HYNIC-PEG₂-c(NGR) were synthesized by Fmoc solid phase peptide synthesis method, radiolabeled with ^{99m}Tc and evaluated in CD13-positive human fibrosarcoma HT-1080 tumor xenografts. The results were compared with earlier reported ^{99m}Tc -NGR peptide prepared using direct labeling method/ conventional method of labeling.

Chapter 4 describes the use of '4+1' mixed ligand strategy to design ^{99m}Tc -radiotracers for the detection of *in vivo* tissue hypoxia. In the present work, isocyanide derivatives of 2-nitroimidazole (2-NimNC) and metronidazole (MetNC) were synthesized and subsequently radiolabeled with ^{99m}Tc using the tripodal tetradentate NS₃ co-ligand to prepare the corresponding ^{99m}Tc -'4+1' mixed ligand complexes. The structural characterization of the complexes and their preliminary evaluation in tumor bearing mice are thoroughly discussed.

In Chapter 5, [$^{99m}\text{TcN}(\text{PNP})$]²⁺ precursor which is known to form lipophilic complexes was chosen for radiolabeling folic acid with ^{99m}Tc with an aim of reducing the high renal uptake, associated with ^{99m}Tc -folate radioconjugates. The biodistribution was carried out in normal mice to study the clearance pattern and the results were compared with the previously reported radiofolates.

CHAPTER 2

PREPARATION OF [$^{99m}\text{Tc}(\text{CO})_3$] $^+$ -LABELED CYCLIC RGD PEPTIDE DERIVATIVES

FOR

TARGETING TUMOR ANGIOGENESIS

2.1. Introduction

The organometallic synthon, *fac*-[^{99m}Tc(CO)₃(H₂O)₃]⁺ introduced by Alberto et al. has attracted considerable interest in the designing of ^{99m}Tc-labeled target specific radiotracers [59]. In [^{99m}Tc(CO)₃(H₂O)₃]⁺ core, ^{99m}Tc exists in +1 oxidation state. The +1 oxidation state of ^{99m}Tc in [^{99m}Tc(CO)₃(H₂O)₃]⁺ core is stabilized by the π-back bonding from the filled d-orbital of metal to the anti-bonding orbital of CO moiety. Technetium has a low-spin d⁶ electronic configuration which gives to this compound, ([^{99m}Tc(CO)₃(H₂O)₃]⁺ core) the property to be chemically inert. The [^{99m}Tc(CO)₃(H₂O)₃]⁺ synthon has an octahedral configuration where three CO ligands and three aqua (H₂O) ligands are coordinated to the metal atom. The metal carbonyl Tc-CO bond is quite strong due to the synergistic effect where CO simultaneously acts as a sigma doner and a π-acceptor. However the three coordinated H₂O molecules are substitution labile and can be easily replaced by variety of functional groups (e.g., amines, thiols, carboxylates etc) either in the form of mono-, bi- or tridentate ligand [61-73]. A tridentate ligand system is most commonly studied as it provides more stability due to chelate effect [74]. The “tricarbonyl core” approach exploits the stability of [^{99m}Tc(CO)₃(H₂O)₃]⁺ core while manipulating the relatively labile water ligands to attach targeting vectors [72].

The preparation of tridentate chelating systems for the complexation with [^{99m}Tc(CO)₃(H₂O)₃]⁺ core generally requires multi-step synthesis and their incorporation into biomolecules often lacks efficiency and selectivity due to cross-reactivity with other functional groups present [115]. In this regard, the chemical orthogonality of Cu(I)-catalyzed azide–alkyne cycloaddition (CuAAC) reaction and ease of incorporation of azide and alkyne in variety of substrates (peptides, antibodies, small molecules) has popularized click reaction as an effective strategy for introduction of a metal chelator in a biological vector [115,116].

2.1.1. Click-chemistry: Cu(I)-catalyzed azide–alkyne cycloaddition (CuAAC) reaction

The term ‘Click chemistry’ was first introduced by Barry Sharpless and refers to the reactions which satisfy a set of conditions [117]. The reactions are characterized by (a) simple reaction conditions, using no solvent or solvent that is benign or easily removed and simple product isolation, (b) high to excellent reaction yields, (c) generation of inoffensive byproducts that can be easily removed by non-chromatographic methods, (d) stereospecific products [117,118]. Examples of click reaction are nucleophilic ring opening reactions, cycloaddition reactions, Diels-Alder reaction etc.

The CuAAC reaction has become the icon of click chemistry since its introduction by the Sharpless and Meldal laboratories [119,120]. This reaction satisfies all the conditions of click chemistry concept like mild reaction conditions, selectivity and the comparatively straight forward preparation of alkyne and azide building blocks etc. and is popularly known as Cu-catalyzed click chemistry or simply click chemistry. Unlike the uncatalyzed cycloaddition of azides and alkynes which results in a mixture of 1,4- and 1,5-triazole regioisomers at higher temperature, CuAAC provides selectively and efficiently 1,4-disubstituted 1,2,3-triazoles under mild reaction conditions [119,120]. The unique orthogonal reactivity of alkynes and azides, and the mild reaction conditions of cycloaddition are well suited for the modification of a wide variety of biomolecules. Due to these attractive features, click chemistry has found tremendous applications across different scientific disciplines, including development of radiotracers [115]. This method finds significant application in the synthesis of biomolecule-chelator conjugates in high yield and purity that are needed for preparation of radiopharmaceuticals as molecular imaging probes or therapeutic agents for different diseased sites. Mindt and Schibli et al. reported the first example of an application of the CuAAC to metallic radionuclides [121]. In

their approach, the click reaction is employed to the synthesis of tridentate ligand systems for the stable complexation of $[\text{}^{99\text{m}}\text{Tc}(\text{CO})_3(\text{H}_2\text{O})_3]^+$ while conjugating them simultaneously to biomolecules. The 1,2,3,-triazoles formed by 1,3-cycloaddition reaction of azides and alkynes act as excellent ligands particularly for organometallic cores of Mo, Tc and Re [115,121]. Thus, the reaction of azide-functionalized compounds with alkyne prochelators (for e.g., propargyl glycine) provides 1,4-disubstituted 1,2,3-triazole-containing tridentate ligand systems for complexation with $[\text{}^{99\text{m}}\text{Tc}(\text{CO})_3(\text{H}_2\text{O})_3]^+$ precursor (**Fig. 2.1**). This approach has been successfully applied for radiolabeling of carbohydrates, peptides and steroids with $^{99\text{m}}\text{Tc}(\text{CO})_3$ core [122,123]. This chapter demonstrates the application of click chemistry route in preparing $[\text{}^{99\text{m}}\text{Tc}(\text{CO})_3]^+$ labeled cyclic RGD peptide derivatives for targeting tumor angiogenesis.

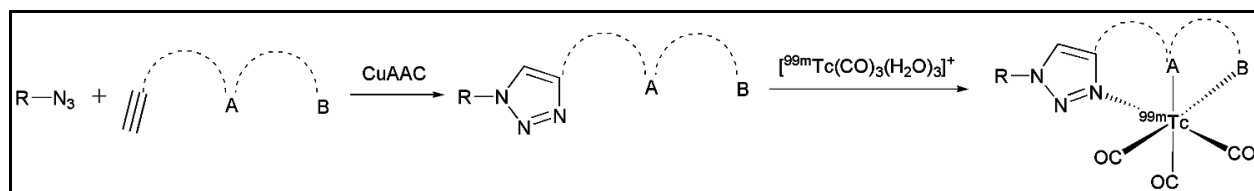


Fig. 2.1. Schematic representation of the synthesis of 1,2,3-triazolyl ligand systems for complexation with $[\text{}^{99\text{m}}\text{Tc}(\text{CO})_3(\text{H}_2\text{O})_3]^+$ precursor. A and B represents various functional groups for coordination of the tricarbonyl core.

2.1.2. RGD peptide: Valuable tool for targeting tumor angiogenesis

Angiogenesis, the formation of new blood vessels from pre-existing vessel constitutes a fundamental step in tumor metastasis [124-127]. Imaging of tumor-angiogenesis in a targeted fashion can provide early diagnosis, thus aiding in treatment planning and monitoring of anti-angiogenic therapies in cancer [128-130]. Integrin $\alpha_v\beta_3$ receptors which are overexpressed in some cancers are suitable targets for tumor-angiogenesis imaging because it is highly expressed

on activated and proliferating endothelial cells during tumor angiogenesis and metastasis but are absent in most organs [131,132]. Integrin $\alpha_v\beta_3$ is known to recognize ligands containing the arginine-glycine-aspartic acid (RGD) amino acid sequence present in several extracellular proteins such as vitronectin, fibronectin etc [133,134]. The high affinity of RGD binding motif towards integrin $\alpha_v\beta_3$ has led to the designing of a plethora of linear and cyclic RGD peptide analogs [135,136]. The cyclic RGD peptides have shown enhanced affinity and selectivity towards $\alpha_v\beta_3$ receptors over the linear ones. Among the cyclic RGD analogs, c(RGDfK) motif has been the most extensively explored for development of radiometallated peptides, profiting from the presence of the ϵ -NH₂ group of lysine amenable for derivetization or conjugation to a BFC and/or pharmacokinetic modifiers [137]. Radiolabeled multimeric RGD peptide analogs have also been studied extensively and are reported to have higher tumor accumulation. However the prohibitively high cost of synthesis along with increased uptake in non-target organs, limits the clinical utility of these radiotracers [138,139]. Different ^{99m}Tc-cores have been employed for radiolabeling of RGD peptides derivatives [140-142]. Among these, ^{99m}Tc-HYNIC labeled RGD peptides have been studied extensively [140]. The small size, kinetically inert [^{99m}Tc(CO)₃(H₂O)₃]⁺ is yet another promising radio-precursor that has also been explored for radiolabeling of RGD peptides with different tridentate ligands [129]. ^{99m}Tc(CO)₃-iminodiacetate (IDA) complex of cRGDfK monomer has been studied with and without PEG₄ linker as well as with glucosamine, as the pharmacokinetic modifier (PKM) [129]. However these negatively charged complexes were observed to have either low uptake, retention in the tumor or high intestinal uptake. These studies indicate that there is a definite scope of research towards modifying and preparing potential RGD-based radiotracers with improved pharmacokinetics.

In the present study, two neutral $^{99m}\text{Tc}(\text{CO})_3$ -labeled cRGDfK monomers with and without PEG₇ as the PKM have been designed via click chemistry route. The two spacers, medium-PEG (PEG₇) and a single methylene unit ($-\text{CH}_2-$) were incorporated at ϵ -amino group of lysine of cRGDfK peptide by conjugation with $\text{N}_3\text{-PEG}_7\text{-COOH}$ and $\text{N}_3\text{CH}_2\text{COOH}$. The two azide-modified cRGDfK peptides were then clicked with propargyl glycine (Pra) to introduce a tridentate chelator for radiolabeling with $[\text{}^{99m}\text{Tc}(\text{CO})_3(\text{H}_2\text{O})_3]^+$ precursor. The pharmacokinetics of PEGylated cRGDfK peptide was compared with a non-PEGylated cRGDfK peptide bearing a single methylene ($-\text{CH}_2-$) unit as the spacer. PEGylation of peptides is a common method to manipulate the pharmacokinetics. Effect of shorter PEGs, PEG₂, PEG₃ and PEG₄ [143-145] as well as longer PEG (MW = 3400) [146] on the *in vivo* kinetics of radiolabeled RGD peptides has been reported in literature. In this study, medium-sized PEG₇ linker was introduced with an aim of increasing the biological half-life of the peptide that may lead to increase in the tumor uptake of the radiotracer.

2.2. Experimental

2.2.1. Materials and methods

The peptide, cRGDfK was procured from ABX chemicals (Radeberg, Germany). 2-azido acetic acid, N,N-diisopropylethylamine (DIPEA), DL-propargyl glycine and sodium borohydride were purchased from Sigma Aldrich, USA. Copper sulphate, sodium ascorbate, sodium carbonate and sodium potassium tartrate were purchased from S.D. Fine Chemicals, Mumbai, India. 1-[Bis(dimethylamino)methylene]-1H-1,2,3-triazolo[4,5-b]pyridinium 3-oxid hexafluorophosphate (HATU) was procured from Alfa Aesar, USA and $\text{N}_3\text{-PEG}_7\text{-COOH}$ was procured from Novabiochem, Germany. The cRGDfK peptide derivatives were purified using a semi-preparative HPLC system (JASCO, Japan) connected with JASCO-PU-2086 Plus, intelligent

prep pump, JASCO UV-2075 Plus absorption detector and having a Megapak Sil C18-10 column (7.5 × 250 mm). The analytical HPLC measurements were performed on a JASCO PU 2080 Plus dual pump HPLC system, Japan, with a JASCO 2075 Plus tunable absorption detector and a Gina Star radiometric detector system, using a C18 reversed phase HiQ Sil column (5 μm, 4 × 250 mm). Mass spectra were recorded on QTOF Micromass Instrument using electron spray ionization (ESI).

2.2.2. Synthesis

2.2.2.1. Synthesis of cRGDfK-CH₂-Tz-Pra (2a)

A solution of azidoacetic acid (2.5 mg) in DMF (50 μL) activated with HATU (9 mg) and DIPEA (5 μL) was added to cRGDfK peptide (12 mg) dissolved in DMF (100 μL). The reaction mixture was incubated at room temperature overnight and then diluted with water before purification using semi-preparative HPLC. The purified product was dried under vacuum and characterized by mass spectrometry. Yield: 7 mg (53.62%)

MS (ESI⁺): m/z = 687.3 [M+H]⁺ (calcd for C₂₉H₄₂N₁₂O₈: 686.3)

The click reaction was then carried out between the azide-modified cRGDfK and DL-propargyl glycine. The azide-modified cRGDfK (2 mg) was dissolved in 1:1 t-butanol/water (100 μL) and to that propargyl glycine (0.35 mg), copper sulphate (0.3 mg) and sodium ascorbate (0.6 mg) were added and incubated at 50°C for 6 h. The product obtained was characterized by mass spectrometry and used for radiolabeling without purification.

MS (ESI⁻): m/z = 799.3 [M]⁻ (calcd for C₃₄H₄₉N₁₃O₁₀: 799.3)

2.2.2.2. Synthesis of cRGDfK-PEG₇-Tz-Pra (2b)

Compound **2b** was synthesized using a procedure similar to that used for synthesis of compound **2a**. The solution of N₃-PEG₇-COOH (6.5 mg) in DMF (50 μL) activated in presence

of HATU (5 mg) and DIPEA (3 μ L), was added to cRGDfK peptide (7 mg) dissolved in DMF (100 μ L). The reaction mixture was stirred at room temperature overnight and then purified by semi-preparative HPLC. The purified compound was characterized by mass spectrometry. Yield: 4.5 mg (33%)

MS (ESI⁺): $m/z = 1140.2$ [M+H]⁺ (calcd for C₄₉H₈₁N₁₃O₁₈: 1139)

Subsequently, click reaction of cRGDfK-PEG₇-N₃ (2 mg) with propargyl glycine (0.2 mg) was carried out in the presence of copper sulphate (0.1 mg) and sodium ascorbate (0.3 mg) for 6 h at 50 °C.

MS (ESI⁻): $m/z = 1251.9$ [M]⁻ (calcd for C₅₄H₈₈N₁₄O₂₀: 1252)

2.2.2.3. Preparation of Re(CO)₃ complexes, Re(CO)₃-Pra-Tz-CH₂-cRGDfK (2c) & Re(CO)₃-Pra-Tz-PEG₇-cRGDfK (2d):

Bis(tetraethylammonium)-*fac*-tribromotricarbonylperrhenate [(NEt₄)₂[ReBr₃(CO)₃] (5 mg) prepared following a reported procedure [147], was added to compound **2a** and/or **2b** dissolved in 1:1 (v/v) mixture of water/methanol. The reaction mixture was stirred at 60°C for 5h. Subsequently the reaction mixture was cooled down to attain room temperature and the product was purified using semi-preparative HPLC, dried under vacuum and characterized by mass spectrometry.

MS (ESI⁺): **2c**, $m/z = 1088.3$ [M+H+H₂O]⁺ (calculated for C₃₇H₄₈N₁₃O₁₃Re: 1069.3); **2d**, $m/z = 771.4$ [M+2H+H₂O]²⁺ (calculated for C₅₇H₈₈N₁₄O₂₃Re: 1522.9)

2.2.3. Radiolabeling

2.2.3.1 Preparation of [^{99m}Tc(CO)₃(H₂O)₃]⁺ precursor

The [^{99m}Tc(CO)₃(H₂O)₃]⁺ precursor was prepared following a procedure reported by Alberto et al [59]. Carbon monoxide gas was purged through an aqueous solution of NaBH₄ (10

mg), Na₂CO₃ (8 mg) and Na/K tartrate (15 mg) in 0.5 mL distilled water for 5 minutes. To this solution, freshly eluted Na^{99m}TcO₄ (1 mL, ~37 MBq) was added and the mixture was heated at 100°C for 15 min. The pH of the reaction mixture was adjusted to 7 using 0.5 M phosphate buffer (pH 7.5): 1 M HCl (1:3 v/v).

2.2.3.2. Preparation of ^{99m}Tc(CO)₃-Pra-Tz-CH₂-cRGDfK (2e) & ^{99m}Tc(CO)₃-Pra-Tz-PEG₇-cRGDfK (2f):

Compounds **2a** and/or **2b** (50 µg) dissolved in distilled water (100µL) were added to the freshly prepared [^{99m}Tc(CO)₃(H₂O)₃]⁺ precursor (500 µL) and incubated at 100°C for 15 min. The solutions were then allowed to cool to room temperature before carrying out HPLC analysis.

2.2.3.3. Quality control

The radiochemical purity (RCP) of the radiotracers was determined by HPLC using a gradient elution method. The eluting solvents were water (solvent A) and acetonitrile (solvent B) containing 0.1% trifluoroacetic acid; 0-28 min: 90% A-10% A; 28-30 min: 10% A; 30-32 min: 10% A-90% A. Flow rate was maintained at 1 mL/min. About 10 µL of the radiotracer was injected into the column for analysis. The RCP of the complex was determined by measuring the peak area from the chromatogram.

2.2.3.4. Determination of octanol-water partition coefficient (Log P_{o/w})

The radiotracer (0.1 mL, ~3.7 MBq) was mixed with distilled water (0.9 mL) and *n*-octanol (1 mL) on a vortex mixer for about 1 min and then centrifuged (3500 g) for 5 min to get clear separation of the two layers. The *n*-octanol layer (0.8 mL) was withdrawn and equal volume of fresh double-distilled water was added. The mixture was vortexed again and then centrifuged as described above. The above step was repeated and then equal aliquots of the two

layers were withdrawn and measured in a γ -counter. The readings thus obtained were used to calculate the Log $P_{o/w}$ of the complex.

2.2.3.5. Stability studies

In vitro stability

The radiotracers were incubated in saline at room temperature till 24 h post-preparation and their stabilities were assayed by HPLC analyses.

Serum stability

The radiotracers (25 μ L) were incubated in human serum (250 μ L) at 37°C for 24 h. 100 μ L of the mixture was taken and to that 100 μ L of acetonitrile was added to precipitate the serum proteins and centrifuged at 3500 g for 10 minutes. The supernatant was analyzed by HPLC to assess the stability of the complex in serum.

2.2.4. In vitro cell studies

B16F10 murine melanoma cells [National Center for Cell Sciences (NCCS) Pune, India] were cultured in Minimum Essential Medium (MEM) supplemented with 10% fetal calf serum (Invitrogen Carlsbad, CA) and 1% antibiotic/antimycotic formulation. The cells were incubated at 37°C in a humidified atmosphere containing 5% CO₂. The radiotracers, **2e** and **2f** (0.011, 1.1 and 11.1 μ M) were incubated at 37°C for 1 h with 1×10^5 cells. After incubation, the cell pellet was washed twice with cold phosphate buffer saline (PBS) and radioactivity associated with cells was measured in NaI (TI) gamma counter. The experiment was carried out in triplicate. Inhibition studies were carried out using 100-fold cRGDfK peptide. Percentage inhibition values were calculated as [$\frac{\text{difference between cell binding of radiotracer in absence and in presence of cold cRGDfK peptide}}{\text{cell binding in absence of peptide}} \times 100$].

2.2.5. Biodistribution studies

Biodistribution studies were carried out in C57BL/6 mice bearing melanoma tumor. About 100 μL of melanoma tumor cell suspension containing about 1×10^6 cells was injected subcutaneously on the dorsum of the experimental C57BL/6 mice. After about 14 days of transplantation of the tumor cells, when the tumor size grew approximately to 8-10 mm in diameter, the tumor bearing animals were used for the experiment. For carrying out biodistribution studies, the radiotracer (~ 3.7 MBq/animal, 100 μL) was injected intravenously through the lateral tail vein. The animals ($n = 4/\text{time point}$) were sacrificed at different time intervals (30, 60, and 180 min), and the relevant organs excised for measurement of retained activity. Blocking experiment was carried out by co-administration of the peptide, cRGDfK (15 mg/kg) along with the radiotracer to determine the receptor binding specificity. The animals ($n = 4$) were sacrificed at 180 min p.i. The organs were weighed and the activity associated with them was measured in a flat-bed type NaI(Tl) counter with suitable energy window for $^{99\text{m}}\text{Tc}$. The activity retained in each organ/tissue was expressed as a percent value of the injected dose per gram (%ID/g).

2.2.6. Data analysis

Statistical data are reported as mean \pm standard deviation (S.D.). Paired two-tailed Student's t tests were done to evaluate statistical significance, where $p < 0.05$ was considered to be statistically significant.

2.3. Results and Discussion

2.3.1 Synthesis

The peptide, cRGDfK was derivatized at ϵ -amino group of lysine by introduction of two different azide moieties $\text{N}_3\text{-PEG}_7\text{-COOH}$ and $\text{N}_3\text{CH}_2\text{COOH}$. The azide-modified PEGylated and

non-PEGylated cRGDfK derivatives were reacted with propargyl glycine (Pra) in the presence of copper sulphate and sodium ascorbate to introduce a tridentate chelator for radiolabeling with $[^{99m}\text{Tc}(\text{CO})_3(\text{H}_2\text{O})_3]^+$ precursor (**Fig. 2.2**).

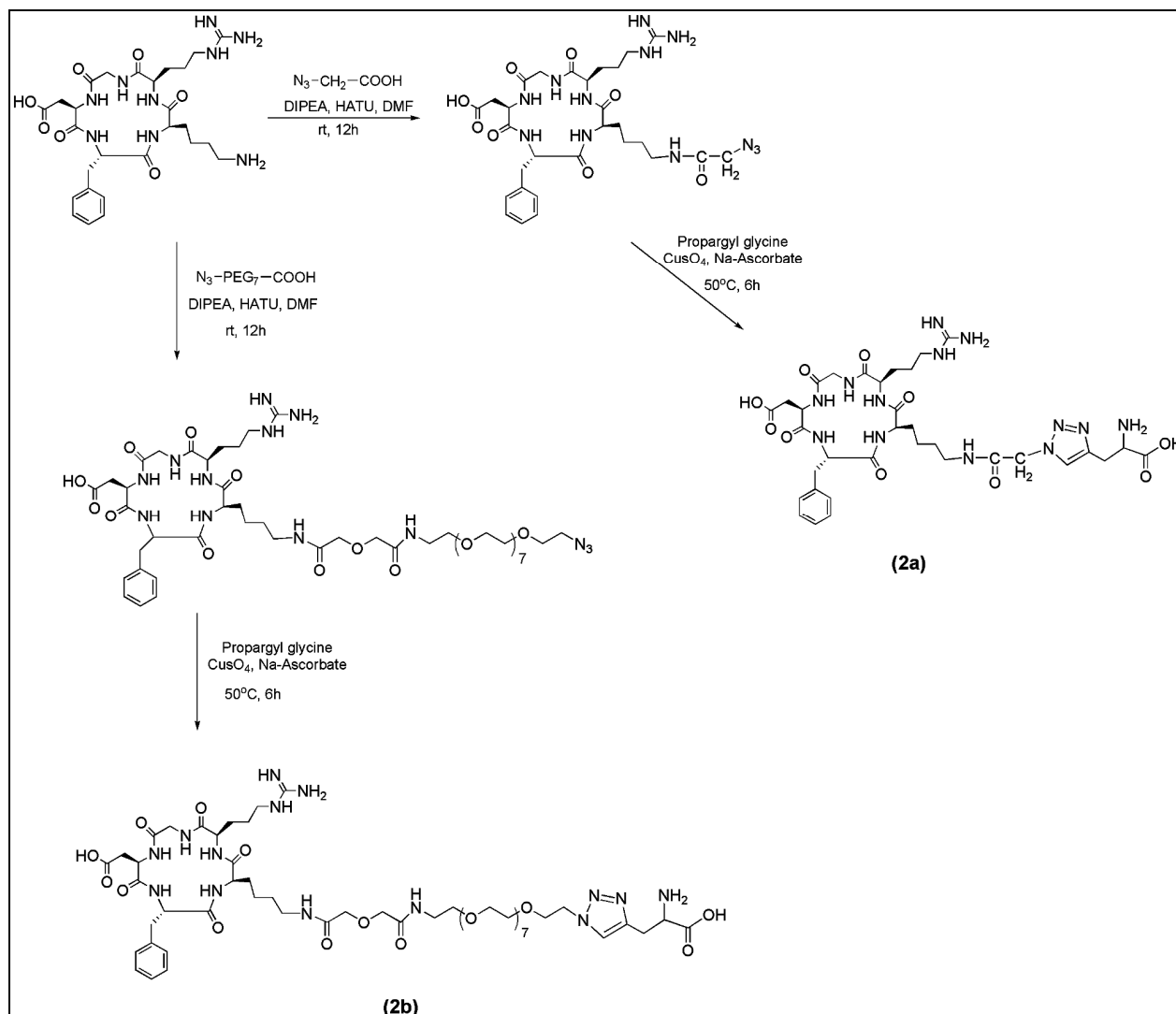


Fig. 2.2. Synthesis scheme of triazole functionalized PEGylated and non-PEGylated cRGDfK peptide analogues

The propargyl glycine was the preferred alkyne for this study as $-\text{NH}_2$ and $-\text{COOH}$ groups from the glycine unit and the N3 of 1,2,3-triazole formed by click reaction can act as a

versatile tridentate chelator for complexation with $[\text{}^{99\text{m}}\text{Tc}(\text{CO})_3(\text{H}_2\text{O})_3]^+$ precursor. Formation of intermediate azides and the cRGDFK peptides functionalized with the tridentate triazole (**2a** and **2b**) were confirmed by mass spectrometry.

2.3.2. Radiolabeling

Compounds **2a** and **2b** were radiolabeled with $[\text{}^{99\text{m}}\text{Tc}(\text{CO})_3(\text{H}_2\text{O})_3]^+$ precursor complex to form neutral complexes of cRGDFK (**Fig. 2.3**). The two imaging probes in this study were neutral as the +1 oxidation state of technetium was neutralized by the -1 charge on the -COOH group of propargyl glycine. The $[\text{}^{99\text{m}}\text{Tc}(\text{CO})_3(\text{H}_2\text{O})_3]^+$ precursor complex as well as the radiotracers, **2e** and **2f** were characterized by reversed phase HPLC following the gradient elution program. Radiotracers, **2e** and **2f** were obtained in >90% RCP as determined from the peak area measurements of the respective HPLC elution profiles. The $\text{Re}(\text{CO})_3$ complexes **2c** and **2d** prepared in macroscopic level were characterized by mass spectrometry. The structural identities of $^{99\text{m}}\text{Tc}$ -labeled radiotracers were confirmed by comparing the radio-HPLC retention time with that of the UV profile of the corresponding cold Re-complexes. While the UV-HPLC retention times of cold complexes **2c** and **2d** were observed to be 15.5 and 18.2 min respectively, the corresponding radio-HPLC retention times of radiotracers **2e** and **2f** were 15.9 and 18.8 min respectively (**Fig. 2.4**) whereby the structural similarity of the two complexes could be inferred. The $\text{Log } P_{\text{o/w}}$ values, a measure of lipophilicity, were found to be 0.19 for radiotracer **2e** and 0.25 for **2f**. The radiotracers showed excellent *in vitro* stability in saline as well in serum till 24 h as determined by no change in the radiochemical purity on storage.

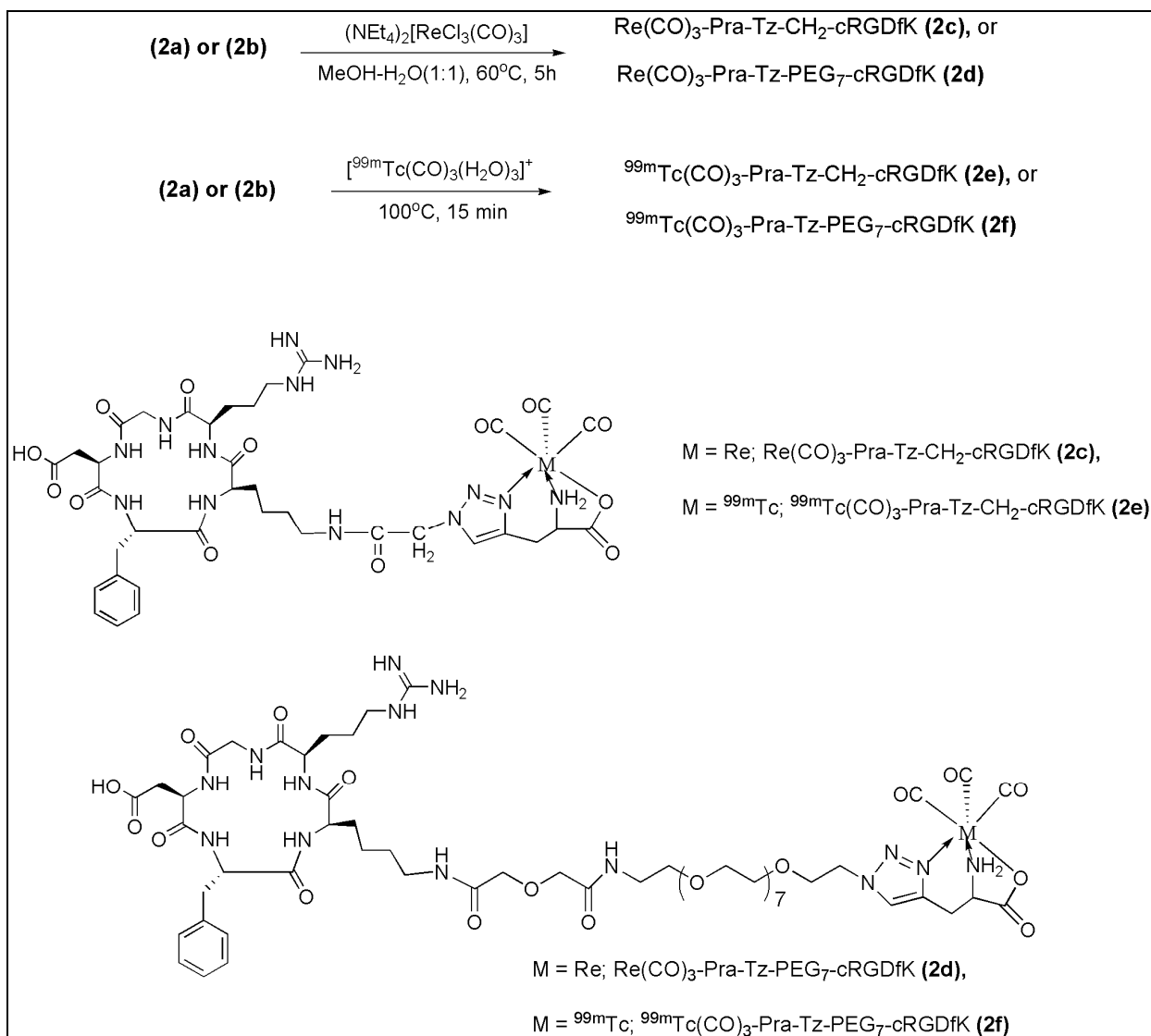


Fig. 2.3. Metal carbonyl complexes of triazole functionalized cRGDfK peptide analogues

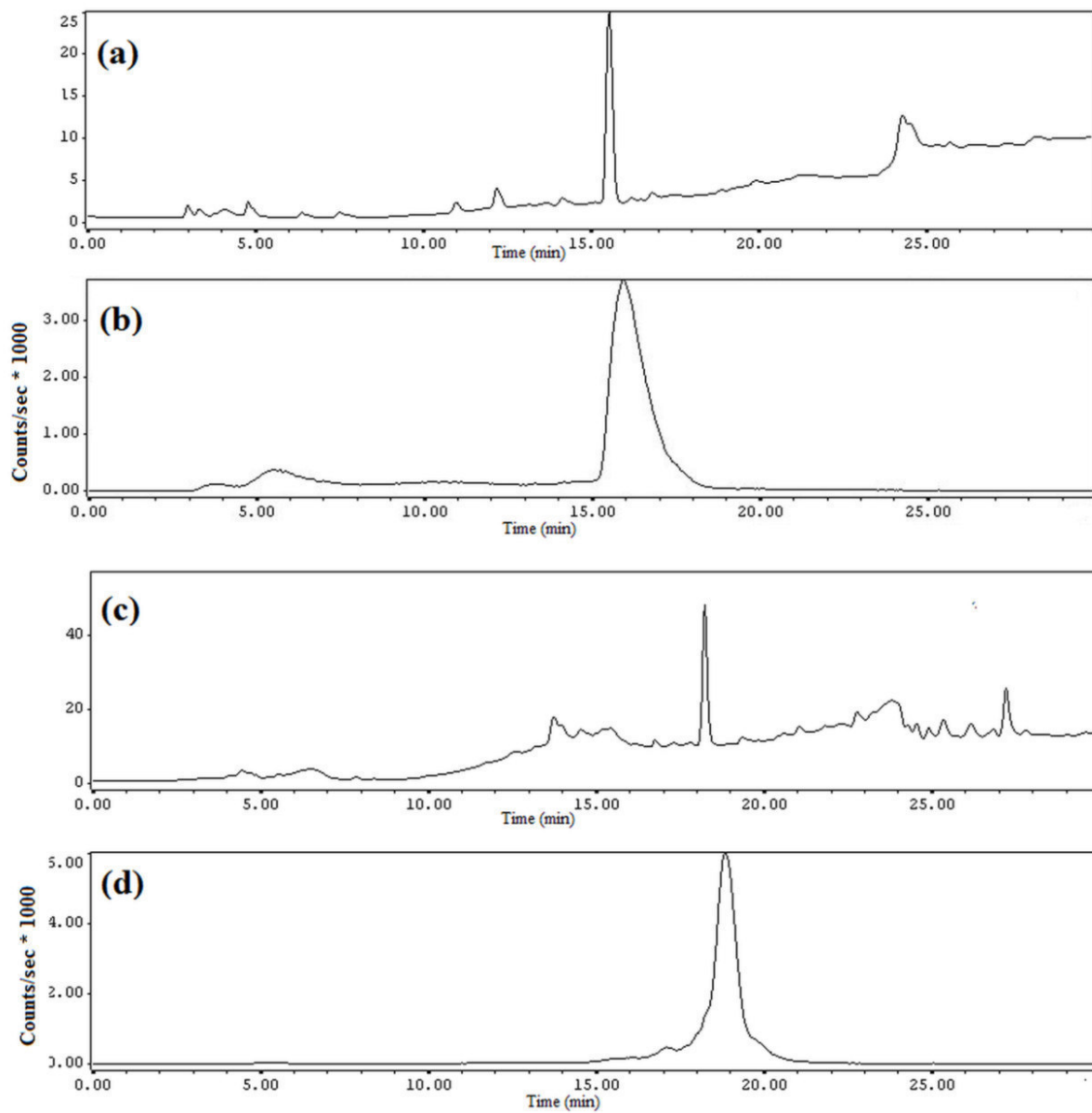


Fig. 2.4. HPLC profile of (a) $\text{Re}(\text{CO})_3\text{-Pra-Tz-CH}_2\text{-cRGDfK}$ (b) $^{99\text{m}}\text{Tc}(\text{CO})_3\text{-Pra-Tz-CH}_2\text{-cRGDfK}$ (c) $\text{Re}(\text{CO})_3\text{-Pra-Tz-PEG}_7\text{-cRGDfK}$ and (d) $^{99\text{m}}\text{Tc}(\text{CO})_3\text{-Pra-Tz-PEG}_7\text{-cRGDfK}$

2.3.3. *In vitro* cell studies

The binding of the radiotracers **2e** and **2f** in *in-vitro* cell binding studies in B16F10 cells were observed to be nearly similar at all the concentrations studied [Table 2.1]. This binding was found to be specific as addition of excess unlabeled cRGDfK (100-fold) resulted in nearly 80% inhibition for both the radiotracers. Similar binding and inhibition pattern for the two radiotracers indicates that specific binding remained unaltered upon PEGylation.

Table-2.1: Percentage binding and inhibition of $^{99m}\text{Tc}(\text{CO})_3\text{-Pra-Tz-CH}_2\text{-cRGDfK}$ (**2e**) and $^{99m}\text{Tc}(\text{CO})_3\text{-Pra-Tz-PEG}_7\text{-cRGDfK}$ (**2f**) in B16F10 murine melanoma cells

Compound	Concentrations (μM)	% Binding	% Binding (with excess cold)	Inhibition(%)
2e	0.01	2.34 ± 0.49	1.34 ± 0.09	42.86%
	1.1	3.75 ± 0.59	0.73 ± 0.09	80.6%
	11.1	5.96 ± 0.02	1.17 ± 0.04	80.3%
2f	0.01	2.32 ± 0.54	1.19 ± 0.45	48.75%
	1.1	3.614 ± 0.459	0.78 ± 0.21	78.38%
	11.1	4.782 ± 0.164	0.76 ± 0.07	84.19%

2.3.4. Biodistribution studies

Bio-evaluation of the radiotracers **2e** and **2f** was carried out in C57BL/6 mice bearing melanoma tumor, which are known to over-express $\alpha_v\beta_3$ receptors. The uptake and retention of radiotracers in different organs/tissue is summarized in Table 2.2.

Table-2.2: Biodistribution pattern of $^{99m}\text{Tc}(\text{CO})_3\text{-Pra-Tz-CH}_2\text{-cRGDfK}$ (**2e**) and $^{99m}\text{Tc}(\text{CO})_3\text{-Pra-Tz-PEG}_7\text{-cRGDfK}$ (**2f**) in C57BL/6 mice bearing melanoma tumor

Organ	%ID/g of organ (s.d) [#]					
	30 min		60 min		180 min	
	2e	2f	2e	2f	2e	2f
Blood	3.80 (0.18)	4.51 (0.35)	2.61 (0.11)	3.30 (0.21)	0.44 (0.20)	2.13 (0.10)
Liver	5.73 (1.36)	11.43 (0.65)	11.3 (1.50)	8.60 (0.82)	1.95 (0.47)	7.68 (1.59)
GIT	9.27 (0.83)	8.71 (4.36)	9.92 (2.73)	6.98 (0.44)	15.49 (3.64)	8.27 (1.54)
Kidney	7.41 (0.44)	23.91 (1.72)	21.03 (1.28)	19.82 (2.47)	2.64 (0.49)	20.87 (3.09)
Stomach	2.22 (0.49)	4.28 (0.32)	2.57 (0.92)	2.94 (0.75)	1.83 (0.56)	2.53 (0.36)
Heart	2.91 (1.54)	1.98 (0.59)	1.16 (0.02)	1.48 (0.49)	0.34 (0.04)	1.11 (0.12)
Lungs	5.08 (1.59)	3.63 (0.36)	1.99 (0.82)	2.82 (0.27)	1.53 (0.60)	2.24 (0.01)
Muscle	1.02 (0.49)	0.77 (0.25)	0.34 (0.00)	0.44 (0.38)	0.19 (0.01)	0.09 (0.07)
Spleen	3.17 (0.19)	1.96 (0.43)	1.11 (0.77)	1.65 (0.56)	1.04 (0.40)	0.52 (0.09)
Tumor	3.01 (0.77)	4.11 (0.51)	1.73 (0.02)	3.27 (0.13)	1.13 (0.09)	2.16 (0.28)
Excretion*	56.57 (3.24)	39.78 (1.06)	50.22 (2.59)	45.13 (1.66)	68.45 (2.63)	56.52 (2.29)
Tumor/Blood	0.73 (0.27)	0.91 (0.09)	0.66 (0.02)	0.99 (0.1)	2.79 (0.55)	1.03 (0.13)
Tumor/Muscle	3.17 (0.77)	4.8 ± 0.09	5.07 (0.06)	4.85 (0.19)	6.25 (0.51)	15.52 (2.45)

[#]%ID/g – Percentage injected dose per gram; s.d – standard deviation, *%Excretion has been indirectly calculated by subtracting the activity accounted for all the organs from total injected activity.

The maximum tumor accumulation of **2e** and **2f** was observed at 30 min p.i; (3.01 ± 0.77) % ID/g and (4.11 ± 0.51) % ID/g respectively. PEGylation has been widely used for improving the pharmacokinetics of various radiolabeled small peptides. In the present study, PEG₇ linker was introduced with an aim of increasing the biological half-life of the peptide that may lead to increase in the tumor uptake of the radiotracer [145]. This was indeed observed for radiotracer **2f** in biodistribution studies where nearly two-fold higher tumor uptake was observed at 60 min and 180 min p.i. in comparison to that for radiotracer **2e**. The higher lipophilicity of PEGylated radiotracer led to its slower clearance from the blood and the liver. The longer circulation half-life of **2f** also resulted in higher renal activity. Radiotracer **2e** cleared through both the hepatobiliary and renal pathway as indicated by increase in the uptake in liver and kidneys at 60 min p.i. and that of intestine at 180 min p.i. Excretion of radiotracers was calculated by subtracting the activity corresponding to all the organs from the total activity injected. For radiotracer **2e**, $56.57 \pm 3.24\%$ excretion was observed at 30 min p.i. which increased to $68.45 \pm 2.63\%$ at 180 min p.i. whereas the corresponding values for the radiotracer **2f** were $39.78 \pm 1.06\%$ and $56.52 \pm 2.29\%$ respectively. Though the tumor uptake was higher for **2f**, high uptake in other non-target organs resulted in lower target/non-target ratios. Tumor to blood ratio improved for radiotracer **2e** from (0.73 ± 0.27) at 30 min p.i. to (2.79 ± 0.55) at 180 min p.i. whereas the higher blood pool activity of radiotracer **2f** resulted in lower tumor to blood ratio (1.03 ± 0.13) at 180 min p.i.

Specific *in vivo* integrin $\alpha_v\beta_3$ -targeting of the radiotracers was ascertained through blocking experiment carried out by co-injection of excess of cRGDfK peptide. The blocking of receptors by the cold cRGDfK peptide resulted in significant reduction ($p < 0.05$) in the tumor uptake of the radiotracers **2e** and **2f**, (0.47 ± 0.09) %ID/g and (1.01 ± 0.22) %ID/g respectively at

180 min p.i. (**Fig. 2.5**), thereby confirming the uptake to be receptor-mediated. Reduction in the tracer uptake in other non-target organs was also observed during blocking studies which is consistent with the low expression levels of integrin $\alpha_v\beta_3$ in these tissues [148].

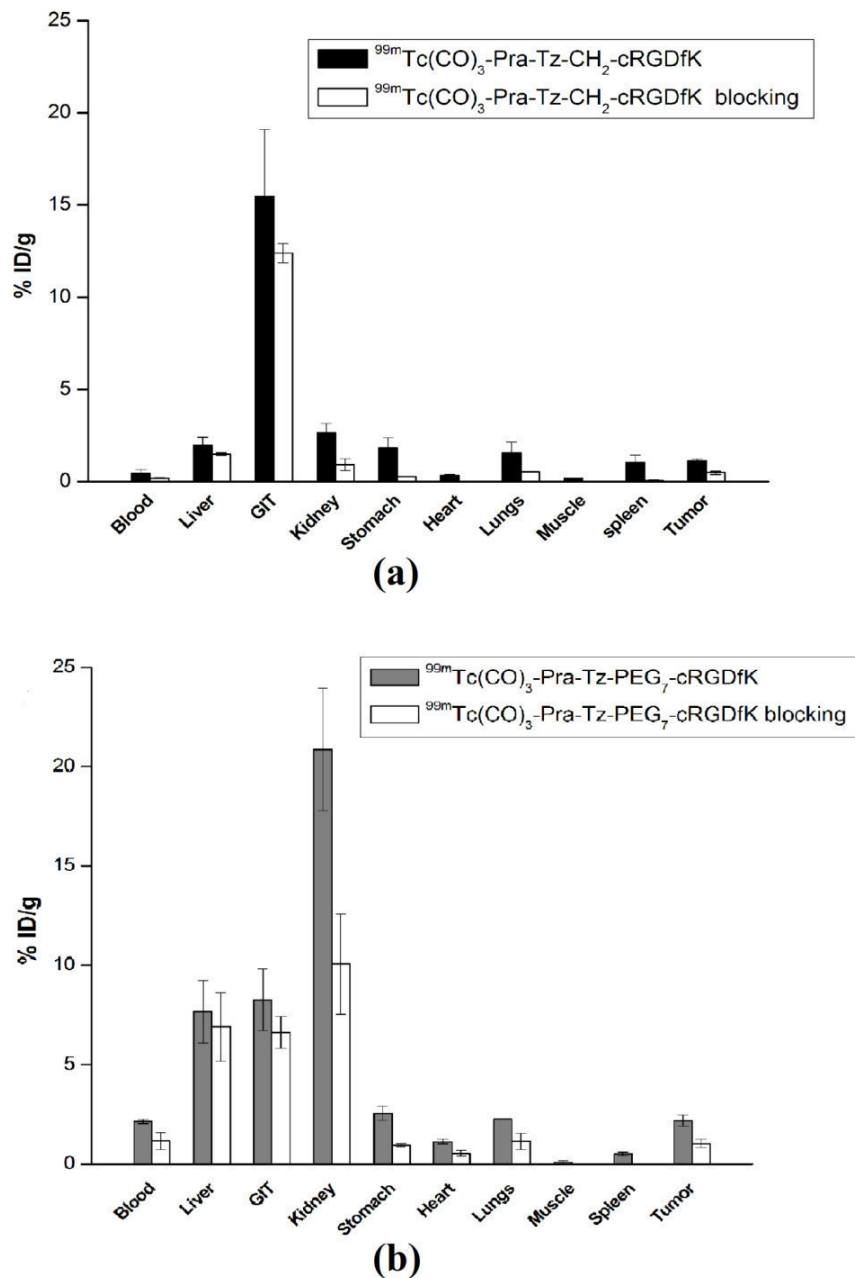


Fig 2.5. Comparison in the uptake of (a) $^{99m}\text{Tc}(\text{CO})_3\text{-Pra-Tz-CH}_2\text{-cRGDfK}$ and (b) $^{99m}\text{Tc}(\text{CO})_3\text{-Pra-Tz-PEG}_7\text{-cRGDfK}$ in different organs/tissue of C57BL/6 mice bearing melanoma tumor with/without receptor blockade at 180 min p.i.

2.4. Conclusion:

The click chemistry reaction led to facile introduction of a tridentate chelator to the azide-modified PEGylated and non-PEGylated cRGDfK peptide analogues, which were subsequently radiolabeled with ^{99m}Tc using $[^{99m}\text{Tc}(\text{CO})_3(\text{H}_2\text{O})_3]^+$ precursor. The radiotracers, $^{99m}\text{Tc}(\text{CO})_3$ -Pra-Tz-CH₂-cRGDfK (**2e**) and $^{99m}\text{Tc}(\text{CO})_3$ -Pra-Tz-PEG₇-cRGDfK (**2f**) were prepared in good radiochemical yield (~90%) and were found to be stable in serum, with no significant degradation till 24 h. The $^{99m}\text{Tc}(\text{CO})_3$ complexes (**2e**) and (**2f**) were characterized by comparing the radio-HPLC profile with UV-HPLC chromatogram of corresponding rhenium analogues (**2c**) and (**2d**). The two radiotracers showed specificity towards the $\alpha_v\beta_3$ receptors both in *in vitro* and *in vivo* studies. The PEGylated cRGDfK peptide analogue had higher tumor uptake than the non-PEGylated analogue but high uptake in other non-target organs resulted in lower target/non-target ratios.

CHAPTER 3

**PREPARATION OF ^{99m}Tc -HYNIC LABELED CYCLIC NGR PEPTIDE DERIVATIVES
FOR
TARGETING CD13 SPECIFIC TUMORS**

3.1. Introduction

In this Chapter HYNIC is used as the BFCA for ^{99m}Tc labeling of target specific peptide. Towards this the cyclic NGR (Asparagine-Glycine-Arginine) peptide for targeting CD13 receptors over-expressed in various tumor cells is used as the vector. HYNIC is one of the most promising BFCA generally used for radiolabeling peptides with ^{99m}Tc as it allows ^{99m}Tc labeling with higher specific activity under mild labeling conditions [78-86]. A brief discussion on the following aspects viz., (i) advantages of radiolabeled peptides in tumor imaging, (ii) the role of NGR peptide based ligands for targeting CD13 specific tumors, (iii) the logical consideration while choosing the ^{99m}Tc -HYNIC core for radiolabeling NGR peptide, (iv) solid phase peptide synthesis method for the synthesis of peptides have been presented in subsequent sections .

3.1.1 Radiolabeled peptides for imaging of tumors

There has been an exponential growth in the development of radiolabeled peptides for diagnostic and therapeutic applications in the last decade [149-151]. Peptides have a high affinity for characteristic receptors that are overexpressed on malignant tumor cells [152]. Peptide-based ligands which are specific towards binding with these receptors can be used as vectors for radiolabeling with suitable diagnostic and therapeutic isotopes [149-151]. The radiolabeled peptides thus obtained serve as target-specific radiotracers towards application in imaging as well as therapy of tumors. Peptides have many key properties including fast clearance, rapid tissue penetration, and low immunogenicity, and can be produced easily and inexpensively [149-151]. Peptides which are smaller units of complex proteins can tolerate harsher reaction conditions which may be required for carrying out structural modifications as well as radiolabeling. Additionally, the availability of automated means of synthesizing these compounds in large quantities along with the simplified methods of purifying, characterizing,

have kindled attention of researchers to peptides as carrier molecule in designing targeted agents for radiodiagnosis. Few peptide based radiolabeled agents for receptor targeted tumor imaging are presented in the **Table 3.1**.

Table 3.1. List of few radiolabeled peptides and the corresponding target receptors

Radiolabeled Peptides	Targets/Application	Ref
^{99m} Tc-Hynic-TOC, ^{99m} Tc-Hynic-TATE	[#] SSTR overexpressing cancer	153
¹¹¹ In-DOTA-TATE	SSTR overexpressing cancer	154
⁶⁸ Ga-DOTA-TATE, ⁶⁸ Ga-DOTA-TOC	SSTR overexpressing cancer	155
⁶⁸ Ga-AMBA	[#] GRP receptor based imaging of Prostate cancer	156
¹⁸ F-galacto-RGD	$\alpha_v\beta_3$ targeted imaging of cancer	133
⁶⁸ Ga/ ¹¹¹ In-DOTA-RGD	$\alpha_v\beta_3$ targeted imaging of cancer	133
⁶⁸ Ga-PSMA	[#] PSMA overexpressing Prostate cancer	157
⁶⁸ Ga-DOTA-Exendin-4	[#] GLP-1R expressing tumors (insulinomas)	158

[#]SSTR-Somatostatin receptors; GRP-Gastrin releasing peptide; PSMA-Prostate specific membrane antigen; GLP1R-Glucagen-like peptide-1-receptor

Asparagine-Glycine-Arginine is one such peptide-based ligand which shows high affinity towards APN(CD13) receptors.

3.1.2. NGR motif for targeting APN/CD13 expressing tumor

Development of target specific agents depends on the identification of cellular or vascular epitopes that distinguish cancer cells from normal cells. Aminopeptidase N (APN referred to as CD13) receptors are among one such molecular markers which are highly expressed in cancer cells and are implicated in tumor progression and invasion [159-161]. APN/CD13 is a zinc-dependent, trans-membrane exopeptidase that plays an important role in metastatic tumor cell invasion through enzyme-catalyzed degradation of extracellular matrix components [159]. High expression of CD13 can be detected in a number of human solid tumors, including melanoma, prostate, lung and ovarian cancer [162,163]. CD13 is selectively recognized by peptides containing the Asn-Gly-Arg (NGR) sequence, a tumor-homing motif discovered by phage display technologies [164,165]. Owing to their tumor homing properties, NGR containing peptides have a major implication in delivery of therapeutic and imaging agents to the targeted diseased site thereby reducing systemic toxicity. A noteworthy example is NGR-hTNF conjugate (NGR peptide conjugated anti-cancer drug, human tumor necrosis factor) which is under clinical investigation for malignant pleural mesothelioma, colorectal, lung (small-cell and non-small-cell), liver and ovarian cancers, and soft tissue sarcomas [166]. Furthermore, the NGR containing peptides have also been studied as molecular probes for *in vivo* detection of APN expression in solid tumors [167].

In recent years CD13-receptor targeted various peptides with NGR-signature motif have been synthesized and radiolabeled with different isotopes (^{64}Cu , ^{68}Ga , $^{99\text{m}}\text{Tc}$) for molecular imaging [168-172]. The $^{99\text{m}}\text{Tc}$ -labeled NGR peptides reported earlier were either directly radiolabeled or radiolabeled using $^{99\text{m}}\text{Tc}$ -oxo core [170-172]. These complexes were observed to have either low uptake, retention in the tumor or high liver and intestinal uptake. These studies

indicate that there is a definite scope of research to modify and prepare potential ^{99m}Tc -labeled NGR based radiotracers with improved pharmacokinetics. Amongst the various approaches available ^{99m}Tc -HYNIC core (HYNIC = 6-hydrazinonicotinic acid) was chosen for this study as it offers high radiolabeling efficiency and allows for preparation of molecular imaging probes with high specific activity and promising pharmacokinetic profile. HYNIC also has an advantage of simple and easier conjugation with peptides either on-resin during solid phase peptide synthesis or synthesis in solution phase [78,173].

The susceptibility of linear peptides to proteolytic degradation and reports of cyclic NGR peptides exhibiting higher efficacy towards their target (CD13 receptors) validates the superiority of cNGR peptides as molecular probes in comparison to linear peptides [174]. Thus cyclic NGR peptide, c(KCNGRC) [cyclic(lysine-cysteine-asparagine-glycine-arginine-cysteine amide)] was selected for this particular study. The lysine amino acid at N-terminal allows the possibility of further conjugation of a chemotherapeutic drug at ϵ -amine group for tumor targeted drug delivery. The peptide c(KCNGRC) was synthesized manually by standard ***Fmoc solid phase synthesis strategy***. The N-terminus of the peptide was conjugated with HYNIC-Boc to synthesize HYNIC-c(KCNGRC). With the aim of increasing the circulating half-life and modulating the pharmacokinetics, polyethylene glycol moiety (PEG₂) was introduced as a spacer at the N-terminus prior to conjugation with HYNIC for preparation of another peptide ligand, HYNIC-PEG₂-c(KCNGRC). The HYNIC conjugated peptides, HYNIC-cKCNGRC and HYNIC-PEG₂-cKCNGRC were subsequently radiolabeled with ^{99m}Tc . The two radiotracers, ^{99m}Tc -HYNIC-cKCNGRC (^{99m}Tc -HYNIC-c(NGR)) and ^{99m}Tc -HYNIC-PEG₂-cKCNGRC (^{99m}Tc -HYNIC-PEG₂-c(NGR)) were subsequently investigated for their efficacy as tumor targeted molecular imaging probes.

3.1.3. Solid phase peptide synthesis

The concept of solid phase peptide synthesis (SPPS) was introduced by Robert Bruce Merrifield for achieving more efficient synthesis of peptides in terms of yield and purity [175]. In SPPS, the peptide chain is assembled in a stepwise manner while the C-terminal end of the peptide is anchored to an inert cross-linked polymeric support and the peptide is grown from C-terminal to N-terminal residue. This method employs an insoluble and filterable polymeric support such as cross-linked polystyrene that functions as the carboxyl protecting group for the C-terminal amino acid of the peptide. The target peptide sequence is formed in a stepwise manner by attaching temporary N α -protected C-terminal amino acid to the resin. After the removal of N α -protection, the next N α -protected amino acid is coupled and the process is repeated until the entire desired peptide is assembled on the polymer support. For coupling the peptides, the carboxyl group is usually activated. This is important for speeding up the reaction. The two main types of activating groups used are carbodiimides and triazolols [180]. All the reactions are carried out under non-aqueous conditions in organic solvents. The target peptide is deprotected and cleaved from the polymer matrix by acidolysis with HF (hydrofluoric acid) or anhydrous TFA (Trifluoroacetic acid) in the presence of suitable scavenger.

There are two majorly used forms of SPPS based on the type of N α -protecting groups: Fmoc and Boc. The Boc group is deprotected with strong acids such as TFA while the Fmoc protecting group can be removed using a mild base usually piperidine (20–50%) in DMF [180]. The advantage of Fmoc is that it is cleaved under very mild basic conditions but is stable under acidic conditions. This allows the use of protecting groups that are stable under basic conditions and are labile under mildly acidic conditions. These types include Boc and benzyl groups, which can be used on the side-chains of amino acid residues of the target peptide. Thus, by using Fmoc,

orthogonal protecting group strategy can be used with the added advantage over Boc in terms of the ease of cleavage.

3.2. Experimental

3.2.1. Materials and methods

The amino acid derivatives N α -Fmoc-N γ -trityl-L-asparagine, N α -Fmoc-N Ω -(2,2,4,6,7-pentamethyl-2,3-dihydrobenzo[b]furan-5ylsufonyl)-L-arginine, N ϵ -Boc-N α -Fmoc-L-lysine were purchased from Alfa Aesar, USA. Fmoc-Cys(Acm)-OH and Fmoc-Gly-OH were purchased from Sigma Aldrich. NovaSyn TGR resin and Fmoc-NH-(PEG)₂-COOH were procured from Novabiochem, Germany. 1-[Bis(dimethylamino)methylene]-1H-1,2,3-triazolo[4,5-b]pyridinium 3-oxid hexafluorophosphate (HATU) was procured from Alfa Aesar, USA. N,N-diisopropylethylamine (DIPEA), Piperidine, 6-chloronicotinic acid, di-tert-butyl dicarbonate, sodium dihydrogen phosphate, disodium hydrogen phosphate, ethylenediaminediacetic acid (EDDA), N-[Tris(hydroxymethyl)methyl]glycine (Tricine) were procured from Sigma Aldrich, USA. Stannous chloride dihydrate was procured from Fluka. The HYNIC-c(KCNGRC) and HYNIC-PEG₂-c(KCNGRC) peptide ligands were purified using a semi-preparative HPLC system (JASCO, Japan) connected with JASCO-PU-2086 Plus, intelligent prep pump, JASCO UV-2075 Plus absorption detector and having a Megapak Sil C18-10 column (7.5 × 250 mm). The analytical HPLC measurements were performed on a JASCO PU 2080 Plus dual pump HPLC system, Japan, with a JASCO 2075 Plus tunable absorption detector and a Gina Star radiometric detector system, using a C18 reversed phase HiQ Sil column (5 μ m, 4 x 250 mm). The eluting solvents (1 mL/min) used in HPLC were; water with 0.1% trifluoroacetic acid (solvent A) and acetonitrile with 0.1% trifluoroacetic acid (solvent B) following the gradient: 0-3 min: 0% B; 3-5 min: 0-20% B; 5-10 min: 20% B; 10-20 min: 20-90% B; 20-22 min: 90-0% B;

22-30 min: 0% B. Mass spectra were recorded on QTOF Micromass Instrument using electron spray ionization (ESI).

3.2.2. Synthesis

3.2.2.1. Synthesis of HYNIC-Boc (6-BOC-hydrazinopyridine-3-carboxylic acid) (3a)

HYNIC-Boc was synthesized as reported in literature [78]. Briefly, 80% hydrazine hydrate (8 mL) was added to 6-chloronicotinic acid (1 g, 6.35 mmol) and stirred at 100°C for 4 h. After cooling to room temperature, the reaction mixture was concentrated under reduced pressure to give a white solid. The solid was dissolved in water and further adjustment of pH of the solution to 5.5 resulted in precipitate formation. The precipitate was filtered, washed with ethanol and dried in vacuum to give 6-hydrazinopyridine-3-carboxylic acid (845 mg). In the next step, Boc protection of hydrazine group was carried out. To 6-hydrazinopyridine-3-carboxylic acid (200 mg, 1.31 mmol) in DMF, triethylamine (365 μ L, 2.62 mmol) and di-tert-butyl-dicarbonate (285 mg, 1.31 mmol) were added and the reaction mixture was stirred overnight at room temperature. The reaction mixture was concentrated and the crude product obtained was purified by silica gel column chromatography using ethyl acetate as the eluting solvent to obtain 6-Boc-hydrazinopyridine-3-carboxylic acid (230 mg, 69.5% yield). R_f (ethyl acetate) = 0.2; IR (KBr, $\nu_{\max}/\text{cm}^{-1}$): 3259 (m), 2976 (m), 2930 (s), 1703 (s), 1610 (s), 1487 (w), 1250 (s), 1159 (s), 1018 (w). ^1H NMR (300 MHz, CD_3OD): δ = 1.42 (s, 9H), 6.53 (d, J = 8.7 Hz, 1H), 7.96 (d, J = 8.7 Hz, 1H) 8.57 (s, 1H); MS (ESI⁺): m/z = 253.8 $[\text{M}+\text{H}]^+$, 275.9 $[\text{M}+\text{Na}]^+$ (calcd for $\text{C}_{11}\text{H}_{15}\text{N}_3\text{O}_4$: 253.1) (**Fig 3.1**).

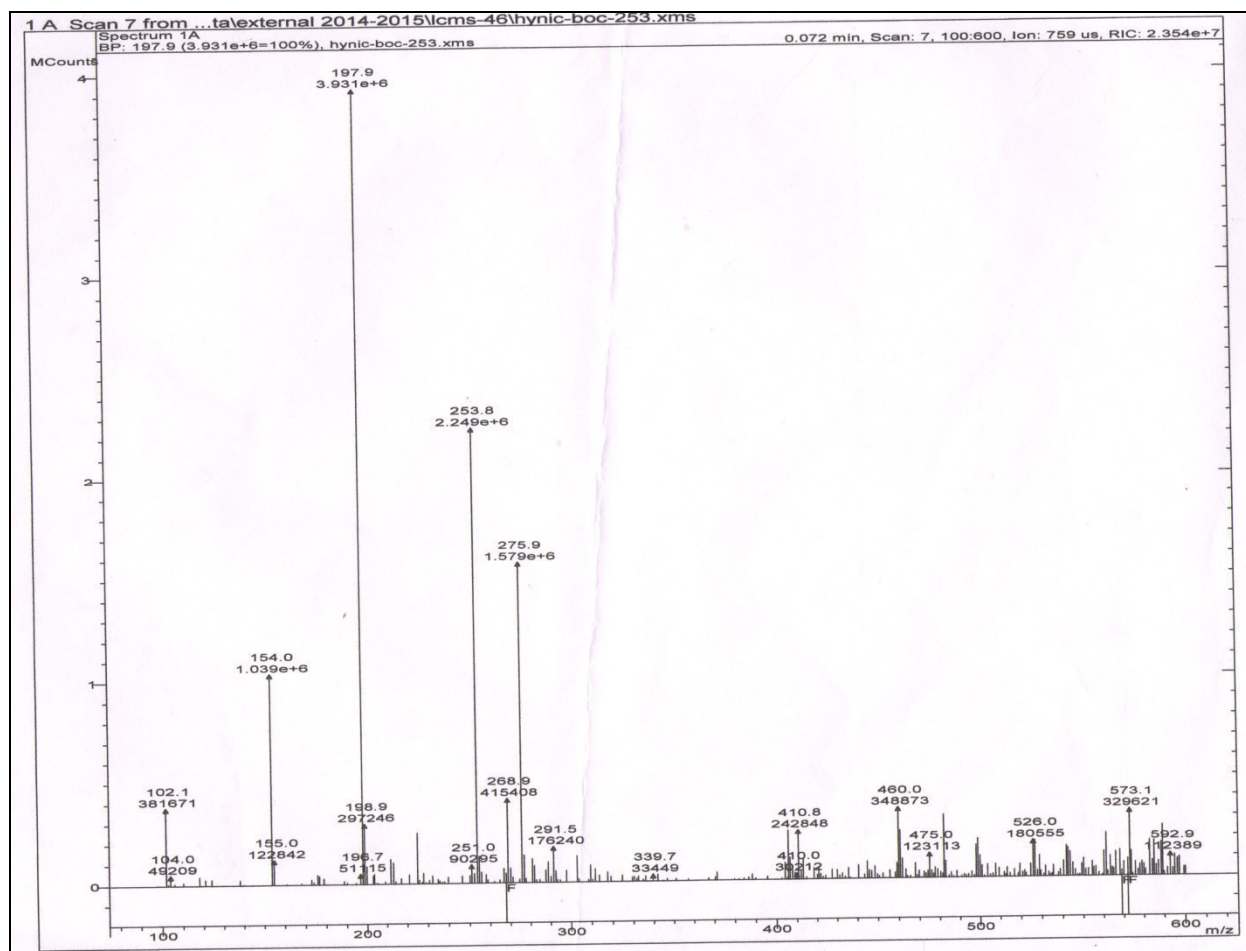


Fig 3.1. ESI-MS of HYNIC-Boc (**3a**)

3.2.2.2. Synthesis of HYNIC conjugated cyclic NGR peptides

Scheme for synthesis of HYNIC-c(KCNGRC) [HYNIC-c(NGR)] and HYNIC-PEG₂-c(KCNGRC) [HYNIC-PEG₂-c(NGR)] is shown in (Fig. 3.2).

Synthesis of HYNIC-c(NGR) (**3b**)

The fully protected peptide H-Lys(Boc)-Cys(Acm)-Asn(Trt)-Gly-Arg(Pbf)-Cys(Acm)-NH₂ was assembled on Novasyn TGR resin manually by standard Fmoc solid phase peptide synthesis. Coupling of each amino acid was carried out using standard Fmoc strategy where 3-fold excess of amino acid as well as O-(7-azabenzotriazol-1-yl)-N,N,N',N'-tetramethyluronium hexafluorophosphate (HATU) was used along with 6-fold excess of N,N-diisopropylethylamine

(DIPEA) in dimethylformamide (DMF) for 90 min. The reaction was monitored by picrylsulphonic acid test and the Fmoc groups were removed by treatment with 20% piperidine in DMF for 30 min. Subsequently, on-resin cyclization of cysteine sulphides was carried out with 1.2 eq of thallium(III)trifluoroacetate in DMF. The chelator HYNIC-Boc (2 eq) was then coupled to the N-terminus of the peptide in presence of HATU and DIPEA. Subsequently the resin was treated with cocktail mixture of trifluoroacetic acid (TFA)/tri-isopropylsilane (TIPS) (99:1, v/v) for cleavage of the peptide and deprotection of side chain groups. The crude peptide was precipitated and washed three times with diethyl ether. The crude peptide was then purified by semi-preparative HPLC and lyophilized to obtain a white fluffy powder. MS (ESI⁺): m/z = 835.0 [M+Na]⁺ (calcd for C₃₀H₄₉N₁₅O₈S₂: 811.94) (**Fig 3.3**).

Synthesis of HYNIC-PEG₂-c(NGR) (3c)

The peptide ligand HYNIC-PEG₂-c(KCNGRC) was synthesized according to the above mentioned procedure. The peptide at N-terminus was conjugated with Fmoc-NH-PEG₂-COOH (2 eq) followed by conjugation with HYNIC-Boc (2 eq) after deprotection of Fmoc group. MS (ESI⁺): m/z = 1038.1 [M+Na]⁺ (calcd for C₃₉H₆₆N₁₆O₁₂S₂: 1015.17) (**Fig 3.4**).

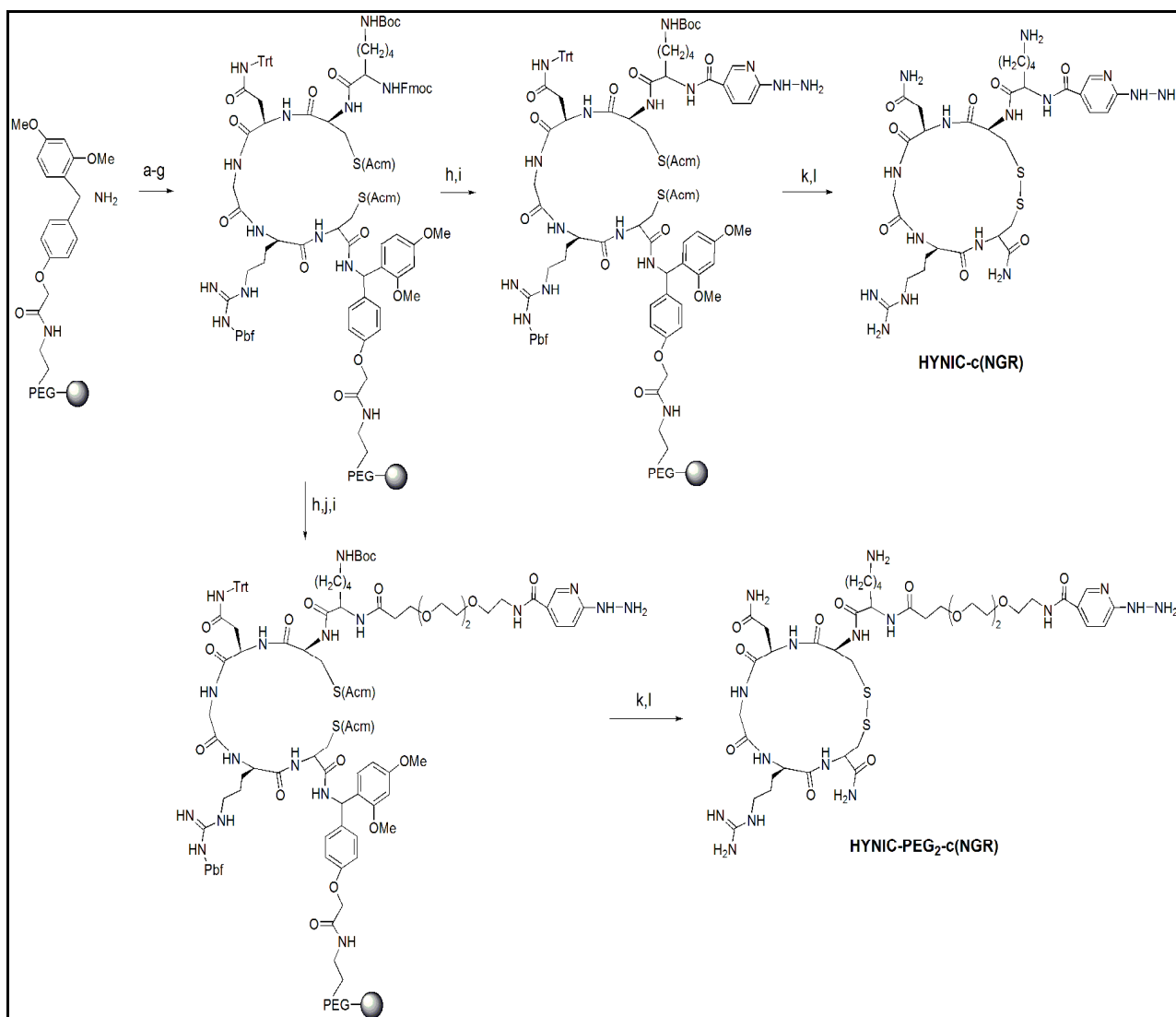


Fig 3.2. Synthesis scheme of HYNIC-c(NGR) and HYNIC-PEG₂-c(NGR)

Reagents and conditions: a) N-Fmoc-Cys(Acm)-OH, HATU, DIPEA, DMF, rt, 2 h; b) 20% piperidine in DMF, rt, 30 min (x 2); c) N-Fmoc-Arg(Pbf)-OH, HATU, DIPEA, DMF, rt, 2 h; d) N-Fmoc-Gly-OH, HATU, DIPEA, DMF, rt, 2 h; e) N-Fmoc-Asn(Trt)-OH, HATU, DIPEA, DMF, rt, 2 h; f) N-Fmoc-Cys(Acm)-OH, HATU, DIPEA, DMF, rt, 2 h; g) N-Fmoc-Lys(Boc)-OH, HATU, DIPEA, DMF, rt, 2 h; h) 20% piperidine in DMF, rt, 30 min (x 2); i) HYNIC-Boc, HATU, DIPEA, DMF, rt, 2 h; j) Fmoc-NH-(PEG)₂-COOH, HATU, DIPEA, DMF, rt, 2 h; k) Tl(III)trifluoroacetate, DMF, rt, 2 h; l) TFA/ethanedithiol/triisopropylsilane/water (94:2.5:2.5:1 v/v), rt, 2 h.

Spectrum Plot - 4/6/2016 12:36 PM

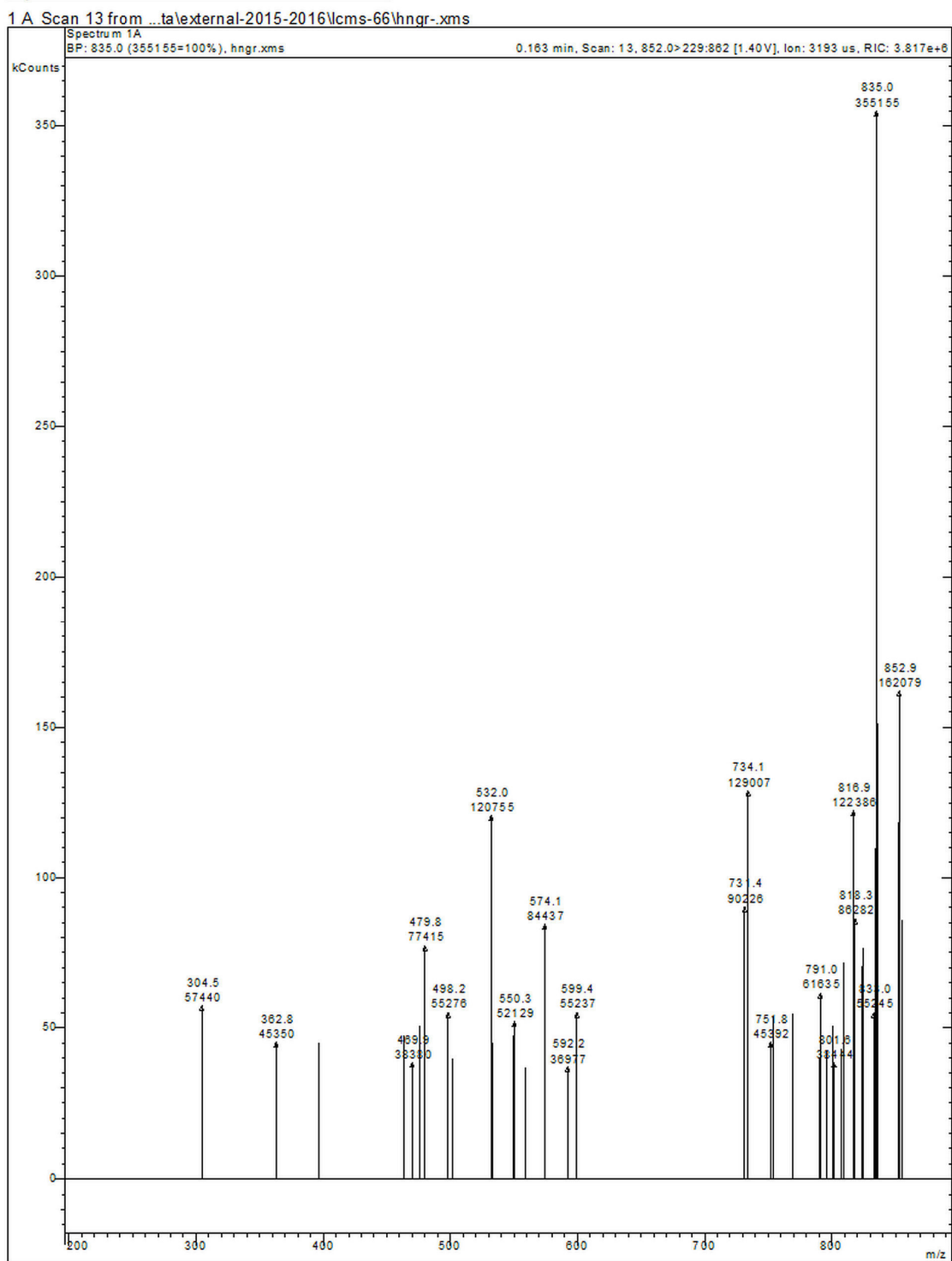


Fig 3.3. ESI-MS of HYNIC-c(NGR) (3b)

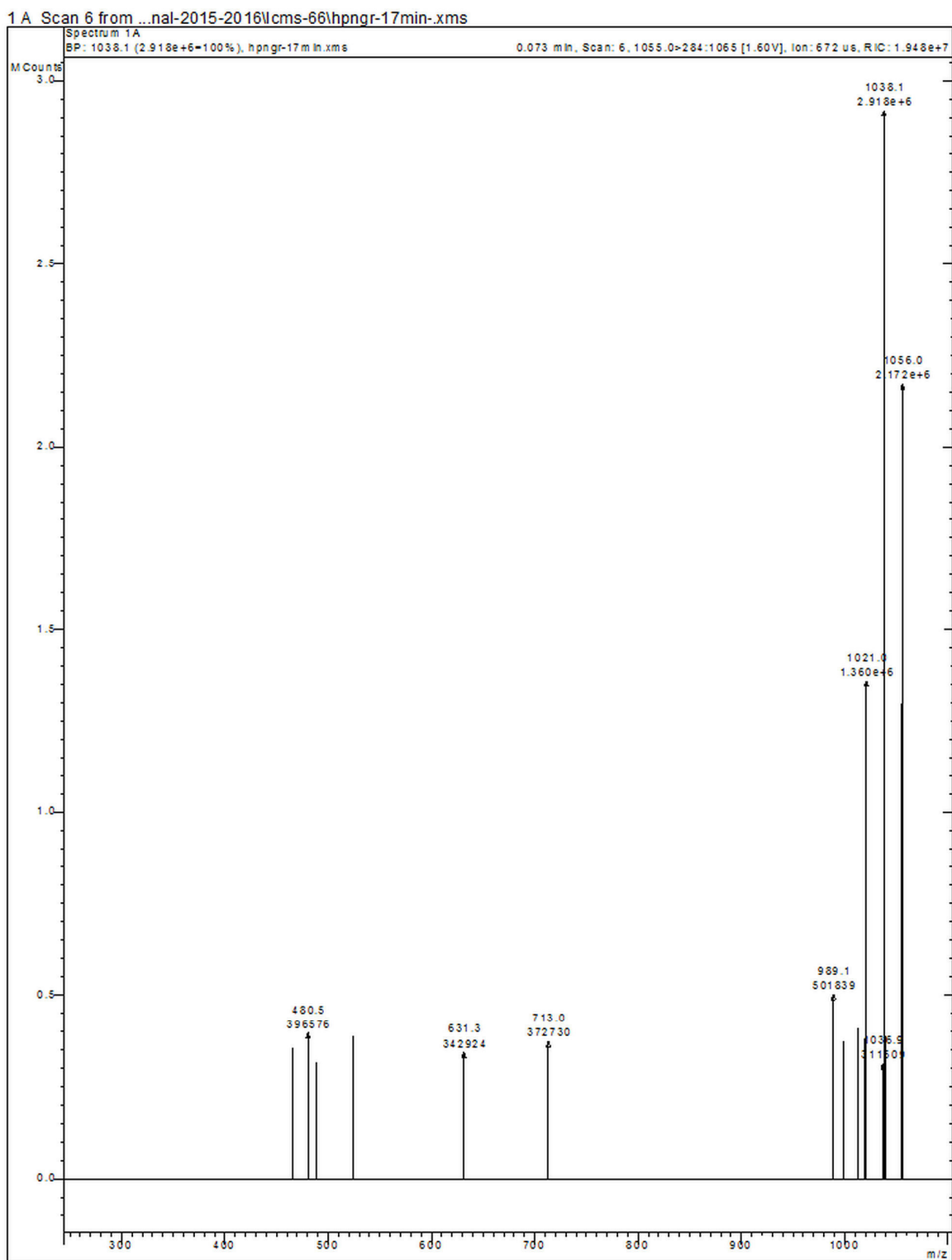


Fig 3.4. ESI-MS of HYNIC-PEG₂-c(NGR) (**3c**)

3.2.3. Radiolabeling and quality control

3.2.3.1. Preparation of ^{99m}Tc -HYNIC-c(NGR) and ^{99m}Tc -HYNIC-PEG₂-c(NGR)

The purified peptide ligands HYNIC-c(NGR) and HYNIC-PEG₂-c(NGR) were radiolabeled with ^{99m}Tc using stannous chloride (SnCl_2) as the reducing agent and EDDA and tricine as co-ligands. The peptide ligands (40 μg) were mixed with EDDA (200 μL , 50 mg/mL in 0.1N NaOH), tricine (100 μL , 200 mg/mL in distilled water), disodium hydrogen phosphate (6.4 mg), sodium dihydrogen phosphate (21 mg), $\text{Na}^{99m}\text{TcO}_4$ (500 μL , 740 MBq) and SnCl_2 (20 μg). The reaction mixture was subsequently incubated at 90°C for about 15 min. The radiochemical purity (RCP) of the radiotracers was determined by HPLC and the radiochemical yields (RCY) were determined by TLC using methanol/1M ammonium acetate (1:1) and MEK as mobile phase.

3.2.3.2. Determination of octanol-water partition coefficient ($\text{Log } P_{o/w}$)

Radiotracers (50 μL , ~3.7 MBq) were mixed with distilled water (950 μL) and *n*-octanol (1 mL) on a vortex mixer for about 1 min and then centrifuged (3500 g) for 5 min to get clear separation of the two layers. The radioactivity in 100 μL samples of both the aqueous and the organic phases was measured in a γ -counter. The experiment was repeated thrice to calculate the $\text{Log } P_{o/w}$ of radiotracers.

3.2.3.3. Stability studies

The stability of the radiotracers, ^{99m}Tc -HYNIC-c(NGR) and ^{99m}Tc -HYNIC-PEG₂-c(NGR) was tested in saline and human serum. The radiotracers were incubated in saline at 37°C till 6 h post-preparation and their stabilities were assessed by HPLC analyses. To determine serum stability, the radiotracers (50 μL) were incubated in human serum (0.5 mL) at 37°C for 6 h. 100 μL of the mixture was taken and to that 100 μL of acetonitrile was added to precipitate the

serum proteins and centrifuged at 3500 g for 10 minutes. The supernatant was analyzed by HPLC to assess the stability of the radiotracers in serum.

3.2.4. *In vitro* cell uptake studies

The human fibrosarcoma HT-1080 and breast adenocarcinoma MCF7 cells were obtained from National Center for Cell Sciences (NCCS) Pune, India. The cells were cultured in Dulbecco's Modified Eagle's Medium (DMEM) supplemented with 10% fetal calf serum (Invitrogen Carlsbad, CA) and 1% antibiotic/antimycotic formulation and were incubated at 37°C in a humidified atmosphere containing 5% CO₂. For cell uptake studies, HT-1080 cells (1×10^5) were seeded in 24-well tissue culture plates and incubated at 37°C overnight. The cells were subsequently incubated with ^{99m}Tc-HYNIC-c(NGR) and ^{99m}Tc-HYNIC-PEG₂-c(NGR) (3.5 KBq/well), at 37°C for 1 h. After incubation, cells were washed twice with ice-cold phosphate buffer saline (PBS) and the cells were harvested by trypsinization. At the end of trypsinization, wells were examined under a light microscope to ensure complete detachment of cells. Cell suspensions were collected and radioactivity associated with cells was measured in a NaI (TI) gamma counter. The activity in these cell suspensions as percentage of total input radioactivity was calculated to determine the cell uptake data. The experiment was carried out in triplicate. Specific uptake was determined by pre-incubation of cells with 100-fold excess of peptide [c(KCNGRC)]. Percentage inhibition values were calculated as $[\{\text{difference between cell binding of radiotracer in absence and presence of cold peptide}\}/\text{cell binding in absence of peptide}] \times 100$.

3.2.5. Biodistribution studies

Biodistribution studies were carried out in athymic nude mice bearing human fibrosarcoma (HT-1080) tumor. The HT-1080 human fibrosarcoma xenograft model was

generated by subcutaneous injection of 1×10^6 cells on the dorsum of athymic nude mice. After about 14 days of transplantation of the tumor cells, when the tumor size grew approximately to 300-500 mm³ in volume, the tumor bearing animals were used for the experiment. The radiotracers (~3.7 MBq/animal, 100 μ L) were injected intravenously into the tail vein of each mice (n = 4). The animals were sacrificed at different time intervals (30, 60, and 180 min), and the relevant organs excised for measurement of retained activity. For blocking studies the peptide, c(NGR) (15 mg/kg) was co-administered along with the radiotracer to determine the receptor binding specificity. The mice were sacrificed at 60 min p.i. and the organs were weighed and the activity associated with them was measured in a flat-bed type NaI(Tl) counter with suitable energy window for ^{99m}Tc. The activity retained in each organ/tissue was expressed as a percent value of the injected dose per gram (%ID/g). All the animal experiments were carried out in compliance with the relevant national laws, as approved by the local committee on the conduct and ethics of animal experimentation.

3.2.6. Data analysis

Statistical data are reported as mean \pm standard deviation (S.D.). Paired two-tailed Student's t tests were done to evaluate statistical significance, where $p < 0.05$ was considered to be statistically significant.

3.3. Results and discussion

3.3.1. Synthesis

The CD13 receptor expressions are more pronounced on tumor endothelial cells and angiogenic tumor blood vessels as against minimal or no expression on normal blood vessels making these receptors attractive molecular targets. The peptides containing NGR sequence are selective ligands towards CD13 receptors hence radiolabeled NGR peptides have potential for

molecular imaging and detection of CD13 receptor-positive tumors, tumor angiogenesis and follow the disease progression (tumor growth and metastasis).

In the present study, two HYNIC conjugated cNGR peptide ligands were synthesized, in one of the ligand HYNIC chelator was directly conjugated to the N-terminus of the peptide [HYNIC-c(NGR)] whereas in the other a PEG₂ linker was inserted between the chelator and the N-terminal of the peptide [(HYNIC-PEG₂-c(NGR))] with the hypothesis to improve the tumor uptake and retention and pharmacokinetics of the radiotracer. Pharmacokinetics of radiotracers is influenced by the charge, molecular size, spatial hindrance (steric factor) and hydrophilicity of the chelators/linkers. Polyethylene glycol (PEG) units being neutral, non-immunoreactive and hydrophilic are excellent pharmacokinetic modifiers. Small PEG units (PEG₂, PEG₃, PEG₄) conjugated with different peptides are reported to improve the tumor targeting capability and pharmacokinetics [143-145].

The NGR peptide ligands, HYNIC-c(NGR) (**3b**) and HYNIC-PEG₂-c(NGR) (**3c**) could be prepared in >99% purity by standard Fmoc solid phase synthesis method. The peptide ligands were characterized by mass spectrometry.

3.3.2. Radiolabeling

The peptide ligands HYNIC-c(NGR) (**3a**) and HYNIC-PEG₂-c(NGR) (**3b**) were radiolabeled with ^{99m}Tc using EDDA and tricine as co-ligands. Probable structures of ^{99m}Tc-HYNIC-c(NGR) and ^{99m}Tc-HYNIC-PEG₂-c(NGR) is presented in **Fig. 3.5**.

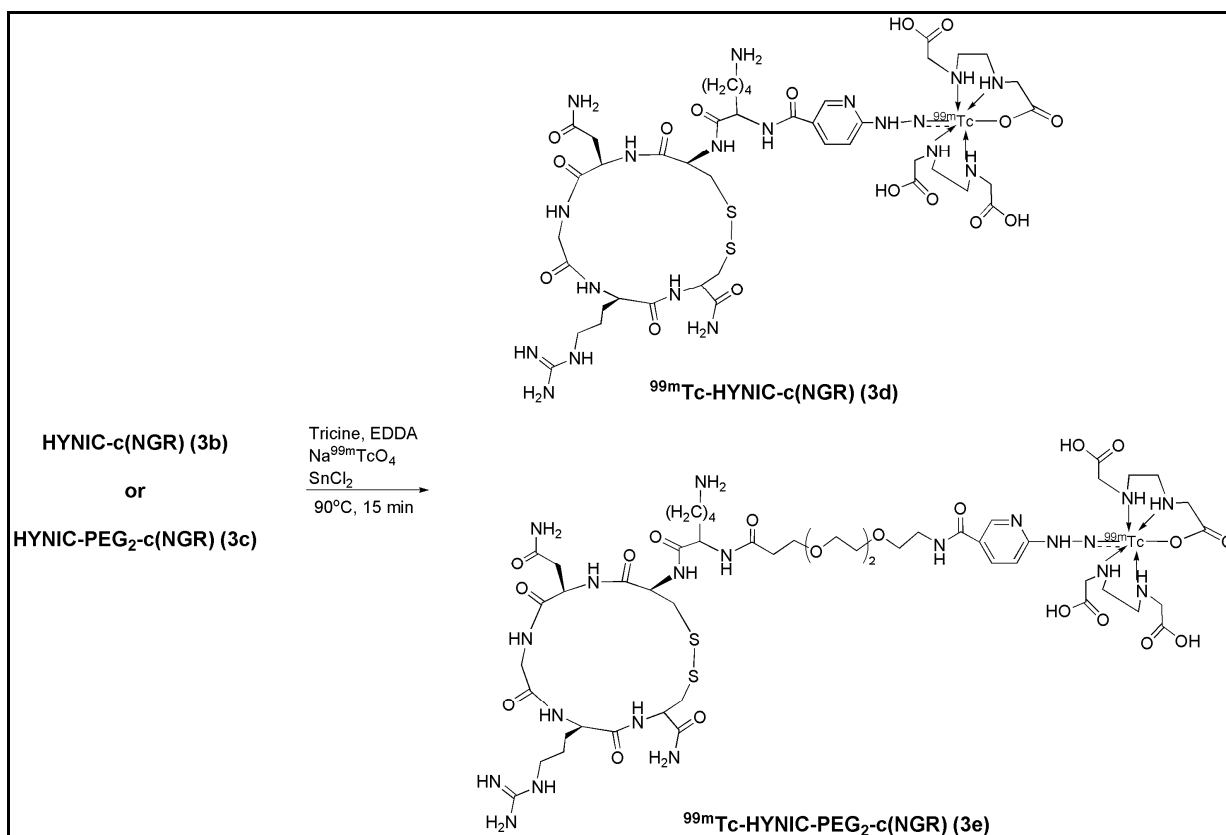


Fig. 3.5. Radiosynthesis of ^{99m}Tc-HYNIC-c(NGR) and ^{99m}Tc-HYNIC-PEG₂-c(NGR)

The two radiotracers ^{99m}Tc-HYNIC-c(NGR) and ^{99m}Tc-HYNIC-PEG₂-c(NGR) were obtained with specific activity of 14.5 GBq/μmol and 16.7 GBq/μmol respectively. Radiochemical yield of the radiotracers was determined by TLC in methanol/1M ammonium acetate (1:1) and MEK. In MEK, ^{99m}Tc-HYNIC-c(NGR), ^{99m}Tc-HYNIC-PEG₂-c(NGR) and ^{99m}TcO₂ remained at the point of spotting ($R_f = 0$) while Na^{99m}TcO₄ moved to the solvent front ($R_f = 0.9-1.0$). In 1:1 methanol/1M ammonium acetate, ^{99m}Tc-HYNIC-c(NGR), ^{99m}Tc-HYNIC-PEG₂-c(NGR) and Na^{99m}TcO₄ moved to the solvent front ($R_f = 0.8-0.9$) while ^{99m}TcO₂ remained at the point of spotting ($R_f = 0$). The radiochemical yield of ^{99m}Tc-HYNIC-c(NGR) and ^{99m}Tc-HYNIC-PEG₂-c(NGR) was thus determined to be $93.8 \pm 1.01\%$ and $96.2 \pm 0.8\%$ respectively. The RCP as determined by HPLC radiochromatograms for ^{99m}Tc-HYNIC-c(NGR) and ^{99m}Tc-HYNIC-PEG₂-

c(NGR) was $95 \pm 0.75\%$ and $97.5 \pm 1.3\%$ respectively. Radiochemical purity (RCP) of the radiotracers was analyzed by radio-HPLC chromatograms. Retention times of $^{99m}\text{TcO}_4^-$, $^{99m}\text{Tc-HYNIC-c(NGR)}$ and $^{99m}\text{Tc-HYNIC-PEG}_2\text{-c(NGR)}$ were found to be 3.6, 13.4 and 14.2 min respectively (**Fig.3.6**).

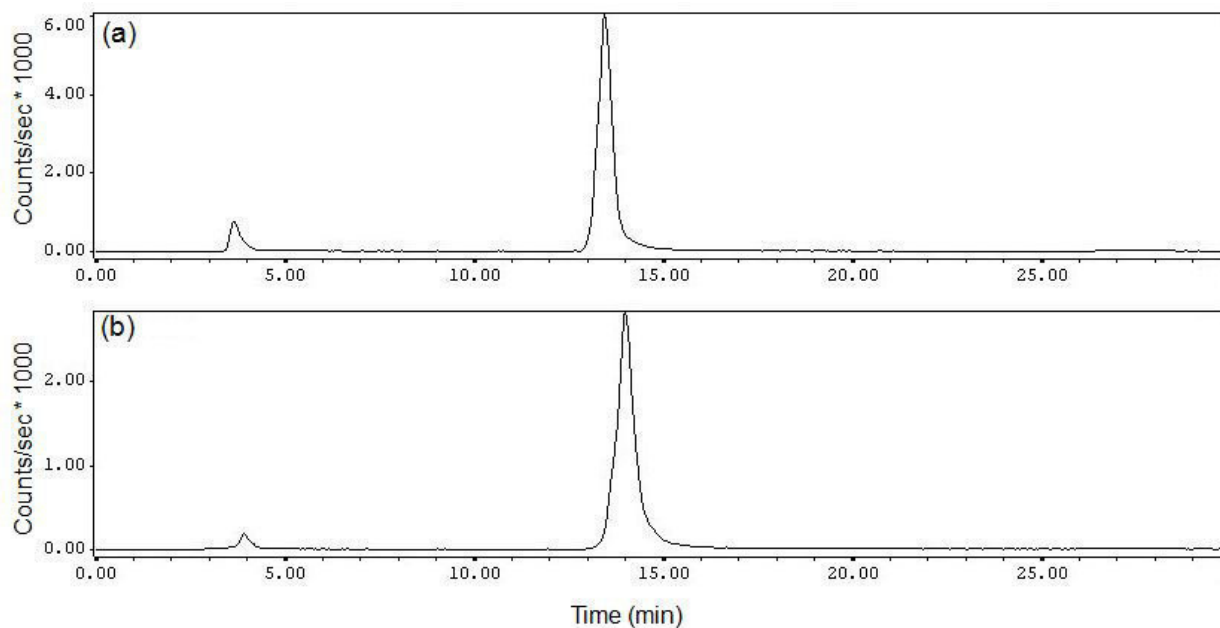


Fig.3.6. HPLC profile of (a) $^{99m}\text{Tc-HYNIC-c(NGR)}$ and (b) $^{99m}\text{Tc-HYNIC-PEG}_2\text{-c(NGR)}$

The octanol/water partition coefficient ($\text{Log } P_{o/w}$) was determined to be -2.33 ± 0.05 for $^{99m}\text{Tc-HYNIC-c(NGR)}$ and -2.61 ± 0.08 for $^{99m}\text{Tc-HYNIC-PEG}_2\text{-c(NGR)}$, suggesting that both the radiotracers are hydrophilic in nature. The radiotracers showed excellent *in vitro* stability in saline and in human serum at 6 h as determined by no change in the radiochemical purity (RCP).

3.3.3. *In-vitro* cell uptake studies

The cell uptake studies revealed similar uptake and inhibition of the two radiotracers in HT-1080 cells (**Fig.3.7**). Similar binding and inhibition pattern for the two radiotracers indicates that specific binding remained unaltered upon PEGylation. In *in-vitro* cell binding studies with

HT-1080 cells the uptake values of ^{99m}Tc -HYNIC-c(NGR) and ^{99m}Tc -HYNIC-PEG₂-c(NGR) were estimated to be $1.02\pm 0.15\%$ and $1.0\pm 0.18\%$ respectively. However, the two radiotracers exhibited negligible uptake in MCF7 cells which do not express CD13 receptors, the values being $0.18\pm 0.1\%$ for ^{99m}Tc -HYNIC-c(NGR) and $0.19\pm 0.08\%$ for ^{99m}Tc -HYNIC-PEG₂-c(NGR). The negligible accumulation of the radiotracers in CD13-negative MCF7 cells as compared to CD13 expressing HT-1080 cells indicates receptor-mediated uptake of the two radiotracers.

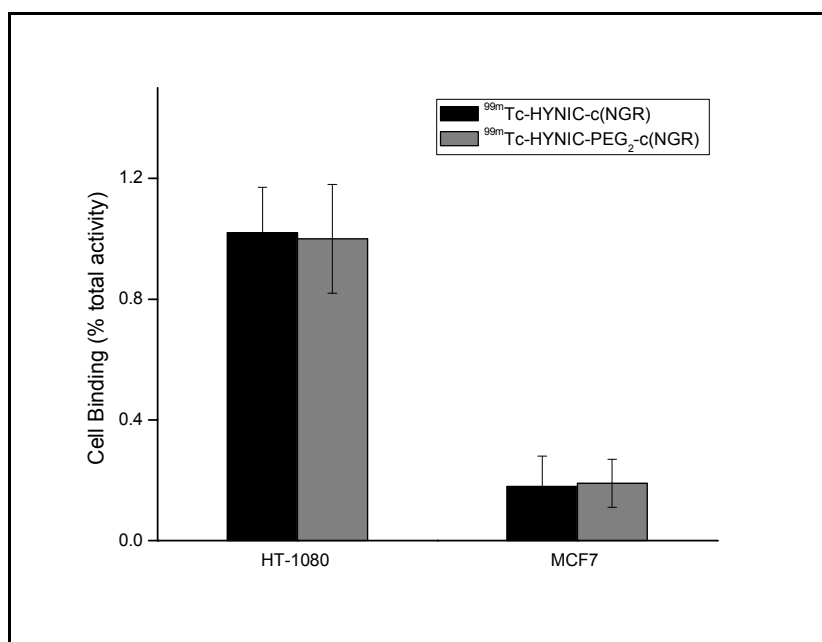


Fig.3.7. Cell binding of ^{99m}Tc -HYNIC-c(NGR) and ^{99m}Tc -HYNIC-PEG₂-c(NGR) in HT-1080 cells and MCF7 cells

3.3.4. Biodistribution studies

Results of biodistribution studies of ^{99m}Tc -HYNIC-c(NGR) and ^{99m}Tc -HYNIC-PEG₂-c(NGR) in HT-1080 tumor xenografts are summarized in **Table 3.2**.

Table-3.2: Biodistribution pattern of ^{99m}Tc -HYNIC-c(NGR) and ^{99m}Tc -HYNIC-PEG₂-c(NGR) in athymic nude mice bearing human fibrosarcoma, HT-1080 tumor

Organs	%ID/g of organ (s.d) [#]					
	^{99m}Tc -HYNIC-c(NGR)			^{99m}Tc -HYNIC-PEG ₂ -c(NGR)		
	30 min	1 h	3 h	30 min	1 h	3 h
Blood	1.70 (0.07)	0.58 (0.08)	0.27 (0.01)	1.53 (0.26)	0.66 (0.18)	0.25 (0.07)
Liver	1.14 (0.04)	0.71 (0.08)	0.61 (0.07)	0.63 (0.10)	0.42 (0.02)	0.39 (0.13)
Intestine	1.20 (0.45)	2.09 (1.16)	0.74 (0.11)	0.46 (0.09)	0.37 (0.01)	0.54 (0.20)
Stomach	0.77 (0.18)	1.70 (0.01)	0.39 (0.24)	1.78 (1.18)	1.65 (0.12)	0.46 (0.07)
Kidney	8.51 (1.22)	7.66 (1.40)	4.15 (1.11)	19.61(1.08)	16.54(2.67)	10.51(0.56)
Heart	1.30 (0.45)	0.29 (0.05)	0.25 (0.16)	0.91 (0.20)	0.29 (0.07)	0.21 (0.11)
Lungs	2.52 (0.72)	0.85 (0.26)	0.30 (0.11)	1.51 (0.25)	0.56 (0.01)	0.45 (0.14)
Spleen	0.70 (0.09)	1.11 (0.22)	0.76 (0.46)	0.62 (0.05)	0.41 (0.01)	0.43 (0.20)
Muscle	0.67 (0.08)	0.27 (0.03)	0.19 (0.05)	0.50 (0.13)	0.21 (0.01)	0.15 (0.04)
Tumor	1.55 (0.08)	0.77 (0.02)	0.68 (0.08)	1.74 (0.20)	0.86 (0.08)	0.76 (0.07)
Excretion*	59.32 (2.61)	66.27 (5.84)	82.61 (4.06)	50.83 (1.69)	59.29 (2.21)	68.87 (2.78)
Tumor/Blood	0.91 (0.01)	1.32 (0.19)	2.52 (0.13)	1.16 (0.33)	1.33 (0.26)	3.04 (0.16)
Tumor/Muscle	2.31 (0.15)	2.98 (0.35)	3.58 (0.31)	3.48 (0.35)	4.09 (0.07)	4.96 (0.59)

[#]%ID/g – Percentage injected dose per gram; s.d – standard deviation, *%Excretion has been indirectly calculated by subtracting the activity accounted for all the organs from total injected activity.

The uptake of the two radiotracers in HT-1080 tumor was observed to be maximum at 30 min p.i. being $1.55 \pm 0.08\%$ ID/g for ^{99m}Tc -HYNIC-c(NGR) and $1.74 \pm 0.2\%$ ID/g for ^{99m}Tc -HYNIC-PEG₂-c(NGR). The insertion of PEG₂ linker did not significantly affect the tumor uptake and retention. However target/non-target ratios (tumor/blood, tumor/muscle, tumor/liver)

were observed to be higher for ^{99m}Tc -HYNIC-PEG₂-c(NGR) at 3 h p.i. in comparison to that of ^{99m}Tc -HYNIC-c(NGR). The tumor/blood, tumor/muscle, tumor/liver ratios were calculated to be 2.52 ± 0.13 , 3.58 ± 0.31 , 1.11 ± 0.14 for ^{99m}Tc -HYNIC-c(NGR) and 3.04 ± 0.16 , 4.96 ± 0.59 , 1.95 ± 0.18 for ^{99m}Tc -HYNIC-PEG₂-c(NGR), at 3 h p.i. The higher hydrophilicity of ^{99m}Tc -HYNIC-PEG₂-c(NGR) led to significantly rapid clearance from liver and intestine at 30 min p.i. in comparison to that of ^{99m}Tc -HYNIC-c(NGR). However the larger molecular mass associated with PEG units is expected to result in slower renal clearance which was indeed observed for the ^{99m}Tc -HYNIC-PEG₂-c(NGR) complex. The preferential route of excretion of the two radiotracers was the renal pathway. Uptake of the two radiotracers in the non-target organs except kidneys was reduced to <1% ID/g at 3 h p.i.

The radiotracers, ^{99m}Tc -HYNIC-c(NGR) and ^{99m}Tc -HYNIC-PEG₂-c(NGR) exhibited excellent in vivo stability as inferred from the HPLC analyses of the urine sample of the nude mice bearing human fibrosarcoma (HT-1080) tumor where no degradation of radiotracers to any other species was observed at 3 h p.i. for both the radiotracers (**Fig 3.8**).

The blocking experiment carried out by co-injection of 15 mg/kg of unlabeled c(NGR) peptide, resulted in significant reduction in the tumor uptake of the two radiotracers, ^{99m}Tc -HYNIC-c(NGR): ($0.39 \pm 0.10\%$ ID/g, $p = 0.031$) and ^{99m}Tc -HYNIC-PEG₂-c(NGR) ($0.52 \pm 0.04\%$ ID/g, $p = 0.019$) at 60 min p.i. in comparison with the non-blocking group (**Fig. 3.9**). The reduction in the tumor uptake reflects CD13 receptor specificity of the two radiotracers.

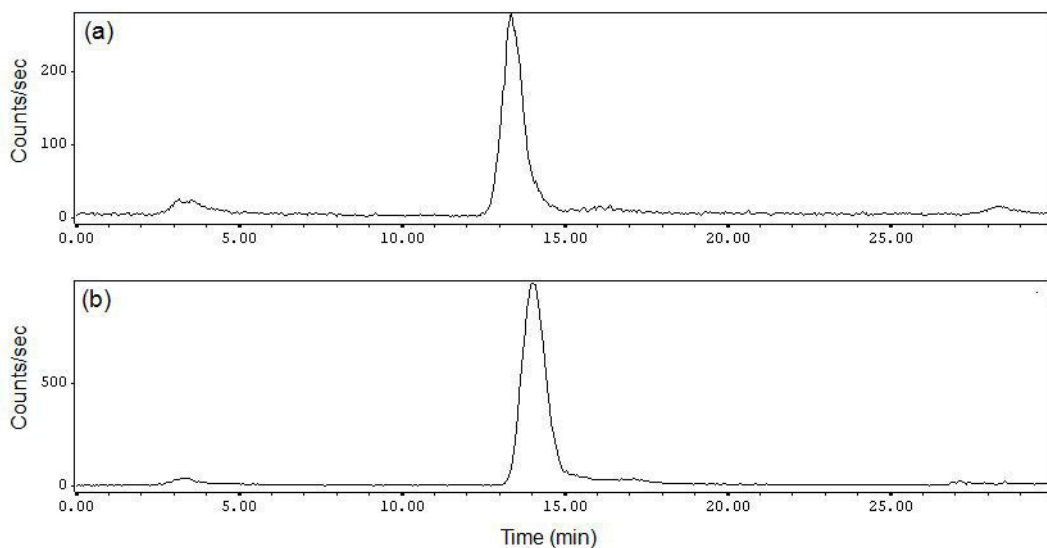


Fig. 3.8. Radio-HPLC chromatogram of (a) ^{99m}Tc -HYNIC-c(NGR) and (b) ^{99m}Tc -HYNIC-PEG₂-c(NGR) in the urine sample of nude mice bearing HT-1080 tumor at 3 h p.i.

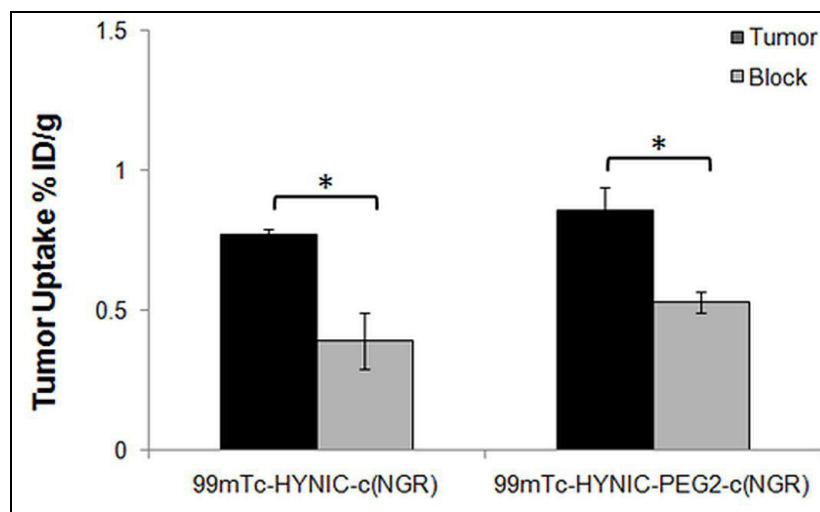


Fig.3.9. Tumor uptake of ^{99m}Tc -HYNIC-c(NGR) and ^{99m}Tc -HYNIC-PEG₂-c(NGR) in human fibrosarcoma (HT-1080) tumor with and without receptor blockade at 1 h p.i. * = statistically significant ($p < 0.05$)

Ma et al reported the biodistribution studies of NGR peptide directly labeled with ^{99m}Tc [170]. The tumor model being different, direct comparison is not possible but higher uptakes in

non-target organs, liver ($3.85 \pm 0.73\%$ ID/g), blood ($1.75 \pm 0.39\%$ ID/g) and intestine ($2.18 \pm 0.96\%$ ID/g) were observed for ^{99m}Tc -NGR even at 4 h p.i. contrary to rapid non-target clearance of presently studied radiotracers. The tumor/liver and tumor/blood ratios for ^{99m}Tc -NGR were 0.62 ± 0.33 and 0.65 ± 0.15 respectively at 1 h p.i. which are lower than those obtained for ^{99m}Tc -HYNIC-c(NGR) and ^{99m}Tc -HYNIC-PEG₂-c(NGR). The tumor/muscle ratio for ^{99m}Tc -NGR was 4.75 ± 0.91 at 1 h p.i. which is comparable with that of ^{99m}Tc -HYNIC-PEG₂-c(NGR). The radiotracer ^{99m}Tc -MAG₃-PEG₈-c(NGRyk) studied by Oliveira et al [171] displayed higher intestinal (small + large intestine) levels ($\sim 4\%$ ID/g at 1 h p.i.) whereas higher renal retention was observed for ^{99m}Tc -HYNIC-c(NGR) and ^{99m}Tc -HYNIC-PEG₂-c(NGR). Difference in the chelator, number of PEG units and amino acid sequence are possibly responsible for the difference in the retention in the excretory organs (intestine and kidneys). Kim et al had studied the biodistribution of ^{99m}Tc -ECG-NGR in HT-1080 human fibrosarcoma tumor model [172]. The tumor uptake values for ^{99m}Tc -ECG-NGR were 1.66 ± 0.67 and 0.95 ± 0.39 at 1 h and 4 h p.i. respectively. The radiotracer, ^{99m}Tc -ECG-NGR exhibited slower clearance from blood with the tumor/blood ratio of 0.57 and 1.0 at 1 h and 4 h respectively which is lower than the tumor/blood ratio obtained for ^{99m}Tc -HYNIC-c(NGR) and ^{99m}Tc -HYNIC-PEG₂-c(NGR). The tumor/muscle ratios at 1 h and 4 h p.i. for ^{99m}Tc -ECG-NGR were 3.2 and 5.2 respectively which are comparable with our results

3.4. Conclusion

Two novel NGR peptide conjugates HYNIC-c(NGR) and HYNIC-PEG₂-c(NGR) were synthesized and radiolabeled with ^{99m}Tc using EDDA/tricine as coligands in high radiochemical yield and purity. Both the radiotracers exhibited excellent *in vitro* and *in vivo* stability. The two radiotracers, ^{99m}Tc -HYNIC-c(NGR) and ^{99m}Tc -HYNIC-PEG₂-c(NGR) exhibited receptor

mediated uptake in HT-1080 cells *in vitro* as well as HT-1080 tumor *in vivo*. The target-to-non-target ratios (tumor-to-blood, tumor-to-liver) of presently studied radiotracers were observed to be better with respect to the ^{99m}Tc -labeled NGR peptides reported in literature. However rapid washout of tumor-associated activity was observed for the radiotracers, ^{99m}Tc -HYNIC-c(NGR) and ^{99m}Tc -HYNIC-PEG₂-c(NGR). The PEG₂ introduced as the pharmacokinetic modifier did not significantly increase the tumor uptake and retention. Thus, future studies will be emphasized on introduction of a longer PEG unit or a hydrophobic linker in order to improve the tumor-targeting properties while retaining the favourable tumor-to-background ratio.

CHAPTER 4

**PREPARATION OF ^{99m}Tc -‘4+1’ MIXED LIGAND COMPLEXES OF
NITROIMIDAZOLE LIGANDS FOR TARGETING TUMOR HYPOXIA**

4.1. Introduction

Chapter 4 describes the use of ‘4+1’ mixed ligand strategy to design ^{99m}Tc -radiotracers for the detection of *in vivo* tissue hypoxia. The strategy used for ^{99m}Tc -labeling herein, is using the tripodal tetradentate NS_3 chelator and nitroimidazole-isocyanide as the monodentate ligand. The role of nitroimidazoles in targeting tumor hypoxia, synthesis of isocyanide derivatives of 2-nitroimidazole and metronidazole (2-NimNC and MetNC), their radiolabeling with ^{99m}Tc via ‘4+1’ mixed ligand strategy and preliminary bioevaluation studies have been discussed.

4.1.1. Hypoxia

Tissue hypoxia is a pathophysiological condition in which the demand for oxygen by the tissue exceeds the supply it receives. Hypoxic tissues are hallmark of certain solid tumors in advanced stage [177,178]. Hypoxic regions in solid tumors are a result of available oxygen being consumed within 70 to 150 μm of tumour vasculature by rapidly proliferating tumor cells thus limiting the amount of oxygen available to diffuse further into the tumor tissue [179,180]. Presence of hypoxic regions in tumors is one of the major reasons for the resistance to conventional radiotherapy and chemotherapy [181,182]. The decrease in the response to radiotherapy of hypoxic cells then leads to an increased risk of metastasis and poor prognosis for the patient [183-187]. Detection of hypoxia and its extent in cancerous lesions therefore help physicians in patient selection for hypoxia-directed treatment and to plan a treatment regime towards a better clinical outcome.

There are several methods to detect and quantify hypoxia in tumor which can be broadly classified under invasive and non-invasive categories. Due to the inherent drawbacks of invasive techniques [188], non-invasive techniques are a preferred choice. Among the non-invasive techniques, nuclear medicine based on the administration of small amount of

radiopharmaceuticals, followed by the detection of the radiation escaping from the body, is considered to be the most promising modality due to high sensitivity and ability to provide functional information of organs/tissue [7,8,188].

Hypoxia detection by a radiopharmaceutical is based on the oxygen dependent chemical modification of the radiotracer, which will lead to selective accumulation in hypoxic cells thus delineating them from normal cells. Radiopharmaceuticals for hypoxia detection can be classified as nitroimidazole based and non-nitroimidazole based radiopharmaceuticals [189]. A brief discussion on nitroimidazoles and nitroimidazole based radiopharmaceuticals is presented in the following sections.

4.1.2. Nitroimidazoles as hypoxia markers

Nitroimidazoles which undergo selective oxygen-dependent reduction and accumulation in hypoxic tumor cells have received most attention as bioactive moiety for targeting hypoxia [190,191]. Nitroimidazoles are substituted imidazoles which are planar and pi-electron rich heteroaromatic compounds. 2-nitroimidazole (azomycin) was the first nitroimidazole isolated from a natural source and was originally found to be an antibiotic against anaerobic bacteria and protozoa [192,193]. Its selective toxicity was determined by biological reduction to the reactive species in the absence of oxygen [194]. This particular behaviour of nitroimidazole derivatives in oxygen deficient environment led to their study in the detection of hypoxia [195,196]. The mechanism underlying hypoxia selectivity demonstrated by nitroimidazole involves a series of one-electron reductions mediated by nitro-reductase enzymes present in the cells [180,181]. Initial step in the nitroimidazole reduction process involves the formation of nitroimidazole radical anion. In normoxic cells where due to the presence of sufficient oxygen concentration the radical anion is quickly oxidized to its initial state and after conversions several times between

oxidized and reduced states the molecule diffuses out of the cell. However, in hypoxic cells the low oxygen concentration is not able to effectively compete with the reoxidation of the molecule and further reduction of the nitroimidazole radical anion takes place which results in trapping of the metabolites in the cells (**Fig 4.1**).

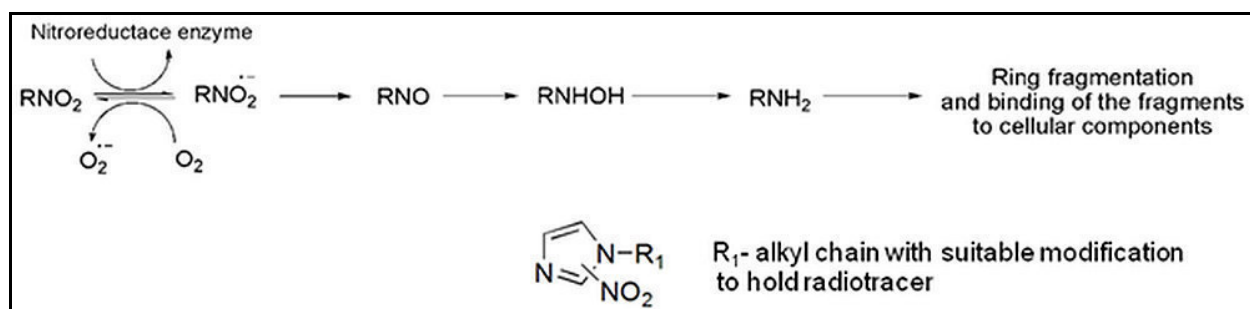


Fig. 4.1. Schematic representation of reduction of nitroimidazole

The single electron reduction potential (SERP) is an important molecular parameter, which determines the efficiency of reduction of nitroimidazoles in hypoxic cells. Among differently substituted nitroimidazoles, viz. 2-, 4- and 5-nitroimidazoles, owing to the more positive SERP, the 2-nitroimidazole was found to be most suitable for targeting hypoxic tissues [197,198]. The SERP values of 2-, 4- and 5-nitroimidazoles are in the order -418 mV, -527 mV and -450 mV, respectively, with respect to the standard hydrogen electrode.

4.1.3. Nitroimidazole radiopharmaceuticals:

Several nitroimidazoles radiopharmaceuticals labeled with PET or SPECT radioisotope have been evaluated for in vivo detection of hypoxia [198-206]. At present, [¹⁸F]Fluoromisonidazole ([¹⁸F]FMISO), a 2-nitroimidazole derivative, is the radiopharmaceutical of choice for the clinical imaging of tumor hypoxia [207]. Apart from [¹⁸F]FMISO, various other ¹⁸F-labeled agents which have been evaluated clinically are [¹⁸F]FAZA [¹⁸F]fluoroazomycin

arabinofuranoside), [^{18}F]FETNIM ([^{18}F]fluoroerythronitroimidazole), [^{18}F]FETA (^{18}F fluoroetanidazole) etc.[208,209]. Among the SPECT radiopharmaceuticals, BMS181321 and BRU59-21 are the two important $^{99\text{m}}\text{Tc}$ -based radiotracers clinically evaluated for the detection of tissue hypoxia [210,211]. However, both of them are highly lipophilic and exhibited poor target to non target ratio when tested in vivo.

Though, [^{18}F]Fluoromisonidazole ([^{18}F]FMISO) is currently the agent of choice for clinical detection of tumor hypoxia, its use is limited by number of PET centers and cyclotrons. Owing to a larger number of SPECT centers, a $^{99\text{m}}\text{Tc}$ -radiopharmaceutical for this purpose may find wider applicability. There are a number of $^{99\text{m}}\text{Tc}$ -labeled nitroimidazole radiopharmaceuticals prepared and evaluated for detecting hypoxia [203-206], however none has so far matched the pharmacokinetics of [^{18}F]FMISO, the gold standard in terms of the clinical utility. This factor provided the necessary impetus for investigating new $^{99\text{m}}\text{Tc}$ -labeled nitroimidazole radiotracer for targeting tumor hypoxia.

It has been observed from the previous studies that overall efficacy of a nitroimidazole radiotracer depends not only on SERP but other molecular parameters such lipophilicity, charge of the complex etc [212,213]. Lipophilicity plays an important role in promoting the intracellular accumulation of the radiolabeled agents via passive diffusion pathway, as more lipophilic complexes will have greater affinity for lipid bilayer of the cell membrane. The overall charge of the complex (positive, negative and neutral) on the other hand will be the determining factor for the overall pharmacokinetic behavior of the radiopharmaceutical [204,205]. In the present work, $^{99\text{m}}\text{Tc}$ -‘4+1’ mixed ligand approach is used to prepare neutral lipophilic complexes of nitroimidazole derivatives for targeting tumor hypoxia.

One of the studies involving the evaluation of a number of nitroimidazole complexes labeled with ^{99m}Tc had shown that residence time of the radiotracer in hypoxic cells is an important parameter, which decides the overall efficacy of the radiotracer in vivo [205]. Lipophilicity and charge on the complex had a strong influence on the residence time of the complex in hypoxic cells. It was observed that a complex with more positive SERP value, for example, a 2-nitroimidazole complex of ^{99m}Tc , need not be always effective to target hypoxic cells in vivo, if its residence time in tumor is less. On the contrary, it may be possible that a nitroimidazole complex with SERP value lower than 2-nitroimidazole, shows better uptake in hypoxic cells. Therefore, in addition to a derivative of 2-nitroimidazole, a derivative of metronidazole, a common anti-microbial agent containing a 5-nitroimidazole moiety is also included in the present study.

4.2. Experimental

4.2.1. Materials and methods

2-Nitroimidazole, *tert*-butyl-N-(3-bromopropyl)carbamate, anhydrous potassium carbonate, phenyl dichlorophosphate, triethylamine, dimethylphenylphosphine, ammonium perrhenate, triethanolamine, potassium thioacetate and ethylenediaminetetraacetic acid disodium salt were procured from M/s. Sigma Aldrich, USA. Metronidazole was procured from Acros Organics, USA. Ethyl formate and thionyl chloride were purchased from S. D. Fine Chemicals, India. Sodium pertechnetate ($\text{Na}^{99m}\text{TcO}_4$) was obtained from $^{99}\text{Mo}/^{99m}\text{Tc}$ generator built in-house. Silica gel plates (silica gel 60 F₂₅₄) used for thin layer chromatography (TLC) as well as silica gel (60–120 mesh) used for column chromatography were obtained from Merck, India. IR spectra were recorded on JASCO-FT/IR-420 spectrometer, Japan. ^1H -NMR and ^{13}C -NMR (^1H decoupled) spectra were recorded using 300 MHz Bruker Avance II, spectrometer, Germany.

Mass spectra of the rhenium complexes were recorded on high-resolution mass spectrometer, Bruker MicroTOFQ-2, Germany. Mass spectra of other ligands were recorded on Advion Mass Spectrometer, USA using electron spray ionization (ESI) in positive mode. The HPLC analyses were performed on a JASCO PU 2080 Plus dual pump HPLC system, Japan, with a JASCO 2075 Plus tunable absorption detector and a Gina Star radiometric detector system, using a C18 reversed phase HiQ Sil column (5 μm , 4 x 250 mm). Radioactivity distribution on TLC strips was recorded on MiniGITA γ -radioactivity TLC scanner, obtained from Raytest, Germany. All the solvents used for HPLC were degassed and filtered prior to use and were of HPLC grade. Cyclic voltammograms were recorded on a CH instrument (CHI760D), USA.

4.2.2. Synthesis

Synthesis of tetradentate ligand 2,2',2''-nitrilotriethanethiol (NS₃):

Synthesis of tripodal tetradentate NS₃ ligand was carried out in three steps following a reported procedure [93]. Scheme for synthesis of NS₃ ligand is presented in **Fig 4.2**.

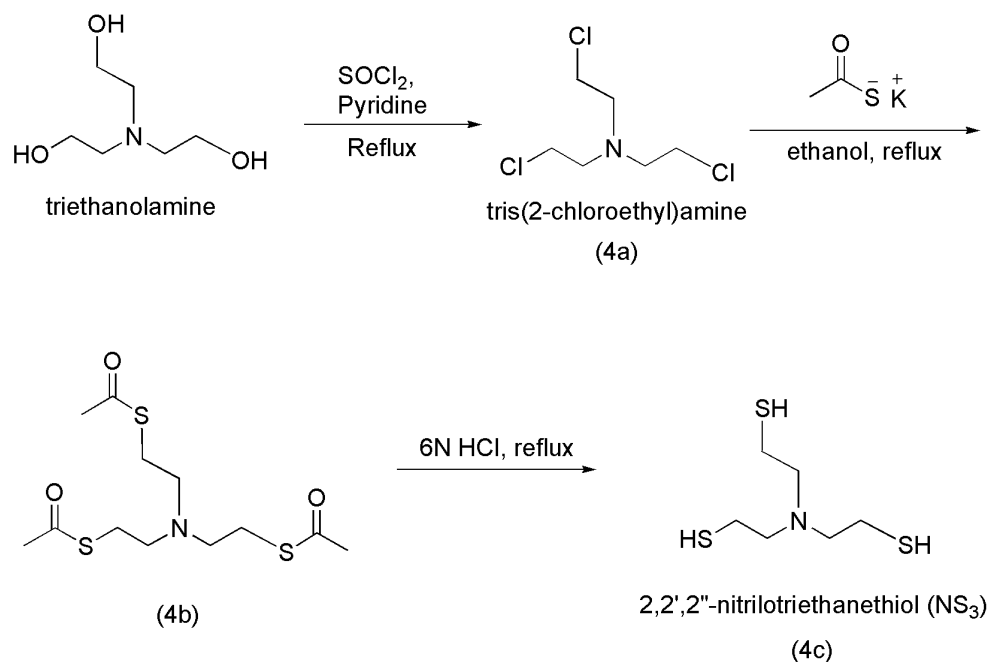


Fig. 4.2 Synthesis scheme of tetradentate ligand (NS₃)

4.2.2.1. Synthesis of tris(2-chloroethyl)amine (4a)

To a solution of triethanolamine (2.24 g, 15 mmol) in pyridine (2.5 mL), thionyl chloride (6.5 mL, 90 mmol) was added and the reaction mixture was stirred overnight at room temperature. After completion of reaction it was treated with 30% Na₂CO₃ and extracted with diethyl ether. Combined organic extracts were pooled together, concentrated and purified by silica gel column chromatography to obtain compound **4a**. R_f = 0.7 (chloroform); IR (neat, $\nu_{\max}/\text{cm}^{-1}$): 2956 (m), 2840 (m), 1450 (s), 1307 (m), 1256 (m), 1108 (s), 940 (w), 735 (s), 657 (s). ¹H-NMR (δ ppm, CDCl₃): 3.00 (t, $J = 6.8$, 6H), 3.54 (t, $J = 6.8$ Hz, 6H).

4.2.2.2. Synthesis of tris(S-ethylethanethioate)amine (4b)

Compound **4a** (500 mg, 2.44 mmol) was refluxed with potassium thioacetate (1.67g, 14.64 mmol) in 10 mL of ethanol for 6 h. Thereafter, the solvent was removed under vacuum and the residue was dissolved in 1 M KOH solution. The aqueous layer was extracted with diethylether (15 mL x 3) and combined ether extracts were pooled together and dried under vacuum. The crude product obtained was purified by silica gel column chromatography to obtain compound **4b**. R_f = 0.25 (hexane/ethyl acetate); IR (neat, $\nu_{\max}/\text{cm}^{-1}$): 2956 (m), 2840 (m), 1687 (s), 1423 (s), 1360 (m), 1114 (s), 953 (m). ¹H-NMR (δ ppm, CDCl₃) 2.33 (s, 9H), 2.71 (t, $J = 6.9$ Hz, 6H), 2.95 (t, $J = 6.9$ Hz, 6H) (**Fig 4.3**). ESI-MS: mass (calculated) C₁₂H₂₁NO₃S 323.5; m/z (observed) 324.6 [M+H]⁺ (**Fig 4.4**).

4.2.2.3. Synthesis of 2,2',2''-nitrilotrisethanethiol (NS₃) (4c)

Compound **4b** was dissolved in 6 N HCl and the solution was refluxed for overnight with continuous stirring. Subsequently, the solvent was removed under vacuum to obtain compound **4c**. IR (KBr, $\nu_{\max}/\text{cm}^{-1}$): 2946 (m), 2840 (m), 2539 (br,s), 1451 (m). ESI-MS: mass (calculated) MS(ESI): C₆H₁₅NS₃ 197.0 m/z (observed) 196.0 [M-H]⁻ (**Fig 4.5**).

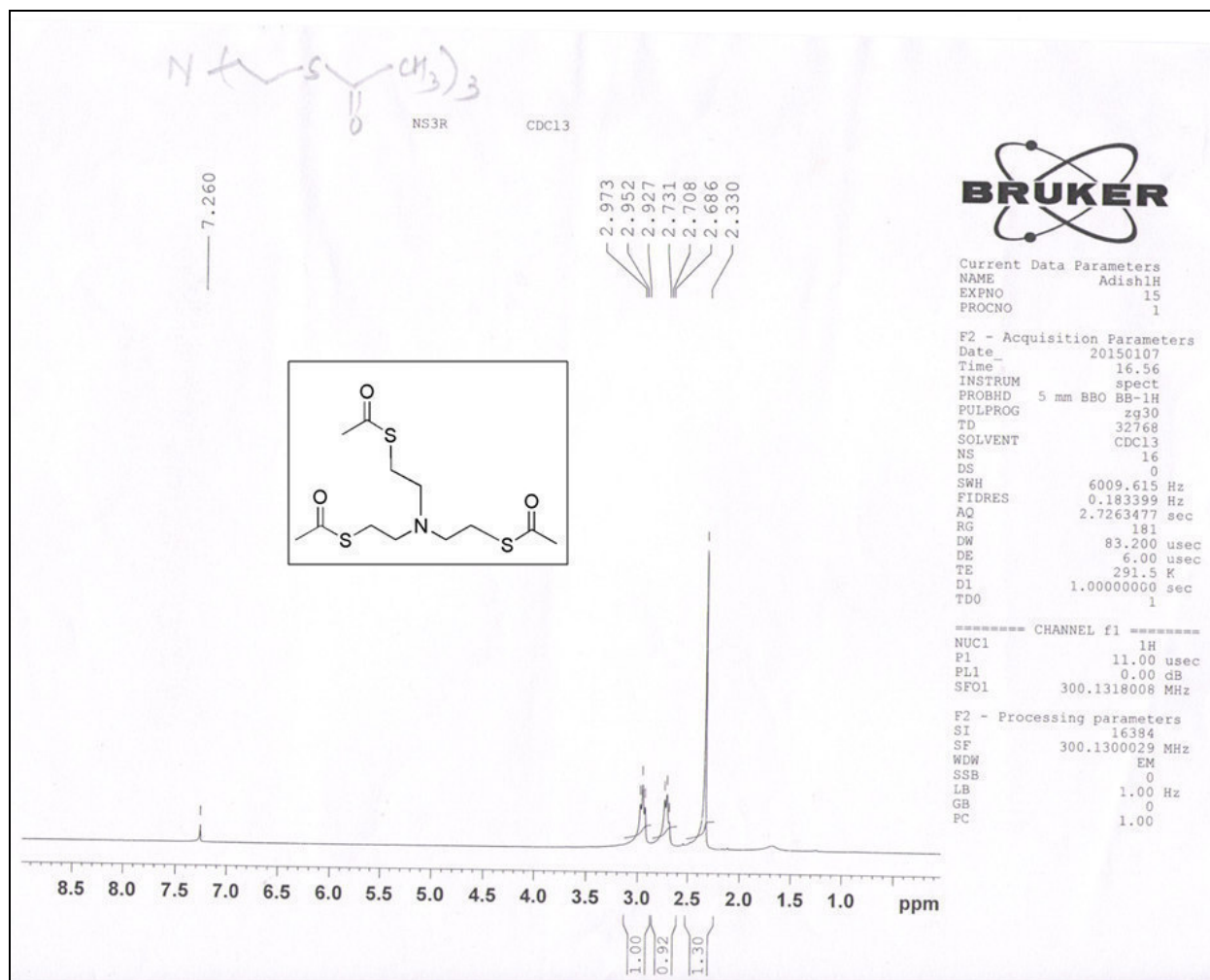


Fig. 4.3. $^1\text{H-NMR}$ spectra of tris(*S*-ethylethanethioate)amine (**4b**)

Spectrum Plot - 6/19/2013 1:17 PM

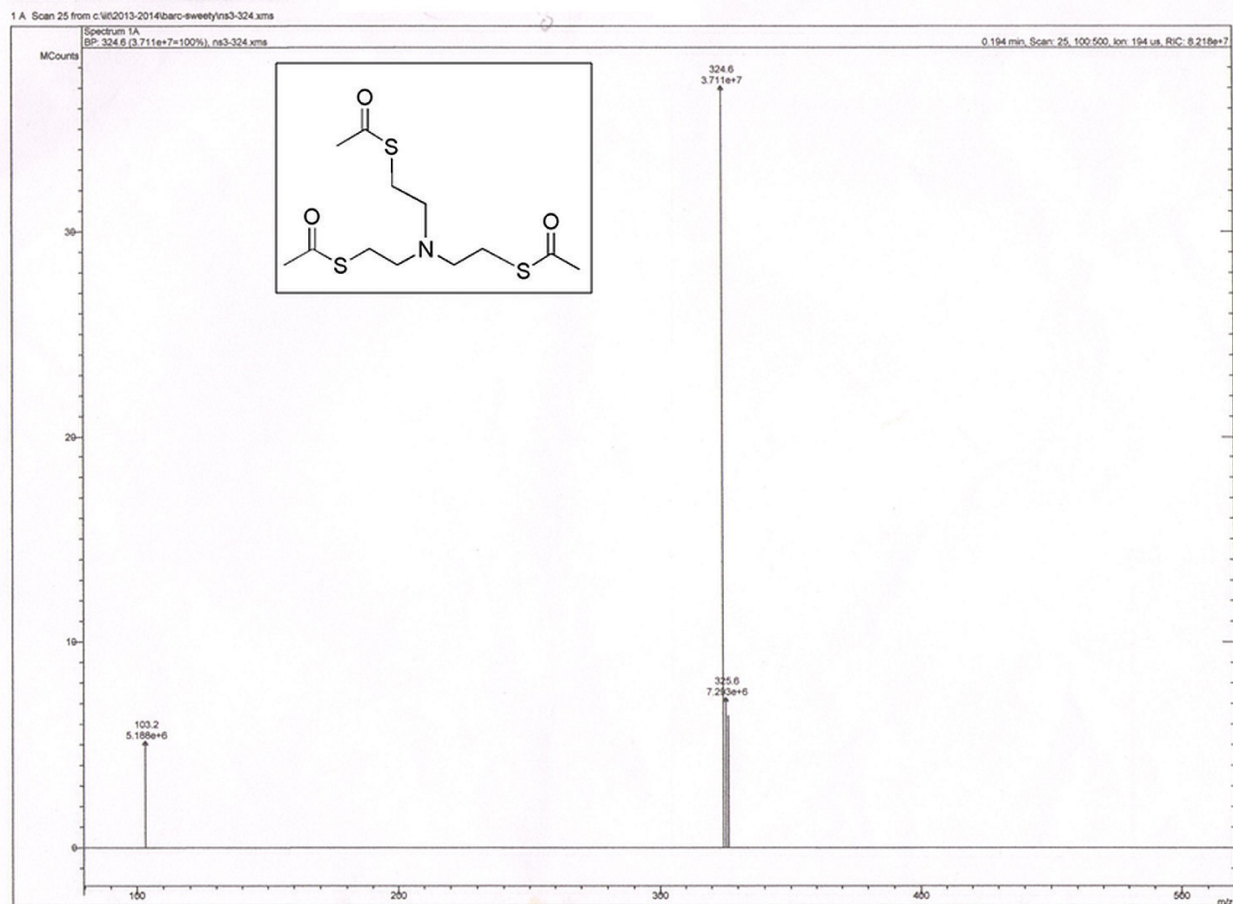


Fig. 4.4. ESI-MS of tris(*S*-ethylethanethioate)amine (**4b**)

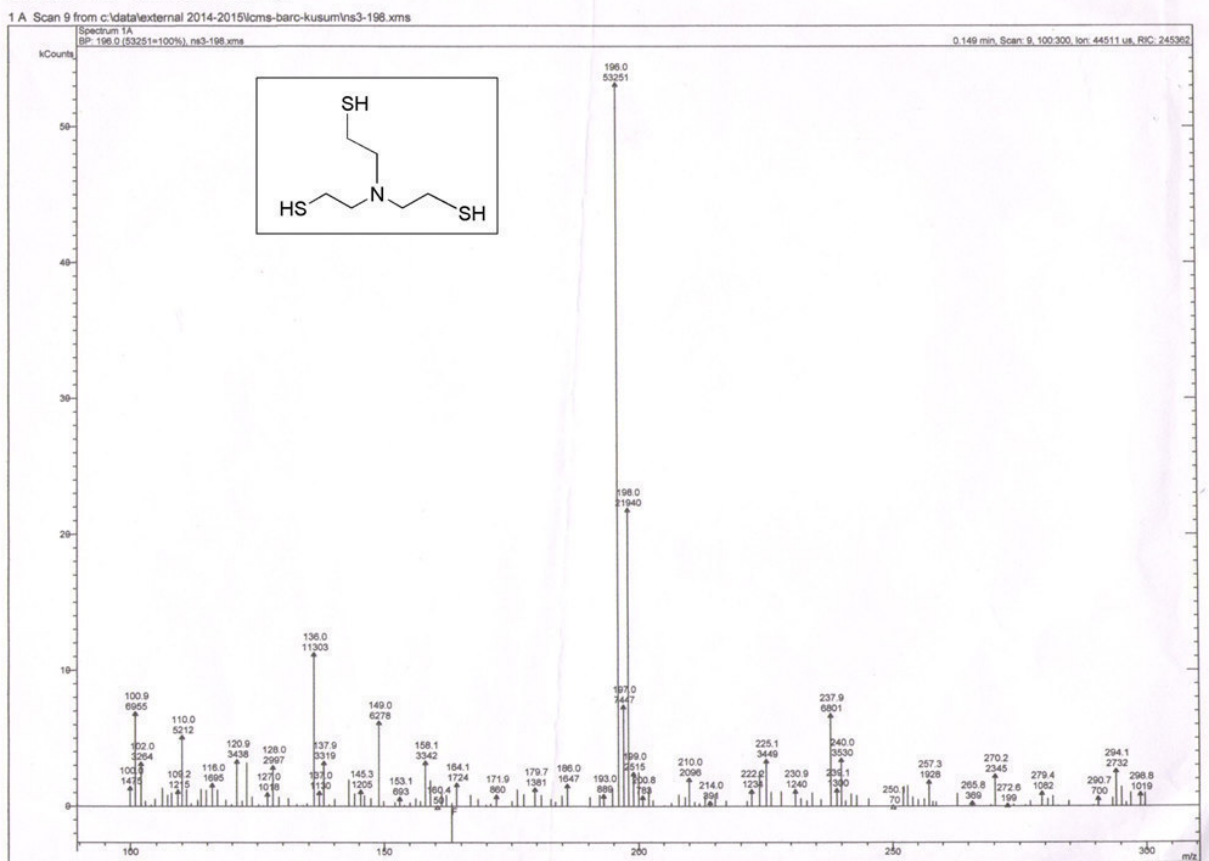


Fig. 4.5. ESI-MS of 2,2',2''-nitrilotrisethanethiol (NS₃) (**4c**)

Synthesis monodentate isocyanide ligands (2NimNC and MetNC)

4.2.2.4. Synthesis of *tert*-Butyl-3-(2-nitro-1*H*-imidazol-1-yl)propylcarbamate (**4d**)

2-nitroimidazole (0.17 g, 1.5 mmol), *tert*-butyl N-(3-bromopropyl)carbamate (0.33 g, 1.36 mmol) and crushed anhydrous K₂CO₃ were refluxed in acetonitrile (10 mL) for 20 h with continuous stirring. Thereafter, the solvent was removed under vacuum and the residue was dissolved in water (30 mL). The aqueous layer was extracted with chloroform (15 mL x 3). Combined organic extracts were pooled together, concentrated and purified by silica gel column chromatography to obtain compound **4d** (0.32 g, 82%). R_f = 0.4 (ethyl acetate). IR (neat,

$\nu_{\max}/\text{cm}^{-1}$: 3336(m); 3111 (m); 2971(s); 2929 (m); 1694(s); 1536 (s); 1493 (s); 1451 (m); 1366 (s); 1268 (s); 1250 (m); 1164 (m); ^1H NMR (δ ppm, CDCl_3): 1.41 (s, 9H), 2.02 (quin, 2H, $J = 6.9$, $-\text{CH}_2\text{CH}_2\text{CH}_2\text{NHBoc}$), 3.18 (q, 2H, $J = 6.9$ Hz, $-\text{CH}_2\text{CH}_2\text{CH}_2\text{NHBoc}$), 4.44 (t, 2H, $J = 6.9$ Hz, $-\text{CH}_2\text{CH}_2\text{CH}_2\text{NHBoc}$), 7.10 (s, 1H, 2-nitroimidazole-C5-H), 7.28 (s, 1H, 2-nitroimidazole-C4-H) (**Fig 4.6**); ^{13}C NMR (δ ppm, CDCl_3): 28.3 ($(\text{CH})_3\text{C}$), 31.3 ($-\text{CH}_2-\text{CH}_2-\text{NH}$), 37.3 ($-\text{CH}_2-\text{CH}_2-\text{NH}$), 47.6 ($\text{Ar}-\text{CH}_2-\text{CH}_2-$), 79.7 ($(\text{CH})_3\text{C}-\text{O}$), 126.3 (imidazole $\text{N}=\text{C}(\text{NO}_2)-\text{N}-\text{CH}_2-\text{CH}_2$), 128.3 (imidazole $\text{N}=\text{C}(\text{NO}_2)-\text{N}-\text{CH}_2-\text{CH}_2$), 144.8 (imidazole $\text{N}=\text{C}(\text{NO}_2)-\text{N}-\text{CH}_2-\text{CH}_2$), 156.2 ($-\text{NH}-\text{C}=\text{O}(\text{O})$). ESI-MS (+ve mode): mass (calculated) $\text{C}_{11}\text{H}_{18}\text{N}_4\text{O}_4$ 270.1; m/z (observed) 271.1 $[\text{M}+\text{H}]^+$.

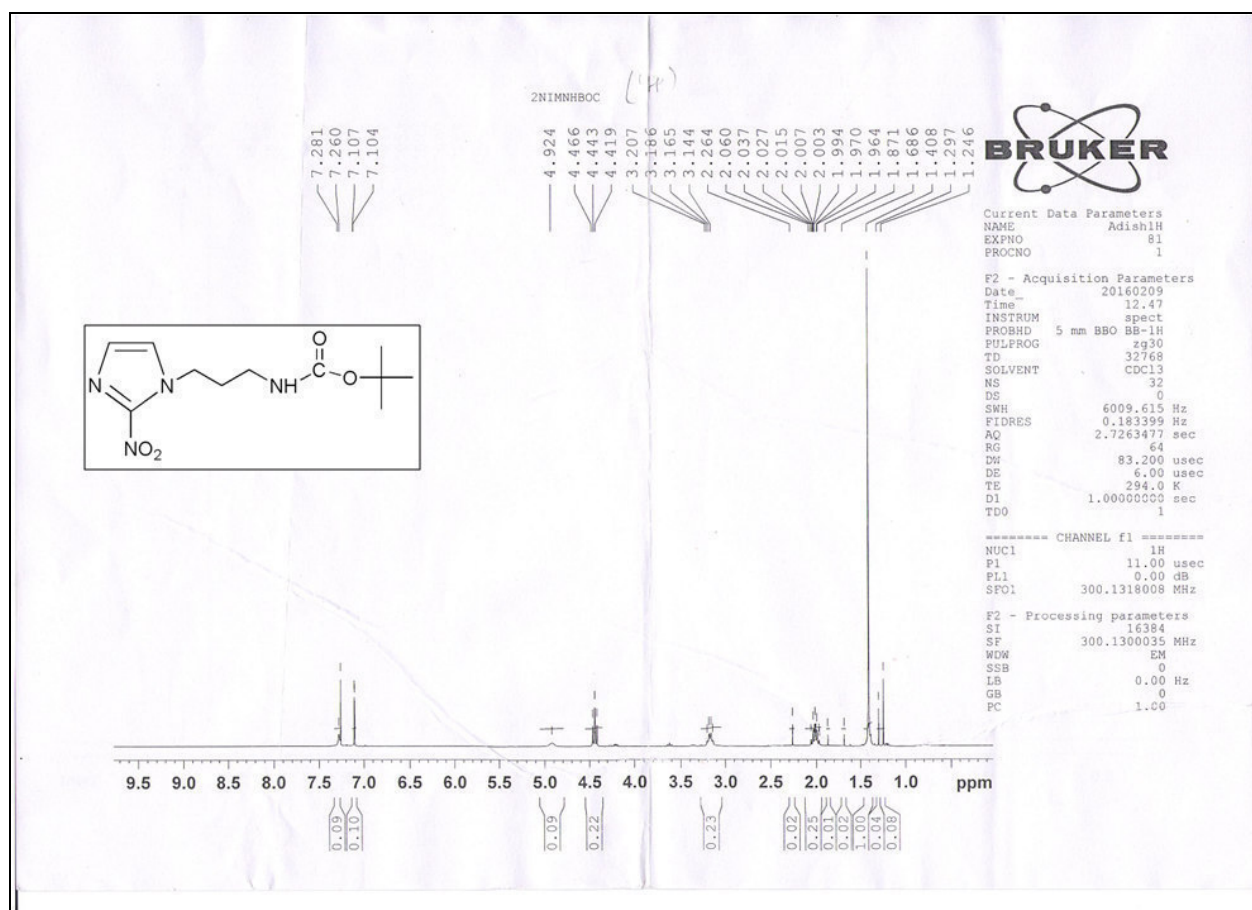


Fig. 4.6. ^1H -NMR spectra of tert-Butyl-3-(2-nitro-1H-imidazol-1-yl)propylcarbamate (**4d**)

4.2.2.5. Synthesis of 3-(2-nitro-1H-imidazol-1-yl)propan-1-amine hydrochloride (4e)

Compound **4d** (0.32 g, 1.18 mmol) was dissolved in methanol (2 mL) and 6 N HCl (5 mL). This solution was heated at 50°C for 12 h with continuous stirring. Thereafter, the solvent was removed under vacuum to obtain compound **4e** in quantitative yield as hydrochloride salt. IR (KBr, $\nu_{\max}/\text{cm}^{-1}$): 3098 (m); 2971 (s); 2929 (m); 1536 (s); 1508 (s); 1488 (s); 1356 (s); 1278 (m); 1158 (m); ^1H NMR (δ ppm, D_2O): 1.96 (quin, 2H, $J = 6.8$ Hz, $-\text{CH}_2\text{CH}_2\text{CH}_2\text{NH}_2\cdot\text{HCl}$), 3.04 (t, 2H, $J = 6.8$ Hz, $-\text{CH}_2\text{CH}_2\text{CH}_2\text{NH}_2\cdot\text{HCl}$), 4.41 (t, 2H, $J = 6.8$ Hz, $-\text{CH}_2\text{CH}_2\text{CH}_2\text{NH}_2\cdot\text{HCl}$), 7.09 (s, 1H, 2-nitroimidazole-C5-H), 7.37 (s, 1H, 2-nitroimidazole-C4-H); ^{13}C NMR (δ ppm, D_2O): 29.4, 37.2, 47.8, 128.0, 148.7, 158.2. ESI-MS (+ve mode): mass (calculated) $\text{C}_6\text{H}_{10}\text{N}_4\text{O}_2$ 170.1; m/z (observed) 171.1 $[\text{M}+\text{H}]^+$.

4.2.2.6. Synthesis of N-(3-(2-nitro-1H-imidazol-1-yl)propyl)formamide (4f)

Compound **4e** (0.20 g, 0.97 mmol) and triethylamine (0.59 g, 6 mmol) were dissolved in ethylformate (10 mL) and the reaction mixture was refluxed for 8 hours [214]. Thereafter, excess of ethylformate was removed under vacuum and the crude product obtained was further purified by silica gel column chromatography to obtain compound **4f** (0.15 g, 75%). $R_f = 0.15$ (ethyl acetate). IR (neat, $\nu_{\max}/\text{cm}^{-1}$): 3110 (m); 2953 (m); 2922 (m); 1670 (s); 1536 (s); 1493 (s); 1359 (s); 1268 (m); 1164 (m). ^1H NMR (δ ppm, CDCl_3): 2.12 (quin, 2H, $J = 6.3$ Hz, $-\text{CH}_2\text{CH}_2\text{CH}_2\text{NHCHO}$), 3.40 (q, 2H, $J = 6.3$ Hz, $-\text{CH}_2\text{CH}_2\text{CH}_2\text{NHCHO}$), 4.47 (t, 2H, $J = 6.3$ Hz, $-\text{CH}_2\text{CH}_2\text{CH}_2\text{NHCHO}$), 7.15 (s, 1H, 2-nitroimidazole-C5-H), 7.30 (s, 1H, 2-nitroimidazole-C4-H), 8.24 (s, 1H, $-\text{CH}_2\text{CH}_2\text{CH}_2\text{NHCHO}$) (**Fig 4.7**). ^{13}C NMR (δ ppm, CDCl_3): 30.5 ($-\text{CH}_2-\text{CH}_2-\text{NH}$), 34.8 ($-\text{CH}_2-\text{CH}_2-\text{NH}$), 47.8 ($\text{Ar}-\text{CH}_2-\text{CH}_2-$), 127.0 (imidazole $\text{N}=\text{C}(\text{NO}_2)-\text{N}-\text{CH}_2-\text{CH}_2$), 128.3 (imidazole $\text{N}=\text{C}(\text{NO}_2)-\text{N}-\text{CH}_2-\text{CH}_2$), 144.6

(N=C(NO₂)-N-CH₂-CH₂), 162.2 (-NH-CHO). ESI-MS (+ve mode): mass (calculated) C₇H₁₀N₄O₃ 198.1; m/z (observed) 221.2 [M+Na]⁺.

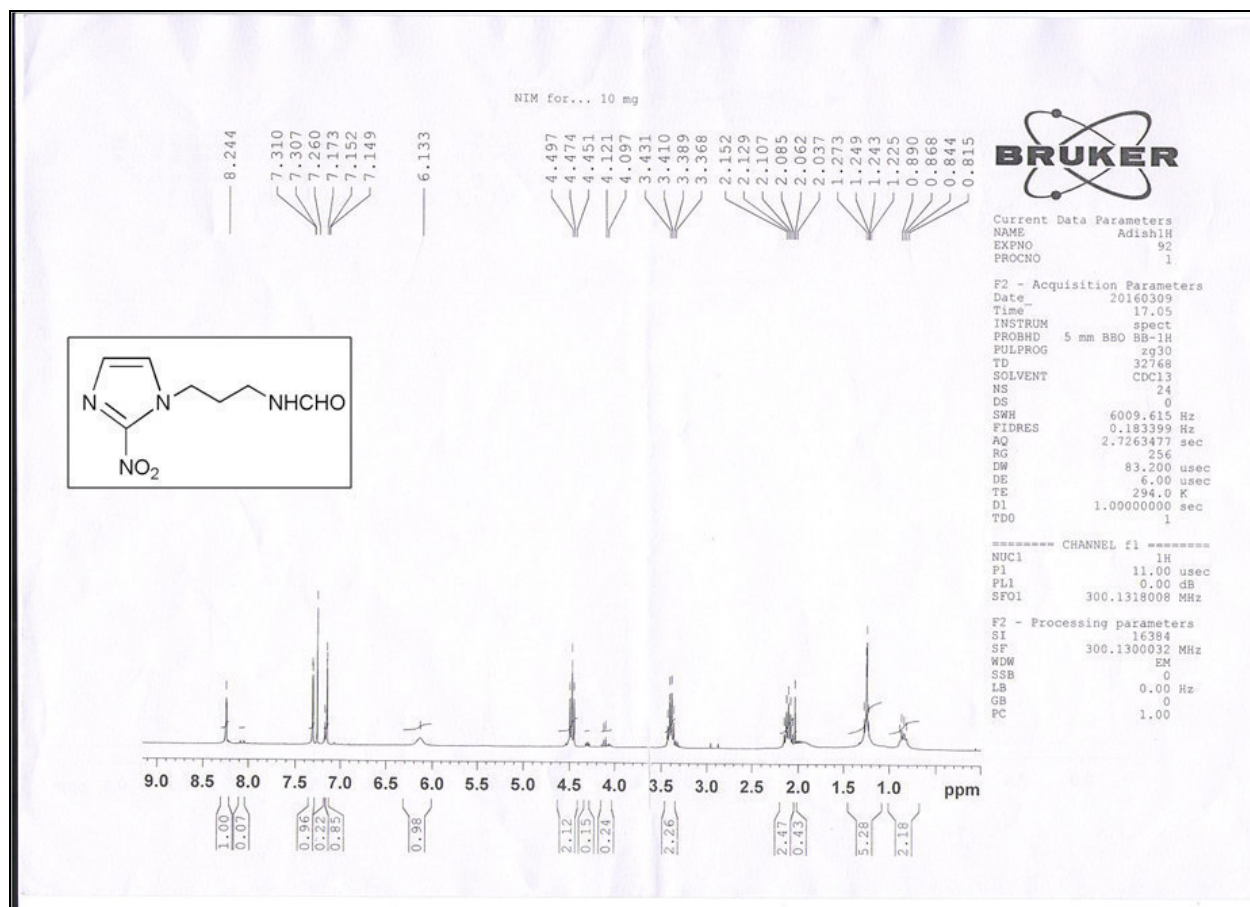


Fig. 4.7. ¹H-NMR spectra of N-(3-(2-nitro-1H-imidazol-1-yl)propyl)formamide (**4f**)

4.2.2.7. Synthesis of 1-(3-isocyanopropyl)-2-nitro-1H-imidazole (2NimNC) (**4g**)

To Compound **4f** (75 mg, 0.38 mmol) dissolved in 1:1 v/v triethylamine/dichloromethane solution (2 mL), phenyldichlorophosphate (96 mg, 0.46 mmol) was added. The reaction mixture was stirred at room temperature for 1 h [215]. Thereafter, saturated NaHCO₃ solution (10 mL) was added to the reaction mixture and vigorously stirred for another 30 minutes. The crude compound was extracted from the reaction mixture using chloroform (3 × 10 mL). Pooled chloroform layers were concentrated and further purified by silica gel column chromatography eluting with ethyl

acetate to obtain compound **4g** (33 mg, 48% yield). $R_f = 0.6$ (ethyl acetate). IR (neat, $\nu_{\max}/\text{cm}^{-1}$): 3117 (m); 2959 (m); 2922 (m); 2149 (C≡N stretch, s); 1536 (s); 1487 (s); 1359 (s); 1268 (m); 1164 (m). ^1H NMR (δ ppm, CDCl_3): 2.26 (quin, 2H, $J = 6.3$ Hz, $-\text{CH}_2\text{CH}_2\text{CH}_2\text{NC}$), 3.47 (t, 2H, $J = 6.3$ Hz, $-\text{CH}_2\text{CH}_2\text{CH}_2\text{NC}$), 4.61 (t, 2H, $J = 6.3$ Hz, $-\text{CH}_2\text{CH}_2\text{CH}_2\text{NC}$), 7.19 (s, 2H, 2-nitroimidazole-C4,C5-*H*) (**Fig 4.8**); ^{13}C NMR (δ ppm, CDCl_3): 29.3 ($-\text{CH}_2-\text{CH}_2-\text{NH}$), 38.5 ($-\text{CH}_2-\text{CH}_2-\text{NC}$), 46.9 (Ar- CH_2-CH_2-), 126.3 (imidazole $\text{N}=\text{C}(\text{NO}_2)-\text{N}-\text{CH}_2-\text{CH}_2$), 128.7 (imidazole $\text{N}=\text{C}(\text{NO}_2)-\text{N}-\text{CH}_2-\text{CH}_2$), 158.9 ($-\text{CH}_2-\text{CH}_2-\text{NC}$) (**Fig 4.9**). ESI-MS (+ve mode): mass (calculated) $\text{C}_7\text{H}_8\text{N}_4\text{O}_2$ 180.1; m/z (observed) 181.1 $[\text{M}+\text{H}]^+$.

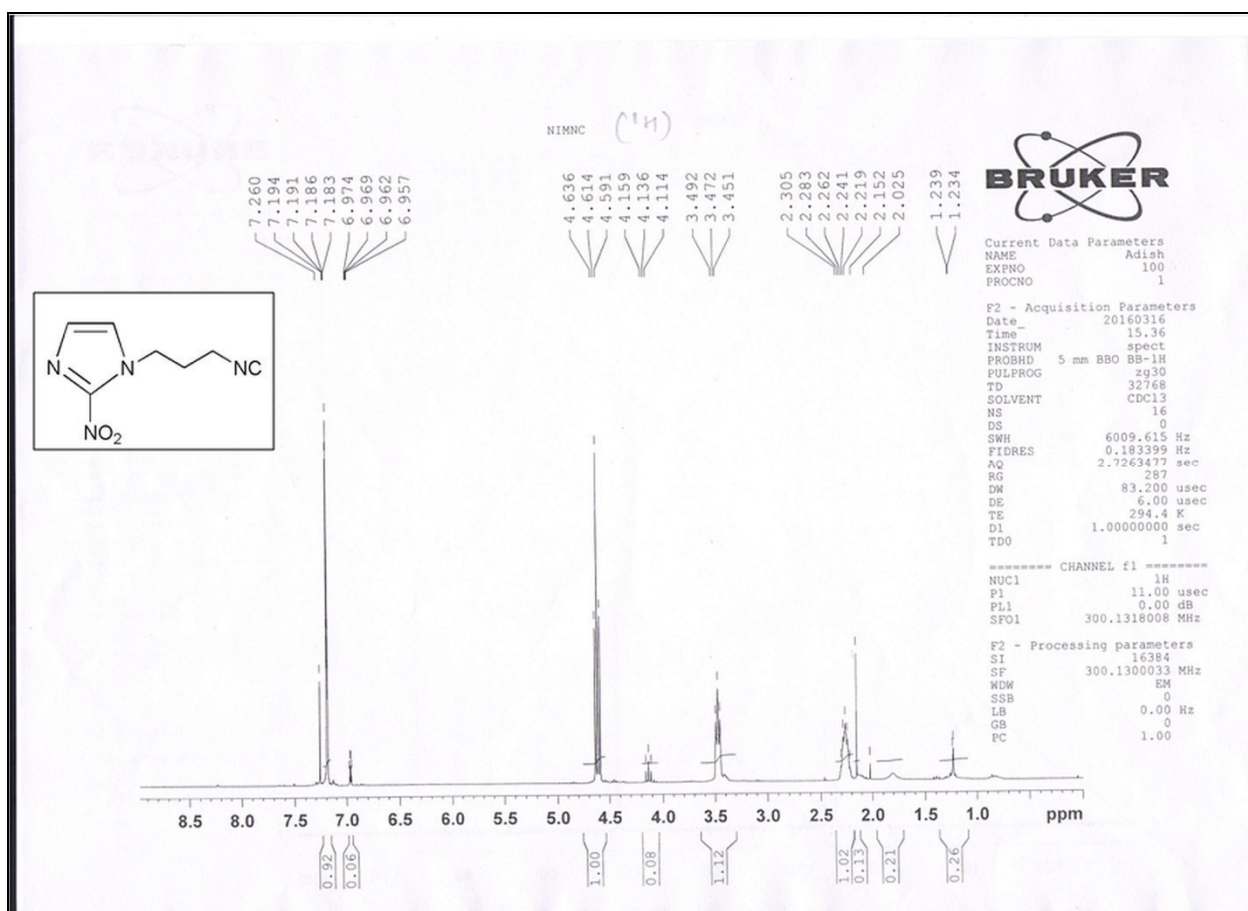


Fig. 4.8. ^1H -NMR spectra of 1-(3-isocyanopropyl)-2-nitro-1H-imidazole (2NimNC) (**4g**)

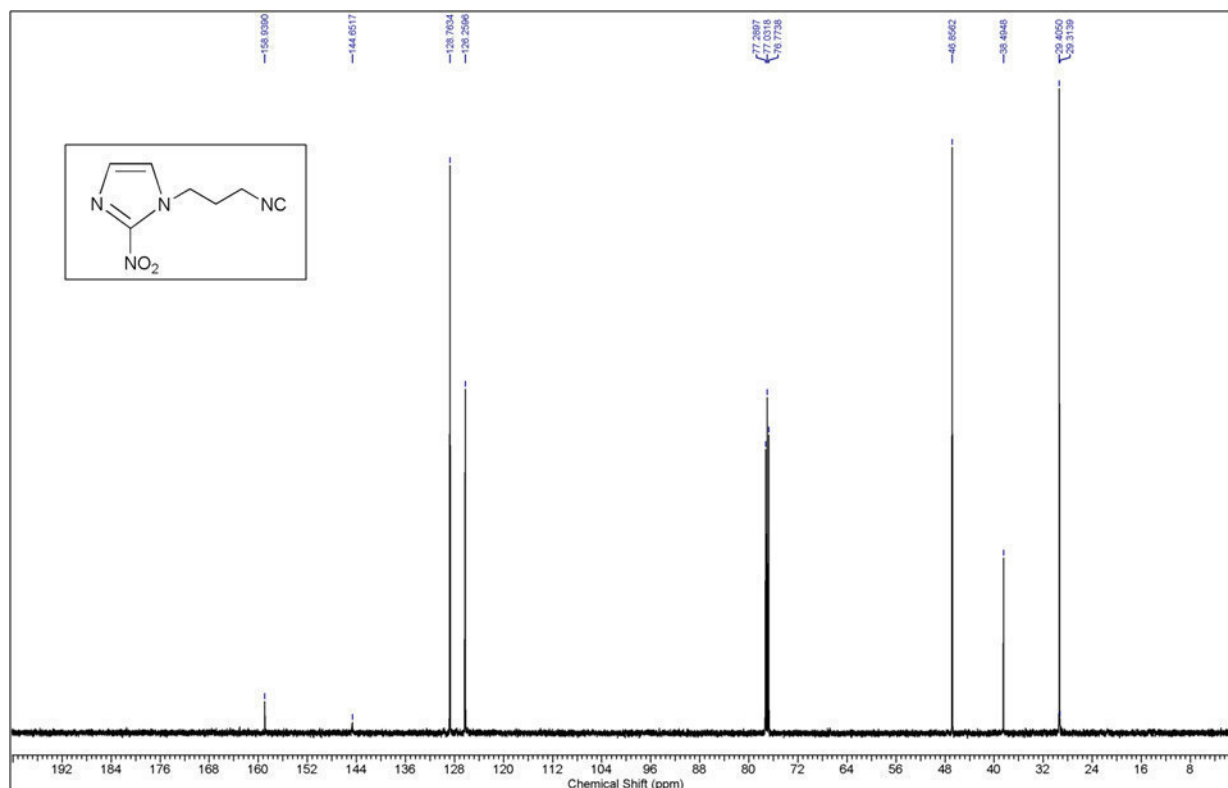


Fig. 4.9. ¹³C-NMR spectra of 1-(3-isocyanopropyl)-2-nitro-1H-imidazole (2NimNC) (**4g**)

4.2.2.8. Synthesis of *N*-(2-(2-methyl-5-nitro-1H-imidazol-1-yl)ethyl)formamide (**4h**)

Compound **4h** was synthesized from 2-(2-methyl-5-nitro-1H-imidazol-1-yl)ethanamine hydrochloride (0.30 g, 1.45 mmol) using triethylamine (0.89 g, 8.8 mmol) and ethylformate (15 mL) following a procedure similar to the synthesis of compound **4f**. $R_f = 0.15$ (ethyl acetate). IR (neat, $\nu_{\max}/\text{cm}^{-1}$) 3243 (s); 3122 (m); 3044 (m); 2912 (m); 2852 (m); 1674 (s); 1518 (s); 1464 (s); 1428 (s); 1386 (s); 1357 (s). ¹H NMR (δ ppm, CDCl₃): 2.55 (s, 3H, -CH₃), 3.68 (q, 2H, $J = 6.3$ Hz, -CH₂CH₂NHCHO), 4.51 (t, $J = 6.3$ Hz, 2H, -CH₂CH₂NHCHO), 7.98 (s, 1H, Metronidazole-C4-H), 8.23 (s, 1H, -CH₂CH₂NHCHO) (**Fig 4.10**); ¹³C NMR (δ ppm, CDCl₃): 14.1 (-CH₃), 37.8 (-CH₂CH₂NC), 44.9 (-CH₂CH₂NC), 133.3 (-C(CH₃)=N-CH=), 151.2 ((-C(CH₃)=N-CH=), 162 (CH₂CH₂NC). ESI-MS (+ve mode): mass (calculated) C₇H₁₀N₄O₃ 198.1; m/z (observed) 199.1 (M+H)⁺ and 221.1 [M+Na]⁺.

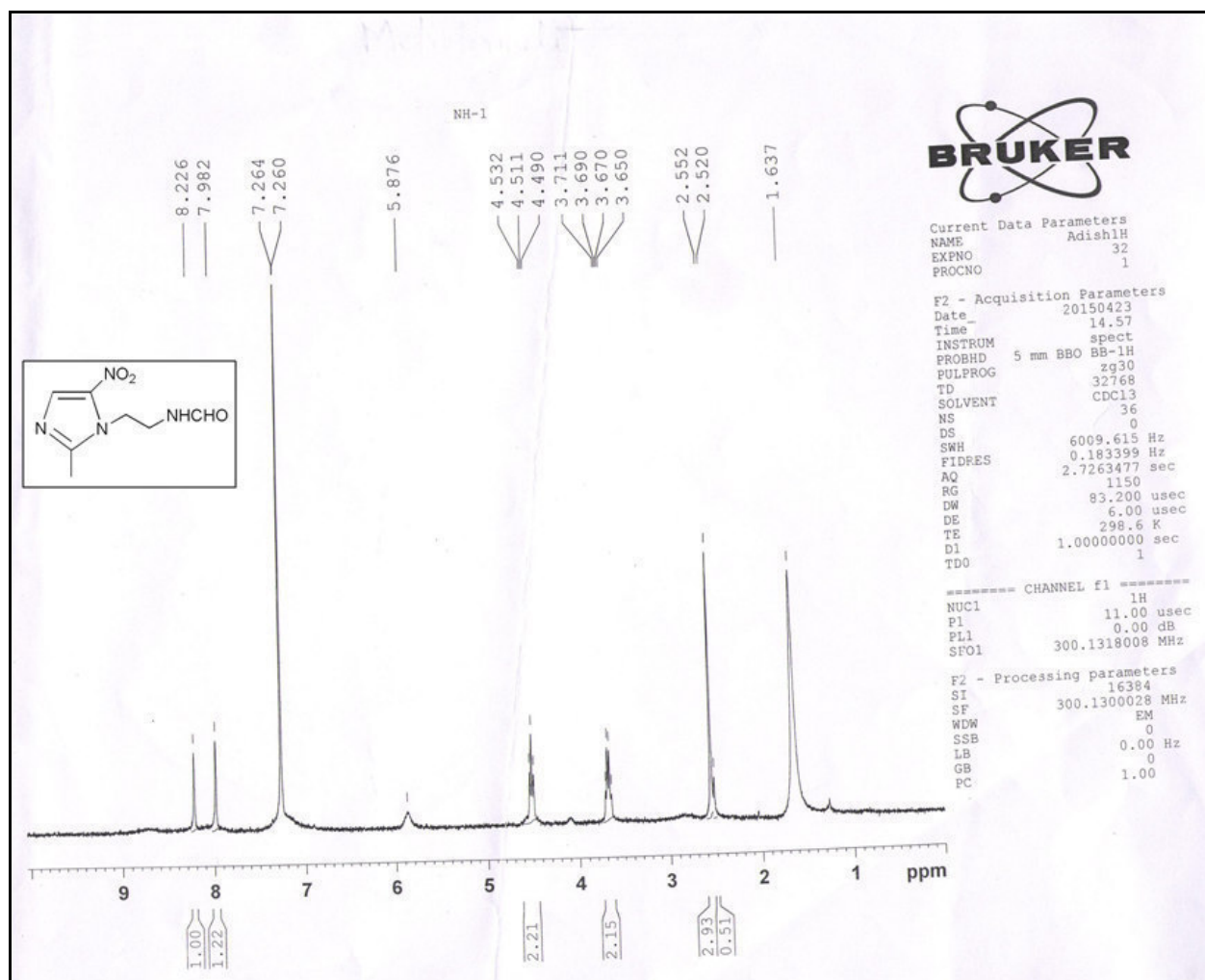


Fig. 4.10. ^1H -NMR spectra of N-(2-(2-methyl-5-nitro-1H-imidazol-1-yl)ethyl)formamide (**4h**)

4.2.2.9. Synthesis of 1-(2-isocyanoethyl)-2-methyl-5-nitro-1H-imidazole (MetNC) (**4i**)

Synthesis of compound **4i** was carried out starting from compound **4h** (60 mg, 0.3 mmol), 1:1 v/v triethylamine/dichloromethane solution (2 mL) and phenyldichlorophosphate (80 mg, 0.38 mmol), following a procedure similar to compound **4g**. Overall yield of compound **4i** (27 mg, 50%). $R_f = 0.6$ (ethyl acetate). IR (neat, $\nu_{\text{max}}/\text{cm}^{-1}$): 3124 (m); 3045 (m); 2916 (m); 2850 (m); 2150 ($\text{C}\equiv\text{N}$ stretch, s); 1530 (s); 1462 (s); 1427 (s); 1366 (s); 1356 (s). ^1H NMR (δ ppm, CDCl_3): 2.64 (s, 3H, $-\text{CH}_3$), 3.92 (t, 2H, $J = 5.7$ Hz, $-\text{CH}_2\text{CH}_2\text{NC}$), 4.59 (t, 2H, $J = 5.7$ Hz, $-\text{CH}_2\text{CH}_2\text{NC}$),

8.02 (s, 1H, Metronidazole-C4-H) (**Fig 4.11**); ^{13}C NMR (δ ppm, CDCl_3): 14.6 ($-\text{CH}_3$), 41.6 ($-\text{CH}_2\text{CH}_2\text{NC}$), 44.9 ($-\text{CH}_2\text{CH}_2\text{NC}$), 133.7 ($-\text{C}(\text{CH}_3)=\text{N}-\text{CH}=\text{}$), 151.4 ($-\text{C}(\text{CH}_3)=\text{N}-\text{CH}=\text{}$), 161 ($\text{CH}_2\text{CH}_2\text{NC}$). ESI-MS (+ve mode): mass (calculated) $\text{C}_7\text{H}_8\text{N}_4\text{O}_2$ 180.1; m/z (observed) 181.1 $[\text{M}+\text{H}]^+$.

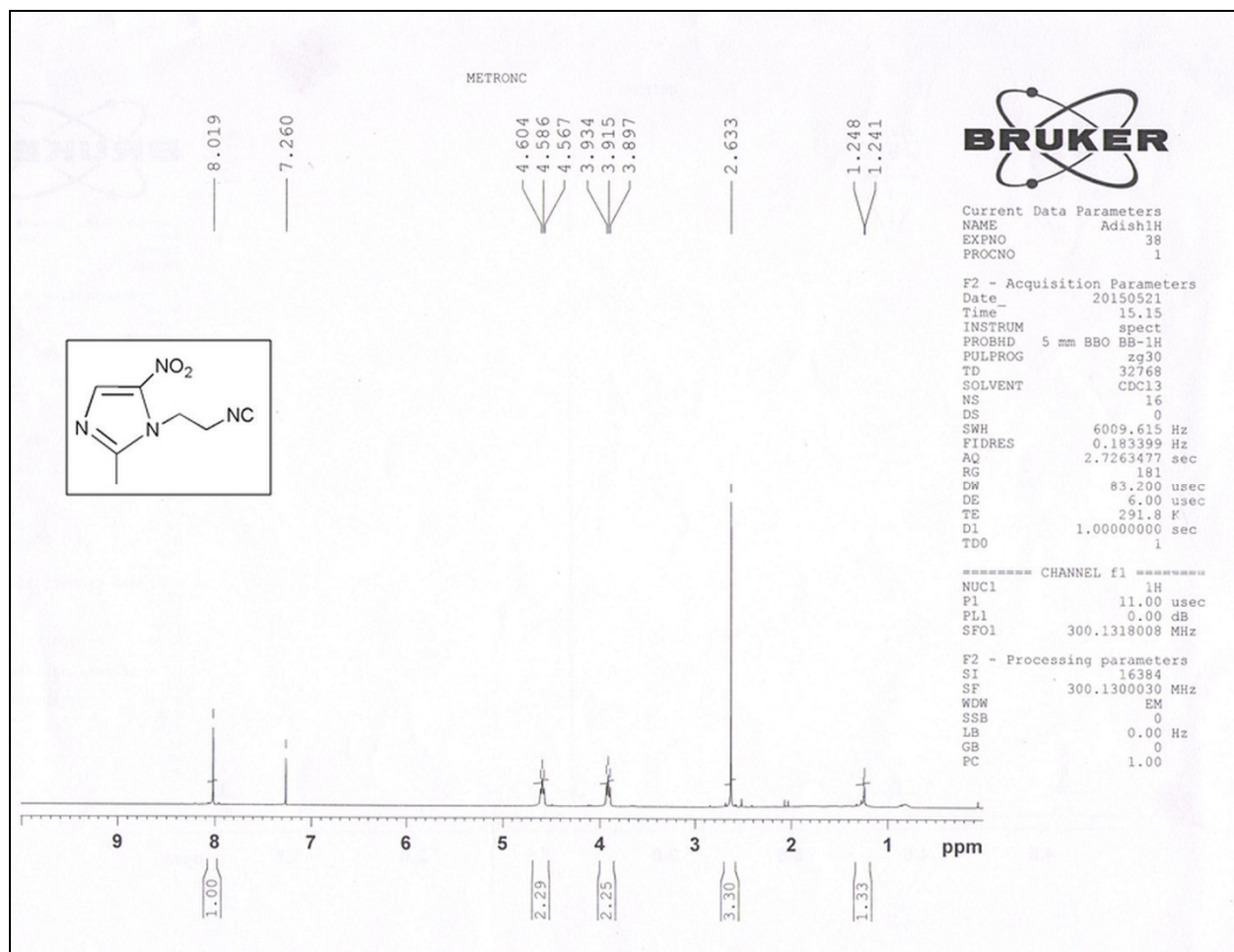


Fig. 4.11. ^1H -NMR spectra of 1-(2-isocyanoethyl)-2-methyl-5-nitro-1H-imidazole (MetNC) (**4i**)

4.2.2.10. Preparation of inactive Rhenium ($^{185/187}\text{Re}$) analogs of $^{99\text{m}}\text{Tc}$ -complexes

General procedure for the preparation of $\text{Re}(\text{NS}_3)$ -complexes of 2NimNC (4g) and MetNC (4i)

The rhenium complexes, $[\text{Re}(\text{NS}_3)(2\text{NimNC})]$ (**4j**) and $[\text{Re}(\text{NS}_3)(\text{MetNC})]$ (**4k**), were prepared using $[\text{Re}(\text{NS}_3)(\text{PMe}_2\text{Ph})]$ precursor complex, which was synthesized following a reported procedure [93]. To $[\text{Re}(\text{NS}_3)(\text{PMe}_2\text{Ph})]$ (12 mg, 0.023 mmol) in dichloromethane (0.5 mL), a solution of **4g** or **4i** (1.2 eq.) in dichloromethane (0.5 mL) was added. The reaction mixture was stirred at room temperature for 1 h. The $\text{Re}(\text{NS}_3)$ -complex formed was subsequently purified by silica gel column chromatography eluting with chloroform.

$[\text{Re}(\text{NS}_3)(2\text{NimNC})]$: R_f (chloroform) = 0.2, IR (neat, $\nu_{\text{max}}/\text{cm}^{-1}$): 2924 (m); 2850 (m); 1989 (N \equiv C stretch, br s) 1714(m); 1505(m); 1464(s); 1465(s); 1359(s). ^1H NMR (δ ppm, CDCl_3): 2.35 (quin, 2H, $-\text{CH}_2\text{CH}_2\text{CH}_2\text{NC}$), 2.99-3.23 (m, 12H, $-\text{SCH}_2\text{CH}_2\text{N}-$) 4.68 (m, 2H, $-\text{CH}_2\text{CH}_2\text{CH}_2\text{NC}$), 4.83 (t, 2H, $J = 6.6$ Hz, $-\text{CH}_2\text{CH}_2\text{CH}_2\text{NC}$), 7.16 (s, 1H, 2-nitroimidazole-C5-H), 7.52 (s, 1H, 2-nitroimidazole-C4-H) (**Fig 4.12**). ESI-MS (+ve mode): mass (calculated) $\text{C}_{13}\text{H}_{20}\text{N}_5\text{O}_2\text{S}_3\text{Re}$ 561; m/z (observed) 584 $[\text{M}+\text{Na}]^+$ (**Fig 4.13**).

$[\text{Re}(\text{NS}_3)(\text{MetNC})]$: R_f (chloroform) = 0.18, IR (neat, $\nu_{\text{max}}/\text{cm}^{-1}$): 2922 (m); 2840 (m); 1977 (N \equiv C stretch, br m); 1670(m); 1539(s); 1486 (s); 1361(m). ^1H NMR (δ ppm, CDCl_3): 2.71 (s, 3H, $-\text{CH}_3$), 2.98-3.23 (m, 12H, $-\text{SCH}_2\text{CH}_2\text{N}-$), 4.63 (m, 2H, $-\text{CH}_2\text{CH}_2\text{NC}$), 5.19 (m, 2H, $-\text{CH}_2\text{CH}_2\text{NC}$), 8.01 (1H, s, metronidazole-C4-H) (**Fig 4.14**). ESI-MS (+ve mode): mass (calculated) $\text{C}_{13}\text{H}_{20}\text{N}_5\text{O}_2\text{S}_3\text{Re}$ 561; m/z (observed) 562 $[\text{M}+\text{H}]^+$ (**Fig 4.15**).

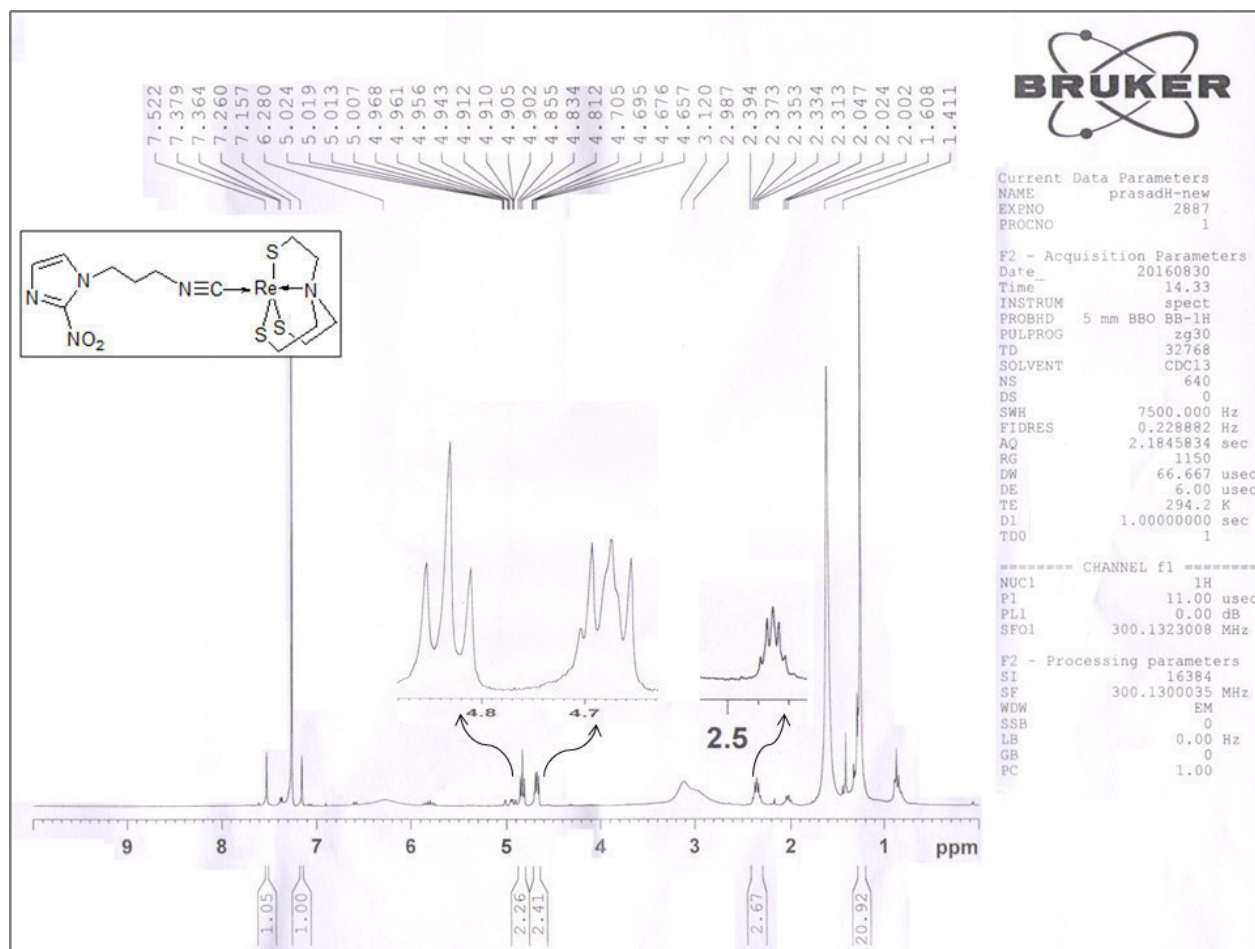


Fig. 4.12 ¹H-NMR spectra of [Re(NS₃)(2NimNC)] (**4j**)

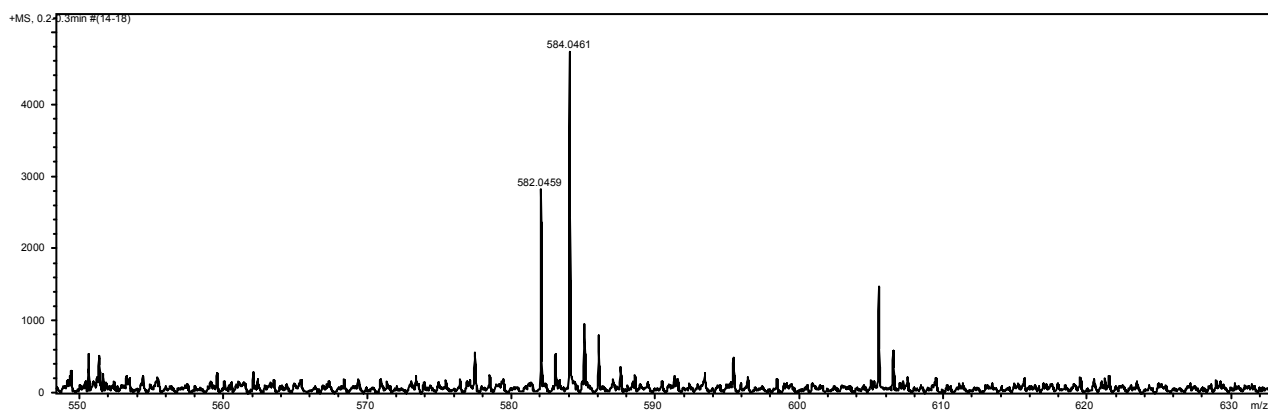


Fig. 4.13. ESI-HRMS of [Re(NS₃)(2NimNC)] complex (**4j**)

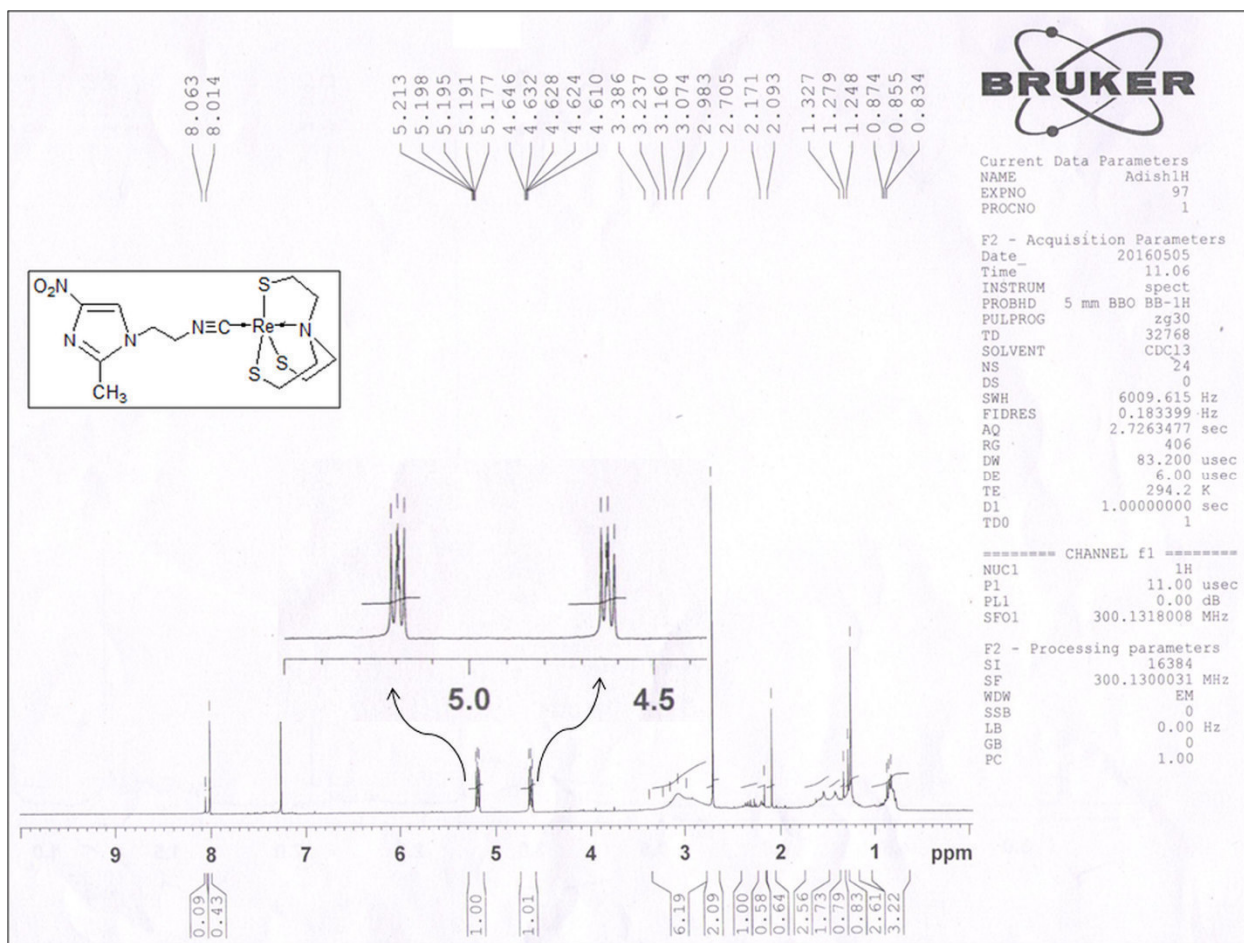


Fig. 4.14. $^1\text{H-NMR}$ spectra of $[\text{Re}(\text{NS}_3)(\text{MetNC})]$ (**4k**)

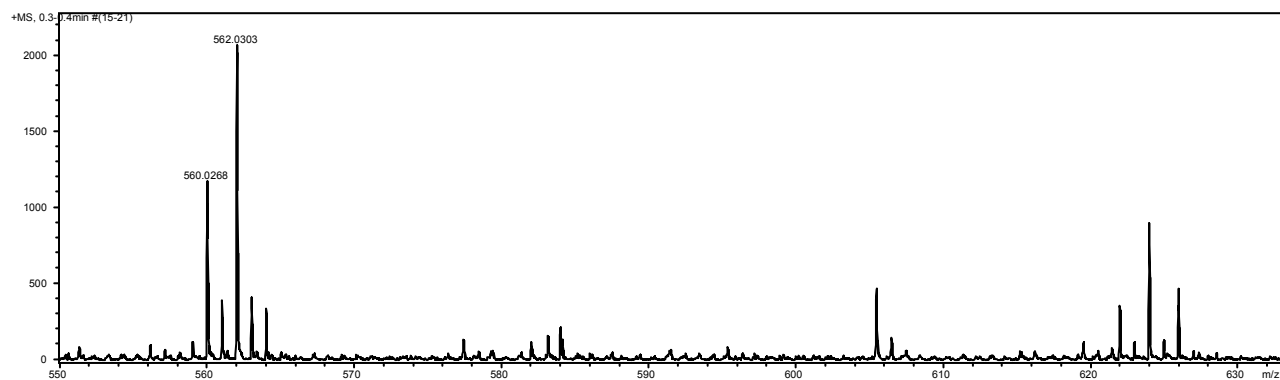


Fig. 4.15. ESI-HRMS of $[\text{Re}(\text{NS}_3)(\text{MetNC})]$ complex (**4k**)

4.2.3. Radiolabeling

4.2.3.1. Preparation of ^{99m}Tc-EDTA complex (EDTA – ethylene diamine tetraacetic acid)

The ^{99m}Tc-EDTA precursor complex was prepared by adding freshly eluted Na^{99m}TcO₄ (37 MBq) to an aqueous solution of Na₂EDTA (5 mg, 100 μL) and mannitol (5 mg), followed by addition of freshly prepared SnCl₂ solution (100 μg/ 50 μL) in 0.1N HCl. The reaction mixture was incubated at room temperature for 30 min. Formation and radiochemical purity (RCP) of ^{99m}Tc-EDTA complex was determined by TLC. The pH of ^{99m}Tc-EDTA solution was adjusted to 7 and used for subsequent studies.

4.2.3.2. General procedure for preparation of ^{99m}Tc(NS₃)-complex

To NS₃ ligand (5 × 10⁻² M in 400 μL ethanol) and 2NimNC/MetNC (10⁻² M in 100 μL ethanol), freshly prepared ^{99m}Tc-EDTA complex (19 MBq, 500 μL) was added. Subsequently, the reaction mixture was incubated at 100°C for 30 minutes. After cooling, the formation and RCP of the radioactive preparation was analyzed by HPLC.

4.2.4. Quality Control

4.2.4.1. TLC

The RCP of the precursor complex, ^{99m}Tc-EDTA, was determined by TLC. About 2 μL of test solution was spotted on two separate TLC strips and they were developed in water and acetone, respectively. Subsequently, the radioactivity distribution on the TLC strips was recorded using a TLC scanner.

4.2.4.2. HPLC

The RCP of the complexes [^{99m}Tc(NS₃)(2NimNC)] and [^{99m}Tc(NS₃)(MetNC)] was determined by HPLC. Water (A) and acetonitrile (B), both solvents containing 0.1% trifluoroacetic acid, was used as mobile phase for HPLC analyses. Following gradient elution

program was employed to effect separation of various species in the analyte. 0 min–90% A; 28 min–10% A, 30 min–90% A. Flow rate was maintained at 1 mL/min. About 15 μ L of the test solution was injected into the column for analysis and the elution was monitored observing the radioactivity profile as a function of time. The RCP of the complex was determined by peak area measurements from the chromatogram.

4.2.4.3. Octanol-water partition co-efficient ($\text{Log}P_{o/w}$)

The radiolabeled compound (0.1 mL, \sim 3.7 MBq) was mixed with double distilled water (0.9 mL) and *n*-octanol (1 mL) and vortexed for about 3 min. The mixture was then centrifuged (3500 g) for 5 min to effect clear separation of the two layers. The *n*-octanol layer (0.8 mL) was withdrawn and equal volume of fresh double distilled water was added. The mixture was vortexed again and then centrifuged as described above. Equal aliquots of the two layers were withdrawn and measured for associated radioactivity using NaI(Tl) counter. The measurements were used to calculate the $\text{Log}P_{o/w}$ of the complex.

4.2.4.4. In-vitro serum stability

The radiolabeled complex (50 μ L) was added to 300 μ L of serum and incubated at 37°C. About 100 μ L aliquot of this solution was withdrawn after 3 h and the serum proteins were precipitated by the addition of 100 μ L of acetonitrile. The mixture was centrifuged at 3500 g for 10 minutes and the supernatant was analyzed by HPLC to check the stability of the complex in serum.

4.2.5. Cyclic voltammetry studies

The redox behavior of the ligands, 2NimNC (**4g**) and MetNC (**4i**) and the corresponding Re-‘4+1’ mixed ligand complexes (**4j**) and (**4k**) were evaluated by carrying out cyclic voltammetric studies, following a previously reported procedure [196]. Glassy carbon is used as

working electrode; platinum wire is used as counter electrode and an Ag/Ag⁺ is used as reference electrode. About 5 mM solutions (5 mL) of various ligands and complexes were prepared in anhydrous DMF. The solutions also contained tetrabutylammoniumperchlorate (TBAP) (1 mmol/mL) as the supporting electrolyte. The solutions were purged with high purity argon to remove dissolved oxygen, which otherwise may interfere while recording the voltammograms of the analyte. Ferrocene was used as reference standard for which the one-electron redox potential was observed to be at $E_{1/2} = 0.47$ V under similar conditions [216].

4.2.6. *In vivo* studies

All procedures performed herein were in strict compliance with the national laws governing the conduct of animal experiments. The *in vivo* behavior of the complexes, [^{99m}Tc(NS₃)(2NimNC)] and [^{99m}Tc(NS₃)(MetNC)], were evaluated by carrying out biodistribution in Swiss mice bearing fibrosarcoma tumor. The fibrosarcoma tumor was induced by subcutaneous injection about 10⁶ HSDM1C1 murine fibrosarcoma cells on the dorsum of the Swiss mice. The tumor was allowed to grow till it reached about 10 mm in diameter. The radioactive preparation (~3.7 MBq per animal in 100 μL volume) was administered intravenously via lateral tail vein. After the injections, animals (n = 3) were incubated for different time intervals (30 min, 1 h and 3 h). At the end of respective time interval, the animals were sacrificed and relevant organs/tissue excised, weighed and activity associated with them were measured in a flat-bed type NaI(Tl) counter with energy window set for ^{99m}Tc. Results were expressed as percentage injected activity per gram of organ (%ID/g).

4.3. Results and discussion

4.3.1. Synthesis

The use of '4+1' mixed ligand strategy for radiolabeling with ^{99m}Tc requires modification of nitroimidazole into a monodentate ligand such as isocyanide. Isocyanide derivative of 2-nitroimidazole (2NimNC, compound **4g**) was synthesized in a four step synthetic procedure starting from 2-nitroimidazole (**Fig 4.16**). Dehydration of intermediate **4f** in the presence of phenyl dichlorophosphate and triethylamine resulted in target compound 2NimNC (**4g**) in good yield. All intermediate compounds as well as the target compound, 2NimNC (**4g**), were characterized by appropriate spectroscopic techniques. A characteristic peak at 2150 cm^{-1} in IR spectra of 2NimNC (**4g**) confirmed the presence of isocyanide group. The $^1\text{H-NMR}$ and $^{13}\text{C-NMR}$ of all the compounds were consistent with the expected structure. A molecular ion peak at m/z 181.1 in the mass spectra of the 2NimNC (**4g**) served as an additional evidence for the formation of expected compound. A strategy similar to the synthesis of 2NimNC (**4g**) was followed for the synthesis of MetNC (**4i**), starting from amine derivative of metronidazole. Similar to 2NimNC (**4g**), a characteristic peak at 2150 cm^{-1} in the IR spectrum of MetNC (**4i**) indicated the presence of isocyanide group in the molecule. $^1\text{H-NMR}$ and $^{13}\text{C-NMR}$ of the compound was also consistent with the expected structure and a molecular ion peak at m/z 181.1 confirmed the formation of expected product, MetNC (**4i**).

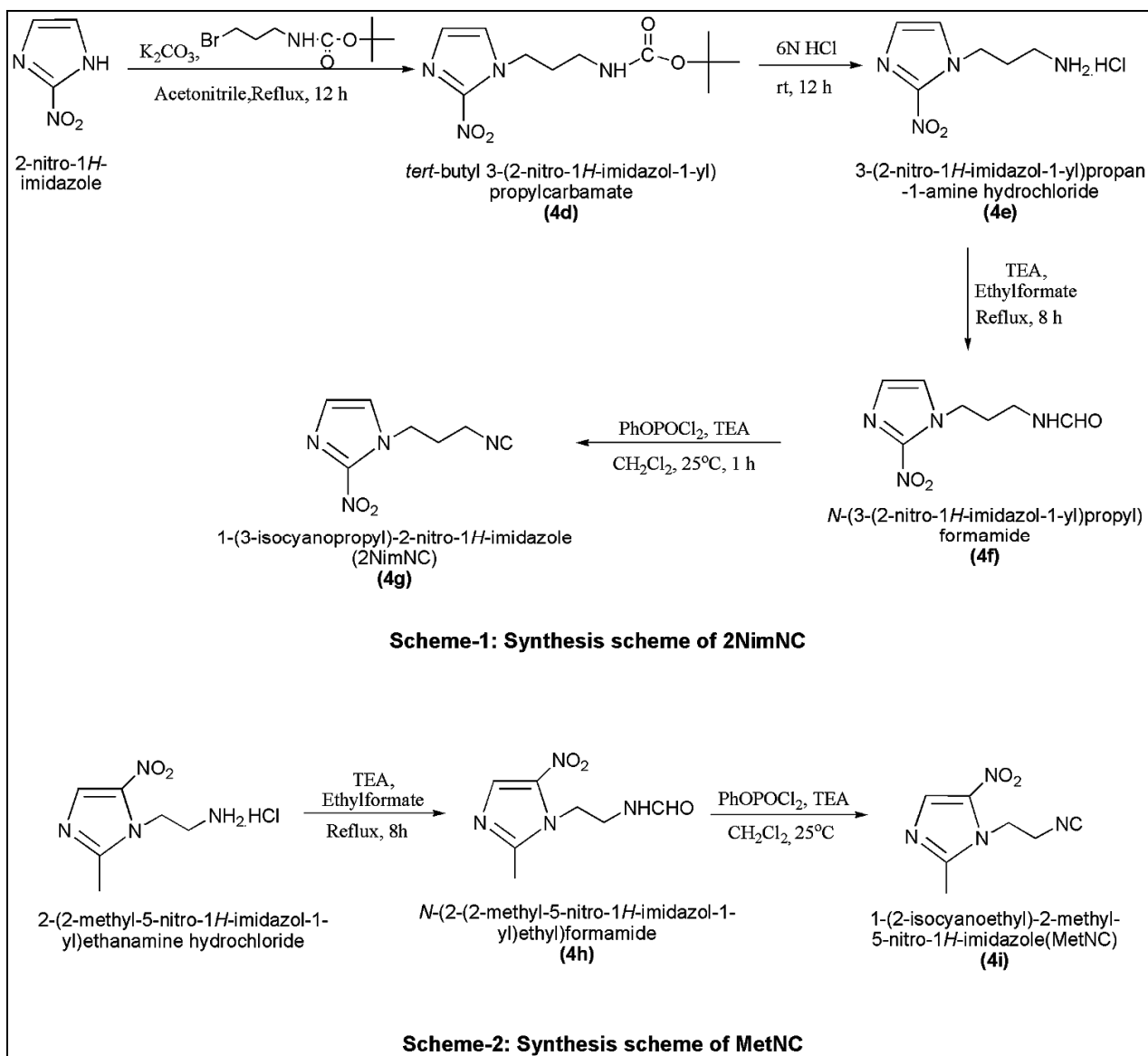


Fig. 4.16. Synthesis of isocyanide derivative of 2-nitroimidazole (2NimNC, **4g**) and metronidazole (MetNC, **4i**)

4.3.2. Radiolabeling

The ^{99m}Tc -‘4+1’ mixed ligand complexes were prepared in two steps following reported procedures.^[20] In the first step, ^{99m}Tc -EDTA precursor complex was prepared from $\text{Na}^{99m}\text{TcO}_4$ and Na_2EDTA in presence of mannitol using SnCl_2 as the reducing agent. Formation and

radiochemical purity (RCP) of $^{99m}\text{Tc-EDTA}$ precursor complex was analyzed by TLC using acetone and water as developing solvents. In acetone, $^{99m}\text{Tc-EDTA}$ complex and reduced Technetium [$^{99m}\text{Tc(IV)O}_2$] remained at the point of spotting ($R_f = 0$), while $\text{Na}^{99m}\text{TcO}_4$ moved to the solvent front ($R_f = 0.8-0.9$). In water, $^{99m}\text{Tc-EDTA}$ complex as well as $\text{Na}^{99m}\text{TcO}_4$ moved to the solvent front ($R_f = 0.8-0.9$), while $^{99m}\text{Tc(IV)O}_2$ remained at the point of spotting (**Fig 4.17**). The $^{99m}\text{Tc-EDTA}$ precursor complex could be consistently prepared in >95% RCP. In the second step, EDTA ligand in $^{99m}\text{Tc-EDTA}$ precursor complex was simultaneously exchanged with monodentate isocyanide ligand, 2NimNC (10^{-3} M) or MetNC (10^{-3} M), and tetradentate co-ligand NS_3 (5×10^{-3} M), resulting in the formation of corresponding nitroimidazole- $^{99m}\text{Tc(NS}_3)$ complex.

Classical method of ^{99m}Tc labeling requires high ligand concentration for obtaining satisfactory labeling yields. This problem was alleviated to a significant extent using pre-formed cores of ^{99m}Tc , such as [$^{99m}\text{Tc(V)N}$] $^{2+}$ core, [$^{99m}\text{Tc(I)(CO)}_3$] $^+$ core etc. The ‘4+1’ approach used in the present case is equally efficient in terms of low ligand concentration required for obtaining excellent radiolabeling yields. The $^{99m}\text{Tc-‘4+1’}$ nitroimidazole complexes could be prepared with >90% RCP using millimolar concentration (10^{-3} M) of the ligand, similar to the preparation of $^{99m}\text{Tc(CO)}_3$ complexes and [^{99m}TcN] $^{2+}$ complexes reported earlier [204-206]. While overall time required for the radiotracer preparation via ‘4+1’ mixed ligand route is comparable to other routes, it does not involve the use of toxic gases or specialized reagents.

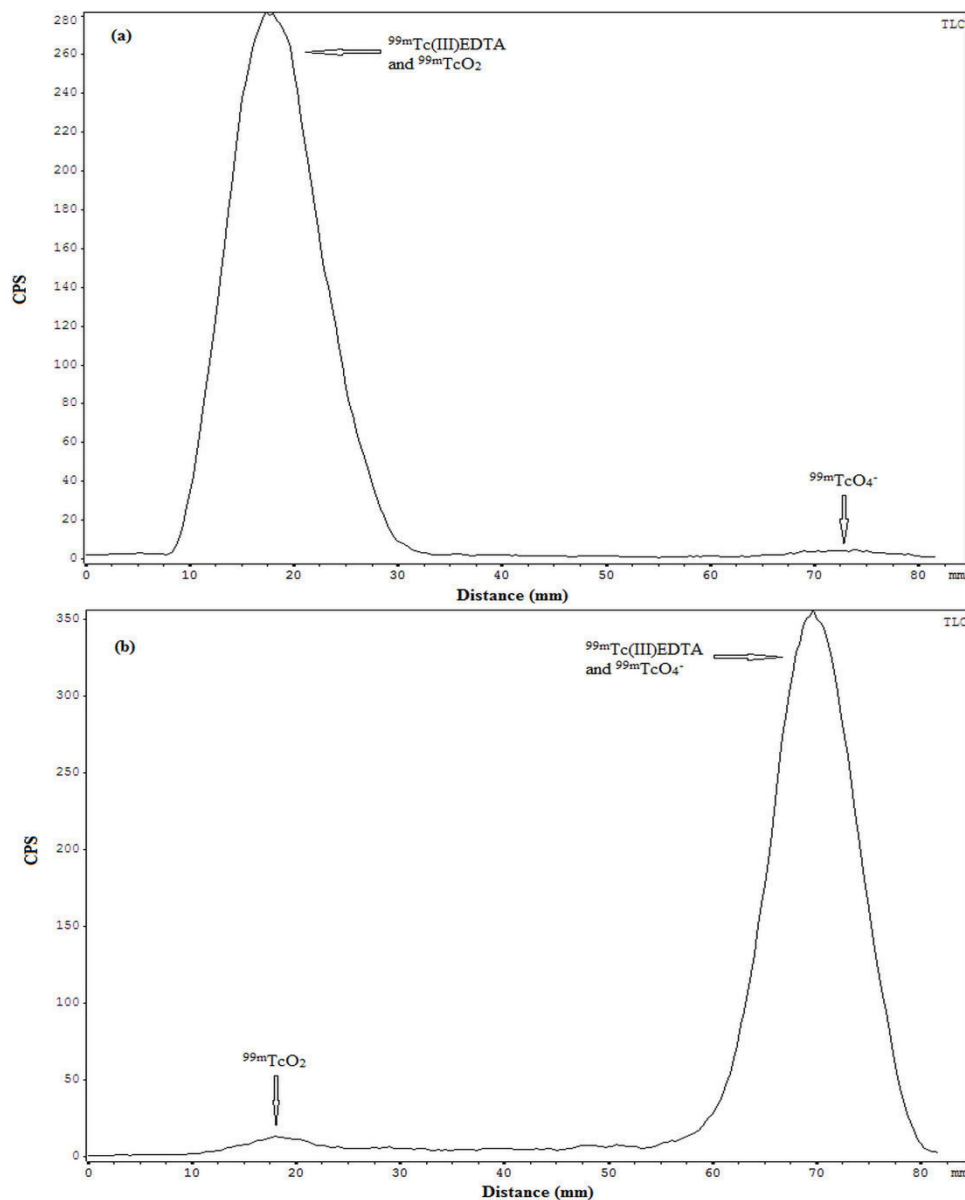


Fig. 4.17. TLC of ^{99m}Tc -EDTA complex in (a) acetone and (b) water

The nitroimidazole- $^{99m}\text{Tc}(\text{NS}_3)$ complexes thus prepared were analyzed by HPLC. The HPLC chromatogram of [$^{99m}\text{Tc}(\text{NS}_3)(2\text{NimNC})$] complex showed a sharp peak at 24.2 ± 0.5 min (RCP = $94.3 \pm 1.2\%$, $n = 4$) (**Fig 4.18**). Similarly, [$^{99m}\text{Tc}(\text{NS}_3)(\text{MetNC})$] complex appeared as a single sharp peak at 20.4 ± 0.5 min (RCP = $94.91 \pm 1.5\%$, $n = 4$) [**Fig 4.18**]. It could be noted here that ^{99m}Tc -EDTA precursor complex was eluted at 2.9 ± 0.1 min (chromatogram not shown).

Radiochemical purity of both nitroimidazole- $^{99m}\text{Tc}(\text{NS}_3)$ complexes were $>90\%$, as determined from the HPLC peak integration. Specific activity of the complexes $[^{99m}\text{Tc}(\text{NS}_3)(2\text{NimNC})]$ and $[^{99m}\text{Tc}(\text{NS}_3)(\text{MetNC})]$ at the end of preparation (without applying any decay correction for ^{99m}Tc during preparation) was found to be 438.6 ± 1.9 and $443 \pm 1.2 \mu\text{Ci}/\mu\text{mol}$ of ligand ($n = 3$).

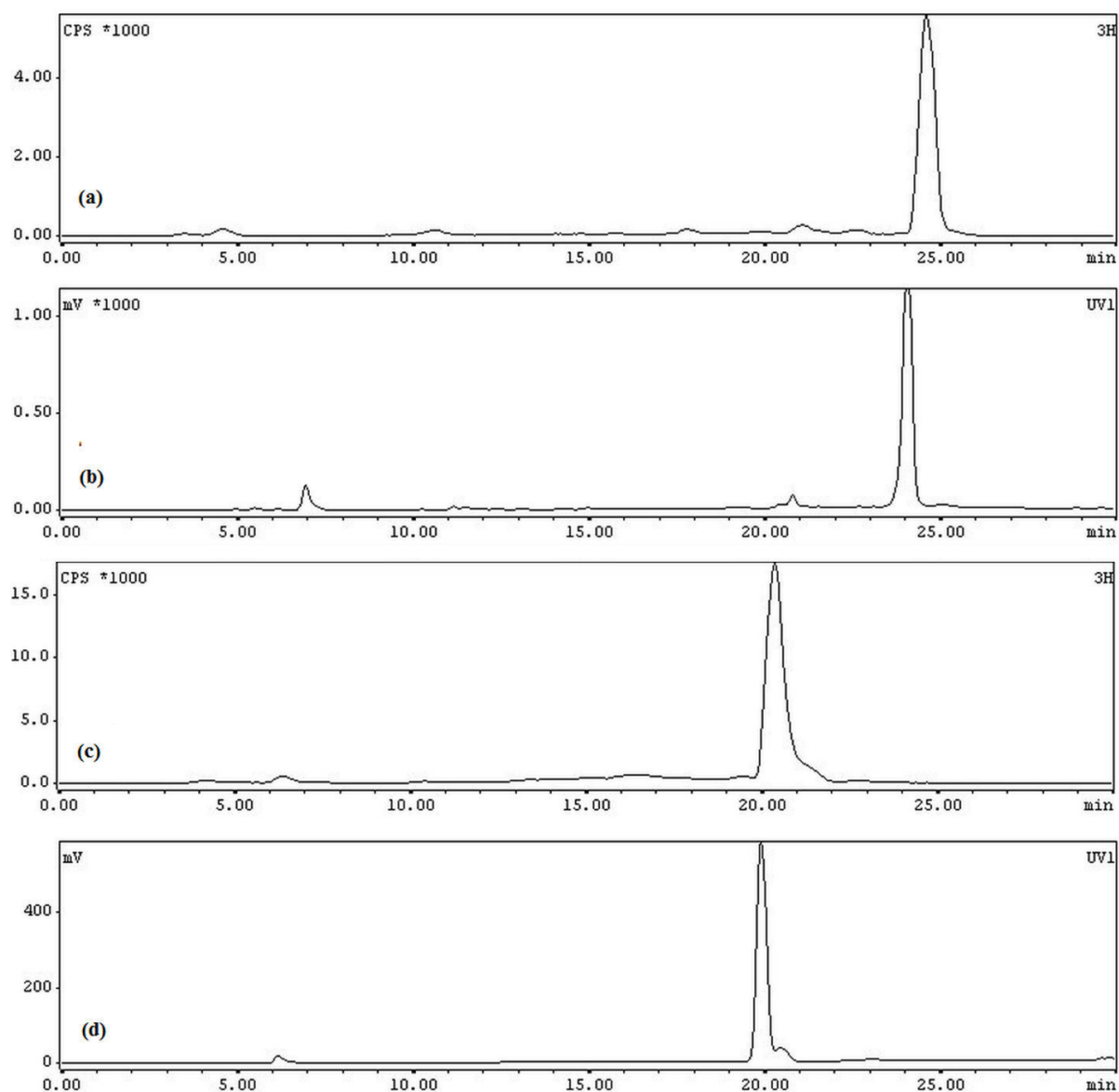


Fig. 4.18. HPLC elution profile of (a) $[^{99m}\text{Tc}(\text{NS}_3)(2\text{NimNC})]$ and (b) $[\text{Re}(\text{NS}_3)(2\text{NimNC})]$, (c) $[^{99m}\text{Tc}(\text{NS}_3)(\text{MetNC})]$ and (d) $[\text{Re}(\text{NS}_3)(\text{MetNC})]$

Serum stability of the two nitroimidazole- $^{99m}\text{Tc}(\text{NS}_3)$ complexes were studied by incubating the complexes in human serum at 37°C . The complexes did not show significant degradation (determined by HPLC) in human serum during the study period (3 h) (**Fig 4.19**).

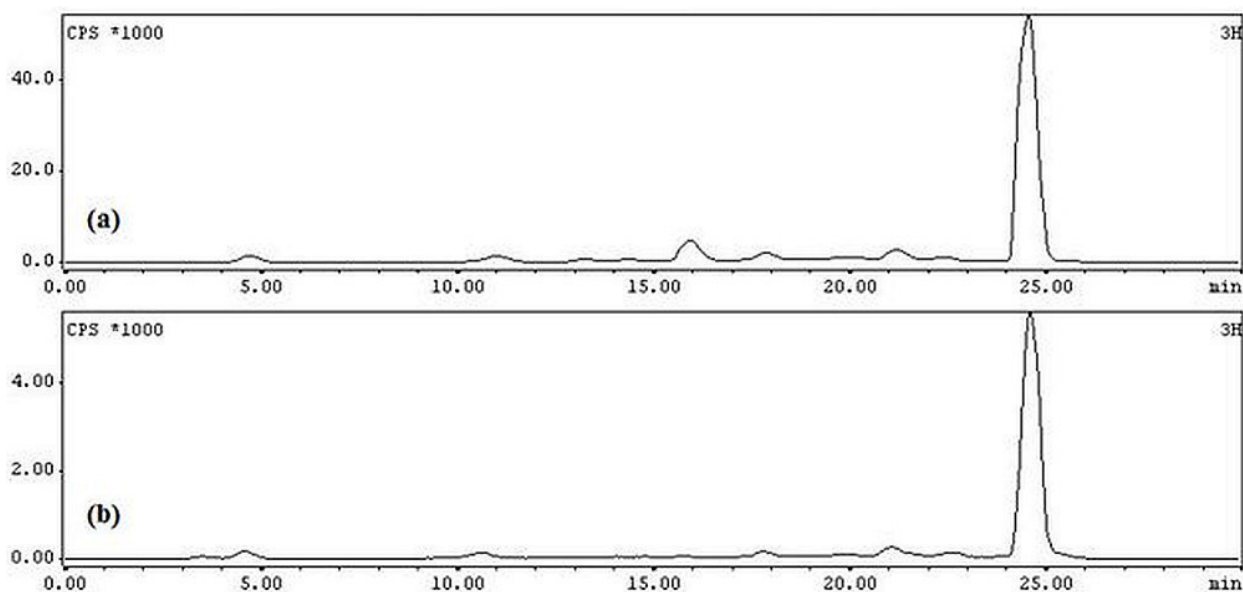


Fig. 4.19. HPLC elution profile of (a) [$^{99m}\text{Tc}(\text{NS}_3)(2\text{-NimNC})$] and (b) supernatant obtained after the precipitation of serum proteins

The $\text{Log } P_{o/w}$ value, a measure of lipophilicity, of the two nitroimidazole- $^{99m}\text{Tc}(\text{NS}_3)$ complexes was found to be 0.94 ± 0.1 and 0.97 ± 0.07 ($n = 3$), for [$^{99m}\text{Tc}(\text{NS}_3)(2\text{NimNC})$] complex and [$^{99m}\text{Tc}(\text{NS}_3)(\text{MetNC})$] complex, respectively. The values indicated highly lipophilic nature of the complexes.

4.3.3. Preparation of inactive Rhenium ($^{185/187}\text{Re}$) analogs of ^{99m}Tc -complexes

Due to difficulties involved in the structural characterization of ^{99m}Tc -complexes prepared at the nca level, corresponding rhenium analogues were synthesized at macroscopic level (**Fig 4.20**). This was achieved using [$\text{Re}(\text{NS}_3)(\text{PMe}_2\text{Ph})$] precursor complex and the

nitroimidazole isocyanide ligand, 2NimNC or MetNC. The rhenium analogues could be prepared in moderate to good yields. **Figure 4.18** shows the UV-chromatogram of Re-‘4+1’ mixed ligand complexes, $[\text{Re}(\text{NS}_3)(2\text{NimNC})]$ and $[\text{Re}(\text{NS}_3)(\text{MetNC})]$. It could be noted that UV-chromatograms of the two rhenium complexes matched with the radioactivity profile of the corresponding $^{99\text{m}}\text{Tc}$ -‘4+1’ complexes prepared at the nca level. This observation indicated the formation of structurally similar complexes, both at nca level as well as macroscopic level. The nitroimidazole-Re(NS_3) complexes were further analyzed by various spectroscopic techniques to obtain additional structural information.

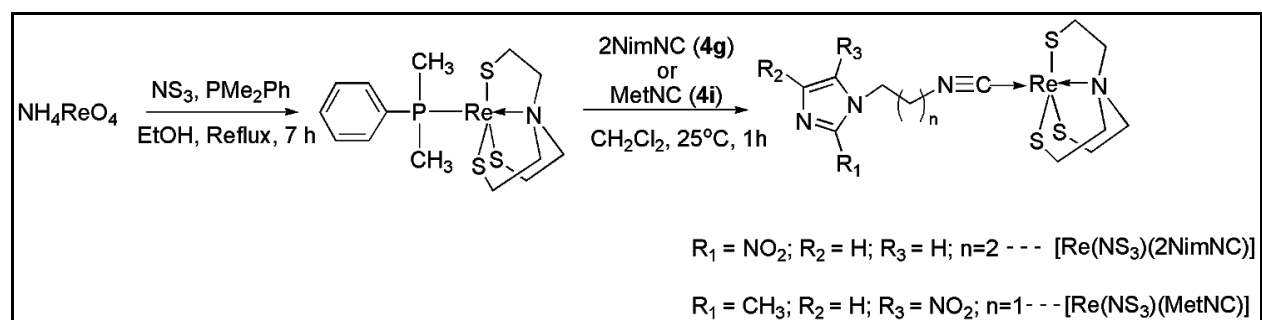


Fig. 4.20. Preparation of Re-‘4+1’ complexes of isocyanide derivatives of nitroimidazole

A red-shift in the stretching frequency of $-\text{N}\equiv\text{C}$ group in the infrared spectrum of the nitroimidazole-Re(NS_3) complexes (1989 cm^{-1}) compared to the free ligand (2150 cm^{-1}) (**Fig 4.21**), similar to the observation made by Spies et. al. on $[\text{Re}(\text{NS}_3)(\text{CNR})]$ complexes [93], indicated the coordination of the ligand to central Re-metal through the $-\text{NC}$ group. The ^1H -NMR spectrum of $[\text{Re}(\text{NS}_3)(2\text{NimNC})]$ (**Fig 4.12**) showed a downfield shift in all the methylene protons of the propyl spacer compared to the free ligand. The protons of the methylene group directly attached to the $-\text{NC}$ group (α -carbon) showed complex splitting patterns of AB spin system indicating that the two protons attached to α -methylene group are not equivalent. This

could be attributed to the coordination of -NC group to the Re-metal centre. Similar observations were made with $[\text{Re}(\text{NS}_3)(\text{MetNC})]$ complex.

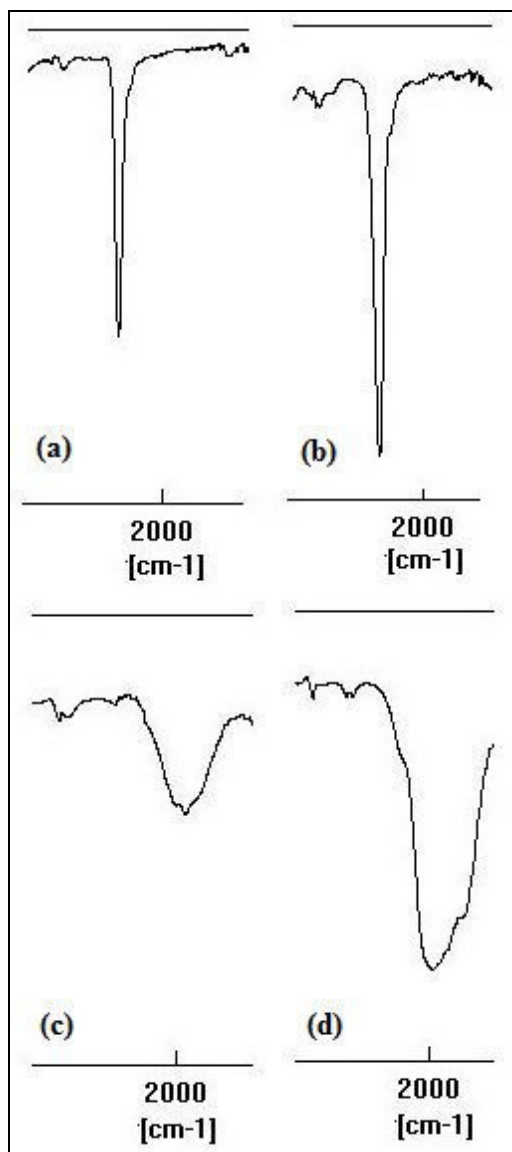


Fig. 4.21. IR absorption of $\text{N}\equiv\text{C}$ bond in ligands (a) 2NimNC and (b) MetNC, their respective Re-‘4+1’ complexes (c) $[\text{Re}(\text{NS}_3)(2\text{NimNC})]$ and (d) $[\text{Re}(\text{NS}_3)(\text{MetNC})]$

In the $^1\text{H-NMR}$ spectrum of $[\text{Re}(\text{NS}_3)(\text{MetNC})]$, the methylene protons of the ethyl spacer exhibited a complex AA'BB' splitting pattern (**Fig 4.14**), which could be attributed to the

steric hindrance in C-C bond rotation by the relatively large nitroimidazole ring at one end and the $\text{Re}(\text{NS})_3$ complex core at the other. Observation of $(\text{M}+\text{Na})^+$ ion peak at m/z 584.0461 in the mass spectrum of $[\text{Re}(\text{NS}_3)(2\text{NimNC})]$ (**Fig 4.13**) and $(\text{M} + \text{H})^+$ ion peak at m/z 562.0303 in the mass spectrum of $[\text{Re}(\text{NS}_3)(\text{MetNC})]$ (**Fig 4.14**) with typical isotopic pattern of mononuclear rhenium complexes confirmed the formation of expected complexes.

4.3.4. Cyclic voltammetry studies

Single electron reduction potential of the nitroimidazole is one of the important parameters that determine the efficiency of reduction of the radiotracer in hypoxic cells. Therefore, any modification in the nitroimidazole ring or its electronic environment can potentially alter the SERP value, affecting its ability to target hypoxic cells. The modification can either increase or decrease the SERP value of the nitroimidazole ligand. A change in SERP value can be expected when the native ligand, 2-nitroimidazole or metronidazole, is modified to isocyanide derivative. Additionally, a change in SERP can also be expected when the nitroimidazole-isocyanide ligand coordinates with $\text{M}(\text{NS}_3)$ core [$\text{M} = {}^{99\text{m}}\text{Tc}, \text{Re}$] to form the ‘4+1’ mixed ligand complex, since this process may potentially alter the electronic environment of the nitroimidazole ligand in the complex. Adams et al. had carefully studied and reported that modifications made at sites two to three carbon-carbon bond distances away from the nitroimidazole group had no significant effect on its SERP value [217,218]. However, in the present work cyclic voltammetric studies of the nitroimidazole ligand as well as the nitroimidazole- $\text{Re}(\text{NS}_3)$ complexes were carried out to evaluate the effects of synthetic modification and coordination of the ligand to the metal in the final complex. The voltammogram of the ligand 2NimNC (**4g**) and corresponding Re -‘4+1’ mixed ligand complex, $[\text{Re}(\text{NS}_3)(2\text{NimNC})]$, is shown in **Fig. 4.22**. The SERP of 2NimNC ligand was -0.93 V, while

that reported for unsubstituted 2-nitroimidazole was -0.92 V (obtained from literature) [205]. This observation is in accordance with the observation made by Adams et al [217,218]. The voltammogram of $[\text{Re}(\text{NS}_3)(2\text{NimNC})]$ complex showed a single electron reduction wave at -0.88 V, which is more positive than SERP of both 2-nitroimidazole as well as 2NimNC ligand. Similar observations were made with $[\text{Re}(\text{NS}_3)(\text{MetNC})]$ complex and MetNC ligand. The SERP of MetNC ligand and $[\text{Re}(\text{NS}_3)(\text{MetNC})]$ complex were observed to be -0.96 V and -0.91 V, respectively, while that of metronidazole was -0.99 V. Thus cyclic voltammetric study provides an indication that the ability of 2-nitroimidazole/metronidazole moiety to get reduced in hypoxic cells was not affected after forming '4+1' complex.

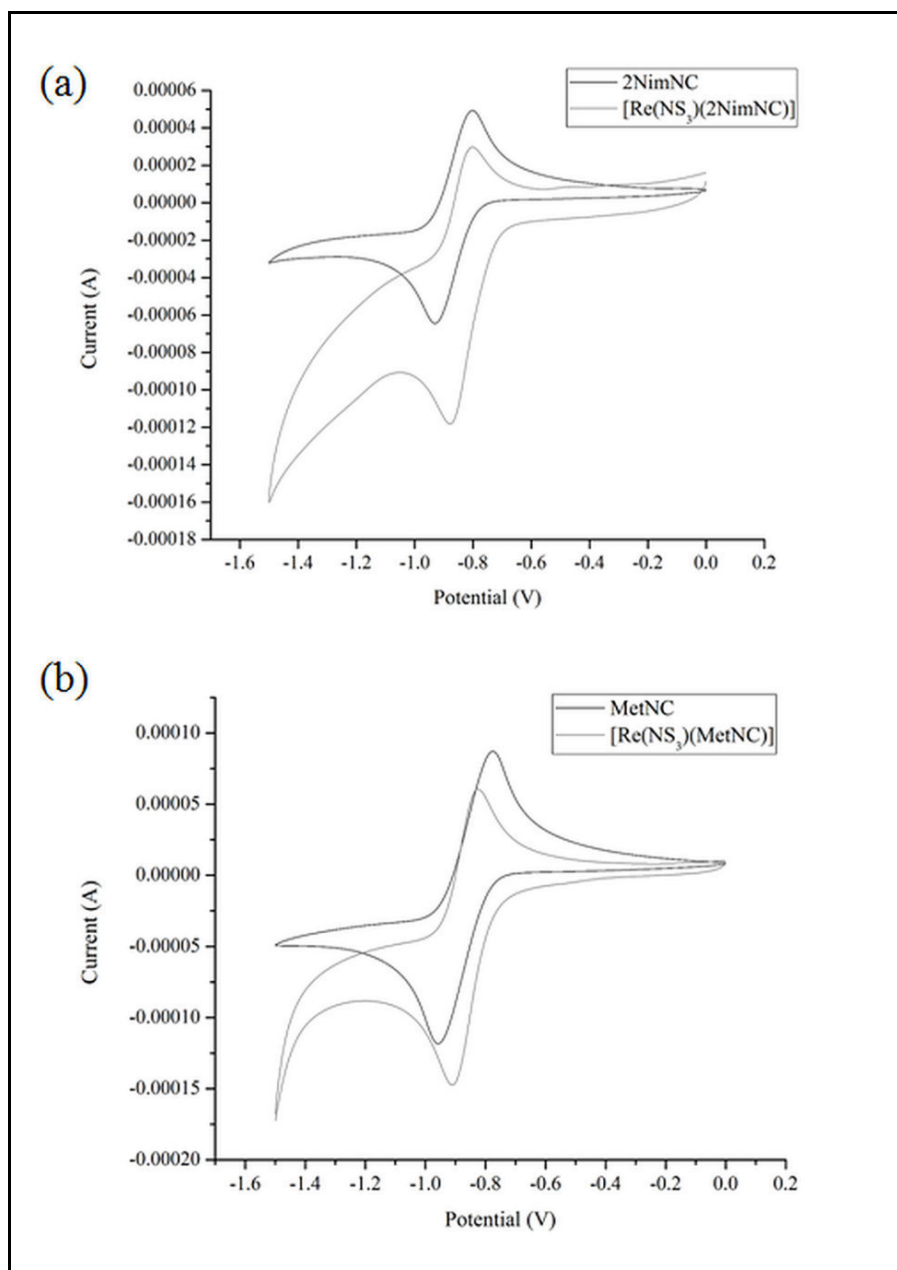


Fig. 4.22. Voltammogram of (a) 2NimNC and [Re(NS₃)(2NimNC)] and (b) MetNC and [Re(NS₃)(MetNC)]

4.3.5. *In vivo* studies

Biodistribution studies of the complexes [$^{99m}\text{Tc}(\text{NS}_3)(2\text{NimNC})$] and [$^{99m}\text{Tc}(\text{NS}_3)(\text{MetNC})$] were carried out in Swiss mice bearing fibrosarcoma tumor. Though the absolute hypoxic status of the solid fibrosarcoma tumor used for the present study was not determined, control experiments with [^{18}F]FMISO, the clinically used radiopharmaceutical for imaging hypoxia, in the same tumor model provided an indirect evidence for the hypoxic nature of this tumor [205]. **Table 4.1** summarizes the *in vivo* distribution of [$^{99m}\text{Tc}(\text{NS}_3)(2\text{NimNC})$] and [$^{99m}\text{Tc}(\text{NS}_3)(\text{MetNC})$] complexes in different organs/tissues in tumor bearing animal model expressed as percentage injected dose per gram of the organ (%ID/g).

The complex [$^{99m}\text{Tc}(\text{NS}_3)(2\text{NimNC})$] showed an initial tumor uptake of 0.84(0.05) %ID/g at 30 min p.i., which then reduced to 0.40(0.07) %ID/g at 60 min p.i. Thereafter, clearance of activity from tumor was slow, about 85% of activity [0.34(0.03) % ID/g] retained in tumor even at 180 min p.i. Similar trend was observed with [$^{99m}\text{Tc}(\text{NS}_3)(\text{MetNC})$] complex. It is pertinent to note that activity associated with the muscle is less than that in tumor at all time points, which rules out the possibility of tumor associated activity to be due to non-specific uptake. This is also reflected in the gradual increase in tumor-to-muscle ratio of the complexes with time.

Major clearance of [$^{99m}\text{Tc}(\text{NS}_3)(2\text{NimNC})$] and [$^{99m}\text{Tc}(\text{NS}_3)(\text{MetNC})$] complexes from the animal body was through hepatobiliary route. This is evident from the level of activity in liver and gastrointestinal tract. Presence of significant level of activity in liver and gastrointestinal tract as early as 30 min also indicates fast clearance of activity from blood pool. This was further corroborated by very low-level of activity in blood pool as early as 30 min p.i.

A possible reason for this observation could be the high lipophilicity ($\text{LogP}_{o/w}$) of the complexes, 0.94 ± 0.1 and 0.97 ± 0.07 for $[^{99m}\text{Tc}(\text{NS}_3)(2\text{NimNC})]$ and $[^{99m}\text{Tc}(\text{NS}_3)(\text{MetNC})]$, respectively.

Table 4.1. Distribution pattern of nitroimidazole- $^{99m}\text{Tc}(\text{NS}_3)$ complexes ($[^{99m}\text{Tc}(\text{NS}_3)(2\text{NimNC})]$ and $[^{99m}\text{Tc}(\text{NS}_3)(\text{MetNC})]$) in various organs at different time points

Organs	% ID/g (s.d) [#]					
	(n = 3)					
	$[^{99m}\text{Tc}(\text{NS}_3)(2\text{NimNC})]$			$[^{99m}\text{Tc}(\text{NS}_3)(\text{MetNC})]$		
	30 min	60 min	180 min	30 min	60 min	180 min
Liver	18.53 (2.39)	12.72 (2.42)	10.26 (0.48)	15.71 (3.70)	16.52 (4.36)	14.23 (4.55)
Intestine	16.89 (1.78)	20.86 (0.63)	22.16 (0.28)	17.76 (4.46)	18.44 (2.09)	17.51 (2.98)
Stomach	1.32 (0.2)	1.25 (0.4)	0.89 (0.33)	1.62 (0.09)	0.99 (0.15)	1.14 (0.03)
Kidney	2.08 (0.39)	1.29 (0.15)	0.93 (0.03)	1.86 (0.39)	1.27 (0.35)	1.36 (0.10)
Heart	1.08 (0.05)	0.96 (0.20)	0.57 (0.06)	0.46 (0.09)	0.31 (0.16)	0.31 (0.31)
Lungs	1.97 (0.49)	1.71 (0.21)	1.16 (0.42)	0.99 (0.06)	0.91 (0.03)	0.52 (0.04)
Spleen	2.72 (0.46)	1.34 (0.14)	0.47 (0.16)	1.90 (0.25)	1.46 (0.05)	1.13 (0.66)
Blood	0.99 (0.05)	0.42 (0.09)	0.27 (0.01)	1.01 (0.06)	0.59 (0.01)	0.35 (0.04)
Muscle	0.28 (0.08)	0.13 (0.05)	0.07 (0.01)	0.17 (0.02)	0.12 (0.02)	0.07 (0.03)
Tumor	0.84 (0.05)	0.40 (0.07)	0.34 (0.03)	0.78 (0.08)	0.44 (0.06)	0.31 (0.05)
Tumor/Blood	0.84 (0.02)	0.95 (0.05)	1.24 (0.08)	0.77 (0.04)	0.76 (0.09)	0.89 (0.07)
Tumor/Muscle	3.13 (0.89)	3.36 (0.33)	4.76 (1.08)	4.08 (0.12)	4.17 (0.11)	4.84 (1.49)

[#]%ID/g – Percentage injected dose per gram; s.d – standard deviation

As mentioned earlier, residence time of the complex in hypoxic cells plays a crucial role in deciding its overall efficacy in vivo. Fast clearance of the radiotracer from blood significantly limits its distribution in the tumor and residence time in hypoxic cells. In the present case, we speculate that due to fast blood clearance, the complexes [$^{99m}\text{Tc}(\text{NS}_3)(2\text{NimNC})$] and [$^{99m}\text{Tc}(\text{NS}_3)(\text{MetNC})$] might not have spent sufficient time in tumor to undergo oxygen dependent reduction and trapping in hypoxic cells. On the contrary, relatively slow clearance from blood must have facilitated better diffusion and distribution of [^{18}F]FMISO ($\text{LogP}_{\text{o/w}}$ of [^{18}F]FMISO -0.41) [191] in tumor, which resulted in significantly higher uptake in tumor than the nitroimidazole- $^{99m}\text{Tc}(\text{NS}_3)$ complexes evaluated in present study [**Table 4.2**].

Table 4.2. Activity of nitroimidazole- $^{99m}\text{Tc}(\text{NS}_3)$ complexes ([$^{99m}\text{Tc}(\text{NS}_3)(2\text{NimNC})$] and [$^{99m}\text{Tc}(\text{NS}_3)(\text{MetNC})$]) and [^{18}F]FMISO observed in tumor and blood at different time points

	Time p.i. (min)	[$^{99m}\text{Tc}(\text{NS}_3)(2\text{NimNC})$]	[$^{99m}\text{Tc}(\text{NS}_3)(\text{MetNC})$]	[^{18}F]FMISO
Tumor	30 min	0.84 (0.05)	0.78 (0.08)	4.65 (0.86)
%ID/g (s.d) [#]	60 min	0.40 (0.07)	0.44 (0.06)	3.70 (0.09)
	180 min	0.34 (0.03)	0.31 (0.05)	2.04 (0.14)
Blood	30 min	0.99 (0.05)	1.01 (0.06)	3.95 (0.31)
%ID/g (s.d) [#]	60 min	0.42 (0.09)	0.59 (0.01)	2.38 (0.42)
	180 min	0.27 (0.01)	0.35 (0.04)	0.53 (0.07)

[#]%ID/g – Percentage injected dose per gram; s.d – standard deviation

The tumor-to-muscle ratio of both the complexes improved with time attaining a maximum of 4.76 (1.08) and 4.84 (1.49) at 180 min p.i. for [$^{99m}\text{Tc}(\text{NS}_3)(2\text{NimNC})$] and [$^{99m}\text{Tc}(\text{NS}_3)(\text{MetNC})$] respectively. Also, the tumor-to-blood ratio of both the complexes

improved with time attaining a maximum of 1.24 (0.08) for [$^{99m}\text{Tc}(\text{NS}_3)(2\text{NimNC})$] and 0.89 (0.07) for [$^{99m}\text{Tc}(\text{NS}_3)(\text{MetNC})$] at 180 min p.i.

4.4. Conclusions

The '4+1' mixed ligand strategy was successfully employed for the preparation of ^{99m}Tc complexes of 2-nitroimidazole and metronidazole. The complexes could be prepared at low ligand concentration and showed high stability in labelling mixture and human serum. Cyclic voltammetry studies of the ligand and rhenium complexes clearly indicated that there is no significant change in SERP value of nitroimidazole ligand upon forming the complex. Preliminary biological evaluation of [$^{99m}\text{Tc}(\text{NS}_3)(2\text{NimNC})$] and [$^{99m}\text{Tc}(\text{NS}_3)(\text{MetNC})$] in Swiss mice bearing fibrosarcoma tumor showed acceptable tumor-to-blood and tumor-to-muscle ratio. However, low uptake in tumor was observed. This is possibly attributed to fast clearance of the complex from blood, whereby the complex spends insufficient time in tumor to get reduced and trapped. Thus, the results obtained with ^{99m}Tc -'4+1' nitroimidazole complexes provided pertinent insights towards further modifications using an amine or a carboxylic acid functionalized NS_3 chelator (NS_3en or $\text{NS}_3\text{-COOH}$) in order to decrease the lipophilicity of the complex which may considerably improve the residence time of the complex in hypoxic cells.

CHAPTER 5

PREPARATION OF A ^{99m}Tc -FOLIC ACID RADIOTRACER USING

$[\text{}^{99m}\text{TcN}(\text{PNP})]^{2+}$ METAL FRAGMENT

5.1. Introduction

Folic acid is a water soluble B vitamin that is essential for cell survival and proliferation [219,220]. Folic acid is constituted of pteronic acid covalently bound to a glutamic acid moiety. Entry of folate into the cell is mediated by membrane-bound folate receptors (FRs) or reduced folate carriers (RFCs), whose affinities differ for different forms of folate and the distribution varies in normal and malignant tissues [221,222]. FRs are over-expressed in a variety of malignancies including epithelial, ovarian, cervical, breast, lung, kidney and colorectal tumors, while being generally absent in normal tissues apart from epithelial cells in kidney and placenta [223]. FRs thus acts as potential molecular target for imaging and therapy of FR-positive tumors [224,225]. In the recent past, several folic acid conjugates with drugs [226,227] or fluorescent probes [228] have been studied for treatment or detection of FR positive tumors. The vitamin folic acid, emerged as an almost ideal targeting agent for imaging purposes and therapy of cancer and inflammatory diseases because of the very high affinity ($K_D < 10^{-9}$ M) to the FRs and because of its non-toxic and non-immunogenic properties [224]. With regard to the development of radiotracers, further advantages of using folic acid are its accessibility for chemical modification and its robustness at high temperatures which are often required for radiolabeling procedures [229].

While, a number of SPECT- and PET- based folate radioconjugates have been developed in the past [230-234], a few have been clinically evaluated [235,236], and none received regulatory clearance for routine clinical use. A number of these radiotracers experience high renal uptake where FRs are densely populated limiting their utility as an established radiotracer for FR positive cancers [237-239]. Pre-loading with anti-folate drugs (pemetrexed) in some of these cases have reduced affinities of the radiolabeled folates for receptors present on kidney

[240]. However, use of these modalities subject the diseased patients to additional stress. To circumvent the above limitation, an attempt is made to design a radiolabeled folate radiotracer which targets FRs on tumor sites but minimizes the burden of radiation to renal tissue. While designing such a radiotracer with ^{99m}Tc , the advantages of its diverse coordination chemistry can be utilized whereby fine tuning of the *in vivo* pharmacokinetics could be envisaged by varying the linker, bifunctional chelator as well as the radiosytron.

The high renal uptake of radio-folates is attributable to the highly hydrophilic nature of these complexes which facilitates clearance mainly via the renal pathway. Thus, a rational approach in designing a new ^{99m}Tc -folate complex is to introduce lipophilicity to the final complex, so as to favor the clearance via the hepatic route. In this direction, use of the $[\text{}^{99m}\text{TcN}(\text{PNP})]^{2+}$ precursor which is known to form lipophilic complexes and facilitate *in vivo* clearance of the complex via the hepatic route [107-110], was chosen for labeling the parent folic acid molecule. The $[\text{}^{99m}\text{TcN}(\text{PNP})]^{2+}$ metal fragment forms inert complexes with bidentate π -donor ligands containing $[\text{S}^-, \text{S}^-]$, $[\text{N}, \text{S}^-]$ or $[\text{O}^-, \text{S}^-]$ groups [111,112]. Cysteine is a commonly used bi-functional chelator for this metal fragment which has been evaluated in past with several carrier molecules/ biomolecules [110].

Chemical modification of folic acid by covalent attachment of prosthetic groups using the pendant approach can in general be accomplished via any of the two carboxylic functionalities at the alpha (α) and gamma (γ) positions of the glutamate moiety (**Fig. 5.1**) [241]. However, almost all folate-based chemotherapeutic drugs and radiopharmaceuticals have been prepared via derivatization at the γ -position, as the α -carboxylic acid group in the glutamate part of folic acid is synthetically less easily accessible for conjugation due to steric hindrance [242] and also

because the γ -folate conjugates have higher affinity for FRs compared with the α -conjugates [243].

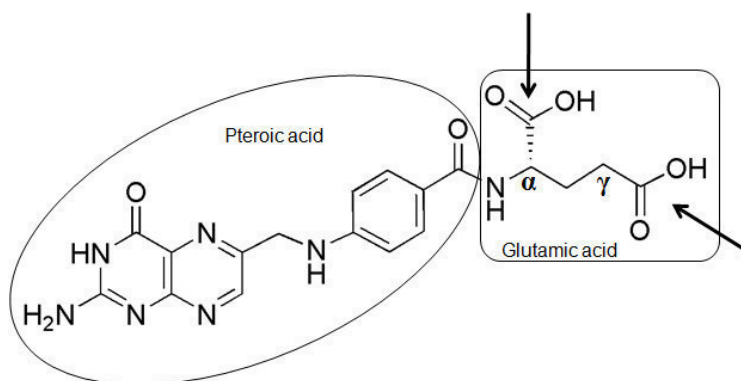


Fig. 5.1. Chemical structure of folic acid. The two carboxylic functionalities are accessible for derivatization (black arrows).

In the present work, conjugation of γ - carboxylic acid of folic acid with the amino group of cysteine BFCA was carried out resulting in the formation of the conjugate, which was subsequently radiolabeled with $[^{99m}\text{TcN}(\text{PNP})]^{2+}$ metal fragment to yield the final complex. Bioevaluation studies of the synthesized conjugate and the tracer in FR positive epithelial carcinoma cell line KB-31 [244] was carried out to evaluate the affinity of the radiotracer for FR imaging. Additionally, a preliminary *in vivo* distribution study of the radiolabeled complex in Swiss mice was carried out to assess its pharmacokinetic behavior.

5.2. Experimental

5.2.1. Materials and methods

Folic acid, S-trityl cysteine, 1-Ethyl-3-(3-dimethylaminopropyl)carbodiimide (EDC), triethyl silane and trifluoroacetic acid were procured from Aldrich. N-(2-methoxyethyl)-2-(diphenylphosphino)-N-(2-(diphenylphosphino)ethyl)ethanamine (PNP2) was synthesized

following a reported procedures [109]. All other reagents used were of analytical grade. ^3H -Folic acid (Specific activity 12 Ci/mmol) was supplied by Board of Radiation in Isotope Technology (BRIT), Navi Mumbai, India. HPLC analyses were carried out on a JASCO PU 2080 Plus dual pump HPLC system, Japan, with a JASCO 2075 Plus tunable absorption detector and a Gina Star radiometric detector system, using a C18 reversed phase HiQ Sil column (5 μm , 4 \times 250 mm). ^1H -NMR spectra were recorded using 300 MHz Bruker Avance II, spectrometer, Germany. Mass spectra were recorded on a Varian Prostar mass spectrometer using the ESI technique. KB-31 cells were obtained from the Cell Repository of the National Centre for Cell Science (NCCS), Pune, India.

5.2.2. Synthesis

5.2.2.1. Synthesis of *S*-trityl cysteine ester (**5a**)

Compound **5a** was synthesized following a reported procedure [110]. Briefly, to a suspension of *S*-trityl-L-cysteine (0.5 g, 1.4 mmol) in ethanol, ethyl p-toluensulfonate (0.5 mL, 3 mmol) was added and the reaction mixture was refluxed under for 48 h, during which time dissolution occurred. Thereafter, the solvent was removed under vacuum and the residue was dissolved in an aqueous solution of KHCO_3 . The aqueous layer was extracted with dichloromethane (15 mL \times 3) and combined organic extracts were pooled together and dried under vacuum. The crude product obtained was purified by silica gel column chromatography eluting with dichloromethane to obtain compound **5a**. ^1H -NMR (300 MHz, CDCl_3): δ = 1.23 (t, 3H, $-\text{CH}_3$), 2.51-2.64 (m, 2H, $-\text{CH}_2\text{S}-$), 3.20 (m, 1H, $-\text{CHNH}_2$), 4.14 (q, 2H, $-\text{OCH}_2\text{CH}_3$), 7.21-7.43 (15H, Ar). ESI-MS (+ve mode): mass (calculated) $\text{C}_{24}\text{H}_{25}\text{NO}_2\text{S}$ 391.53; m/z (observed) 392.5 $[\text{M}+\text{H}]^+$.

Synthesis of folic acid-cysteine conjugate

5.2.2.2. Synthesis of (Ethyl, *S*-trityl cysteinyl amido) Folic acid (**5b**)

Folic acid (100 mg, 0.23 mmol) and compound **5a** (82 mg, 0.21 mmol) were dissolved in minimum volume of DMSO and the mixture cooled to 0°C. To the cooled solution, EDC (50 mg, 0.25 mmol) was added and the reaction mixture stirred for 1 h. Subsequently, it was brought to room temperature and reaction continued overnight. Upon completion of the reaction, the mixture was gradually poured into a vigorously stirred solution of ether cooled to 0°C. The supernatant was slowly decanted and the yellow solid thus obtained was washed with ether (0°C) and dried under vacuum to obtain compound **5b** (148 mg, 80%).

¹H NMR (300 MHz, DMSO-d₆): δ = 1.07 (t, 3H, J = 7.5 Hz), 1.89-2.01 (m, 2H), 2.31 (t, 2H, J = 7.5 Hz), 3.98-3.99 (m, 2H), 4.03-4.1 (m, 1H), 4.28-4.36 (m, 1H), 4.48 (d, 2H, J = 6 Hz), 6.63 (d, 2H, J = 7.8 Hz), 7.22-7.32 (m, 15H), 7.64 (d, 2H, J = 7.8 Hz), 8.64 (s, 1H), 11.43 (br s, 1H) (**Fig. 5.2**). ESI-MS (+ve mode): mass (calculated) C₄₃H₄₂N₈O₇S 814.29; m/z (observed) 815.3 [M+H]⁺.

5.2.2.3. Synthesis of (*S*-trityl cysteinyl amido) Folic acid (**5c**)

A mixture of compound **5b** (100 mg, 0.12 mmol) and 1M KOH solution (0.54 mmol, 540 μ L) in MeOH (1 mL) was stirred overnight at room temperature. Upon completion of the reaction, MeOH was removed under vacuum, water (2 mL) was added and the pH of the mixture was adjusted to 3 using aqueous 2N HCl to precipitate compound **5c**. This was filtered, washed with water and cold ether and dried under vacuum. Yield: (91 mg, 95%).

ESI-MS (-ve mode): mass (calculated) C₂₂H₂₄N₈O₇S 786.2; m/z (observed) 785.0 [M-H]⁻ (**Fig. 5.3**).

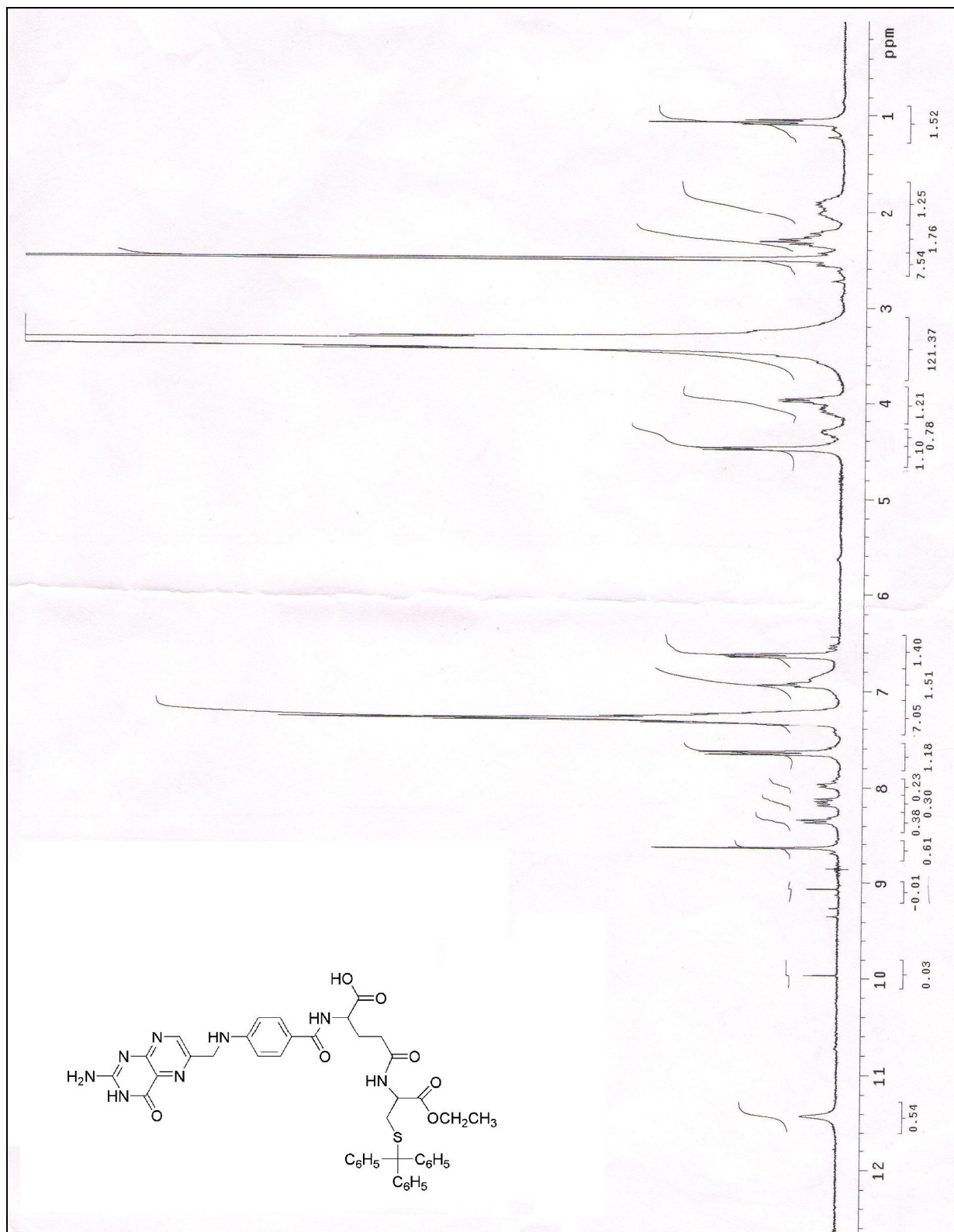


Fig. 5.2. $^1\text{H-NMR}$ spectra of compound **5b**

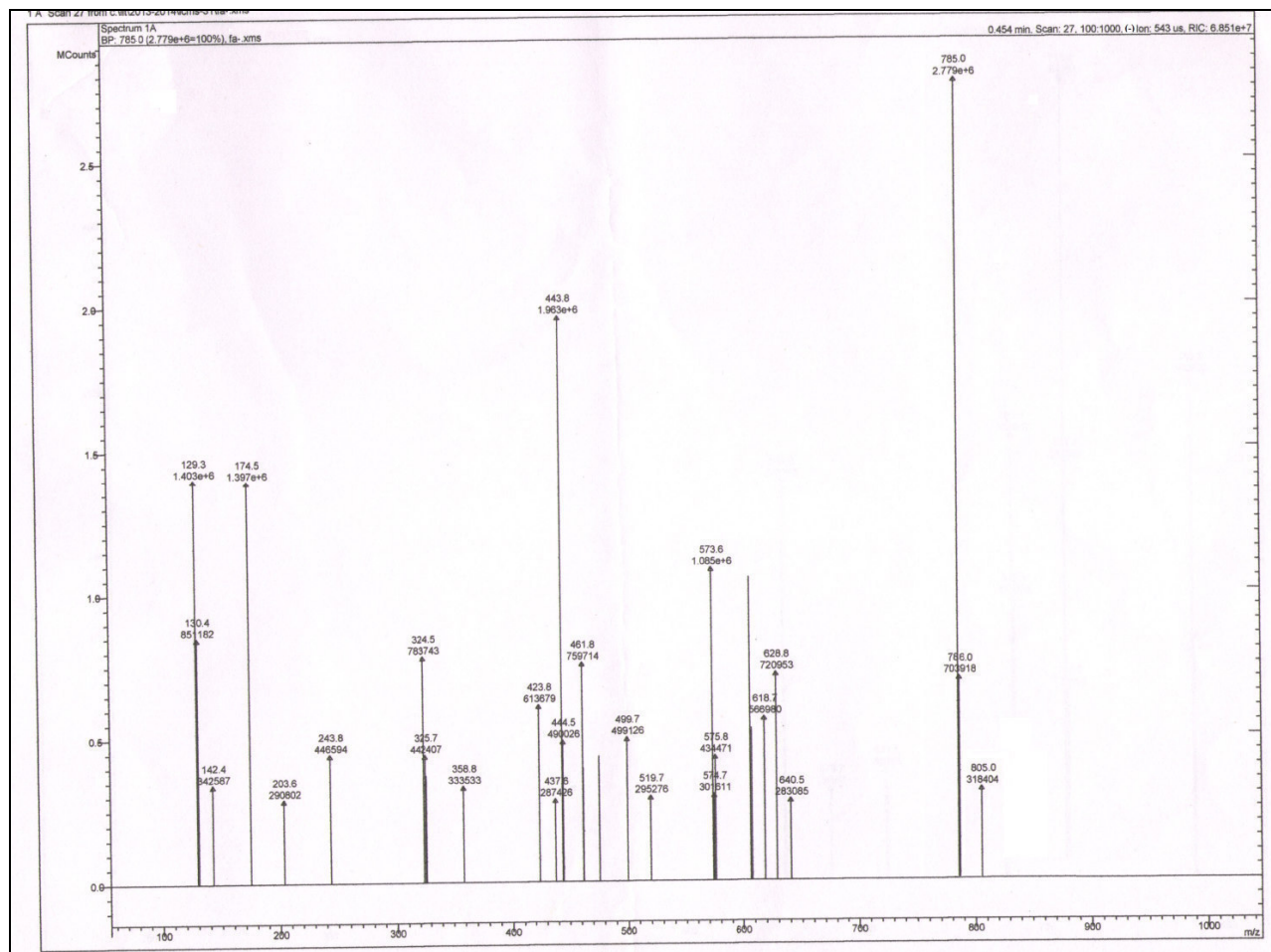


Fig. 5.3. ESI-MS of compound **5c**

5.2.2.4. *Synthesis of (cysteinyl amido) folic acid (5d)*

The compound **5c** (20 mg, 0.025 mmol) was stirred with trifluoroacetic acid (TFA) (2 mL) for 10 min at room temperature. To the resultant yellow solution, triethylsilane was added dropwise until the solution turned colorless. Stirring was continued for another 2 h. The solvent was removed under vacuum to obtain the desired product **5d**.

ESI-MS (+ve mode): mass (calculated) $C_{22}H_{24}N_8O_7S$ 544.1; m/z (observed) 544.1 $[M]^+$ (**Fig.**

5.4)

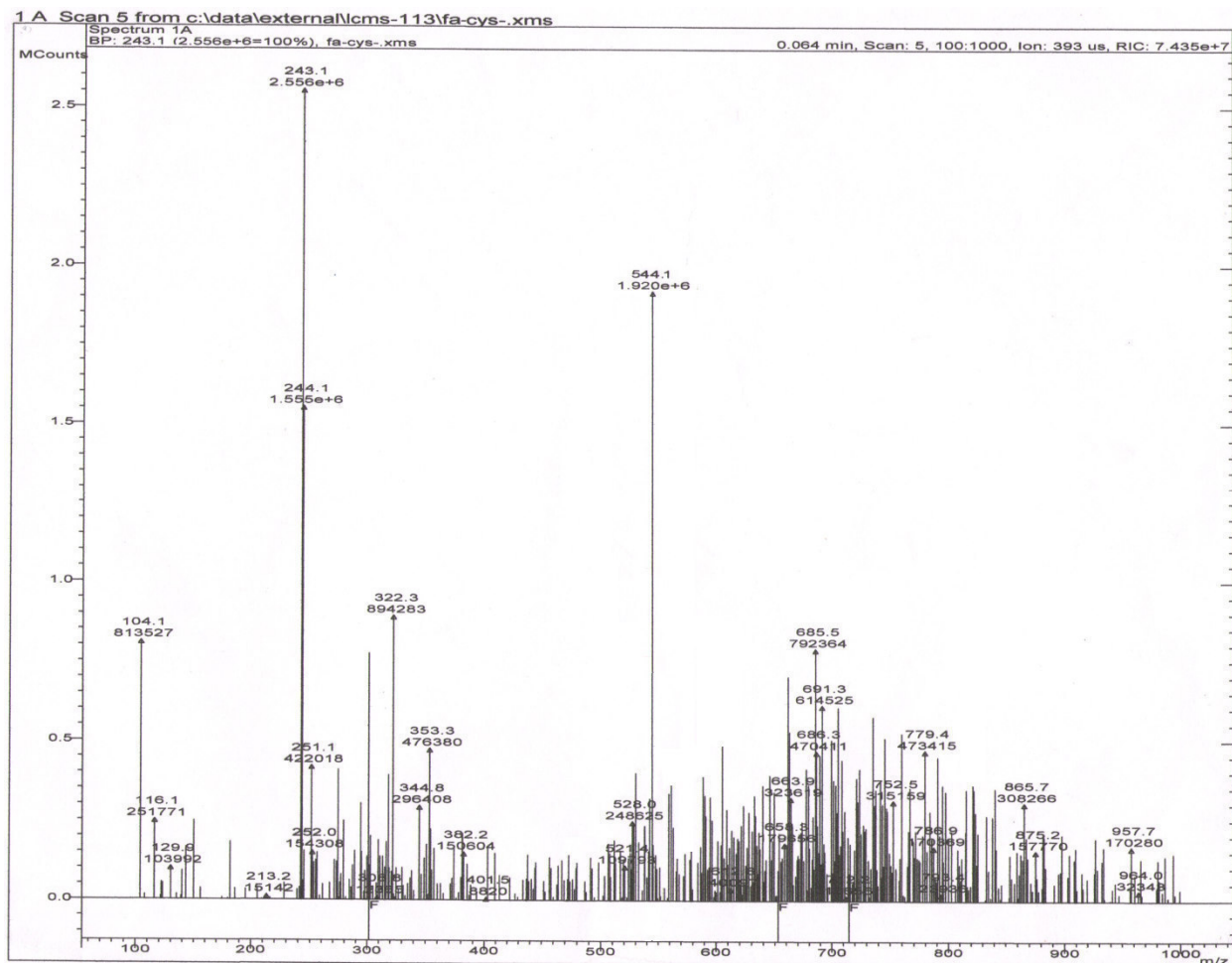


Fig. 5.4. ESI-MS of compound **5d**

5.2.3. Radiolabeling

At first [^{99m}TcN] $^{2+}$ core was prepared following a reported procedure [245]. Briefly, to succinic dihydrazide (5 mg) dissolved in 250 μL of ethanol, SnCl_2 (0.1 mg, 2 mg/mL) and $^{99m}\text{TcO}_4^-$ (750 μL , 30 mCi) were added. The reaction mixture was incubated at room temperature for 30 minutes for formation of [^{99m}TcN] $^{2+}$ intermediate. To this core, PNP2 ligand (2 mg) and compound **5d** (2 mg) were added simultaneously and heated at 100°C for 30 minutes. The formation of [$^{99m}\text{TcN}(\text{PNP})$]-folic acid complex (**5e**) was characterized by reversed phase HPLC.

5.2.4. Quality control studies

5.2.4.1. HPLC

The radiochemical purity of the [$^{99m}\text{TcN}(\text{PNP})\text{]}^{2+}$ intermediate as well as the final complex (**5e**) was assessed by HPLC using a C18 reversed phase column. Water (A) and methanol (B) were used as the mobile phase and the following gradient elution technique was adopted for the separation (0 min 50% A, 15 min 0% A, 50 min 0% A). Flow rate was maintained at 1 mL/min. About 20 μL of the test solution was injected into the column and elution was monitored by observing the radioactivity profile.

The same C18 reversed phase analytical column was used for the purification of complex. On purification through HPLC, around 100 μCi / 3.7 MBq of the radiolabeled folic acid product (**5e**) was obtained in methanol-water medium which was removed under vacuum and reformulated in aqueous 10% ethanol solution. This was used for carrying out the *in vitro* and *in vivo* evaluation studies.

5.2.4.2. Octanol-Water partition coefficient ($\text{Log } P_{o/w}$)

The radiolabeled complex **5e** (0.1 mL, ~3.7 MBq) was mixed with water (0.9 mL) and octanol (1 mL) using a vortex mixer for about 3 minutes and centrifuged for 5 minutes at 3500 g to get clear separation of the two layers. The octanol layer (0.8 mL) was withdrawn and equal volume of fresh double distilled water was added. The mixture was again vortexed and centrifuged as described above. Equal aliquots of the two layers were withdrawn and measured for the radioactivity. The readings thus obtained were used to calculate the $\text{Log } P_{o/w}$ value of the complex.

5.2.4.3. Stability studies

Cysteine challenge studies

The purified [$^{99m}\text{TcN}(\text{PNP})$]-folic acid complex **5e** (100 μCi / 3.7 MBq, 100 μL) was challenged with 10 mM cysteine solution (100 μL) and saline (300 μL) and incubated at 37°C for 1 h to ascertain the kinetic stability of the complex *in vivo*. The complex was then analyzed by HPLC.

Serum stability

The radiolabeled complex **5e** (50 μCi / 1.85 MBq, 50 μL) was added to 250 μL of serum and incubated at 37°C for 1 h. About 100 μL of the mixture was taken and to that 100 μL of acetonitrile was added to precipitate the serum proteins and centrifuged at 3500 g for 10 minutes. The supernatant was analyzed by HPLC to check the stability of the complex in serum.

5.2.5. In vitro cell binding studies

5.2.5.1. Estimation of IC_{50}

In vitro cell study was performed to assess the inhibition of ^3H -folic acid by unlabeled ligand, in epithelial carcinoma cell line KB-31, which is reported to express folate receptors [244]. They were grown at 37°C with 5% CO_2 atmosphere in folate deficient RPMI-1640 medium with 10% fetal bovine serum (FBS) added as a growth supplement. When sufficient cell mass was achieved the cells were harvested by trypsinization and plated into 24-well plates at a concentration of 2×10^5 cells/well in folate deficient RPMI-1640 medium. The plates were kept overnight at 37°C to allow for adhesion of cells to plate surface and formation of a monolayer. On the day of the experiment, the wells were washed twice with ice cold Hank's buffered salt solution (HBSS) and fresh folate deficient RPMI 1640 medium was added.

Prior to addition of ^3H -folic acid tracer, the wells were pre-incubated with a set of concentrations of ligand **5d** (0.0125 to 500 μM) at 4°C for 1 h. The total reaction volume in all wells was adjusted to 1 mL using HBSS. For comparison, another set of similar concentrations of native folic acid were prepared and incubated with KB-31 cells in an identical fashion. After the pre-incubation, ^3H -folic acid (2 μM) was added to all the wells. The plates were then incubated at 4°C for another 3 h to allow uptake of the tracer till equilibrium is reached. At the end of the incubation period, the cells were washed twice with ice cold HBSS. Subsequently, 1 mL of dimethyl sulfoxide (DMSO) was added to dissolve the cell monolayer. The dissolved contents of the wells were added to a set of scintillation tubes, each containing 4 mL of scintillation cocktail. The contents in the tubes were mixed and taken immediately for manual counting on a Hidex Triathler single well liquid scintillation counter with suitable settings for ^3H . Taking the mean value of bound activity from ^3H -folic acid at each concentration of cold ligand **5d** or parent folic acid, a curve of inhibition was plotted using Graphpad Prism software (v6.01).

5.2.5.2. Cell uptake studies of [$^{99\text{m}}\text{TcN(PNP)}$]-folic acid complex

As described in previous section KB-31 cells were cultured in folate-deficient RPMI1640 medium and harvested by trypsinization. They were plated at 10^6 cells/well concentration in 12-well plates and kept overnight at 37°C , 5% CO_2 atmosphere to allow for monolayer formation. On the day of the experiment, the wells were washed twice with ice cold Hank's buffered salt solution (HBSS) and fresh folate deficient RPMI 1640 medium was added. For controls, one set of cells was pre-incubated with 100-fold concentration of unlabeled folic acid at 4°C for 60 min. Purified [$^{99\text{m}}\text{TcN(PNP)}$]-folic acid complex (**5e**) (2 $\mu\text{Ci}/74$ KBq) were added to each wells. Reaction volume was adjusted to 500 μL and the set was incubated at 4°C for 180 min (presumed sufficient for equilibration). After the incubation, the wells were washed twice with

ice cold HBSS. 1mL of 1N NaOH was added to each well to dissolve the cell pellet. The resulting suspension was collected into counting tubes which were then measured in a well-type NaI(Tl) detector with suitable energy window for ^{99m}Tc . The bound activity measurements for binding and inhibition tubes were then compared to obtain a clear idea of specific binding of the tracer to KB-31 cells.

5.2.6. *In vivo* evaluation studies

Normal Swiss mice (20–25 g body weight) were used for the *in vivo* distribution assays of the prepared [$^{99m}\text{TcN}(\text{PNP})$]-folic acid complex (**5e**). The HPLC purified radiolabeled preparation (100 μL , 20 μCi) was administered intravenously. Individual sets of animals (n=4) were utilized for studying the biodistribution at three different time points (30 min, 60 min, 180 min). The animals were sacrificed immediately at the end of the respective time point and the relevant organs and tissue were excised for measurement of associated activity. The organs were weighed and the activity associated with each was measured in a flat-bed type NaI(Tl) counter with suitable energy window for set for ^{99m}Tc . For the sake of comparison the activity retained in each organ/tissue was expressed as a per cent value of the injected dose per gram (% ID/g).

5.3. Results and discussion

Development of radiotracers for FR imaging is of relevant interest to researchers, due to significant overexpression of these receptors on several types of cancer. However, presence of these receptors on kidney entails radiation risk to patients administered with folic-acid based radiotracers. To diminish the renal uptake without compromising the target uptake characteristics, a new ^{99m}Tc folic acid complex was designed via the use of [$^{99m}\text{TcN}(\text{PNP})$] $^{2+}$ metal fragment. The strategy involved synthesizing a suitable folic acid derivative and attaching it to [$^{99m}\text{TcN}(\text{PNP})$] $^{2+}$ metal fragment.

5.3.1. Synthesis

Folic acid has been derivatized with a cysteine BFCA in a three-step synthetic procedure.

The synthetic scheme for the formation of conjugate is shown in **Fig. 5.5**.

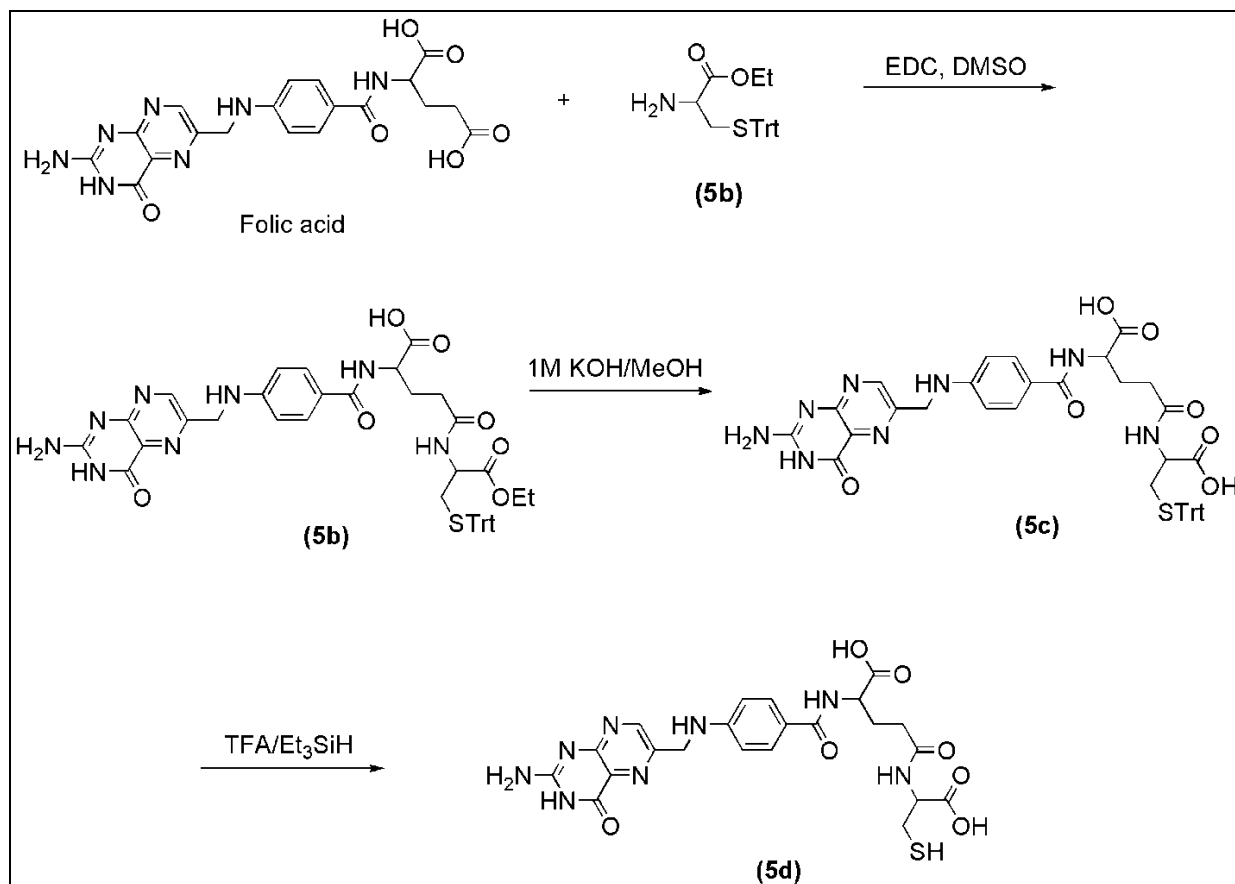


Fig. 5.5. Synthesis scheme of folic acid-cysteine conjugate (5d)

The γ -acid group of folic acid was conjugated with amino residue of *S*-Trt cysteine ester (5a), in presence of EDC activation to yield compound 5b. Alkaline hydrolysis of the ethyl ester group of the resulting conjugate led to formation of the tritylated cysteine-folic acid 5c. The characterization of intermediates were carried using ¹H-NMR and ESI-MS. The δ value 4.28-4.36 (m, 1H) of α -proton observed in ¹H-NMR data of compound 5b confirmed the selective

attachment of cysteine residue at γ -acid. In the final step, the desired ligand **5c** was obtained after trityl deprotection using trifluoroacetic acid (TFA) and triethyl silane. The target ligand **5d** contains free carboxyl and thiol groups suitable for complexation with $[\text{}^{99\text{m}}\text{TcN(PNP)}]^{2+}$ metal fragment.

5.3.2. Radiolabeling and quality control

The scheme for the preparation of $[\text{}^{99\text{m}}\text{TcN(PNP)}]$ -folic acid complex (**5e**) is shown in **Fig. 5.6**.

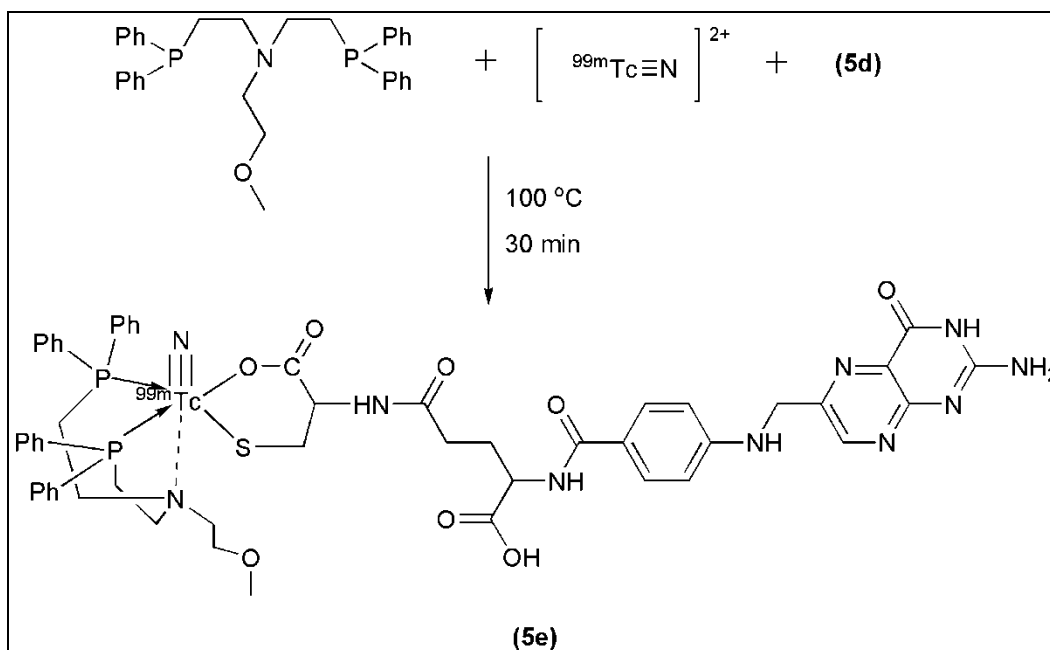


Fig. 5.6. Radiolabeling of folic acid-cysteine conjugate (**5d**)

This involved prior formation of $[\text{}^{99\text{m}}\text{TcN}]^{2+}$ intermediate core. The $[\text{}^{99\text{m}}\text{TcN}]^{2+}$ core was formed with $\sim 95\%$ radiochemical purity as confirmed by TLC using two solvent systems, ethanol/chloroform/toluene/0.5M ammonium acetate (6:3:3:0.5) and saline. This core was further reacted with PNP2 ligand and compound **5d** to form the final complex **5e**. The complex was characterized by HPLC (**Fig. 5.7**). $[\text{}^{99\text{m}}\text{TcN(PNP)}]$ complex formed via cysteine BFCA are known to exist in syn-anti diastereomeric forms which get resolved on HPLC column [110].

Consequently, in the present case two closely spaced peaks were observed at 14.5 min and 15.2 min, different from the peak at 6.45 min assigned to the $[\text{}^{99\text{m}}\text{TcN(PNP)}]^{2+}$ intermediate. Resolving the two diastereomers was not attempted to establish the correctness of stereochemistry as it was beyond the scope of the present work.

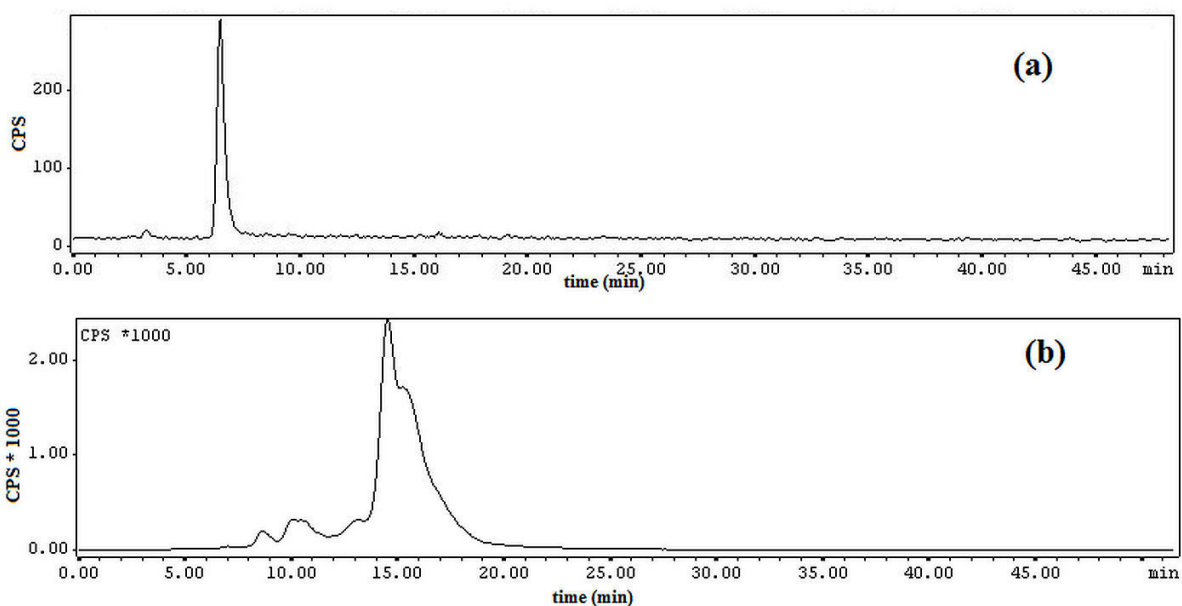


Fig. 5.7. HPLC profile of (a) $[\text{}^{99\text{m}}\text{Tc(N)PNP}_2]^{2+}$ intermediate and (b) $[\text{}^{99\text{m}}\text{Tc(N)PNP}]$ -folic acid complex **5e**

The radiolabeled peak was purified by analytical HPLC (2 times) and the product obtained after solvent removal and re-formulation in 10% ethanol was sufficient for bio-evaluation studies. The $\text{LogP}_{\text{o/w}}$ value of complex **5e** was found to be 0.87. The complex was found to be stable at room temperature and no transchelation of the complex was observed in presence of excess cysteine. Similarly, serum stability studies showed no significant degradation of the tracer up to 1 h.

5.3.3. *In vitro* cell binding studies

In vitro studies in KB-31 cells were carried out using the conjugate **5d** and HPLC purified $[\text{}^{99\text{m}}\text{TcN(PNP)}]$ -folic acid complex **5e**, to ascertain their affinity for FR. The affinity of

the modified folic acid conjugate **5d** was estimated by blocking the uptake of ^3H -folic acid in KB-31 cells. The results of inhibition of ^3H -folic acid by **5d** in comparison with parent folic acid are depicted in **Fig. 5.8**. Using the curve-fitting of the Prism software (one-site fit equation); the IC_{50} of the conjugate **5d** is estimated as 552.7 nM. This is observed to be 10-fold greater than that of parent folic acid (43.11 nM). These results corroborate that the affinity of **5d** for FR has reduced significantly (>10-fold) in the process of synthetic derivatization.

In case of *in vitro* studies with [$^{99\text{m}}\text{TcN}(\text{PNP})$]-folic acid complex **5e**, low level of $^{99\text{m}}\text{Tc}$ activity ($0.5 \pm 0.01\%$ ID/ 10^6 cells) was found to be associated with the cells. This association was however found to be non-specific as addition of excess unlabeled folic acid (100-fold) did not block the uptake of the tracer in the cells. These results conclude that additional modification in the conjugate **5d** via [$^{99\text{m}}\text{TcN}(\text{PNP})$] $^{2+}$ metal fragment adversely affect the folic acid identity, which becomes non-recognizable by FRs present on KB-31 cells.

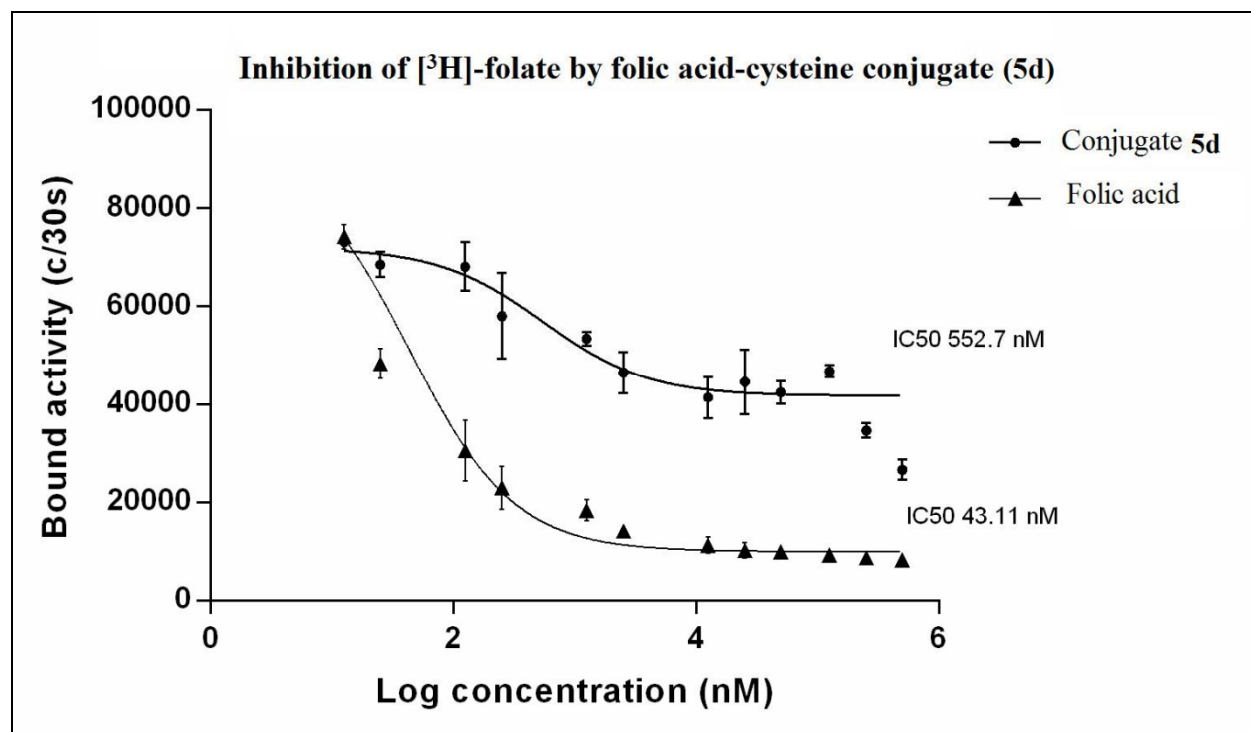


Fig. 5.8. Comparison of inhibition of [³H]-folic acid uptake in KB-31 cells by a) Folic acid-cysteine conjugate **5d** and b) Native folic acid

5.3.4. *In vivo* biodistribution studies

The *in vivo* experiments carried out with the ^{99m}Tc complex indicated favorable features, as was envisaged in the study design, particularly with respect to clearance pattern resulting from the use of the [^{99m}TcN(PNP)]²⁺ pharmacophore. **Table 1** shows the results of biodistribution studies carried in normal Swiss mice. Significant retention of the injected activity was found to be associated with liver (28.9 ± 6.33 %ID/g at 30 min p.i.) and intestines (18.57 ± 3.43 %ID/g at 30 min p.i.) thereby suggesting the role of [^{99m}TcN(PNP)]²⁺ metal fragment in initiating the clearance of the tracer via the hepatic route.

Table 5.1. Biodistribution studies of [$^{99m}\text{TcN}(\text{PNP})$]-folic acid complex (**5e**) in normal Swiss mice

Organs	% ID/g (s.d) [#] (n = 4)		
	30 mins	60 min	180 min
Blood	0.82 ± 0.18	0.30 ± 0.08	0.06 ± 0.02
Liver	28.9 ± 6.33	8.13 ± 0.30	7.14 ± 1.48
Intestine	18.57 ± 3.43	30.53 ± 2.53	31.97 ± 4.13
Kidneys	3.27 ± 0.48	1.71 ± 0.08	1.41 ± 0.34
Stomach	4.06 ± 1.56	1.1 ± 0.55	1.05 ± 0.05
Heart	1.14 ± 0.38	0.37 ± 0.19	0.28 ± 0.14
Lungs	1.93 ± 0.13	0.93 ± 0.23	0.70 ± 0.24
Muscle	0.7 ± 0.28	0.00 ± 0.00	0.00 ± 0.00
Spleen	1.54 ± 0.33	1.63 ± 0.62	0.68 ± 0.04
Excretion*	34.34 ± 4.41	52.15 ± 2.29	56.66 ± 2.82

[#]%ID/g – Percentage injected dose per gram; s.d – standard deviation, *%Excretion has been indirectly calculated by subtracting the activity accounted for all the organs from total injected activity.

Slow movement of activity from liver to intestines is observed for the tracer, which may be due to presence of PNP2 ligand in the final complex **5e**, which clears out slowly from the liver. The latter behavior has been attributed to the presence of non-metabolizable phenyl residues on phosphorus. Hence, use of other PNPs such as 2-((1,1-dimethoxypropyl)phosphanyl)-N-(2-((1,1-dimethoxypropyl)phosphanyl)ethyl)-N-(2-methoxyethyl)etan-1-amine (PNP3)/ 2-(bis(3-methoxypropyl)phosphanyl)-N-(2-bis(3-methoxypropyl)phosphanyl)ethyl)-N-(2-

ethoxyethyl)ethan-1-amine (PNP5)/ 2-(bis(3-ethoxypropyl)phosphanyl)-N-(2-(bis(3-ethoxypropyl)phosphanyl)ethyl)-N-(2-ethoxyethyl)ethan-1-amine (PNP6) carrying ether residues may result in the desirable features of expediting the clearance from the liver and thereby favoring abdominal imaging [246]. The complex was found to clear rapidly from other non-target organs such as blood, lungs and muscle.

5.4. Conclusion

A Folic acid - cysteine conjugate where cysteine functions as a bidentate chelator has been synthesized for complexation with $[\text{}^{99\text{m}}\text{Tc}(\text{N})\text{PNP}]^{2+}$ metal fragment to yield a $^{99\text{m}}\text{Tc}$ -based radiotracer. The radiolabeled complex was obtained in 88% radiolabeling yield. The *in vitro* cell uptake studies in FR positive KB-31 cells revealed reduction in the affinity of the folic acid-cysteine conjugate in comparison with the native folic acid. The preliminary *in vivo* distribution of the complex (**5e**) exhibited high association of activity with liver and intestines and provided support to the rationality of the present design as clearance of labeled folic acid could be effected via the hepatic route. Thus, the study provided pertinent insights towards improving the receptor uptake by designing a similar $[\text{}^{99\text{m}}\text{TcN}(\text{PNP})]$ -folic acid radiotracer by suitable structural modification. This could be possibly achieved by introducing hydrocarbon chain linkers between the cysteine moiety and the folic acid residue, while using the same metal fragment which will ensure clearance via the hepatobiliary route.

SUMMARY

The pharmacokinetics of the radiotracers can be systematically modified by the structural changes in the targeting vector. This can be done either via modification of the coordination environment around the radiometal or by using different pharmacokinetic modifying (PKM) linkers. In this regard, the diverse redox chemistry of ^{99m}Tc provides a wide spectrum of opportunities to modify the structure of Tc-complexes by a careful choice of different cores and chelators. The work carried out in the present thesis demonstrates the use of novel strategies of ^{99m}Tc labeling viz. $[\text{}^{99m}\text{TcN}]^{2+}$ core, $[\text{}^{99m}\text{Tc}(\text{CO})_3]^+$ core, ^{99m}Tc -HYNIC core and ^{99m}Tc -‘4 + 1’ mixed ligand approach towards the preparation of target-specific ^{99m}Tc -radiotracers. Each of these cores has been used in labeling of different biomolecules (cRGDfK peptide, cNGR peptide, Nitroimidazoles, Folic acid) to examine the efficacy of the radiolabeling methodology. The labeling approach for a particular biomolecule was selected considering the fact that biodistribution and targeting capability of the complex depends exclusively on lipophilicity, size and charge. Towards this, the biomolecules used were synthesized/derivatized accordingly to radiolabel with ^{99m}Tc using the desired labeling approach.

The small size, kinetically inert $[\text{}^{99m}\text{Tc}(\text{CO})_3(\text{H}_2\text{O})_3]^+$ is used for preparing two neutral $^{99m}\text{Tc}(\text{CO})_3$ -labeled cRGDfK monomers with and without PEG₇ as the PKM, via click chemistry approach. In this respect the cRGDfK peptide has been derivatized at ϵ -amino group of lysine by conjugation with N₃-PEG₇-COOH/N₃-CH₂-COOH to prepare a PEGylated and a non-PEGylated analogue of cRGDfK. A tridentate chelator was then incorporated by click chemistry conjugation of the two peptide-azides for radiolabeling with $[\text{}^{99m}\text{Tc}(\text{CO})_3(\text{H}_2\text{O})_3]^+$ precursor. The radiotracers, $^{99m}\text{Tc}(\text{CO})_3$ -Pra-Tz-CH₂-cRGDfK (**2e**) and $^{99m}\text{Tc}(\text{CO})_3$ -Pra-Tz-PEG₇-cRGDfK (**2f**) were prepared in good radiochemical yield (~90%) and were found to be stable in serum, with no

significant degradation till 24 h. The two neutral $^{99m}\text{Tc}(\text{CO})_3$ radiotracers prepared exhibited receptor-mediated uptake in melanoma tumor thus showing specificity towards the $\alpha_v\beta_3$ receptors. Comparative *in vivo* evaluation of the two $^{99m}\text{Tc}(\text{CO})_3$ -labeled radiotracers, **2e** and **2f** was carried out in C57BL/6 mice bearing $\alpha_v\beta_3$ -positive melanoma tumors to evaluate their potential towards targeting integrin $\alpha_v\beta_3$ receptors. The $^{99m}\text{Tc}(\text{CO})_3$ -labeled PEGylated cRGDFK peptide (**2f**) analogue had higher tumor uptake than the non-PEGylated analogue (**2e**) however the increase in the tumor uptake on introduction of PEG₇ unit was accompanied by slower clearance from other organs which resulted in decreased target-to-background ratios. The *in vivo* kinetics of $^{99m}\text{Tc}(\text{CO})_3$ -labeled radiotracer, $^{99m}\text{Tc}(\text{CO})_3$ -Pra-Tz-CH₂-cRGDFK (**2e**) with only methylene unit as the spacer was found to be more favorable due to higher tumor/blood, tumor/liver, tumor/kidney and tumor/lung ratios.

^{99m}Tc -HYNIC approach is utilized for labeling NGR peptides. Here two HYNIC conjugated cyclic NGR peptide ligands, HYNIC-c(NGR) (**3b**) and HYNIC-PEG₂-c(NGR) (**3c**) were synthesized by Fmoc solid state peptide synthesis method, radiolabeled with ^{99m}Tc and evaluated in CD13-positive human fibrosarcoma HT-1080 tumor xenografts. The radiotracers, ^{99m}Tc -HYNIC-c(NGR) and ^{99m}Tc -HYNIC-PEG₂-c(NGR) could be prepared in ~95% radiochemical purity (RCP) and exhibited excellent *in vitro* and *in vivo* stability. In *in vitro* cell uptake studies, the two radiotracers demonstrated significantly ($p < 0.05$) higher uptake in CD13-positive human fibrosarcoma HT-1080 cells in comparison to CD13-negative human breast adenocarcinoma MCF-7 cells, indicating receptor-mediated uptake. *In vivo* biodistribution studies carried out in athymic nude mice bearing HT-1080 fibrosarcoma tumor revealed similar uptake of ^{99m}Tc -HYNIC-c(NGR) and ^{99m}Tc -HYNIC-PEG₂-c(NGR) in HT-1080 tumors. The highly hydrophilic nature of the radiotracers led to rapid clearance from liver and intestine with

preferential renal excretion. The target-to-non-target ratios (tumor-to-blood, tumor-to-liver) of presently studied radiotracers were observed to be better with respect to the previously reported ^{99m}Tc -labeled NGR peptides prepared using direct labeling method and ^{99m}Tc -oxo core.

The '4+1' mixed ligand approach is a relatively less explored strategy for radiolabeling molecules with ^{99m}Tc . The '4+1' mixed ligand method of labeling is used to prepare neutral lipophilic complexes of nitroimidazole derivatives for targeting tumor hypoxia. In this work isocyanide derivatives of two nitroimidazoles, viz. 2-nitroimidazole (2NimNC **4g**) and metronidazole (MetNC **4i**), were synthesized and radiolabeled with ^{99m}Tc using '4+1' mixed ligand approach. The complexes $[\text{}^{99m}\text{Tc}(\text{NS}_3)(2\text{NimNC})]$ and $[\text{}^{99m}\text{Tc}(\text{NS}_3)(\text{MetNC})]$ could be prepared in excellent yield (>90%). The structure of ^{99m}Tc -complexes prepared at the no-carrier-added (nca) level was corroborated by spectroscopic analysis with the corresponding rhenium analogues at the macroscopic level. Preliminary biological evaluation of the two nitroimidazole-'4+1' mixed ligand complexes in Swiss mice bearing fibrosarcoma tumor showed uptake and retention of the complexes in tumor.

The $[\text{}^{99m}\text{TcN}(\text{PNP})]^{2+}$ precursor which is known to form lipophilic complexes and facilitate *in vivo* clearance of the complex via the hepatic route, was chosen for labeling the folic acid molecule. In this respect, folic acid was derivatized at the γ -acid group with a cysteine bifunctional chelating agent and subsequently reacted with the preformed $[\text{}^{99m}\text{TcN}]^{2+}$ intermediate in presence of PNP2 (bisphosphine) ligand, to yield the final complex (**5e**). Preliminary, *in vivo* distribution of the complex exhibited high association of activity with liver and intestines and provided support to the rationality of the present design as clearance of labeled folic acid could be effected via the hepatic route.

From the work carried out in this thesis, the following insights are obtained which provide guidelines for carrying out future studies:

In the study with $^{99m}\text{Tc}(\text{CO})_3$ -labeled cRGDfK peptide derivatives, the PEG₇ linker could not impart favorable pharmacokinetic features to the radiolabeled cRGDfK peptide. Hence the introduction of a more hydrophilic chelator/ a smaller PEG (PEG₂, PEG₄) may provide better pharmacokinetics and shall form a part of future studies.

The highly hydrophilic NGR peptide based radiotracers prepared using ^{99m}Tc -HYNIC approach exhibited good target-to-non-target ratio, however with rapid washout of the radiotracers. This issue shall be addressed in future studies by introducing hydrophobic linkers and/or using different ^{99m}Tc labeling approach.

The results obtained with ^{99m}Tc -‘4+1’ nitroimidazole complexes provided pertinent insights towards further modifications envisaging for an optimum radiotracer for diagnostic applications for tumor hypoxia. The NS₃ chelator used for preparing ^{99m}Tc -‘4+1’ nitroimidazole complexes can be modified with an amine or a carboxylic acid (NS₃en or NS₃-COOH) in order to decrease the lipophilicity of the complex which may considerably improve the residence time of the complex in hypoxic cells.

While radiolabeling folic acid using the [$^{99m}\text{TcN}(\text{PNP})$]²⁺ as a radiosynthon, modification in the structure of conjugate by linking the BFCA (cysteine) through a long-chain linker can be envisaged to improve the affinity of [$^{99m}\text{TcN}(\text{PNP})$]-folic acid complex towards folate receptors.

References:

1. World Health Organization Fact Sheet no. 297 – Cancer, **2009**.
2. Higgins LJ, Pomper MG. *Semin Oncol*, **2011**, 38, 3–15.
3. Seaman ME, Contino G, Bardessy N, Kelly KA. *Expert Rev Mol Med*, doi: 10.1017/S1462399410001511.
4. Alford R, Ogawa M, Choyke PL, et al. *Mol BioSyst*, **2009**, 5, 1279–1291.
5. *IAEA-TECDOC*, **2008**, 1597, 1.
6. Weissleder R, Pittet MJ. *Nature*, **2008**, 452, 580–589.
7. Wang X, Feng H, Zhao S, et al. *Oncotarget*, **2017**, 8, 20476-20495.
8. Blankenberg FG, Strauss HW. *J Mag Reson Imaging*, **2002**, 16, 352-361.
9. Coleman RE. *Cancer*, **1991**, 67 (4 Suppl), 1261-1270.
10. Bartholomä MD, Louie AS, Valliant JF, et al. *Chem Rev*, **2010**, 110, 2903-2920.
11. Ametamey SM, Honer M, Schubiger PA. *Chem Rev*, **2008**, 108, 1501-1516.
12. Saha GB. *Fundamentals of Nuclear Pharmacy, 2nd Ed.: Springer-Verlag, New York*, **1984**, 220-225.
13. Liu S. *Chem Soc Rev*, **2004**, 33, 445–461.
14. Jurisson S, Berning D, Jia W, et al. *Chem Rev*, **1993**, 93, 1137-1156.
15. Jurisson S, Lydon JD. *Chem Rev*, **1999**, 99, 2205-2218.
16. Liu S, Edwards DS. *Chem Rev*, **1999**, 99, 2235-2268.
17. Reichert DE, Lewis JS, Anderson CJ. *Coord Chem Rev*, **1999**, 184, 3-66.
18. Casey ME, Nutt R. *IEEE Trans Nucl Sci*, **1986**, NS33, 460-463.
19. Rahmima A, Zaidib H. *Nucl Med Commun*, **2008**, 29,193-207.
20. Firestone R. *John Wiley and Sons Inc*, **1996**, 8th edition.

21. Pimlott SL, Sutherland A. *Chem Soc Rev*, **2011**, 40, 149–162.
22. Eckelman WC. *J Am Coll Cardiol Img*, **2009**, 2, 364–368.
23. Srivastava SC. *Semin Nucl Med*, **1996**, 26, 119–131.
24. Pillai MRA, Dash A, Knapp Jr FF (Russ). *J Nucl Med*, **2013**, 54, 313–323.
25. Volkert WA, Hoffman TJ. *Chem Rev*, **1999**, 99, 2269-2292.
26. Dilworth JR, Parrott SJ. *Chem Soc Rev*, **1998**, 27, 43-55.
27. Banerjee S, Pillai MRA, Ramamoorthy N. *Semin Nucl Med*, **2001**, 31, 260–277.
28. Schwochau K. *Angew Chem Int Ed*, **1994**, 33, 2258-2267.
29. Schubiger PA, Alberto R, Smith A. *Bioconjug Chem*, **1996**, 7, 165-179.
30. Liu S. *Adv Drug Deliv Rev.*, **2008**, 60, 1347-1370.
31. Sood DD, Reddy AVR, Ramamoorthy N. *Fundamentals of Radiochemistry*, **2004**, 298.
32. Richards P, Tucker WD, Srivastava SC. *Int J Appl Rad Isot*, **1982**, 33, 793-799.
33. Saha GB. *Fundamentals of Nuclear Pharmacy*, 5th Ed.: Springer-Verlag, New York, **2004**, 64-78.
34. *Special Issue on 'Radionuclide Generator Technology', Radiochimica Acta* 41(2/3) (1987).
35. Zeglis BM, Houghton JL, Evans MJ, et al. *Inorg Chem*, **2014**, 53, 1880–1899.
36. Banerjee SR, Maresca KP, Francesconi L, et al. *Nucl Med Biol*, **2005**, 32, 1–20.
37. Mewis RE, Archibald SJ. *Coord Chem Rev*, **2010**, 254, 1686–1712.
38. Alberto R. in *Technetium-99m Radiopharmaceuticals: Status and Trends, IAEA*, **2009**, ch. 2, pp. 19–34.
39. Liu S, Edwards DS, Barrett JA. *Bioconjugate Chem*, **1997**, 8, 621–636.
40. Arano Y. *Annals Nucl Med*, **2002**, 16, 79-93.

41. Alberto R. *Technetium in Comprehensive Co-ordination Chemistry II*, **2004**, 5, 127.
42. Hom RK, Katzenellenbogen JA. *Nucl Med Biol*, **1997**, 24, 485-498.
43. Mease RC, Lambert C. *Sem Nucl Med*, **2001**, 32, 278-285.
44. Fichna J, Janecka A. *Bioconjugate Chem*, **2003**, 14, 3-17.
45. Eckelman WC. *Eur J Nucl Med*, **1995**, 22, 249-263.
46. Leonard JP, Novotnik DP, Nierinckx RD. *J Nucl Med*, **1986**, 27, 1819-1823.
47. Kung HF, Kim H-J, Kung MP, et al. *Eur J Nucl Med*, **1996**, 23, 1527-1530.
48. Itoh K. *Ann Nucl Med*, **2001**, 15, 179-190.
49. Johnson G, Nguyen KN, Liu ZG, et al. *J Nucl Cardiol*, **1998**, 5, 285-294.
50. Rao TN, Adhikesavalu D, Camerman A, et al. *J Am Chem Soc*, **1990**, 112, 5798-5804.
51. Eshima D, Taylor A Jr, Fritzberg AR, et al. *J Nucl Med*, **1987**, 28, 1180-1186.
52. Bormans G, Cleynhens B, Adriaens P, et al. *J Labelled Compounds Radiopharm*, **1993**, 33, 1065-1078.
53. Kung HF, Guo YZ, Yu CC, et al. *J Med Chem*, **1989**, 32, 433-437.
54. Francesconi LC, Graczyk G, Wehrli S, et al. *Inorg Chem*, **1993**, 32, 3114-3124.
55. Marchi A, Marvelli L, Rossi R, et al. *J Chem Soc Dalton Trans*, 1992, 1485-1490.
56. Ianoz E, Mantegazzi D, Lerch P. *Inorg Chim Acta*, **1989**, 156, 235-239.
57. Kelly JD, Forster AM, Archer CM, et al. *J Nucl Med*, **1993**, 34, 222-227.
58. Level SZ. *Principles of Nuclear Medicine. Technetium and Rhenium compounds. Saunders, Philadelphia*, **1995**, 213.
59. Alberto R, Schibli R, Egli A, et al. *J Am Chem Soc*, **1998**, 120, 7987-7988.
60. Alberto R, Ortner K, Wheatly N, et al. *J Am Chem Soc*, **2001**, 123, 3135-3136.
61. Schibli R, Alberto R, Abram U, et al. *Inorg Chem*, **1998**, 37, 3509-3516.

62. Alberto R, Egli A, Schibli R, et al. *Coord Chem Rev*, **1999**, 190–192, 901-919.
63. Alberto R, Schibli R, Schubiger PA. *J Am Chem Soc*, **1999**, 121, 6076-6077.
64. Schibli R, Bella RL, Alberto R, et al. *Bioconjugate Chem*, **2000**, 11, 345-351.
65. Schibli R, Schwarzbach R, Alberto R, et al. *Bioconjugate Chem*, **2002**, 13, 750-756.
66. Banerjee SR, Levadala MK, Lavarova N, et al. *Inorg Chem*, **2002**, 41, 6417-6425.
67. Kunze S, Zobi F, Kurz P, et al. *Angew Chem Int Ed*, **2004**, 43, 5025-5029.
68. Alves S, Paulo A, Correia JD, et al. *Bioconjugate Chem*, **2005**, 16, 438-449.
69. Stichelberger A, Waibel R, Dumas C, et al. *Nucl Med Biol*, **2003**, 30, 465-470.
70. Psimadas D, Fani M, Gourni E, et al. *Bioorg Med Chem*, **2012**, 20, 2549–2557.
71. Spagnul C, Alberto R, Gasser G, et al. *J Inorg Biochem*, **2013**, 122, 57–65.
72. North AJ, Hayne DJ, Schieber C, et al. *Inorg Chem*, **2015**, 54, 9594–9610.
73. Palma E, Correia JDG, Domingos A, et al. *J Organomet Chem*, **2004**, 689, 4811-4819.
74. Schibli R, Schubiger PA. *Eur J Nucl Med*, **2002**, 29, 1529-1542.
75. Kasten BB, Ma X, Cheng K, et al. *Bioconjugate Chem*, **2016**, 27, 130–142.
76. Muller C, Dumas C, Hoffmann U, et al. *J Organomet Chem*, **2004**, 689, 4712-4721.
77. Stephenson KA, Banerjee SR, Sogbein OO, et al. *Bioconjugate Chem*, **2005**, 16, 1189–1195.
78. Abrams MJ, Juweid M, tenKate CI, et al. *J Nucl Med*, **1990**, 31, 2022-2028.
79. Schwartz DA, Abrams, MJ, Hauser MM, et al. *Bioconjugate Chem*, **1991**, 2, 333–336.
80. King RC, Surfraz MB, Finucane C, et al. *J Nucl Med*, **2009**, 50, 591-598.
81. Babich JW, Fischman AJ. *Nucl Med Biol*, 1995, 22, 25-30.
82. Decristoforo C., Mather S.J. *Bioconjug. Chem.*, **1999**, 10, 431-438.

83. Decristoforo C., Melendez L., Sosabowski J.K., Mather S.J. *J. Nucl. Med.*, **2000**, *41*, 1114-1119.
84. Decristoforo C., Mather S.J. *Nucl. Med. Biol.*, **1999**, *26*, 389-396.
85. Decristoforo C., Mather S.J. *Eur. J. Nucl. Med.*, **1999**, *26*, 869-876.
86. Liu S, Edwards DS, Looby RJ, et al. *Bioconjug Chem*, **1996**, *7*, 63–71.
87. King RC, Surfraz MB, Biagini SCG, et al. *Dalton Trans*, **2007**, *43*, 4998–5007.
88. Decristoforo C, Mather SJ. *Q J Nucl Med*, **2002**, *46*, 195–205.
89. Babich JW, Coco WG, Barrow S, et al. *Inorg Chim Acta*, **2000**, *309*, 123–136.
90. Liu S, Edwards DS, Harris AR. *Bioconjugate Chem*, **1998**, *9*, 583-595.
91. Liu S, Harris AR, Williams NE, et al. *Bioconjugate Chem*, **2002**, *13*, 881-886.
92. Pietzsch HJ, Gupta A, Syhre R, *Bioconjugate Chem*, **2001**, *12*, 538-544.
93. Spies H, Glaser M, Pietzsch HJ, et al. *Inorg Chim Acta*, 1995, *240*, 465–478.
94. Drews A, Pietzsch HJ, Syhre R, et al. *Nucl Med Biol*, **2002**, *29*, 389–398.
95. Künstler JU, Seidel G, Bergmann R, et al. *Eur J Med Chem*, **2010**, *45*, 3645–3655.
96. Künstler JU, Seidel G, Pietzsch HJ. *Appl Rad Isot*, **2010**, *68*, 1728–1733.
97. Giglio J, Fernandez S, Pietzsch HJ, et al. *Nucl Med Biol*, **2012**, *39*, 679-686.
98. Sakhare N, Das S, Mathur A, et al. *RSC Adv*, **2016**, *6*, 64902–64910.
99. Seifert S, Künstler JU, Schiller E, et al. *Bioconjugate Chem*, **2004**, *15*, 856-863.
100. Baldas J, Bonnyman J, Pojer PM, et al. *J Chem Soc Dalton Trans*, **1981**, 1798-1801.
101. Baldas J, Bonnyman J. *Int J Appl Rad Isot*, **1985**, *36*, 133-139.
102. Duatti A, Uccelli L. *Trends Inorg Chem*, 1996, *4*, 27-41.
103. Bolzati C, Boschi A, Uccelli L, et al. *Inorg Chem*, **1999**, *38*, 4473-4479.
104. Pasqualini R, Duatti A. *J Chem Soc Chem Commun*, **1992**, 1354-1355.

105. Pasqualini R, Comazzi V, Bellande E, et al. *Appl Radiat Isot*, **1992**, 43, 1329-1333.
106. Pasqualini R, Duatti A, Bellande E, et al. *J Nucl Med*, **1994**, 35, 334-341.
107. Bolzati C, Boschi A, Duatti A, et al. *J Am Chem Soc*, **2000**, 122, 4510-4511.
108. Boschi A, Bolzati C, Benini E, et al. *Bioconjugate Chem*, **2001**, 12, 1035-1042.
109. Bolzati C, Boschi A, Uccelli L, et al. *J Am Chem Soc*, **2002**, 124, 11468-11479.
110. Boltzati C, Muhmood A, Malago E, et al. *Bioconjugate Chem*, **2003**, 14, 1231-1242.
111. Tisato F, Refosco F, Porchia M, et al. *Inorg Chem*, **2004**, 43, 8617-8625.
112. Bolzati C, Refosco F, Cagnolini A, et al. *Eur J Inorg Chem*, **2004**, 9, 1902-1912.
113. Bolzati C., Benini E, Cazzola E, et al. *Bioconjugate Chem*, **2004**, 15, 628-637.
114. Saha GB. *Fundamentals of nuclear pharmacy. 5th edition, Springer-Verlag, New York, 2004*, 151-172.
115. Kluba CA, Mindt TL. *Molecules*, **2013**, 18, 3206-3226.
116. Struthers H, Spingler B, Mindt TL, et al. *Chem Eur J*, **2008**, 14, 6173-6183.
117. Kolb HC, Finn MG, Sharpless KB. *Angew Chem Int Ed*, **2001**, 40, 2004-2021.
118. Tiwari VK, Mishra BB, Mishra KB, et al. *Chem Rev*, **2016**, 116, 3086-3240.
119. Rostovtsev VV, Green LG, Fokin VV, et al. *Angew Chem Int Ed*, **2002**, 41, 2596-2599.
120. Tornøe CW, Christensen C, Meldal M. *J Org Chem*, 2002, 67, 3057-3064.
121. Mindt TL, Struthers H, Brans L, et al. *J Am Chem Soc*, **2006**, 128, 15096-15097.
122. Dhyani MV, Satpati D, Korde A, et al. *Nucl Med Biol*, **2010**, 37, 997-1004.
123. Fernández S, Crócamo N, Incerti M, et al. *J Label Compd Radiopharm*, **2012**, 55, 274-280.
124. Mousa SA. *Emerging Ther Targets*, **2000**, 4, 143-153.
125. Carmeliet, P. *Nat Med*, **2000**, 6, 389-395.

126. Bögler O, Mikkelsen T. *Cancer J*, **2003**, 9, 205-213.
127. Folkman J. *Semin Oncol*, **2002**, 29, 15-18.
128. Michalski MH, Chen X. *Eur J Nucl Med Mol Imaging*, **2011**, 38, 385-390.
129. Lee BC, Moon BS, Kim JS, et al. *RSC Adv*, **2013**, 3, 782-792.
130. Fass L. *Mol Oncol*, **2008**, 2, 115-152.
131. Eliceiri BP, Cheresch DA. *J Clin Invest*, **1999**, 103, 1227-1230.
132. Chattopadhyay N, Chatterjee A. *J Exp Clin Cancer Res*, **2001**, 20, 269-275.
133. Haubner R. *Eur J Nucl Med Mol Imaging*, **2006**, 33, 54-63.
134. Schottelius M, Laufer B, Kessler H et al. *Acc Chem Res*, **2009**, 42, 969-980.
135. Zhou Y, Chakraborty S, Liu S. *Theranostics*, **2011**, 1, 58-82.
136. Gaertner FC, Kessler H, Wester HJ, et al. *Eur J Nucl Med Mol Imaging* **2012**, 39, S126-S138.
137. Correia JDG, Paulo A, Raposinho PD, et al. *Dalton Trans*, **2011**, 40, 6144-6167.
138. Ji S, Czerwinski A, Zhou Y et al. *Mol Pharm*, **2013**, 10, 3304-3314
139. Liu S. *Mol Pharm*, **2006**, 3, 472-487.
140. Decristoforo C, Faintuch-Linkowski B, Rey A, et al. *Nucl Med Biol*, **2006**, 33, 945-952.
141. Shi J, Kim YS, Chakraborty S, et al. *Bioconjugate Chem*, **2009**, 20, 1559-1568.
142. Decristoforo C, Santos I, Pietzsch HJ, et al. *Q J Nucl Med Mol Imaging*, **2007**, 51, 33-41.
143. Hernandez R, Czerwinski A, Chakravarty R, et al. *Eur J Nucl Med Mol Imaging*, **2015**, 42, 1859-1868.
144. Wu Z, Li ZB, Cai W, et al. *Eur J Nucl Med Mol Imaging*, **2007**, 34, 1823-1831.
145. Harris JM, Chess RB. *Nat Rev Drug Disc*, **2003**, 2, 214-221.
146. Chen X, Hou Y, Tohme M, et al. *J Nucl Med*, **2004**, 45, 1776-1783.

147. Alberto R, Egli A, Abram U, et al. *J Chem Soc*, **1994**, 19, 2815-2820.
148. Wu Z, Li ZB, Chen K, et al. *J Nucl Med*, **2007**, 48, 1536-1544.
149. Weiner RE, Thakur ML. *BioDrugs*, **2005**, 19, 145-163.
150. Fani M, Maecke HR, Okarvi SM. *Theranostics*, **2012**, 2, 481-501.
151. Kaltsas GA, Papadogias D, Makras P, et al. *Endocr Relat Cancer*, **2005**, 12, 683-699.
152. Spear MA, Breakefield XO, Beltzer J, et al. *Cancer Gene Ther*, **2001**, 8, 506-511.
153. Gabriel M, Decristoforo C, Donnemiller E, et al. *J Nucl Med*, **2003**, 44, 708-716.
154. Forrer F, Uusijarvi H, Waldherr C, et al. *Eur J Nucl Med Mol Imaging*, **2004**, 31, 1257-1262.
155. Koukouraki S, Strauss LG, Georgoulas V, et al. *Eur J Nucl Med Mol Imaging*, **2006**, 33, 460-466.
156. Schroeder RP, van Weerden WM, Krenning EP, et al. *Eur J Nucl Med Mol Imaging*, **2011**, 38, 1257-1266.
157. Lütje S, Heskamp S, Cornelissen AS, et al. *Theranostics*, **2015**, 5, 1388-1401.
158. Wild D, Wicki A, Mansi R, et al. *J Nucl Med*, **2010**, 51, 1059-1067.
159. Bhagwat SV, Lahdenranta J, Giordano R, et al. *Blood*, **2001**, 97, 652-659.
160. Pasqualini R, Koivunen E, Kain R, et al. *Cancer Res*, **2000**, 60, 722-727.
161. Guzman-Rojas L, Rangel R, Salameh A, et al. *Proc Natl Acad Sci U S A*, **2012**, 109, 1637-1642.
162. Tokuhara T, Hattori N, Ishida H, et al. *Clin Cancer Res*, **2006**, 12, 3971-3978.
163. Hashida H, Takabayashi A, Kanai M, et al. *Gastroenterology*, **2002**, 122, 376-386.
164. Arap W, Pasqualini R, Ruoslahti E. *Science*, **1998**, 279, 377-378.
165. Corti A, Curnis F, Arap W, et al. *Blood*, **2008**, 112, 2628-2635.

166. Gregorc V, Zucali PA, Santoro A, et al. *J Clin Oncol*, **2010**, 28, 2604–2611.
167. Von Wallbrunn A, Waldeck J, Höltke C, et al. *J Biomed Opt*, **2008**, 13, 011007.
168. Chen K, Ma W, Li G, et al. *Mol Pharmaceutics*, **2013**, 10, 417–427.
169. Zhang J, Lu X, Wan N, et al. *Nucl Med Biol*, **2014**, 41, 268–275.
170. Ma W, Wang Z, Yang W, et al. *Bio Med Res Int*, **2014**, 618096–618102.
171. Oliveira EA, Faintuch BL, Núñez EGF, et al. *Melanoma Res*, **2012**, 22, 45–53.
172. Kim DW, Kim WH, Kim MH et al. *J Label Compd Radiopharm*, **2015**, 58, 30–35.
173. Greenland WEP, Howland K, Hardy J, et al. *J Med Chem*, **2003**, 46, 1751–1757.
174. Curnis F, Cattaneo A, Longhi R et al. *J Biol Chem*, **2010**, 285, 9114–9123.
175. Merrifield RB. *J Am Chem Soc*, **1963**, 85, 2149.
176. https://en.wikipedia.org/wiki/Solid-phase_synthesis.
177. Weibe LI, Machulla HJ. *Imaging Hypoxia, Kluwer Academic Publishers, Netherlands*, **1999**, 1.
178. Höckel M, Vaupel P. *J Natl Cancer Inst*, **2001**, 93, 266–276.
179. https://en.wikipedia.org/wiki/Tumor_hypoxia
180. Mees G, Dierckx R, Vangeste C, et al. *Eur J Nucl Med Mol Imaging*, **2009**, 36, 1674–1686.
181. Splith K, Bergmann R, Pietzsch J, et al. *ChemMedChem*, **2012**, 7, 57–61.
182. Gray LH, Conger AD, Ebert M. *Br J Radiol*, **1953**, 26, 638–648.
183. Brown JM. *Methods in Enzymology*, **2007**, 435, 297–321.
184. Höckel M, Schlenger K, Aral B, et al. *Cancer Res*, **1996**, 56, 4509–4515.
185. Fyles AW, Milosevic M, Wong R, et al. *Radiother Oncol*, **1998**, 48, 149–156.
186. Nordmark M, Bentzen SM, Rudat V, et al. *Radiother Oncol*, **2005**, 77, 18–24.

187. Brizel DM, Scully SP, Harrelson JM, et al. *Cancer Res*, **1996**, 56, 941–943.
188. (a) <http://www.hbni.ac.in/phdthesis/chem/CHEM01200604036.pdf>;
(b) <http://www.hbni.ac.in/phdthesis/chem/CHEM01201004013.pdf>
189. Joyard Y, Le Joncour V, Castel H et al. *Bioorg Med Chem Lett*, **2013**, 23, 3704–3708.
190. Tocher JH. *Gen Pharmacol*, **1997**, 28, 485–487.
191. Krohn KA, Link JM, Mason RP. *J Nucl Med*, **2008**, (Suppl 2), 129S–148S.
192. Bock M. *Arzneimittelforschung*, **1961**, 11, 587.
193. Hoffer M, Grunberg E. *J Med Chem*, **1974**, 17, 1019–1020.
194. 22. Nakamura S. *Pharm Bull*, **1955**, 3, 379–383.
195. Nunn A, Linder K, Strauss HW. *Eur J Nucl Med*, **1995**, 22, 265–280.
196. Mei L, Wang Y, Chu T. *Eur J Med Chem*, **2012**, 58, 50–63.
197. Wardman P, *J Phys Chem Ref Data*, **1989**, 18, 1637–1755.
198. Mallia MB, Mittal S, Sarma HD, Banerjee S. *Bioorg Med Chem Lett*, **2016**, 26, 46–50.
199. Rasey JS, Hofstrand PD, Chin LK, et al. *J Nucl Med*, **1999**, 40, 1072–1079.
200. Lewis JS, McCarthy DW, McCarthy TJ, et al. *J Nucl Med*, **1999**, 40, 177–183.
201. Grunbaum Z, Freauff SJ, Krohn KA, et al. *J Nucl Med*, **1987**, 28, 68–75.
202. Evans SM, Kachur AV, Shiue CY, et al. *J Nucl Med*, **2000**, 41, 327–336.
203. Ballinger JR. *Semin Nucl Med*, **2001**, 31:321–329.
204. Mallia MB, Kumar C, Mathur A, et al. *Nucl Med Biol*, **2012**, 39, 1236–1242.
205. Mallia MB, Subramanian S, Mathur A, et al. *Nuc Med Biol*, **2014**, 41, 600–610.
206. Fernández S, Giglio J, Rey AM, et al. *Bioorg Med Chem*, **2012**, 20, 4040–4048.
207. Lee ST, Scott AM. *Semin Nucl Med*, **2007**, 37, 451–461.
208. Piert M, Machulla HJ, Picchio M, et al. *J Nucl Med*, **2005**, 46, 106–113.

209. Yang DJ, Wallace S, Cherif A, et al. *Radiology*, **1995**, 194, 795–800.
210. Melo T, Duncan J, Ballinger JR, Rauth AM. *J Nucl Med*, **2000**, 41, 169–176.
211. Linder KE, Chan YW, Cyr JE, et al. *J Med Chem*, **1994**, 37, 9–17.
212. Chu T, Hu S, Wei B, et al. *Bioorg Med Chem Lett*, **2004**, 14, 747–749.
213. Li Z, Zhang J, Jin Z, et al. *Med Chem Commun*, **2015**, 6, 1143–1148.
214. Dhake KP, Tambade PJ, Singhal RS, Bhanage BM. *Green Chem Lett Rev*, **2011**, 4, 151–157.
215. Kobayashi G, Saito T, Kitano Y. *Synthesis*, **2011**, 20, 3225–3234.
216. Connelly NG, Geiger WE. *Chem Rev*, **1996**, 96, 877–910.
217. Adams GE, Cooke MS. *Int J Radiat Biol Relat Stud Phys Chem Med*, **1969**, 15, 457–471.
218. Adams GE, Flockhart IR, Smithen CE, et al. *Radiat Res*, **1976**, 67, 9–20.
219. Leamon PC, Low PS. *Drug Discov Today*, **2001**, 6, 44–51.
220. Stover PJ. *Nutr Rev*, **2004**, 62, S3–S12.
221. Sirotnak FM, Tolner B. *Annu Rev Nutr*, **1999**, 19, 91–122.
222. Wibowo AS, Singh M, Reeder KM, et al. *Proc Natl Acad Sci USA*, **2013**, 38, 15180–15188.
223. Parker N, Turk MJ, Westrick E et al. *Anal Biochem*, **2005**, 338, 284–293.
224. Low PS, Henne WA, Doorneweerd DD. *Acc Chem Res*, **2008**, 41, 120–129.
225. Morris RT, Joyrich RN, Naumann RW, et al. *Ann Oncol*, **2014**, 25, 852–858.
226. Lu J, Zhao W, Huang Y, et al. *Mol Pharmaceutics*, **2014**, 11, 4164–4178.
227. Vlahov IR, Leamon CP. *Bioconjugate Chem*, **2012**, 23, pp 1357–1369.
228. Quici S, Casoni A, Foschi F, et al. *J Med Chem*, **2015**, 58, 2003–2014.
229. Müller C. *Molecules*, **2013**, 18, 5005–5031.

230. Müller C, Schibli R. *J Nucl Med*, **2011**, 52, 1-4.
231. Müller C, Schubiger PA, Schibli R. *Bioconjugate Chem*, **2006**, 17, 797-806.
232. Fani M, Tamma ML, Nicolas GP et al. *Mol Pharmaceutics*, **2012**, 9, 1136-1145.
233. Mathias CJ, Wang S, Lee RJ et al. *J Nucl Med*, **2006**, 37, 1003-1008.
234. Leamon CP, Parker MA, Vlahov IR et al. *Bioconjugate Chem*, **2002**, 13, 1200-1210.
235. Mathias CJ, Wang S, Waters DJ et al. *J Nucl Med*, **1998**, 39, 1579-1585.
236. Fisher RE, Siegel BA, Edell SL et al. *J Nucl Med*, **2008**, 49, 899-906.
237. Trump DP, Mathias CJ, Yang Z et al. *Nucl Med Biol*, **2002**, 29, 569-573.
238. Chen Y, Guo H, Xie F, Lu J. *J Labelled Compd Radiopharm*, **2014**, 57, 12-17.
239. Guo W, Hinkle GH, Lee RJ. *J Nucl Med*, **1999**, 40, 1563-1569.
240. Müller C, Schibli R, Forrer F et al. *Nucl Med Biol*, **2007**, 34, 603-608.
241. Boss SD, Betzel T, Müller C, et al. *Bioconjugate Chem*, **2016**, 27, 74–86.
242. Ke CY, Mathias CJ, Green MA. *Adv Drug Delivery Rev*, **2004**, 56, 1143–1160.
243. Trindade AF, Frade RFM, Maçôas EMS, et al. *Org Biomol Chem*, **2014**, 12, 3181-3190.
244. Bettio A, Honer M, Muller C et al. *J Nucl Med*, 2006, 47, 1153-1160.
245. Mathur A, Mallia MB, Banerjee S et al. *Bioorg Med Chem Lett*, **2013**, 23, 1394-1397.
246. Bolzati C, Cavazza-Ceccato M, Agostini S, et al. *J Nucl Med*, **2008**, 49, 1336-1344.